CHARACTERISATION OF SYNTACTIC FOAMS FOR MARINE APPLICATIONS

A Thesis submitted by

Zulzamri Salleh, MSc, BSc. (Hons.)

For the award of

Doctor of Philosophy

2017

Abstract

Syntactic foams are light weight particulate composites that use hollow particles (microballoons) as reinforcement in a polymer resin matrix. High strength microballoons provide closed cell porosity, which helps in reducing the weight of the material. Due to their wide range of possible applications, such as in marine structures, it is desirable to modify the physical and mechanical properties of syntactic foams in particular to achieve both high specific compressive strength and high energy absorption with minimal or no increase in density. Based on a literature review, it was found that marine applications of syntactic foams mainly focus on mechanical properties, on light weight as buoyancy aid materials, and on enhanced thermal insulators in the deep water pipeline industry. In order to achieve all these characteristics, attention needs to be placed on the determination of the effects on wall thickness, on the radius ratio (η) of glass microballons and on the presence of porosity in syntactic foams. The size of these parameters can be calculated and compared with observation by using SEM micrograph machine.

In this study, the specific mechanical properties, particularly compressive and tensile properties with 2-10 weight percentages (wt.%) of glass microballoons, are investigated and discussed. It is shown that the mechanical properties, particularly compressive and tensile strength, decreased when glass microballoons with vinyl ester resin were added. The effect of porosity and voids content mainly contributed to a reduction of these results and this is discussed further in this study. Tensile and compressive characteristics of the vinyl ester matrix syntactic foam were investigated and it was revealed that tensile strength was 70-80 % higher than compressive strength when glass content was reduced.

The fabrication of syntactic foam sandwich composites is also investigated and discussed in this study. It was found that mechanical properties such as compressive, tensile and flexural strength were varied with different amounts of glass microballoon content as core material. The compressive strength of the sandwich panels was significantly affected by a low density core foam, particularly 2 wt.% of glass

microballoon, as well as their modulus of elasticity and maximum stress value. The tensile failure of the syntactic foam sandwich panels was also significantly affected by lower glass microballoon content (2 wt.%) and the core failure was clearly observed compared to other failure modes, such as cohesive and adhesive failure modes. The flexural shear testing or three-point bending (TPB) of the syntactic foam sandwich panels indicated a higher strength when the glass microballoon content was increased in the core materials compared to the un-symmetrical shear failure mode.

The investigation into water absorption in room temperature (T: 25 ^{o}C) and a higher temperature (70 ^{o}C) have been investigated in this study to check the sustainability and reliability of syntactic foam for marine applications that were immersed in three different types of water (FW-Fresh water, DD-Double Distil water and SW-Salt water). Water absorption rates varied due to the effect of the density of syntactic foam as a result of the pores and void containment attributed to a higher glass microballoon content. The diffusion rate or coefficient D, could be estimated by using Fick's law, which also predicted that the equilibrium stage could be achieved better at high temperature conditions when compared to room temperature. The diffusion rate also varied when immersed with different water conditions, for example SW being slower than FW and DD waters due to the effect of the pores' activity. The mechanical properties of syntactic foam, when immersed in different types of waters at room temperature and under hygrothermal conditions, also varied with the duration at 30 days and at 60 days. It can be seen that the modulus of elasticity for both compressive and tensile properties showed decreases when more glass microballoon content was added, and when immersed for a long duration such as 60 days.

The thermal stability of syntactic foam is also investigated in this study. The compressive and tensile specimens were subjected to a hygrothermal analysis to determine the glass transition temperature, T_g and thermal expansion, α of syntactic foams. In this parametric thermogravimentric analysis (TGA) study, the results for T_g of syntactic foam with different (wt.%) of glass microballoon showed an increase after a hygrothermal process in which three different types of water were compared with dry specimens. Within the TGA/DTGA curve it was also found that T_{onset}, $T_{peak,}$ and T_{end}, showed varied temperatures when more glass microballoon content in syntactic foam was added. Moreover, their composition properties, such as their weight loss

residue as well as their temperature residue, also decreased until all specimens changed properties in the ash coal type. The thermomechanical analysis (TMA) on kinetic energy was conducted according to the first-order reaction Broido method, which is commonly used in polymer composites that have been discovered. In this study, it is revealed that the parameter, such as activation energy (E_a), decreased when the degradation temperature increased. Within this finding, E_a was varied and depended on the (wt.%) of glass microballoon in syntactic foam. The lower activation energy was required to complete the decomposition process. A linear expansion study was done, especially with a focus on the thermal dimension stability of syntactic foam, and the result showed a decrease when more glass microballoon in syntactic foam was added. The lower thermal stability at a higher temperature could be very useful for an insulator product, particularly in marine and aerospace engineering applications. The linear dimension stability, also called coefficient of thermal expansion (CTE), decreased when the glass microballoon content increased. The modification of Turner's model was applied in this study for a comparison of CTE in three different temperatures: 30 ^{o}C, 50 ^{o}C, and 70 ^{o}C for syntactic foam. The modification included parametric study involvement with the effect of radius ration, porosity and voids content in syntactic foam. As a result, the porosity content contributed much more to the CTE value, especially gap of ratio, which was different from the matrix porosity.

In order to achieve a better quality of syntactic foams, the study also investigated the stress intensity factor (SCF) by modelling particularly from the tensile specimens, K around holes at the microballoons. The prediction of strain value between local strains from the experimental strain gauge was compared with the finite element analysis (FEA) simulation when their varied load in longitudinal and transverse axes was applied to a tensile and flexural sandwich panel's syntactic foam. For the tensile specimen, the determination of the SCF used one strain gauge, which was attached near the hole in the middle of the extensometer length. The results show that the SCF values were comparable between experiments with extensometer and strain gage (SG) values, with percentages ranging from 0.40 % to 1.36 %. A comparison and a prediction were made between experimental values and the FEA analysis results. It could be estimated that the experimental values of around 90 % and 70 % followed the FEA values for SG1 and SG2, respectively. An investigation on the strain value for flexural sandwich panel syntactic foam was also carried out using the FEA approach

to predict the properties' behaviour in this study. It was found that the micro strain for SG1 in the FEA approach was 17% higher than the experimental value, even though they were at the same loading setting. However, the prediction for the micro strain of SG2 was only 2.7 % different, which was considered a good agreement to predict the properties of a syntactic foam core sandwich panel for different loading values.

Certification of Thesis

This thesis is entirely the work of *Zulzamri Salleh* except where otherwise acknowledged. The work is original and has not previously been submitted for any other award, except where acknowledged.

Student and supervisors signatures of endorsement are held at USQ.

Dr Mainul Islam

_____

Principal Supervisor

Dr Jayantha Epaarachchi

_____

Associate Supervisor

Acknowledgements

This research program, established and supported under Malaysian Government (MARA). The undertaking and completion of this study would not have been possible without the help and assistance of a significant number of people, to whom I wish to express my sincere gratitude and appreciation.

Firstly, heartfelt and sincere thanks to my supervisor team;

Dr Mainul Islam – Thank you very much for providing me with invaluable insight, expertise and assistance in the many facets of this work, and for the generosity of your time in reviewing this thesis and also journal papers.

Dr Jayantha Epaarachchi – Thank you very much for sharing your knowledge and support particularly your expertise on FEA study which is knowledgeable for me to apply in future research.

CFM team members – Mr Wayne Crowell and Mr Martin Geach for advices, support and helping on the guidance used for testing machine, cutting and grinding machine at the Centre. Last but not least, helping from Dr Venkata Chevali who taught and guided me during thermal analysis. Finally, all CFM/HES postgraduates and post doctorates, Dr Rajab Abousnina, Dr Belas Ahmed Khan, Mr Majid Muttashar, Mr Wessam Al-Azzawi, Mr Wahid Ferdous and all members who gave me advices and beneficial guidance and tips how to make success for my thesis completion.

Heartfelt thanks and appreciation for Prof Peter Schubel as Director of Centre for Future Materials and Prof Thiru Aravinthan as Associate Dean Research Training, who recognised my potential research, encouraged me to succeed of completion of my study and make this journey meaningful and worthwhile.

I greatly appreciate the academic scholarship and financial family sponsorship provided from MARA and Universiti Kuala Lumpur (UniKL). I am also thankful to

UniKL Top management, Deans of UniKL MIMET, PMTC group and all the colleagues.

I would like to express my sincere appreciation to my parents and my family in-law for their unconditional and endless support. The most important thank you goes to my dear wife Sukinah Mohamed (Hitam), all my kids Nur Shafiqa Adriana, Nur Shifa Kamilia and Mohamed Adib Zikry. Thank you for your endless patience for comforting and encouraging me during the challenging periods of this phase of my life. Without your support I would not have been able to put a close to this phase of my life.

All praise and thanks is to Almighty Allah who has blessed me with understanding and strength. His blessings towards me are innumerable as it is through Him that I have developed a sincere thirst for knowledge. To those whom I have failed to mention but have played a contributing part of this endeavour, thank you very much.

Associated Publications

Journals

Salleh, Z, Islam, MM and Ku, H (2014). 'Study on Compressive Properties of Syntactic Foams for Marine Applications'. *Journal of Multifunctional Composites*, 2(1), 21-27.

Salleh, Z, Islam, MM and Epaarachchi, JA (2015). 'Compressive Behaviour of Low Density Polymeric Syntactic Foams'. *Applied Mechanics and Materials,*799-800, 135-139.

Salleh, Z, Islam, MM and Epaarachchi, JA (2016). 'Analysis of Stress Concentration Factor Around the Hole of Syntactic Foam Tensile'. *International Journal of Advances in Science Engineering and Technology*, 4(3), 102-106.

Salleh, Z, Islam, MM and Epaarachchi, JA (2016). 'Mechanical properties of sandwich composite made of syntactic foam core and GFRP skins'. *AIMS Materials Science*, 3(4), 1704-1727.

Salleh, Z, Islam, MM and Epaarachchi, JA (2016). 'Analysis of Stress Concentration Factor for Tensile Characteristics of Syntactic Foam Using Finite Element Method'. *Journal of Research Updates in Polymer Science*, 6(1), 1-12.

Salleh, Z, Islam, MM, Epaarachchi, JA and Su, H (2017). 'Vinyl Ester/Glass Microballoon Syntactic Foams with Low Density'. *International Research Journal of Materials Sciences and Applications*, 1(1), 1-25.

Refereed Conference Proceedings

Salleh, Z, Islam, MM and Epaarachchi, JA (2014). 'Compressive Properties of Ceramic Microballoon Syntactic Foams'. *International Conference on Mechanical, Industrial and Energy Engineering*, 26-27 December, Khulna Bangladesh pp 1-5.

Salleh, Z, Islam, MM and Epaarachchi, JA (2015). 'Mechanical Properties of low Density Glass Microballoons/Vinyl ester Syntactic Foam for Marine Application'. C*onference on Game On Winning with Composites, Composites Australia and CRC-ACS,* 21-23 April, Gold Coast, Queensland, Australia, pp 1-10.

Salleh, Z, Islam, MM and Epaarachchi, JA (2016). 'Determination of Coefficient Thermal Expansion of Glass Microballoon/Vinyl Ester Syntactic Foams'. *3rd Advanced Materials Conference (AIP Conference Proceeding)*, 28-29 November, Bayview Hotel, Langkawi Island, Kedah, Malaysia, pp 1-5.

Salleh, Z, Islam, MM and Epaarachchi, JA (2016). 'Thermogravimetry Analysis on Fused Borosilicate Syntactic Foams'. *3rd Advanced Materials Conference (AIP Conference Proceeding)*, 28-29 November, Bayview Hotel, Langkawi Island, Kedah, Malaysia, pp 1-5.

Table of Contents

List of Figures

List of Tables

Nomenclature

Symbol:	Description:
$Al_2O_3.3P_2O_5$	Amorphous substance
B	Width of panel
Ca^{2+}	Calcium ion
CH_3COO^-	Acetate
$CH_2(COO)_2^{2-}$	Carboxyl
$C_2O_4^{2-}$	Ethanedioate
D	Water diffusion coefficient
d_s	Distances from the centre of the skins
d_c	Distances from the centre of the core
dE	Differential Equation of modulus of elasticity
dw	Differential Equation of volume fraction
E_b	Modulus of elasticity of glass microballoon
E_m	Modulus of elasticity of matrix resin
E_c panels	Compressive modulus of elasticity of syntactic foam sandwich
E_t panels	Tensile modulus of elasticity of syntactic foam sandwich
E_{sk} panels	Modulus of elasticity of skin of syntactic foam sandwich
E_{co} panels	Modulus of elasticity of core of syntactic foam sandwich
E_B	Tangent modulus or modulus of elasticity in bending of syntactic foam sandwich panels
$EI_{flatwise}$	Flexural stiffness of flatwise beam sandwich panel
$EI_{edgewise}$	Flexural stiffness of edgewise beam sandwich panel

$E_{compressive}$	Compressive modulus of elasticity
E_{flex}	Flexural Modulus of elasticity
Ea	Activation energy
$F_{max.}$	Maximum force
f_E	Young's modulus function
F^-	Fluoride
F	Force perpendicularly directed to the specimens
$HCOO^-$	Methanoate
He	Helium gas
K_I *or* K_t	Stress concentration factor
K^+	Potassium ion
K^{-1}	Per Kelvin unit
M_{cm}	Mass of composite
M_{fill}	Mass of filler
M_{mx}	Mass of matrix resin
m_{fill}	Mass fraction of filler
m_{mx}	Mass fraction of matrix
M(t)	Water content at time t
M(∞)	Equilibrium water content
Mg^{2+}	Magnesium ion
mol^{-1}	Per mole unit
NH_4^+	Ammonium ion
Na^+	Natrium ion
NO_3^-	Nitric acid
P_{gas}	Pressure of gas
R_H	Heating rate

R^2	Regression value
r_i	Internal radii
r_o	Outer radii
S	midspan
SO_4^{2-}	Sulphate
s^{-1}	Per second unit
T_g	Glass transition temperature
t_s	Thickness of the skin of sandwich panel
t_c	Thickness of the core of sandwich panel
T_m	Temperature of the maximum decomposition rate
T_{onset}	Onset temperature
T_{end}	End temperature
T_{peak}	Peak temperature
V_{cm}	Volume of composite
V_{fill}	Volume of filler
V_{mx}	Volume of matrix
V_{vd}	Volume of void
v_{fill}	Volume fraction of filler
v_{mx}	Volume fraction of matrix
v_{vd}	Volume fraction of void
V_{gas}	Volume of gas
V_f	Volume fraction of filler/glass microballoon
$V_{p,gm}$	Volume of porosity in syntactic foam
V_{gm}	Volume of glass microballoon
$V_{c,gm}$	Volume of glass microballoon composite
V_{void}	Volume of void in syntactic foam

V_{sf}	Volume of syntactic foam
W_{sf}	Weight of syntactic foam
W_r	Weight of matrix resin
W_{gm}	Weight of glass microballoon
w_m	Maximum packing volume fraction of particles
W_f	Weight of filler/glass microballoon
Wt	Weight of the specimens at time *t*
Wo	Initial weight
W^m	Water diffusion in the matrix material
W^s	Weight of specimen at equilibrium condition
$W(t_1)$	Water content associated with the first weight measurement

Greek Symbol

Symbol:	Description:
ρ_{cm}	Density of composite
ρ_{fill} or ρ_f	Density of filler
ρ_{mx} or ρ_m	Density of matrix resin
η	Radius ratio
μm	micrometer
λ	Thermal conductivity
α	Coefficient of thermal expansion
σ_{max}	Maximum stress
σ_{norm}	Nominal stress
ρ_t	Radius of curvature of the flaw
σ_x	Stress at x-axis

σ_y	Stress at y-axis
δ	Angle made by the line joining the point element and the microballoon surface
χ	Parameter depending on the microballoon and specimen sizes
π	Pi
ρ_{sf}	Density of syntactic foam
ρ_{gm}	Density of glass microballoon
ω	Wall thickness of glass microballoon
ρ_r	Density of viny ester resin
φ	Porosity syntactic foam
σ/μ	Standard deviation divided Mean
f_ϕ	Function of Poisson's ratio
ϕ_b	Poisson's ratio of glass microballoon
ϕ_m	Poisson's ratio of matrix resin
σ_{ult}	Ultimate stress
σ_{fc}	Facing stress
$\emptyset_p$	Cavity porosity
ρ_{exp}	Experimental density
ρ_{theo}	Theoretical density
Δl	Change of length
ΔT	Change of temperature
α_m	CTE for matrix resin
α_g	CTE for glass microballoon
β_m	Weight percentage of matrix resin

β_g	Weight percentage of glass microballoon
ν	Poisson's ratio of glass microballoon
$\emptyset_g$	Cavity porosity
$\emptyset_m$	Matrix porosity
$\emptyset_v$	Voids content
f(α)	Function of reaction model
Ω	Ohm (resistance value)
Δ (%)	Different percentage value of coefficient thermal expansion

Abbreviation

3 D	Three Dimensional
AAP	Acetyl Acetone Peroxide
ASTM	American Society for Testing and Materials
BPO	Benzoyl Peroxide
CHP	Cumene hydoperoxide
DD	Double Distil
DGEBA	Diglycidyl Ether of Bisphenol A
DMA	Dimethylaniline
DTGA	Differential Thermogravimetric Analysis
EI	Flexural Stiffness
EXP	Experimental
FEA	Finite Element Analysis
FW	Fresh Water
FLSW	Flexural Flatwise Sandwich

FESW	Flexural Edgewise Sandwich
GFRP	Glass fibre reinforced plastic
GPa	Giga Pascal
HDT	Heat Distortion Temperature
kN	kilo Newton
MAP	Mono-Aluminium Phosphate
MEKP	Methyl Ethyl Ketone Peroxide
MPa	Mega Pascal
PE	Polyethylene
PMMA	Polymethyl Methacrylate
PVC	Polyvinyl Chloride
RIM	Reaction in Moulding
ROM	Rule of Mixture
SCF	Stress Concentration Factor
SCFT	Syntactic Foam Compression and Tensile
SCSW	Syntactic Foam Compression Sandwich
SF2WC-F	Syntactic Foam 2 wt% Compression Fresh water
SF2WC-F-30	Syntactic Foam 2 wt% Compression Fresh water immersed 30days
SF2WC-F-60	Syntactic Foam 2 wt% Compression Fresh water immersed 60days
SF2WC-D	Syntactic Foam 2wt% Compression DD water
SF2WC-DD-30	Syntactic Foam 2 wt% Compression DD water immersed 30days

SF2WC-DD-60	Syntactic Foam 2 wt% Compression DD water immersed 60days
SF2WC-S	Syntactic Foam 2wt% Compression Salt water
SF2WC-S-30	Syntactic Foam 2 wt% Compression Salt water immersed 30days
SF2WC-S-60	Syntactic Foam 2 wt% Compression Salt water immersed 60days
SF2WT-F	Syntactic Foam 2 wt% Tensile Fresh water absorption
SF2WT-F-30	Syntactic Foam 2 wt% Tensile Fresh water immersed 30days
SF2WT-F-60	Syntactic Foam 2 wt% Tensile Fresh water immersed 60days
SF2WT-D	Syntactic Foam 2wt% Tensile DD water absorption
SF2WT-DD-30	Syntactic Foam 2 wt% Tensile DD water immersed 30days
SF2WT-DD-60	Syntactic Foam 2 wt% Tensile DD water immersed 60days
SF2WT-S	Syntactic Foam 2wt% Tensile Salt water absorption
SF2WT-S-30	Syntactic Foam 2 wt% Tensile Salt water immersed 30days
SF2WT-S-60	Syntactic Foam 2 wt% Tensile Salt water immersed 60days
SF2WCH-F	Syntactic Foam 2wt% Compression Hygrothermal Fresh water
SF2WCH-D	Syntactic Foam 2wt% Compression Hygrothermal DD water
SF2WCH-S	Syntactic Foam 2wt% Compression Hygrothermal Salt water
SF2WTH-F	Syntactic Foam 2wt% Tensile Hygrothermal Fresh water
SF2WTH-D	Syntactic Foam 2wt% Tensile Hygrothermal DD water
SF2WTH-S	Syntactic Foam 2wt% Tensile Hygrothermal Salt water
STSW	Syntactic Foam Tensile Sandwich
SEM	Scanning Electron Microscope/Microscopy
SG	Strain Gauge

SW	Salt Water
TDS	Technical Data Sheet
TGA	Thermogravimetric Analysis
TFSW	Tensile Flatwise Sandwich
TESW	Tensile Edgewise Sandwich
TMA	Thermomechanical Analysis
TPB	3–Point Bending
WCS	World Coordinate System

Chapter 1

Basic Information of Syntactic Foam

1.1 Introduction

According to the American Society for Testing and Materials (ASTM, 2012), syntactic foam is defined as a material consisting of hollow spherical fillers in a resin matrix. The hollow spheres are called microballoons. Syntactic foam is a special material made from a matrix (binder) and hollow spherical microspheres (filler) that possess a formal structure like a cellular and solidified liquid. The term 'syntactic' is defined as originating from the Greek *syntaktikos*, meaning an orderly disposed system (Rizzi et al., 2000). Syntactic foams possess a lower density due to the hollow microballoons incorporated in the matrix, as compared to solid particulate composites and fibre reinforced composites. A schematic 3D diagram of a three-phase syntactic foam is shown in Figure 1.1.

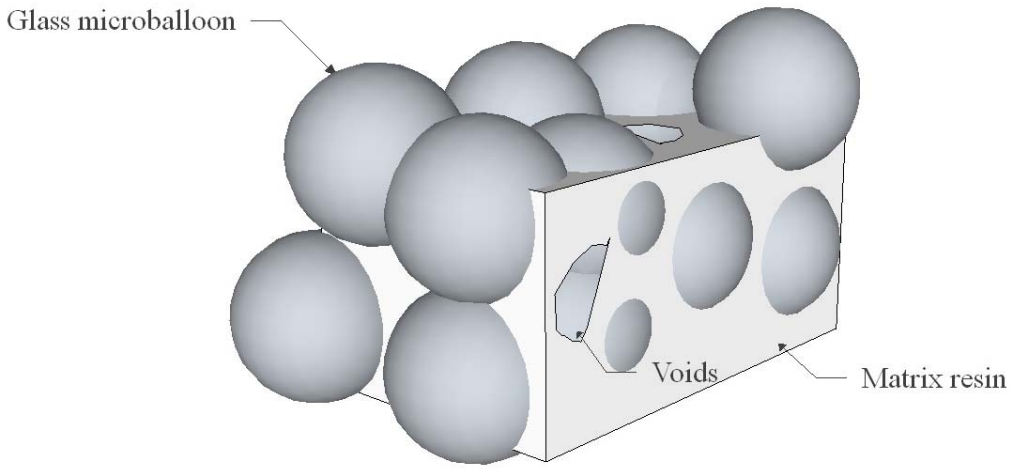

Figure 1.1: Schematic 3D diagram of a three phase syntactic foam

The syntactic foams known as closed foams possess a higher density than open cell foams with difficult to synthesise the existing of porosities in syntactic foams. However, syntactic foams have considerable superior mechanical properties that make them possible to be used in load bearing structural applications. Due to presence of porosity inside hollow particles, called microballoons, leads to lower moisture

absorption and lower thermal expansion, resulting in better dimensional stability (Gupta and Woldesenbet, 2003, Sauvant-Moynot et al., 2006). The size and distribution of porosity can be controlled very closely in these foams by means of microballoon volume fraction and wall thickness. The previous study also indicated that mechanical properties are varied with different filler content (Vasanth et al., 2012).

A comprehensive understanding of the influence of microballoons/matrix adhesion, wall thickness of the matrix on the compressive failure mechanisms of these foams is still lacking (Swetha and Kumar, 2011). This is also supported by (Gupta et al., 2004) that to achieve the better mechanical properties it is needed to consider wall thickness and volume fraction. These parameters always correlate with the density of glass microballoon and filler contents. Previous report shows that, the contents of void or porosities is less when density glass microballoons are increased (Gupta et al., 2010). Therefore, all these main parameters need to be considered in this study to ensure a better understanding to explore for marine applications.

This study expects several outcomes to be achieved to apply syntactic foams in marine applications through analytical studies on the effect of glass microballoon content in mechanical, hygrothermal and thermal insulation properties of syntactic foams. It will provide comprehensive information for the researchers to explore on the characteristic of syntactic foams as the lighter product with durability and sustainability in any conditions. Therefore, this study will achieve good results in mechanical characteristics, hygrothermal properties and thermal insulation properties of glass microballoons/vinyl ester syntactic foams. Determination of stress concentration factor, K for microballoons also enhances the understanding failure of micro crack around the microballoons from the tensile specimens. All these information's are very important to apply for those practically involved in offshore oil and gas industry, military defence technology and all related to the marine industry globally (Woldesenbet, 2008).

1.2 Research Objectives

The main objective of this research is to characterise the syntactic foams for marine applications, with a focus on experimentally investigating the correlations among material parameters, mechanical properties, structural sandwich panels and microstructural parameters of syntactic foams. Therefore, to achieve all these properties it is important to have the elements below.

The main objectives of the research are as follows:

1. To investigate the structural application of syntactic foam using sandwich panels with different weight percentages (wt.%) of glass microballoons as core, and unidirectional glass fibre reinforced plastic (GFRP) as skin.
2. To investigating the behaviour of syntactic foam for marine applications with respect to their water absorption and hygrothermal properties.
3. To investigating the degradation of syntactic foam using thermogravimetric analysis (TGA) and expansion of syntactic foam by thermomechanical analysis (TMA).
4. To develop a simplified closed form analytical model, using the finite element analysis (FEA) to express the stress concentration factor K, between glass microballoons at the crack failure, to express the stress and strain distributions in a single orthotropic laminate tensile shape that is subjected to internal/external pressure.

1.3 Scope of Study

The study focused on the fabrication of low density syntactic foam informed by an understanding of its physical, mechanical and hygrothermal behaviours. During this study, a particular intention was to focus on the following:

1. Fabricating syntactic foam with different weight percentages (wt.%) of glass microballoons, between 2 wt.% to 10 wt.%, used for compression and tensile specimens. From the literature, it was found based on the comparable study that the lower density material with a minimum weight percentage (wt.%) of

glass microballoon is better to be chosen compared to more percentage that will make it more brittle and affect the performance of syntactic foam.

2. Fabricating sandwich panels made from syntactic foam, from 2 wt.% to 10 wt.%, as a core and GFRP as a skin material used for compression, tensile and flexure specimens.
3. Investigating syntactic foam for material degradation behaviour and expansion properties using TGA and TMA.
4. Further investigation of a lower density specimen in terms of its hygrothermal properties for marine applications.
5. Analytical modelling on a lower density specimen, particularly investigating the stress concentration factor (SCF) comparable with experimental data, by using a strain gauge (SG).
6. Numerical simulation for FEA using CREO 3.0 to develop the modelling for isotropic material.
7. Validate the FEA modelling using an experimental investigation.

These findings, hopefully, may be useful to apply to marine engineering as syntactic foam has structural features that are lighter and more durable than existing products available. Because of these characteristics, it may be capable of floating or sinking in the ocean and thus be appropriate for use in marine equipment without significant additional costs. This study is also expected to be strengthened by using finite element analysis, which is used to prove that it can be compared with a numerical model experimental study. The significance of the results of this experiment will also be able to assist other researchers in an effort to advance the study in the future, especially for syntactic foam, based on glass microballoon mixed with a vinyl ester resin matrix.

1.4 Structure of the dissertation

The thesis is organised according to the following structure:

Chapter 1: Introduction

Chapter 2: This chapter focuses on the literature review and technology associated with the development of composite material in marine applications such as types of composite, composite structure, fibre reinforced composites, particulate composites and manufacturing of syntactic foam. It also explains the rule of mixtures for composites, which is related to density and porosity of syntactic foam, while elastic constant is related to mechanical behaviours. These characteristics need to be investigated in order to determine the lower density behaviour of syntactic foam. Since a matrix resin was used in this study, the explanation for the type of polymers should be clearly highlighted together with vinyl ester as a matrix binder. Thus, the chemical properties for glass microballoon and vinyl ester will also be explained in this chapter. The role of hardener, such as methyl ethyl ketone peroxide (MEKP), is also important to explain in this study.

Chapter 3: This chapter covers the fabrication and characterisation of syntactic foams and their constituents. The fabrication uses polyvinyl chloride (PVC) and steel moulds for compression and tensile specimens, respectively. The preparation of constituent materials such as glass microballoon, vinyl ester and MEKP hardener are explained. A conventional method was applied for the fabrication of syntactic foam in this study. The preparation of specimens followed the rule of mixtures with different weight percentages (wt.%) of glass microballoon contents, from 2.0 wt.% to 10 wt.%. The results are discussed including the compressive, tensile, and flexural and density for all specimens. Detailed discussion on density of syntactic foam is also presented, including the wall thickness of glass microballoon, void, and porosity that has occurred in syntactic foam internally. The effect of mechanical properties is also further discussed in this chapter. The scanning electron microscope (SEM) results are also discussed in this chapter for both compressive and tensile specimens. The use of syntactic foam for structural sandwich panels have also been designed and are discussed in the next chapter.

Chapter 4: The structural application of syntactic foam in the form of a syntactic foam core sandwich panel is presented and discussed in this chapter. It was started by the fabrication of a sandwich panel from constituent materials for compression, tensile and flexural testing, respectively. The characterisation of mechanical properties such

as Poisson's ratio, modulus of elasticity, stiffness, shear modulus and tangent modulus are important for sandwich panels. All these results are discussed for both of skin and core material. Furthermore, results from compression and flexure with different failure modes are compared for all different compositions of glass microballoon as a core material. Thus, these results are compared and validated by using strain gage unit, particularly flexural specimens, and this is used for further discussion in the next chapter.

Chapter 5: In this chapter, the mechanical properties between dry specimens and immersed specimens in different types of water is compared with a particular water absorption and hygrothermal treatment for a duration of between 30 and 60 days. Discussion of the effects of different types of water is explained in detail using Fickian Law's equation. The effect of water treatment in syntactic foam is also investigated using SEM analysis.

Chapter 6: This chapter reports on an investigation of a thermogravimetric analysis (TGA) and a thermomechanical analysis (TMA) of syntactic foam. Both degradation and expansion of syntactic foam are determined and discussed in this chapter. The result for glass transition temperature, T_g and coefficient of thermal expansion (CTE), α for all specimens, including pure vinyl ester, are also presented and discussed in this chapter. The effects of different weight percentages (wt.%) of glass microballoon on these analysis items are also discussed for all specimens. These results are discussed in terms of their usefulness in a heat resistance application as a lighter material, particularly when used in marine industries. Another aspect of mechanical properties needs to be investigated in this study, namely the results of the stress concentration factor (SCF), which is also compared between the theoretical and experimental levels, using a stress-strain modelling finite element analysis (FEA) approach in CREO 3.0 software. Design guidelines are proposed in this chapter for future work considerations, especially the development of syntactic foam in marine applications.

Chapter 7: Finally, conclusions and recommendations are made for all the findings in the previous chapters, as well as recommendations for further studies.

1.5 Summary:

The use of low density material in marine engineering became popular because it showed better performance in mechanical strength and has also shown better performance in different environmental conditions. Thus, the introduction of syntactic foam will meet these criteria, as it has the physical characteristics of lightness in particular, and the content of voids and porosity that affect these characteristics.

Although existing research has been conducted on syntactic foam, the use in marine investigation is still lacking, especially in hygrothermal and heat-resistant properties of materials. In addition, the study of numerical modelling on syntactic foam is still lacking. Therefore, this study will expand on the existing research and fill the gap that exists in the area of the properties of low density syntactic foam by renovating comprehensive analyses using a simulation method, in particular the use of sandwich panels of syntactic foam. The research presents an alternative method, useful in numerical modelling, and mainly used for marine applications.

Chapter 2

Literature Review

2.1 Basic Information of Syntactic foam

2.1.1 Overview

When it comes to engineering applications in the context of sea and space, for example in marine and aerospace structural applications, it is important to strive for materials having a combination of low density and high tensile strength, as well as good modulus elasticity and damage tolerance. In order to achieve all these kinds of characteristics, lighter and strong components should be made from composite materials. Composite materials are increasingly being used in recent years in such applications, especially sandwich types. Sandwich composites comprising low density core materials are especially useful in such applications. Use of open cell foams as core materials results in low through-the-thickness compressive strength and modulus of elasticity, thereby limiting the applications of such composites (Mills, 2007), an overview of which can be seen in Figure 2.1. A class of closed cell foams, synthesized by dispersing rigid hollow particles in a matrix material, has shown considerable promise for such applications, and this is called syntactic foam (Shutov, 1996, Hodge et al., 2000, Sauvant-Moynot et al., 2006).

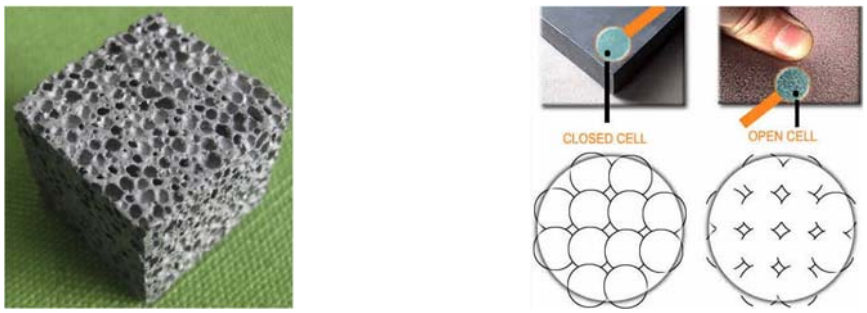

(a) Cross section of syntactic foam (b) Closed cell and open cell

Figure 2.1: Overview of syntactic foam (Abbess, 2011)

This closed foam possesses higher density than open cell foams. However, their considerably superior mechanical properties make it possible for them to be used in

load bearing structural applications, whereas open cell foams cannot be used in these applications. Additionally, the presence of porosity inside hollow particles, called microballoons, leads to lower moisture absorption and lower thermal expansion, resulting in better dimensional stability (Sauvant-Moynot et al., 2006, Gupta and Woldesenbet, 2003). The size and distribution of porosity can be controlled very closely in these foams by means of microballoon volume fraction and wall thickness. An extensive variety of polymer, metal and ceramic matrix syntactic foams has been studied in previously published literature. In polymer matrix syntactic foams, epoxy resins are most commonly used as matrix resin, due to the widespread use of these resins in aerospace applications (Rittel, 2005, Gupta et al., 1999, Karthikeyan et al., 2004, Karthikeyan et al., 2005, Wouterson et al., 2004, Kishore et al., 2005, M. Koopman et al., 2006, Bardella et al., 2003, Gladysz et al., 2006). Figure 2.2 shows the several marine application products made from syntactic foam manufactured by Trelleborg CRP companies such as mooring buoys, deep water ultra-buoys, pipe line installation buoys and umbilical floats porosity (Trelleborg, 2007).

(a) AUV (Autonomous Ultimately Vehicle)

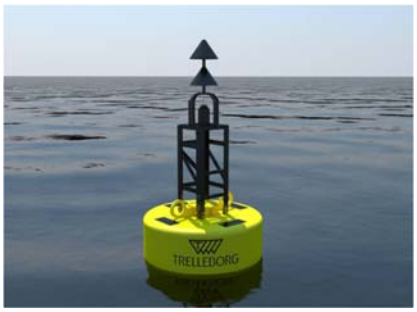

(b) Seismic buoy

(c) Thermal shipping vessel valve insulator

(d) Oil & gas pipe thermal Insulator

Figure 2.2: Several products made from syntactic foams (Trelleborg, 2007, Hiel et al., 1993, Ishai et al., 1995, Bardella and Genna, 2001, Gupta et al., 2002b, Watkins, 1988)

The syntactic foams known as closed foams possess a higher density than open cell foams, and it is difficult to synthesise the existing porosities in syntactic foams. However, syntactic foams have considerable superior mechanical properties that make it possible for them to be used in load bearing structural applications. A previous study also indicated that mechanical properties are varied with different filler content (Vasanth et al., 2012). A comprehensive understanding of the influence of microballoons/matrix adhesion, and wall thickness of the matrix on the compressive failure mechanisms of these foams is still lacking (Swetha and Kumar, 2011). This is also supported by Gupta et al., (2004) who noted that to achieve better mechanical properties wall thickness and volume fraction need to be considered. These parameters always correlate with the density of glass microballoons and filler content. Previous reports show that the void content or porosities are less when the density of glass microballoons is increased (Gupta et al., 2010). Therefore, all these main parameters need to be considered in this study to ensure a better understanding for exploring marine applications.

2.1.2 Performance of syntactic foam

Today, applications of high performance materials are the key for efficient functioning of materials in engineering technology. Thus new materials, which are a combination of two or three different materials, are fabricated to satisfy diverse performance needs in various applications, and such combinations of different materials are called composite materials. Composite materials are engineered materials made from two or more constituent materials with significantly different physical or chemical properties, which remain separate and distinct on a microscopic level within the finished structure. The properties of composite materials are different and have been improved as compared to constituent materials. Syntactic foams are engineered composite materials with a matrix phase and a reinforcing microballoons phase. Gupta and Ricci (2006) found that compressive properties do not significantly improve gradient structure if fabricated with a variation in microballoon volume fraction. Gupta et al., (2001) fabricated syntactic foam using glass microballoons and studied their compressive properties with variations in microballoon volume fractions. They also conducted compressive tests on syntactic foams fabricated with glass microballoons and concluded that compressive strength was higher than syntactic foam with phenolic

microballoons. Gupta et al. (2004) studied the mechanical properties of syntactic foam by taking the radius ratio of microballoons into consideration. Radius ratio is defined as the ratio between the inner and the outer radius of microballoons. A difference in the radius ratio of microballoons causes a change in density of syntactic foams. The lower the radius ratio, the higher the density of microballoons (Gupta et al., 2004). The effect of the microballoon radius ratio (η) and volume fraction on the tensile properties of syntactic foam was studied by Gupta and Nagorny (2006). The syntactic foam fabricated with high density microballoons exhibited high tensile strength and modulus (Gupta and Nagorny, 2006). It was also found that the tensile strength and modulus values of syntactic foam decreased with an increase in volume fraction for similar density microballoons. The effect of microballoon volume fraction on the tensile behaviour of syntactic foam was studied by Kishore et al., (2005). They also concluded that the tensile modulus and strength increase linearly with a decrease in the microballoon volume fraction. Recently, there are several companies supply the glass microballoon in the world with higher demand for fabrication of syntactic foam. Some of them already been listed in Table 2.1 for contributed the supply chain of glass microballoons with different types of physical properties. The majority of suppliers for microballoons were a 3M Company with different varieties of microballoon density.

Table 2.2 shows some collective data for the density and wall thickness of microballoons from past studies. The information shows that the density of microballoons increases with an increase in wall thickness. This is also related to the radius ratio, η which increases when the internal radius r_i also increases. The size of the bubbles is commonly referred to as ranging in diameter from 1- 500μm while the wall thickness range is 1- 4μm, and it is very rare for the diameter to be larger than 500μm (Swetha and Kumar, 2011). Figures 2.3 (a), (b) and (c) show SEM photos of three types of density glass of microballoons that also have a different wall thickness. The photo of microballoons was taken as an observation before incorporation into the matrix resin.

Table 2.1: Summary of glass microballoons suppliers by countries.

Supplier	Country	Density (kgm^{-3})	Mean Effective size (μm)	Radius ratio (η)	Wall Thickness (μm)	References
3M	India	150	60	0.98	0.60	(Vasanth et al., 2012)
		220	35	0.97	0.52	
		460	40	0.94	1.29	
3M, MN	USA	220	35	0.970	0.521	(Lawrence and Pyrz, 2001)
		320	40	0.956	0.878	
		370	40	0.947	1.052	
		460	40	0.936	1.289	
3M	USA	250	25	-	-	(Kishore et al., 2005)
		370	20	-	-	
3M	Australia	125	63	-	-	(Kim and Plubrai, 2004)

Table 2.2. Properties of glass microballoons for syntactic foams.

Microballoon types	Density (kgm^{-3})	Wall thickness (μm)	References
Borosilicate glass	220 - 460	0.521 – 1.289	(Lawrence et al., 2001)
Soda lime borosilicate glass	150 - 460	0.520 – 1.290	(Vasanth et al., 2012)
Hollow glass	600	11 - 50	(Devi et al., 2007)
Soda lime borosilicate glass	762	0.340 - 136	(Kim and Plubrai, 2004)

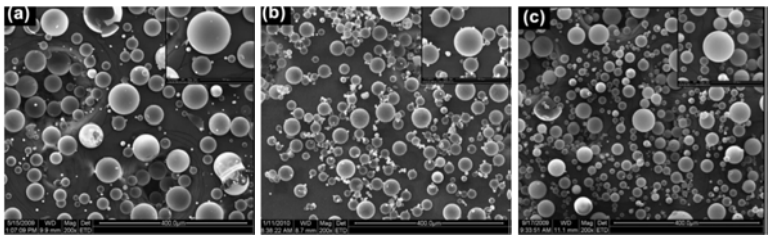

Figure 2.3: SEM photos 3 types of densities (a) 150 kgm^{-3}, (b) 220 kgm^{-3}, (c) 460 kgm^{-3} of glass microballoon (Swetha and Kumar, 2011)

Many researchers commonly use a type of glass microballoon called soda-lime-borosilicate glass. The borosilicate glass microballoons have also been used to fabricate syntactic foam, in which case the properties of the composite can be better related to the properties of constituent materials and their volume fractions (Lawrence et al., 2001). The varieties of density glass microballoon have also been investigated in order to select the best compression result. The measurement of microballoons density is done using pycnometer and is then compared with the TDS (Technical Data sheet) provided by the supplier. Many reports have stated that the wall thickness of glass microballoons affects the compressive properties. Previous studies have also indicated that the strength of the foam is a function of the wall thickness (Devi et al., 2007, Vasanth et al., 2012). The wall thickness can be calculated by considering the ratio of the inner and outer radius as, $\eta = r_i/r_o$ where r_i and r_o are the internal and outer radii of the microballoon. which is also called as radius ratio (Gupta and Ricci, 2006). The illustration of wall thickness of microballoons is shown in Figure 2.4.

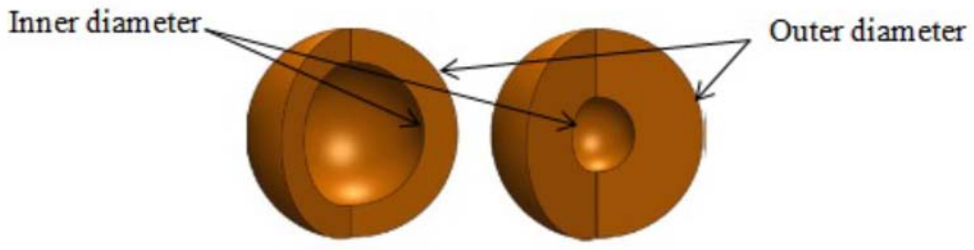

Figure 2.4: Difference in the wall thickness of the microballoon (Shunmugasamy et al., 2012)

2.1.3 Theoretical density using rule of mixtures

It is very important to be able to predict the properties of a composite from the properties of the constituent materials and their geometric arrangement. The rule of mixtures can be derived readily for the composite density of filler and the volume of void composites, as discussed below;

The total mass of the composite is given by,

$$M_{cm} = M_{fill} + M_{mx} \tag{2.1}$$

where M_{cm}, M_{fill} and M_{mx} indicate the masses of composite, filler and matrix resin respectively. Equation (2.1) is also valid when the voids are present in the composite. The volume of the composite needs to include volume of voids,

$$V_{cm} = V_{fill} + V_{mx} + V_{vd} \tag{2.2}$$

where V_{cm}, V_{fill}, V_{mx} and V_{vd} are the volumes of composite, filler, matrix and voids, respectively. Equation (2.1) and (2.2) can be rewritten,

$$m_{fill} + m_{mx} = 1 \tag{2.3}$$

and,

$$v_{fill} + v_{mx} + v_{vd} = 1 \tag{2.4}$$

where, m_{fill} and m_{mx} are the mass fractions of filler and matrix resin respectively, and v_{fill}, v_{mx}, v_{vd} are the volume fractions of filler, matrix and voids respectively.

Composite density, ρ_{cm} is given by,

$$\rho_{cm} = \frac{M_{cm}}{V_{cm}} = \frac{\rho_{fill} M_{fill}}{V_{cm}}$$

or,

$$\rho_{cm} = \rho_{fill} v_{fill} + \rho_{mx} v_{mx} \tag{2.5}$$

Another expression for ρ_{cm} in terms of mass fractions can be given as,

$$\rho_{cm} = \frac{M_{cm}}{V_{cm}} = \frac{1}{\frac{m_{fill}}{\rho_{fill}} + \frac{m_{mx}}{\rho_{mx}} + \frac{v_{vd}}{\rho_{cm}}} \tag{2.6}$$

Rewriting Equation (2.6), volume of voids in composite can be written as below;

$$v_{vd} = 1 - \rho_{cm}\left(\frac{m_{fill}}{\rho_{fill}} + \frac{m_{mx}}{\rho_{mx}}\right) \tag{2.7}$$

2.2 Constituent Materials Relevant to This Study

In this study, the constituent materials for syntactic foam are usually glass microballoon as filler, matrix binder resin and MEKP hardener.

2.2.1 Glass microballoons

Glass hollow microballoons (microspheres or bubbles) are found to be used in manufacturing of syntactic foam in the literature (Kim and Plubrai, 2004, Watkins, 1988, Seamark, 1991, Hinves and Douglas, 1993, Verweiji et al., 1985, Kenig et al., 1984, Narkis et al., 1980, Puterman and Narkis, 1980, Calahorra et al., 1987, Kim et al., 2001, Wouterson et al., 2004, Wouterson et al., 2007, Nijenhuis et al., 1989, Narkis et al., 1982, Gupta et al., 2001, Gupta et al., 2002a, Karthikeyan et al., 2004, M. Koopman et al., 2006).

The hollow glass microballoons are limited to uses in the refractory industry (Cochran, 1998). Ceramic hollow microballoons were used in the work of (Rohatgi et al., 2006) and (Cochran, 1998). Kenig et al., (1985) used carbon microballoons to manufacture syntactic foams. Kim and Oh (2000) fabricated syntactic foam using Q-Cel 520 hollow microballoons. Phenolic microballoons have also been used for syntactic foam manufacturing (Puterman and Narkis, 1980, Bunn and Mottram, 1993).

2.2.2 The role of the polymer matrix

The purpose of the resin is therefore to bind the reinforcement fibres into a single cohesive structural system. In doing so, the resin must hold the reinforcement in place and act as a path for load transfer between the fibres. Through a combination of adhesive and cohesive characteristics, the resin enables the development of a single material system. The new system provides not only tensile capacity but also compressive and shear capacity. The polymer matrix also serves other functions such as protecting the reinforcement fibre from adverse environments. Selection of the appropriate matrix material for environmental durability is critical in ensuring the longer term viability of a composite system.

This is particularly true in harsh service environments such as off-shore and shoreline applications, chemical plants and cold climates where products such as de-icing salts are widely used. The polymer matrix also provides all the inter-laminar shear strength of the composite and also provides resistance to crack propagation and damage. In addition, it can be used to contribute properties such as ductility, toughness or electrical insulation. The resin is also seen to affect the temperature performance of the material, typically determining properties such as the maximum service temperature.

Polymers can be defined as a substance whose molecules consist of a large number of low molar mass base units (monomers) connected by primary (covalent) chemical bonds (Challa, 1993). The base unit monomers are small simple molecules capable of either reacting with each other to form a new polymer chain, or of reacting onto an existing polymer chain. Polymeric materials are generally represented in terms of their monomer base units. For example, a polymer formed by the monomer 'A' (and hence the base unit - A -) would be represented as:

- A - A - A - A - A - or -[- A -]-n

Polymers can be designed with a single monomer species to form what is known as a homopolymer. In order to have superior properties, it is often to obtain by using a mix of type to form a copolymer. Copolymers can be created in a variety of forms as outlined in Table 2.3. The characteristic of a copolymer can be altered through alteration of the sequencing of the monomer base units. Polymers can be classified into two primary types: thermoplastics and thermosets.

Table 2.3: Classification of copolymer types (Challa, 1993).

Polymer Types	Polymer Chain
Random copolymers	- AAABABBABAAB -
Alternating copolymers	- ABABABABABAB - or -[- A - B -]-n
Block copolymers	- AAABBBAAABBB - or -[- A -]-[- B -]-n
Craft copolymers	- AAAAA*AAAAAA - I BBBBBBB -

2.2.3 Thermoplastic polymer matrix

Thermoplastics are polymeric materials that are contained of a series of long carbon chain with no covalent bonding between the individual molecules. Behaviour at room temperature, showed the material behaves as a solid due to the entanglement of the very long molecules; however, when under heat and pressure the individual carbon chains are able to slip relative to one another and the polymer can be deployed into a new shape. Upon cooling period, relative movement of the chains is again restricted and the polymer retains its new shape. When the heating process occurs continuously, shaping and cooling can be provided permanently so that thermal decomposition does not occur.

The common examples of thermoplastic materials include polystyrene, polyethylene, and nylon. Poly (ethylene terephthalate) with clear colour physical properties which is also known as PET is the well-known thermoplastic typically made for soft-drink bottles. From the point of view of the use of matrix composites, thermoplastics commonly used include polyphenylene sulfide (PPS), polyether ether ketone (PEEK), polyether imide (PEI) and polyamide imide (PAI).

Although there has been a significant amount of research was increased particularly into thermoplastic composites every year but it is always being used with unlimited volumes. The primary driver for such work has been the perceived benefits in respect to damage tolerance. Clements (1995) has found that the impact resistance of thermoplastics is potentially far superior to that of thermoset polymers. Juska and Pucket (1997) also found that the high strain to failure characteristics of these materials tend to improved material toughness and improved delamination resistance of resulting composites.

However, these materials have lacking from several processing and performance drawbacks. Processing of thermoplastics requires relatively high temperatures and thus significant energy input. Compounding this, most thermoplastics display low thermal conductivity for conductor behaviour, about 10^{-3} times that of metals (Challa, 1993), and this can have a significant impact on processing times. Clements (1995) also found that the processing temperatures of thermoplastics are normally near the

decomposition temperature and effect in temperature levels or processing times can lead to degradation of the matrix. In addition, thermoplastics also present processing difficulties due to their high viscosity, even at elevated temperatures. Therefore, this creates problems in achieving satisfactory wetting of continuous fibre reinforcements (Mallick, 1997).

In term of performance, thermoplastic composites typically have poor compression performance and this has been attributed to the low modulus found with most neat thermoplastics (Juska and Puckett, 1997). Thermoplastics also display poorer solvent resistance than thermosets; however, they neither absorb nor degrade in water (Clements, 1995). From the perspective of structural engineering, thermoplastic matrix materials will at this time find little application in primary structural composites. Hence, they will be impractical on economic grounds due to high processing and material costs. Usage of these materials will likely be limited to non-structural components utilising short fibre reinforcements. While all these factors are considered, as their application potential is limited, the thermoplastic matrix materials will not be discussed further in this dissertation.

2.2.4 Thermoset polymer matrix

Thermosetting polymers are materials where reactive, low molecular weight compounds are cross-linked via covalent bonds to form a single three-dimensional polymeric network for monomer Bisphenol – A (see Figure 2.5). Upon curing, these materials essentially form one giant network molecule. Unlike thermoplastic polymers, thermosets cannot be reshaped under the application of heat as this would require relative sliding of the initial chains and hence breaking of the covalent cross-links. Heating of the material can in fact have the opposite effect in so far as it can promote further cross-linking of the material and hence can result in a more rigid material.

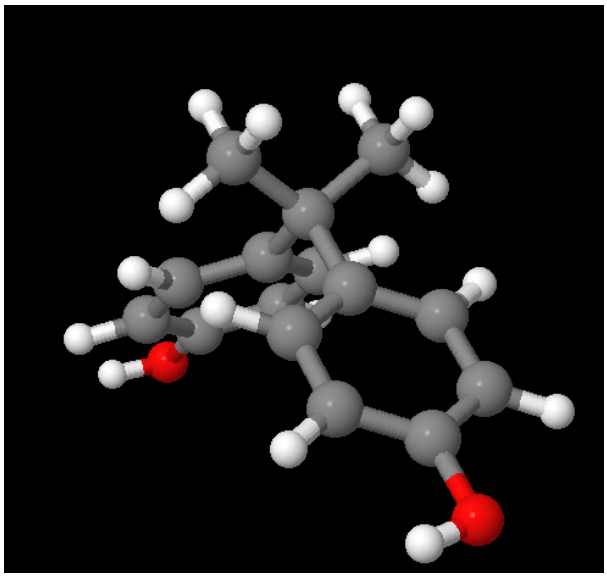

Figure 2.5: 3D Monomer bisphenol-A illustrated using JSmol (Mathias, 2016)

Many of the thermoset polymers used as matrix materials in composites are supplied in the form of liquid pre-polymer, commonly known as a resin. Resins are generally low viscosity liquids which contain low molecular weight polymer species. These molecules are then chemically cross-linked during fabrication processes to form the final thermoset network. Thermoset polymers offer some significant advantages over thermoplastics in terms of their use as composite matrices. Unlike thermoplastics which need to be heated to relatively high temperatures, many of the thermosets used for composite matrices can be formulated for processing at ambient temperatures. Most can also be processed without the use of high pressure. This leads to significant simplification of production and opens the door to a wide range of fabrication techniques. The low viscosity nature of the resins also provides significantly easier impregnation and without fibre reinforcements. Impregnation can be undertaken prior to the curing reaction and upon curing, the continuous thermoset network totally encompasses the fibres. The formation of cross-links in a thermoset network typically results in a stiffer and stronger matrix than that of a thermoplastic. However, thermosets generally tend to have lower elongations and toughness than thermoplastics. Thermosets also display good resistance to a wide array of chemical environments including acids, bases and solvents.

Thermoset polymers are by far the most widely used form of polymeric matrix materials in continuous fibre composites. Common examples include polyesters and vinyl ester, epoxies, phenolic and polyurethanes. Thermoset foam such as cellular cellulose acetate (CCA), polystyrene and polyurethane are very light and resist water, fungi and decay. These materials have very low mechanical properties and polystyrene will be attacked by polyester resin. These foams will not conform to complex curves. Use is generally limited to buoyancy rather than structural applications (Eric, 1999). Polyurethane is often foamed in place when used as a buoyancy material.

Thermoset polymers such as epoxy and phenolic resins, polyimides, polyurethanes, silicones and others are often used as binder for syntactic foams. Various forms of epoxy resins are found to be used as binder in many studies (Rizzi et al., 2000, Kim and Plubrai, 2004, Kim and Oh, 2000, Kim et al., 2001, Wouterson et al., 2004, Wouterson et al., 2005, Narkis et al., 1982, Gupta et al., 2002a, Karthikeyan et al., 2004, Bunn and Mottram, 1993, Gupta et al., 2004). Narkis et al., (1980; 1982) used polyimide and silicone Kenig et al., (1984) powder resins as binders of syntactic foams. Lawrence et al., (2001) and Lawrence & Pyrz (2001) used a low density polyethylene powder as binder. An extensive variety of polymer, metal and ceramic matrix syntactic foam has been studied in previously published literature (Salleh et al., 2014). In polymer matrix syntactic foams, epoxy resins are most commonly used as matrix resin, due to the widespread use of these resins in aerospace applications (Rittel, 2005, Gupta et al., 1999, Karthikeyan et al., 2004, Karthikeyan et al., 2005, Wouterson et al., 2004, Wouterson et al., 2005, Kishore et al., 2005, M. Koopman et al., 2006, Bardella et al., 2003, Gladysz et al., 2006). Studies on epoxy matrix syntactic foams have produced a better understanding of correlations between properties of a composite and properties of matrix and microballoons, including their volume fractions and microballoon wall thickness (Kishore et al., 2005, Gupta et al., 2004). However, in recent years, the increasing price of epoxy resin has required finding lower cost alternatives, especially for bulk structural applications. Additionally, the performance demands for materials are increasing. The demand for applications of syntactic foam in the marine industry is growing every year, particularly in oil and gas, while the market is expected to reach US$115 billion by the year 2020 (Muller, 2014), as shown in Figure 2.6.

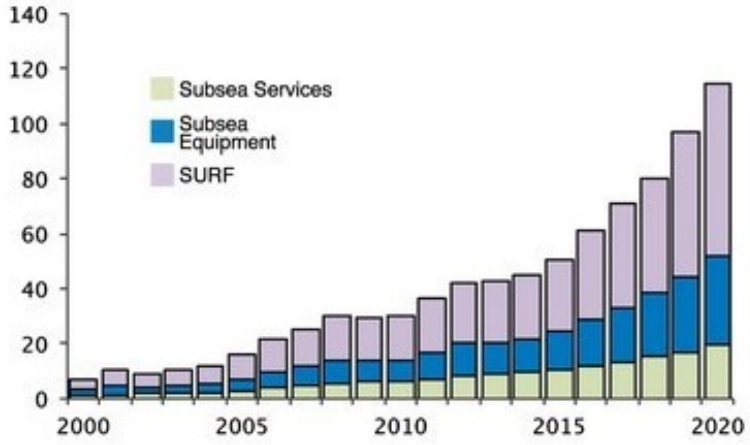

Figure 2.6: Global subsea expenditure ($ billions USD) by market segment (Muller, 2014)

Hence, the development activity is expected to fluctuate every year, and is mainly used in SURF (subsea installation, umbilicals-end product for syntactic foam, risers, and flow lines) and subsea equipment (trees, wellheads, manifolds, etc.). Thus, alternative new matrix materials need to have a lower cost along with higher performance levels. Suitable polymeric material for the foam matrix can be selected from a vast range of thermosetting resins and thermoplastic resins, such as cyanate ester (John et al., 2007), polypropylene (Mae et al., 2007), polysialate (Papakonstantinou et al., 2007), and vinyl ester (Ray and Gnanamoorthy, 2007, Ray et al., 2006), as matrix materials for either cost reduction or for enhanced performance levels. In several cases, additional reinforcement, in the form of fibres for example, can also be added to syntactic foam to obtain certain desired properties (Gupta et al., 1999, Karthikeyan et al., 2001).

2.2.5 Vinyl ester matrix binder

Epoxy resins are typically regarded as covering the high end of the polymer matrix performance spectrum and polyester as covering the lower end, while vinyl ester resins very much hold the middle ground. Originally released unto the market in the mid-1960s, these materials offer a number of the superior performance properties of epoxies in combination with the processing flexibility of polyesters. Vinyl ester resins have been found to offer exceptional chemical resistance characteristics and have been the matrix material of choice in harsh chemical environments for over thirty years. Many such applications are detailed in the literature. Polymeric resin, in the form of for example vinyl esters, is widely used in marine structural applications. Hence, investigating the properties of vinyl ester matrix syntactic foam and developing

structure-property correlations for these materials represent important challenges. The existing studies on vinyl ester syntactic foam have used fly ash ceosphere as the hollow particles (Ray and Gnanamoorthy, 2007, Ray et al., 2006, Gupta et al., 1999).

2.2.6 Chemistry background for DGEBA

The diglycidyl ether of bisphenol A (DGEBA) epoxy which is formed by the reaction of bisphenol A and epichlorohydrin which is consider as epoxide type. It is also known as bisphenol A epoxy, this substance accounts for some 85% of the world's epoxide production (Ayers, 2001). Carbon reaction chain pure bisphenol A epoxides (see Figure 2.7) have a relatively low viscosity; however, due to their high purity these substances tend to crystallise at unlimited time. Therefore, a portion of the epoxide is partially made to react to include an additional bisphenol A and epichlorohydrin chain to join the group (see Figure 2.8). Long carbon chains act as impurities in the system and prevent the onset of the crystallization process.

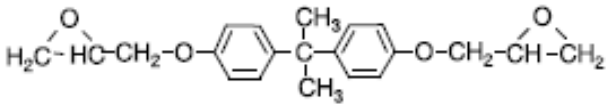

Figure 2.7: Formation of DGEBA for molecule reacted n = 0 (Altuna et al., 2010)

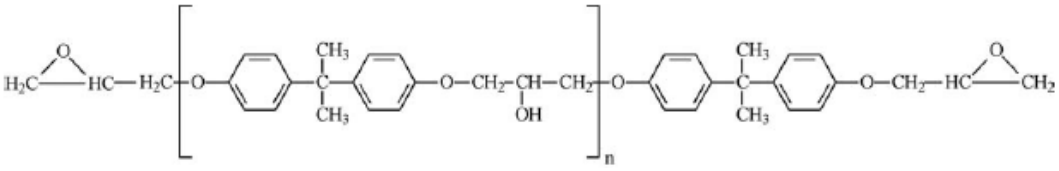

Figure 2.8: Formation of DGEBA for molecule reacted n = 1 (Ratna, 2001)

2.2.7 Chemistry background for vinyl ester

Vinyl ester resins can be formed by the reaction of epoxy resins with acrylic or methacrylic acid. As a result, polymer chain contains terminal unsaturation points, which are capable of cross linking with an unsaturated monomer such as styrene gas. Generally, vinyl ester resin can be formed between the reaction of a DGEBA epoxide

with methacrylic acid (see Figure 2.9). Appropriate levels of unsaturated monomer and polymerisation inhibitors are added to the vinyl ester during or after the esterification process.

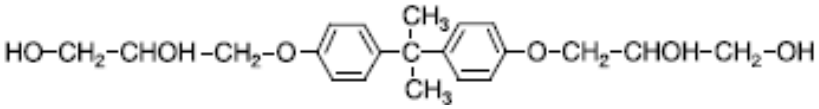

Figure 2.9: Formation of DGEBA base vinyl ester resin

The production of vinyl ester has the advantage that esterification does not produce by-products for example the water produced in polyester production. Therefore, it is considered as minimised the processing job and not much equipment is required. Vinyl esters offer a significant degree of formulation flexibility based on the epoxide backbone used. Other epoxide types such as phenol-novolacs can be successfully substituted for the DGEBA epoxide. Zaske and Goodman (1998) have also noted that alterations in the molecular weight of the epoxide can be used to modify properties of resulting vinyl esters. However, according to Updegraff (1982) the magnitude of these changes is only slight. Substitution of acrylic acid in methacrylic acid can be used to produce vinyl esters particularly for coating applications Huo et al., (2013), while it is also preferred for composites (Zaske and Goodman, 1998). Instantly, a styrene can be formed as gas can be utilised as the unsaturated monomer in vinyl ester resins. However other monomers can also be used to replace part or all of the styrene. One of the company namely as Ashland Chemical Company has recently released a new vinyl ester resin utilising methylmethacrylate monomer to replace a styrene (Adkins and Good, 2001). This is mainly done to eliminate the styrene emission issues normally associated with vinyl ester and polyester resins can be hazardous for human to use it. The resulting product is seen to provide higher HDT (Heat Distortion Temperature) levels and improved rigidity; however, the drawback can be happen to a significant loss in elongation.

2.2.8 Characteristics of vinyl ester

It is a lot of advantages can be compared between structure of the vinyl ester molecule resin and the polyester systems for example it only contains terminal reaction sites. This results in a cured product with a lower crosslink density than typical polyester systems where reaction sites exist at various points along the polyester chain. As a results it become stronger toughness and higher elongation than standard polyester systems. It has also entire length of the molecule that can be used to elongate under stress and thus absorb thermal and mechanical stress or shock according to (Boon and Palfreyman, 1998). The advantages used of bisphenol A in the resin chain also improves the strength and thermal characteristics of the material for verities of applications (Kirk-Othmer, 1996). Based on Figure 2.7 also showed that DGEBA based vinyl ester molecules only possess two ester linkages per molecule compared with the many linkages found on typical polyester molecules. Hence, it is very useful to apply as materials to resist from the water and chemical attack (Updegraff, 1982). In addition to the low concentration of ester linkages, the nearby methyl groups are quite bulky and provide significant shielding to the ester linkage, further enhancing resistance to environmental attack (Zaske and Goodman, 1998). The presence of hydroxyl groups along the polymer chain provides vinyl esters good combination with fibre particularly during mixing process to produce the fibre composites (Huo et al., 2013). Previous report indicated that the secondary hydroxyl groups on the vinyl ester react with hydroxyl groups on the surface of glass fibres, resulting in good wetting and adhesion characteristics (Boon and Palfreyman, 1998). Despite these beneficial characteristics the structural performance of vinyl ester resins is normally lower than that of a corresponding epoxy resins. It is thought that this may be contributed from using styrene to bridge between molecules rather than the amines normally used in normal epoxy resins. It is also thought that the high consumption of styrene used in vinyl esters may successfully “dilute” the performance characteristics of the epoxide part.

As styrene systems, vinyl esters exhibited similar shrinkage characteristics to polyester resins. Comparison can be made where some texts hold that the shrinkage characteristics of vinyl esters are better than those of polyester resins (Updegraff, 1982). Polymer resins such as vinyl esters are widely used in marine structures as an

excellent permeation barrier to resist blistering in marine laminates. Some advantages of the vinyl esters, which may justify their higher cost, include superior corrosion resistance, hydrolytic stability, and excellent physical properties such as impact and fatigue resistance (Gupta et al., 2010). Vinyl ester resins are also widely used as thermoset matrices to fabricate a variety of reinforced structures including pipes, tanks, scrubber and ducts (Sultaniaa et al., 2010). In addition to these applications, vinyl esters are also being used in coatings, adhesives, moulding compounds, structural laminates, electrical applications, etc. Vinyl ester resins combine the best properties of epoxies and unsaturated polyesters. Vinyl ester resins based on epoxy novolac are used for chemical storage tanks, pipes and ducting, fume extraction systems and gas cleaning units, as this particular resin shows superior chemical resistance at high temperatures (Dwivedi et al., 2003). They have high tensile elongation along with better corrosion resistance, which makes them promising material for producing lining coating with outstanding adhesion to other types of plastics and conventional materials such as steel and concrete. Vinyl ester resins also find a variety of applications in optical fibre coating, topcoats for containers, as well as printed circuit boards. Hence, investigating the properties of vinyl ester matrix syntactic foams and developing structure-property correlations for these materials represent important challenges in this study.

2.2.9 MEKP hardener

Organic peroxides are the most common types of initiators used to cure unsaturated polyester resins. For room temperature cure applications, methyl ethyl ketone peroxides (MEKP) are the most common used in composite fabrication. Generally, most of common misconception always occurred within the composites marketplace where all MEKPs are essentially the same. However, it is important to note that there are many differences among the various grades. The common commercial MEKP grades in the market do not normally consist of a single type of peroxide. They are most commonly blended from MEKP-2, MEKP-3 and hydrogen peroxide. The relative proportions of each component have a significant effect on the handling, reactivity and cure characteristics of a particular MEKP grade. In commercial types also contain other components such as residual water from reaction and a non-reactive agent to

reduce reactivity. Figure 2.10 show the formation of MEKP molecules chemical bonding.

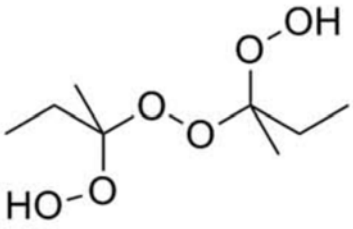

Figure 2.10: Formation of methyl ethyl ketone peroxides (MEKP) (Qian et al., 2014)

Even though these components can be used to significantly reduce the cost of manufacturing process but they typically have a negative effect on reaction and cure characteristics. These materials will be costly; however, a structure can be seriously degraded through attempts to save small amounts of money by using low grade initiators. In order to secure the reactivity during transport and handling, MEKPs are also blended with an agent (diluent). MEKPs are extremely volatile chemicals and easy to explosive decomposition if handled incorrectly. For the safe purpose, products are only permitted to have an active oxygen content of 10% before they are classified as explosive hazards. Chemical agents used to dilute the peroxide tends to act as a plasticizer in the cured resin that reacted in a very short time. Excessively high peroxide addition levels, can result in degradation of the cured product properties due to high levels of these plasticising compounds. To minimise this problem, an initiator addition level of between 1 and 3% has been found to yield optimum cure characteristics and end properties. However, if levels with under 1% have been found to yield incomplete cure characteristics and end properties due to insufficient radical creation. Another peroxides can be utilised from polyester resins such as benzoyl peroxide (BPO), acetyl acetone (AAP) and cumene hydoperoxide (CHP). BPO is typically used in heated processing operations as its reactivity is normally low at room temperature. Precaution need to be taken if using BPO as some grades may resulting in high exothermic temperatures. AAP grades are often used in applications that required in high reactivity and fast processing such as marine and automotive applications which is required dry condition (Hiel et al., 1993, Ishai et al., 1995). CHP grades are used in instances where slower reactivity and lower exothermic temperatures are desired such as aerospace application (Yung et al., 2009).

Free radical addition reaction are commonly used to cure the vinyl ester in polyester resin systems (Marsh, 2007). The combination of vinyl ester and styrene molecules in this reaction to form the final cured network including MEKP/cobalt and BPO/DMA (dimethylaniline). Same as polyester resins, curing systems for vinyl esters employ a combination of initiators, accelerators, promoters and inhibitors, and like polyesters, it is essential that the appropriate components and quantities are selected to ensure full cure of the resin. Therefore, in selecting curing system components for vinyl esters there are a number of differences from polyester systems, which must be understood and accommodated. The most common curing system selected for vinyl ester resins is that of an MEKP initiator, in combination with a cobalt accelerator, and possibly a DMA promoter. In utilising such of the system for vinyl ester, precaution should be taken as to the MEKP grade selected. As noted previously, most of commercial MEKP products contain with an amount of hydrogen peroxide. Therefore, it is an extremely reactive peroxide and in polyesters it provides an initial rapid production of free radicals to initiate the cure process. However, in vinyl ester systems the hydrogen peroxide reacts with the secondary hydroxyl groups on the vinyl ester chain, to form O_2 in the form of bubbles within the resin. Depending on the amount of hydrogen peroxide within the initiator, the creation of small bubbles or called as ("fizzing") within the resin can be quite significant (Davey, 2004).

Many of these bubbles can be trapped within the resin during curing process while to eliminate these problems only grades specifically designated for use with vinyl ester resins should be used. Hence, it was containing with very small residual quantities of hydrogen peroxide to reduce the "fizzing" phenomenon. It can be occurred in thin laminates where the small quantity of bubbles created can migrate out of the part. However, in thick sections and castings, this migration may not occur before gelation, thus trapping the bubbles in the part. In such instances alternative initiator types may have to be adopted. While for CHP based initiators do not contain any hydrogen peroxide and thus do not create problems with oxygen formation. It is also providing lower exothermal temperatures and thus may be preferred for thick sections where temperature build-up is a problem. However, there is drawback with CHP-based systems is that they are less reactive than MEKP systems and thus it is necessary to employ higher levels of accelerators (normally cobalt complexes) and promoters (typically DMA) to achieve rapid curing. There are possibilities to achieve very rapid

curing with CHP initiators if the other curing system components are correctly chosen. Again same as polyesters, vinyl esters will normally require an elevated post-cure temperature to achieve full curing then if post-cure temperatures in excess of 80^{o}C, there is extended reasonable time are recommended to achieve this mission.

2.3 Fabrication of syntactic foam

The variety of fabrication techniques of syntactic foam are discussed below:

2.3.1 Syntactic foam fabrication

A wide variety of syntactic foams can be fabricated by selecting various materials and manufacturing techniques for binder and microballoons, as briefly discussed in Chapter 1. A more detailed discussion on different syntactic foam fabrication techniques is provided below:

2.3.2 Coating technique

Narkis et al., (1982) used VT silica glass microballoons, Scotchcast 256 solid epoxy resin, and Kerimide 601 polyimide for the fabrication of syntactic foams through a coating process. The coating process consists of three steps including resin coating, vacuum filtration, and then polymer precipitation. During resin coating, a thin film of the polymer would lead to undesired agglomeration. Therefore, the slurry is vacuum-filtered and rinsed on the filter. After the vacuum drying of the coated spheres, a moulding powder of the discrete particles is obtained. A predetermined amount of dry coated microballoons is charged into a mould and pressed to the desired volume, and then cured.

2.3.3 Rotational moulding

Rotational moulding was used for producing thermosetting three-phase syntactic foam. The rotational moulding technique is a slow shaping operation using slowly rotating moulds, usually at an atmospheric pressure and with external heat sources. The heat supply from the hot walls to the rotating material can be employed for polymerisation (nylon), melting (thermoplastic), cross-linking (polyesters and cross-linkable polyethylenes), and forming (blowing).

2.3.4 Extrusion technique

For the fabrication of syntactic foams with an extrusion process, Lawrence and Pyrz (2001) and Lawrence et al., (2001) used a low density polyethylene (PE), MP-650-35 as matrix, which is polymer powder with a melting point of 102-104^{o}C. The microballoons were expanded with a grade of 461-20. They had a particle size range of 6-9 μm before expansion and a starting temperature range of 98-104^{o}C for expansion. Syntactic foams comprising PE powder and 5% (by weight) of the microballoons were produced on a laboratory-scale extruder where the material passed through the heated zone in less than one minute. The temperature of the two heating bands was set to 170^{o}C and the temperature of the nozzle to 120^{o}C.

2.3.5 Pressure infiltration

The fabrication of syntactic foams by infiltrating the loose beds of hollow fly ash particles (called *cenospheres*) with an A356 alloy (aluminium alloy) melted was introduced by Rohatgi et al., (2006). The pressure infiltration equipment consisted of a stainless steel chamber, which contained a resistance heater. Inside the chamber was a graphite-coated crucible that rested on a refractory base. A356 alloys were placed in this crucible and melted; the temperature of the melt was raised to either 720 or 800^{o}C according to the desired processing conditions. The preheated borosilicate tubes, containing packed cenospheres, were attached to the heated lid through a Swaglock compression fitting, and the lid was placed onto the heater. Then the lid was held in place through a customised locking system. Once the system was sealed, the pressure was applied to the chamber using nitrogen gas to achieve a pre-determined value and maintained at this level for 2 minutes. The pressure caused the pressure to be released and the composite was removed.

2.3.6 Firing technique

In the fabrication process by firing method, the glass microballoons are bonded using an inorganic binder solution of $Al(H_2PO_4)_3$ and mono-aluminium phosphate (MAP) in water (Verweiji et al., 1985). If a MAP solution is heated, it loses water and a number of complex hydrates are formed. These hydrates decompose to an amorphous substance with formula $Al_2O_3.3P_2O_5$ at temperatures above 300^{o}C. Glass microballoons / MAP slurries are moulded and vacuum-filtrated, and dried at 50-90^{o}C,

and then heated for 24 hours at 230ºC. At this temperature, polymethyl methacrylate (PMMA) spheres depolymerise and evaporate, leaving spherical intergranular cavities in the microballoon compacts. Syntactic foams are made by firing for 3 hours at 600ºC.

2.3.7 Stir mixing technique

The stir mixing or compaction technique has been used by (Kim and Oh, 2000, Kim et al., 2001, Kim and Plubrai, 2004), and (Wouterson et al., 2004, Wouterson et al., 2005) for fabrication of syntactic foams. Generally, hollow microballoons and epoxy resin were used as filler and matrix, respectively. Hollow microballoons were progressively added to the resin system while stirring the mixture gently. The mixture was charged into a mould and then it was compacted under pressure. The moulds could be made from steel, aluminium, copper and plastic PVC materials. Aluminium mould could also be used with a rectangular parallelepiped cavity size of 190 x 230 x 16 mm for flexural, fracture and impact test performance (John et al., 2007). A cylindrical tube shape mould with an inside diameter of 16 and 5 mm in wall thickness could also be used and then cut to a length of 30 mm (Islam and Kim, 2007). The conventional mixer, which uses a glass rod, is commonly used nowadays, but the stir mixer machine using a stir magnetic bar as a mixer yields a better performance, or else the ultrasonic machine could be used. The mixture can also be manually shaken for gelatinising the starch as microballoons in a container (Islam and Kim, 2007). The conventional method needs to be followed carefully to avoid the breakage of microballoons (Tien et al., 2009). This synthesis method consists of mixing measured quantities of glass microballoons in the epoxy resin and mixing them until a slurry of uniform viscosity is obtained.

In this study, this method is selected because it is common to control the quality of the specimens. The fabrication of syntactic foams can be done by preparing the moulds for each type of testing sample. Basically, the type of sample, such as rectangular and cylindrical, has been chosen by many researchers due to better results in compressive, tensile and flexural test performances, and also in line with test standards. Table 2.4 summarises the different types of mould shapes for syntactic foam that have been used in previous work.

The moulds can be made from steel, aluminium, copper and plastic PVC materials. An aluminium mould can also be used with a rectangular parallelepiped cavity size of 190 x 230 x 16 mm for flexural, tensile and impact test performance (John et al., 2007). A cylindrical tube shape mould with an inside diameter of 16 and 5 mm in wall thickness can also be used and then cut to a length of 30 mm (Islam and Kim, 2007). Cylindrical tubes are used for compression moulds, while tray and slab rectangular types are used for flexural moulds.

Table 2.4. Summary of mechanical testing for syntactic foam.

Shape	Test Method	ASTM Standard	Size (mm^3)	Testing Machine	Reference
Rectangular	Tensile	D-3039	5 x 13 x 69	Universal Testing Machine (Instron 4202)	(John et al., 2007)
	Flexural	D-790	5 x 13 x 100		
	Compression	D-695	12 x 12 x24		
Rectangular	Compression	C-365-94	25 x 25 x 12.5	-	(Kim et al., 2001)
Cylindrical	Compression	D 695 M-91	30 x 75	MTS 329.10S	(Rizzi et al., 2000)
	Tensile	D 638	14 x 75		
	Three Point Bending	E 399	14 x 60	Instron 8652	
Cylindrical	Compression	-	10 x 10	-	(Kim et al., 2001)
Cylindrical	Compression	D 5045-91a	12 x 15	Shimadzu 5000	(Shao and Yan, 2011)
Rectangular	Flexural	D 790M-92	125 x 10 x 6		

First of all, the moulds must be cleaned using acetone and the surface must have been coated with mould wax to ensure that the syntactic foams can be removed easily without sticking. The commonly used mould releasing agent is a silicone gel, especially for the stainless steel mould type (Gupta and Woldesenbet, 2003). Stir mixing is the famous method to fabricate syntactic foam. The conventional mixer, using a glass rod, is commonly used nowadays, but the stir mixer machine, using a stir magnetic bar as a mixer, is a better performer, or else the ultrasonic machine can be used. The mixture can also be manually shaken to gelatinise the starch and microballoons in a container (Islam and Kim, 2007). A conventional method needs to be followed carefully to avoid the breakage of microballoons (Lin et al., 2008). This synthesis method consists of mixing measured quantities of glass microballoons in the epoxy resin and mixing them until a slurry of uniform viscosity is obtained. The

hardener is mixed before mixing with glass microballoons, and the diluent is mixed and heated at 50ºC to decrease the viscosity of the resin system (Gupta et al., 1999). Another study for this method also found that the diluent, resin and hardener can be mixed together to decrease the viscosity (Cotgreave and Shortall, 1978). The mixing time is between 4 to 5 minutes approximately. Then, the required amount of microballoons, depending on the volume percentage, is weighed separately and added slowly to the resin mixture.

Since the microballoons are less dense compared to the resin, they have a tendency to float on the top surface slurry. Stirring time is longer for a lower volume percentage (for example 10, 20 and 30) of microballoons to ensure uniform distribution of glass microballoons in the resin. As the amount of the hollow spheres increases, the viscosity also increases and the mixture has a putty-like consistency. The mixture is then transferred to a stainless steel mould, which is smeared with silicone gel (mould releasing agent). The sample, along with the mould, is allowed to cure for 24 hours at room temperature and then removed from the mould. To ensure complete curing, the sample is then post-cured at 60 - 80ºC for 4 hours in a hot air oven.

The quantity of fabrication samples depends on the mechanical testing for each study in syntactic foams. Many research shows that mechanical testing, particularly of compression samples, are the dominant way to fabricate because the results will show the effect of density and wall thickness of glass microballoons (Cotgreave and Shortall, 1978).

2.3.8 Sintering method

Kenig et al., (1984), Kenig et al., (1985), Narkis et al., (1985), Puterman and Narkis (1980), and Meteer and Phillips (1999) used dry resin powder for sintering in fabricating syntactic foam. This invention also have been patented by (Meteer and Philipps, 1999). The powder mixing method was used in their manufacturing processes, where the resin was available in powder form. In general, the measured quantities of solid powder and microballoons were gently mixed in a closed container for a few minutes, until a uniform mixture was achieved. The mixture was poured into a mould, pressed to the desired volume, and then cured.

2.3.9 Stir mixing technique

The fabrication of syntactic foam using stirrer mixing or compaction technique was used by (Kim and Oh, 2000, Kim et al., 2001, Kim and Plubrai, 2004), and (Wouterson et al., 2004, Wouterson et al., 2005). Generally, hollow microballoons and epoxy resin were used as filler and matrix, respectively. Hollow microballoons were progressively added to the resin system while the mixture was stirred gently. The mixture was charged into a mould and then it was compacted under pressure. The moulds could be made from steel, aluminium, copper and plastic PVC materials. The conventional mixer by using the glass rod is commonly used nowadays, but the stir mixer machine using a stir magnetic bar as a mixer creates a better performance or else the ultrasonic machine can be used. The mixture can also be manually shaken to gelatinise the starch as microballoons in a container (Islam and Kim, 2007). A conventional method needs to be followed carefully to avoid the breakage of microballoons (Tien et al., 2009). This synthesis method consists of mixing measured quantities of glass microballoons in the epoxy resin and mixing them until a slurry of uniform viscosity is obtained.

2.3.10 Reaction injection moulding

The reaction moulding (RIM) process is found in the work of (Nijenhuis et al., 1989), and (Methven and Dawson, 1982). Caprolactam is equally placed in two separate glass tubes (A and B) and is heated in a silicone oil bath at a temperature of 135^{o}C. When the caprolactam is molten, a catalyst is added to tube A and an accelerator is added to

tube B. While these additions are molten, heating is continued for another 5-10 minutes. The content of tube B is added to tube A, after adding a desired amount of glass microballoons to tube A, and the mixture is then stirred with a glass rod for about 10 seconds. Then the content of the tube is poured as fast as possible into an upright stainless steel mould, which is preheated for at least 30 minutes in an oven at 145^{o}C. The oven is then closed again and after 5 minutes, the nylon plate filled with microballoons is removed from the mould and allowed to cool in a desiccator.

2.3.11 Buoyancy technique

Fabrication of syntactic foams based on the buoyancy principle is found in the work of (Kim and Oh, 2000, Kim et al., 2001, Kim and Plubrai, 2004). In general, the hollow microballoons are dispersed in aqueous resin in a mixing container as a result of stirring/tumbling, and the container is left until microballoons float to the surface and phase separation happens.

2.4 Mechanical and thermal properties of syntactic foam

A variety of fabrication techniques of syntactic foam for characterising various mechanical and thermal properties are discussed below:

2.4.1 Compressive properties

Compressive failure of syntactic foams has been studied by many researchers. Narkis et al., (1980; 1982) have investigated the compressive properties of three-phase syntactic foam. They found that the failure mechanisms were mainly caused by structure disintegration for the low resin content forms but also by fracture of resin and microballoons for high resin content (Narkis et al., 1982). They also noticed that polyimide foams appeared somewhat stronger than epoxy foams with different weight fractions, but that they had similar strength and moduli when compared to the density composites. In a compressive stress-strain curve for bending dominated structures, the material is elastic linearly up to an elastic limit where cell edges yield, and buckle. The structure continues to collapse at a constant stress until it reaches the densification regime where stress rises steeply (Swetha and Kumar, 2011). The compression graph for syntactic foam consists of three regions: (i) a linear elastic region, (ii) a plateau

region and (iii) a densification region. Figure 2.11 shows the explanation of all these regions.

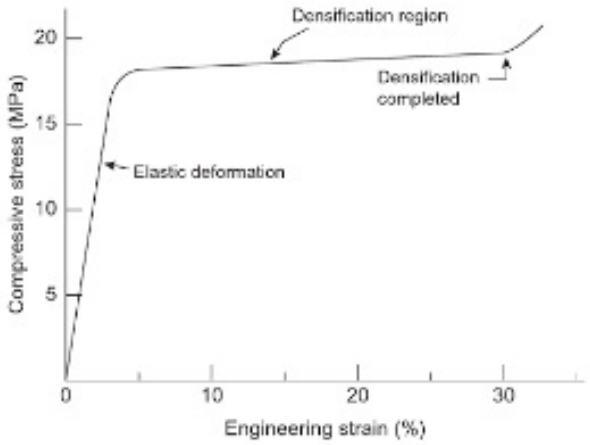

Figure 2.11: Schematic of stress–strain curve for syntactic foams (Swetha and Kumar, 2011)

In the first region, the material is subjected to a uniform deformation and a linear elastic region is observed. Compressive strength of composites is defined as the first peak in the stress-strain curves (Gupta et al., 2010). The plateau region starts after the initial formation of a shear crack, where there is a continued deformation at a constant stress value, which corresponds to the energy absorbed by the material when under compression. This is attributed to the breaking of microspheres, which opens up the enclosed hollow space, providing more space for the compressed material to occupy (Gupta et al., 2006). When significant amounts of microballoons are crushed, the stress level starts to increase again indicating a process of densification and more plastic deformation takes place in the matrix. Rohatgi et al. (2006) found that the compression strength, plateau stress and modulus of composites increased with the composite density. Verweiji et al., (1985) found that the compressive strength of microsphere composites was mainly determined by the intrinsic property of the micoballoons. Gupta et al., (2010) conducted a compression of vinyl ester/glass micoballoons syntactic foam with different densities and found that compressive yield strength, modulus strength, specific compressive and specific modulus decreased with an increase in glass micoballoon content. Similar results have also been found for epoxy/glass microballoons syntactic foam when more glass microballoons were added (Swetha and Kumar, 2011), as shown in Figure 2.12.

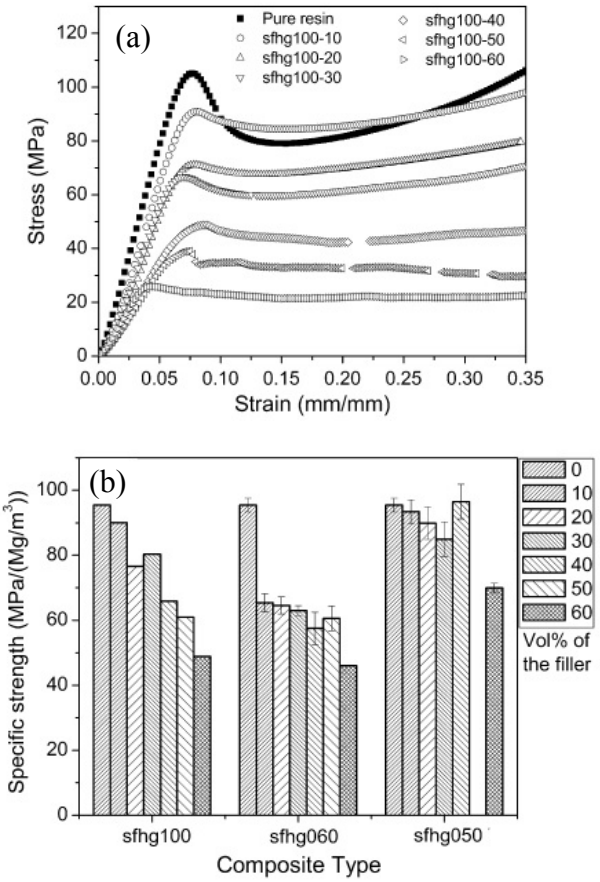

Figure 2.12: (a) Compressive strength (b) Specific compressive strength of glass microspheres/epoxy based syntactic foams (Swetha and Kumar, 2011)

Kim and Plubrai (2004) found that there were two different failure modes of compressive epoxy/glass microballoons syntactic foam, called longitudinal splitting and layered crushing. The effect of the specimen aspect ratio on the stress-strain curve of material is also highlighted by (Gupta et al., 2001, Gupta et al., 2002a, Gupta et al., 2004, Gupta et al., 2010). Investigation into fibre reinforced syntactic foam shows a significant effect on compressive properties, particularly when modulus elasticity was increased with fibre content, due to the influence of both densities and load bearing capacities (Karthikeyan et al., 2004). The behaviour of compressive yield strength and initial tangent modulus of elasticity show that the linearity has a tremendous result, which is dependent on bulk density and volume fraction of glass microballoons (Bunn and Mottram, 1993).

2.4.2 Tensile properties

The tensile properties are very useful, especially for structural syntactic foam of the sandwich type, to characterise their behaviour and failure mode (Caeti et al., 2009). Presently, very few studies are available that deal with the tensile behaviour of syntactic foam (Maharsia and Jerro, 2007). It was concluded by Gupta and Nagony (2006) that tensile strength increased with an increase in microballoon density and decreased with an increase in the volume fraction of microballoons, both having the same density.

An ASTM D 638 standard will be used in this study with the shape of a dog bone, with an appropriate range of relative dimensions. It is easy to grip and has a comfortable workability in a universal testing machine, and axisymmetric bars with tapered cross sections were preferred. Figure 2.13 shows the specimen geometry diagram and the sample specification of the tensile test.

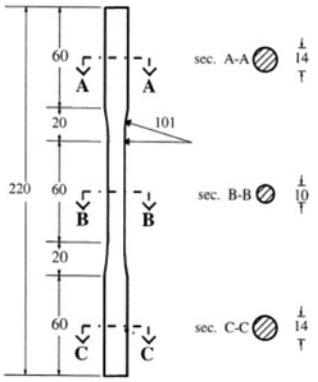

Figure 2.13: A geometry specification for tensile testing (Rizzi et al., 2000)

When the volume fraction of microballoons is increased, it leads to a reduction in tensile strength of syntactic foams. Figure 2.14 shows that the tensile strength decreases when the density of glass microballoons is increased. Further enhancement in tensile strength can be achieved by using high density microballoons; however, this may lead to a reduction in fracture strain and it may damage tolerance properties. Hence, there is a need to determine low cost and efficient methods to increase tensile strength characteristics of syntactic foam without degrading their damage tolerance properties. A report by Maharsia and Jerro (2007) has suggested enhancing the tensile properties in syntactic foam by adding a microstructural modification with nanoclay

particles. Mechanical and thermal properties, particularly tensile strength and tensile modulus of polymers can be enhanced through proper dispersion and exfoliation of nanoclay particles (John et al., 2010).

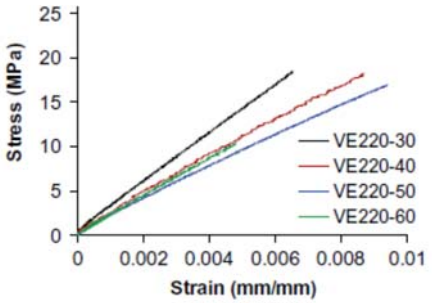

Figure 2.14: Tensile stress-strain curves of vinyl ester syntactic foam (Gupta et al., 2010)

2.4.3 Hygrothermal properties

Moisture absorption is used to identify the sustainability of syntactic foam when different conditions are applied. The ASTM standard that should apply to this test is ASTM D570 or ASTMD 5229-92, or another as specified in the literature. Water absorption has been used to test the final product in marine applications such as the buoyancy effect, which is due to the degradation mechanism of syntactic foam and the combined effect of pressure, temperature and water ingress (Shao and Yan, 2011). Moisture absorption is increased when the void is present, and porosity breakage from glass microballoons in a specific direction occurs (Gupta and Woldesenbet, 2003). Two types of water conditions have been used during this testing: deionised water (D.I. water) and salt water (S.W. water), in two different temperature conditions, room temperature and 70ºC - 80ºC. The unit to determine the water absorption content is in weight percentage (%). Figure 2.15 shows the result of water absorption of three types, and densities of syntactic foam in two water conditions. As can be seen in the graph, both types of syntactic foam where in the equilibrium condition, which was reached in about 1200 hours at high temperatures. Conversely, in line with behaviour at low temperature conditions, moisture absorption reached an equilibrium at 500 hours. At high temperatures, water absorption increased to about 10 times for glass microballoon syntactic foam of 460 kgm^{-3} density specimens, and approximately 5-7 times for density 220 kgm^{-3} type specimens. The strength of syntactic foam was examined after water absorption in these two conditions. Figure 2.16 shows the graph for compression

stress-strain after the hygrothermal test for sample density 220 kgm^{-3}. From the graph, it can be seen that the trends in stress-strain curves were similar in shape to the curves for both dry and moisture absorbed syntactic foam. These materials show trends that are similar to the characteristics of elastic and perfectly plastic materials. After this, the stress characteristic of syntactic foam becomes linearly constant for considerable strain. Even after such a high value of compression, no drop in stress was observed, and stress was observed to be nearly constant in the plastic deformation region, referred to as the plateau region.

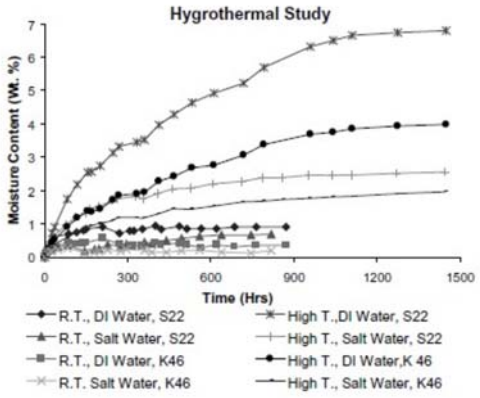

Figure 2.15: Graph of moisture absorption for different water conditions, temperature and density glass microballoons (Gupta and Woldesenbet, 2003)

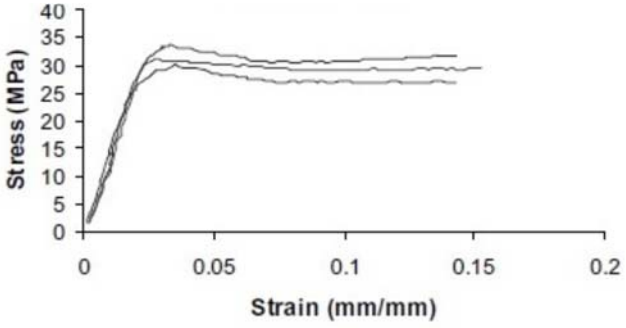

Figure 2.16: Compression stress-strain curve of density 220 kgm^{-3} glass microballoons after hygrothermal condition (Gupta and Woldesenbet, 2003)

2.4.4 Thermal properties

Lightweight structural thermal insulating composites have a limited number of applications in space and deep sea exploration, as well as aerospace, marine, and civil infrastructure. Thus, syntactic foam can be one viable composite solution for structures requiring both enhanced structural and thermal insulation properties. Designing syntactic foam with both high strength and thermal insulating properties is challenging since these two properties are inherently in opposition to one another (Kulesa and Robinson, 2014). Hence, it is evident that the selection of particle, matrix materials and volume fractions of each specimen will impact on the result in desired thermal and mechanical properties. The application to a thermal insulator often focuses on a subject to high temperatures, which leads to interest in thermal properties such as glass transition temperature, T_g using Thermogravimetric Analysis (TGA) testing (Tien et al., 2009), thermal conductivity, λ (Lin et al., 2009), as well as the coefficient of thermal expansion (CTE), α, which is an important design parameter (Vasanth et al., 2012). In Tien et al., (2009) study, the T_g value was decreased when they filled the ceramic phase to fabricate micro- or nano-composites (Tien et al., 2009). In this work, they also found that T_g increases when the volume fraction is increased for epoxy syntactic foam. For the CTE value, it was found that increasing the volume fraction and wall thickness of microballoons could decrease the CTE values.

2.4.5 Stress concentration factor (SCF,K_I)

In order to better understand the fracture and deformation mechanism in syntactic foam, it is imperative to study the micromechanical effects of applied stress in the vicinity of a microballoon. Syntactic foam consists of multi-particle systems, and they involve a large number of parameters which govern their failure mechanism. Therefore, it is very difficult to use a single model to ascertain the behaviour of syntactic foam. Hence, as an initial step, a simple two dimensional model, using the Stress Intensity Factor approach, can be developed to study the loading behaviour of microballoons in a foam matrix. Such a study will help in determining the stress distribution behaviour around a microballoon, and may form the basis for developing future complex models to analyse the behaviour of a multi-particle system involving different types of particles in it. A simple two dimensional model using the Stress Intensity Factor approach is developed in order to study the loading behaviour of microballoons in a foam matrix. It is very interesting to utilise the advantage of low density syntactic foam in marine applications, which has made it necessary to characterise these materials for tensile loading and study various parameters effecting their properties (Gupta and Nagorny, 2006). The existing studies on tensile strength for syntactic foam are very limited, particularly in marine structures where light weight is important to obtain high buoyancy (Bardella and Genna, 2001). Previous reports have also found that tensile strength increases with decreases in glass microballoon content in syntactic foam (Rizzi et al., 2000). Hence, in this study the stress intensity factor K_I, will be calculated from the tensile specimens in order to study the loading behaviour of microballoons in a foam matrix.

The effect of a change in stress intensity factor around a crack or a flaw in a material will be investigated. This flaw shape can be circular, elliptical or randomly shaped, and there are several models available to ascertain the stress intensity factor for different types of flaws (Rizzi et al., 2000), as illustrated in Figure 2.17.

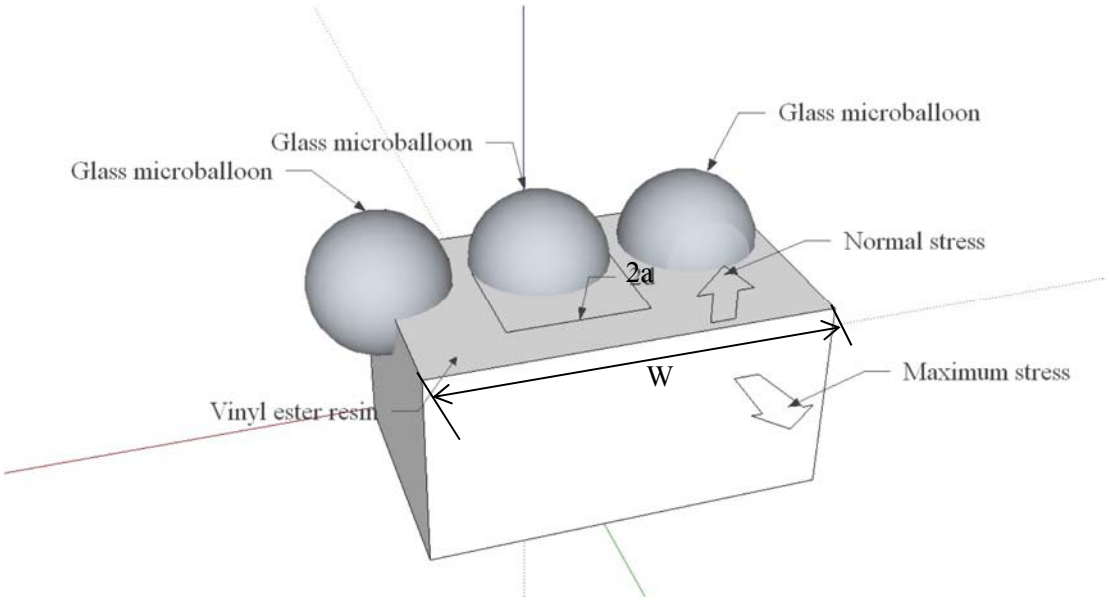

Figure 2.17: Schematic representation of stress distribution around a microballoon (Rizzi et al., 2000)

A microballoon has been considered equivalent to a two-dimensional circular flaw or crack in the system. The particular flaw considered for analysis was a microballoon, therefore the radius of curvature and a half length of the flaw is equal to the microballoon radius. Maximum stress on the surface of the flaw was given by Equation 2.8 below, where 'a' is half length of flaw, ρ_t is the radius of curvature of the flaw and sigma normal is the applied/nominal stress. The ratio of σ_{max} and σ_{norm} gives 'K' as a stress factor value in the Equation 2.9.

$$\sigma_{max} = \sigma_{max}\left[1 + 2\left[\frac{a}{\rho_t}\right]^{\frac{1}{2}}\right] \tag{2.8}$$

$$K = \frac{\sigma_{max}}{\sigma_{norm}}\left[1 + 2\left[\frac{a}{\rho_t}\right]^{\frac{1}{2}}\right] \tag{2.9}$$

Thus, it can be seen that the applied stress is amplified three times on the surface of a microballoon as compared to the nominal stress in the surrounding matrix in which K = 3 at Equation 2.10.

$$\sigma_{max} = \quad 3[\sigma_{norm}] \tag{2.10}$$

$$K = 3 \tag{2.11}$$

The characterisation of the stress concentration around the microballoon can be determined by using the stress intensity factor, K_I. Components to describe the stress elements for the x-component and y-component were stated at below equations:

$$\sigma_x = \frac{K_I}{\sqrt{2\pi d}}\left[cos\frac{\delta}{2}\left[1 - sin\frac{\delta}{2}sin\frac{3\delta}{2}\right]\right] \quad (2.12)$$

$$\sigma_y = \frac{K_I}{\sqrt{2\pi d}}\left[cos\frac{\delta}{2}\left[1 + sin\frac{\delta}{2}sin\frac{3\delta}{2}\right]\right] \quad (2.13)$$

Thus tensile component x-y can be written as Equation 2.14;

$$\tau_{xy} = \frac{K_I}{\sqrt{2\pi d}}\left[sin\frac{\delta}{2}cos\frac{\delta}{2}cos\frac{3\delta}{2}\right] \quad (2.14)$$

where, 'K_I ' in the above equation is the stress intensity factor, which gives the stress distribution around a microballoon, a is the distance between microballoon surface and the point element considered, and δ is the angle made by the line joining the point element and the microballoon surface. Since the plane x-y are considered, therefore $\delta_z = 0$ and the stress intensity factor can be determined as;

$$K_I = \chi \times \sigma \times \sqrt{\pi a} \quad (2.15)$$

$$\chi = \sqrt{\left(\frac{W}{\pi a} \times tan\left(\frac{\pi a}{W}\right)\right)} \quad (2.16)$$

where, χ is a parameter depending on the microballoon and specimen sizes (a, W) and geometries, and the manner of load application, and has units of MPa $(m)^{1/2}$, while σ is applied load. The crack formation and stresses on an element in the vicinity of a microballoon are σ_x, σ_{norm}, σ_y. At a critical value of the stress intensity factor K_I, known as the fracture toughness, fracture will occur in the material and σ_c is critical stress for crack propagation.

2.5 Summary

The use of glass microballoon as a filler in polymer composites is attracting much interest due to its potential mechanical properties, thermal properties, and processing advantages as core of sandwich panels, which has potential benefits for marine applications. However, the presence of porosity and internal voids occurred in the syntactic foam compatibility with the matrix resin, which results in poor mechanical properties of the composites even though it can be made reliable as low density composites. Therefore, water treatment, such as immersion in different types of water, is also one of the methods needed to apply to this syntactic foam, which is an essential processing method for sustainable use in the marine industry. Significant improvements in the mechanical properties of the composites are reported by using different types of water. The effect of a parametric study into syntactic foam also contributed to enhancements for use in many applications on a long term basis.

In this study, glass microballoons were selected to mix with vinyl ester resin as binder to produce syntactic foam. Widely used water treatments, such as de-ionised and salt water, were chosen to perform the water resistance experimental method as reported on in previous reports. The effect of water treatment on syntactic foam were investigated through a hygrothermal and mechanical property analysis. Their stress concentration near to the small hole was also examined, using a connection with a local strain gage, and drawing a comparison through a Finite Element Analysis (FEA) approach.

Chapter 3

Fabrication and Characterisation of Syntactic Foams and their Constituents

3.1 Introduction

This chapter focuses on the physical, compression and tensile properties as well as the fracture mechanism of glass microballoon/vinyl ester syntactic foams. There are fifteen of coupons that are fabricated using only one type of microballoon in five different weight percentages (wt.%) for both tensile and compression testing. The tensile and compressive properties of these materials are characterized, including modulus of elasticity, strength and fracture features. The effect of the weight percentage and wall thickness of microballoons on the mechanical properties of the composite is very important to be investigated. All the specimens are prepared using the open mould method and are tested using universal testing machine (UTM). In order to characterise the fracture mechanism of syntactic foams, microstructure analysis has been introduced with the use of a scanning electron microscope (SEM).

3.2 Constituent materials for syntactic foams

The vinyl ester resin, also scientifically known as diglicidyl ether of bisphenol A-based resin, with methyl ethyl ketone peroxide (MEKP) as catalyst, was used as the matrix material, and was procured from the Australian company is known as NOROX. The glass microballoons used in this study are non-porous in nature and are manufactured and supplied by Potters Industries Inc. The supplier trades under the name of Q-CEL Spherical (R) Hollow Microspheres. The manufacturing data sheet shows that the physical shape of the glass microballoon is spherical, with glass powder typed with chemically-stable fused-borosilicate glass and a non-porous microsphere (Division, 2011). Figure 3.1(a) shows the scanning electron micrograph of the glass microballoons particles before they were incorporated with matrix resin used in this study. The mean inner diameter was calculated by taking the difference between the

average true particle density of solid and hollow particles made up of the same material. The mean particle size distribution and bulk density of this particle supplied by the manufacturer were given as 72μm (5-150μm) and 110 kgm^{-3}, respectively.

Density of syntactic foam was measured by using gas replacement according to ASTM D2840. The helium gas was supplied from a cylinder tank to the multipycnometer unit (Quantachrome Instrument model). The measurement was set up at a room temperature of 25 ^{o}C. First, the specimens were grinded using a mortar and pestle to create smaller granular pieces. The pieces were then placed into a multipycnometer cup before being placed in the measurement area. Figure 3.1(b) shows the overview of multipycnometer unit used for density measurement.

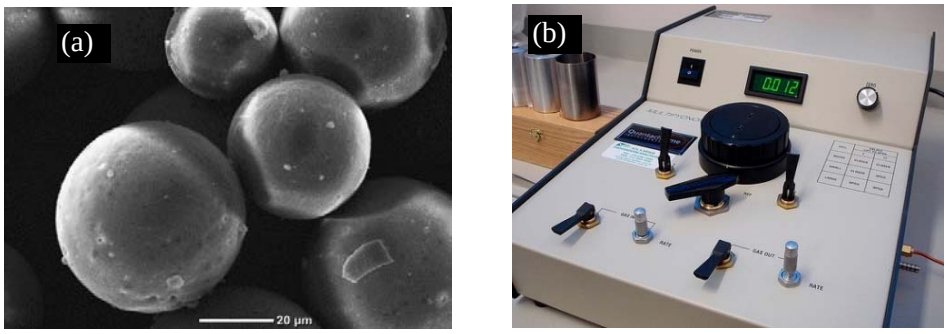

Figure 3.1: (a) A SEM photo for glass microballoon (b) Multipycnometer unit

3.3 Fabrication of syntactic foams

The fabrication of tensile specimens made by steel mould is turned into what is called the shape of a 'dog bone', which has been used in this study. The compression specimens, made with a PVC mould were included with the dimensions diameter, ϕ = 22.0 mm x length, L = 44.0 mm. First, the moulds had to be cleaned by using acetone and the surface had to be coated with mould wax to ensure that the syntactic foams could be removed easily. The commonly used mould releasing agent of a silicone gel type was employed particularly for the stainless steel mould reported by (Gupta et al., 2004).

Stir mixing is a well-known method for fabricating syntactic foams. Mixing with a glass rod is common nowadays, but a mixer machine equipped with a stir magnetic bar as a mixer is better than using the ultrasonic machine for timely manner consuming. The mixture can also be manually shaken to gelatinise the starch and microballoons in a container by (Islam and Kim, 2007). The manual mixing or conventional method needs to be followed carefully to avoid the breakage of microballoons reported by (Tien et al., 2009). This synthesis method consists of mixing measured quantities of glass microballoons in the resin and mixing them until a slurry of uniform viscosity is obtained. The mixing time is approximately between 4 and 5 minutes. Stirring time should be increased for a higher weight percentage of microballoons to ensure uniform distribution of glass microballoons in the resin. As the amount of the glass microballoons increases, the viscosity also increases and the mixtures develops into a putty-like consistency. It is difficult to achieve homogeneity when using the mixer machine.

A putty-like consistency is impossible to stir because it changes into a dough-like consistency and become sticky. Therefore, the selection of composition glass microballoons in weight percentage was also important to ensure that this phenomenon could be avoided during sample preparation. Then, all the mixtures were transferred and cast into moulds for tensile and compressive testing after being waxed with silicone gel (mould releasing agent). The samples along with the mould were allowed to cure for 24 hours at room temperature and then were removed from the moulds. At the final stage of fabrication, all the specimens were post-cured at 60 – 80 ^{o}C for 4 hours in a hot air oven. Steps involved in the processing of syntactic foam are shown in Figure 3.2.

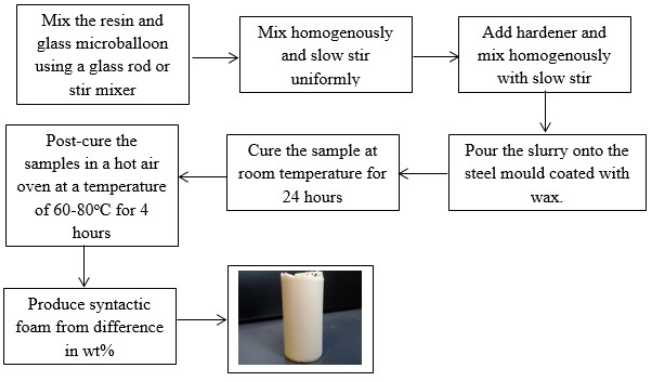

Figure 3.2 : The process flow for the fabrication of syntactic foams by using stir mixing method

3.3.1 Syntactic foam density

Constant temperature was used to determine the densities of syntactic foam by using Boyle's Law where the pressure and volume of the gas are important parameters in ideal gas law (John et al., 2007). According to this law, the pressure of the gas is inversely proportional to the volume of gas, or the multiplication of pressure (P_{gas}) with volume of the gas (V_{gas}) is equal to the constant value. The above parameters can be connected by using R as Boltzmann constant, while T remains constant and n = 1(He gas). This will determine the initial values for the pressure and volume of syntactic foam while the final values are considered as the pressure and volume of the gas. Therefore, it is important to determine the volume of the syntactic foam in order to calculate the density of syntactic foam when mass is divided by their volume itself. To measure the volume fraction for each of the specimens, the rule of mixtures was implemented using Equation (3.1) below,

$$\text{Volume fraction, } Vf = \frac{Wf}{Wf+(1-Wf)\frac{\rho f}{\rho m}} \qquad (3.1)$$

where W_f is weight of filler/glass microballoon, ρf is density of filler/glass microballoon and ρm is density of matrix/vinyl ester resin. Equation (3.1) was very useful for measuring the density of composites particularly for syntactic foam (Islam and Kim, 2007). The compositions of glass microballoons in weight percentage (wt.%) in this study were 2 wt.%, 4 wt.%, 6 wt.%, 8 wt.% and 10 wt.%. The density of syntactic foam was measured, using a crushed microballoons sample in a Quanta-chrome Ultra multipycnometer. The density of syntactic foam affected the mechanical properties, particularly with regards to the porosity content in the syntactic foam, which also needed to be investigated properly in this study.

3.3.2 Syntactic foam porosity

The calculation of the parameters is related to the wall thickness, ω such as radius ratio, η and the volume of porosities as shown below. The ratio of inner, r_i to outer, r_o radius of microballoons, called the radius ratio η, is also reported in Table 3.1. The radius ratio is calculated approximately, based on the standard glass density of 2540 kgm^{-3} or on mean particle density (Tagliavia et al., 2009). The diagram of the outer and inner

radii together with the wall thickness can be seen in Figure 3.3(a). It is clear that if r_o is the same, any difference made in the ρ_{gm} is caused by a difference in η. Two types of porosity occur in syntactic foams: microballoons porosity and matrix porosity (Gupta and Nagorny, 2006). The empty microballoon volume enclosed within the microballoons itself gives the opportunity for the microballoon porosity to rise. The closed cell porosity is required to reduce the density of the syntactic foam material otherwise known as the volume cavity. The contents of matrix porosity of the desired closed cell microballoon in syntactic foams can be defined at Equation (3.2),

$$V_{p,gm} = V_{gm} \times V_{c,gm} \qquad (3.2)$$

where, V_{gm} = volume of glass microballoons in syntactic foam, volume cavity $V_{c,gm}$ = η^3, radius ratio $\eta = \left(1 - \frac{\rho_{sf}}{\rho_{gm}}\right)^{\frac{1}{3}}$, $\eta = 1 - \frac{\omega}{r}$, ρ_{gm} density of glass microballoon, ρ_{sf} density of syntactic foam, ω wall thickness of glass microballoon (Swetha and Kumar, 2011) and r is the average size of the glass microballoons.

The second type of porosity is matrix porosity, which occurs because of the entrapment of air in the syntactic foam structure during the foam synthesis, as shown in Figure 3.32(b). This structure distribution, especially for matrix porosity, relies on the contents of matrix porosity itself. During the mixing of the resin with microballoon, entrapment of air is inevitable, leading to voids in syntactic foams.

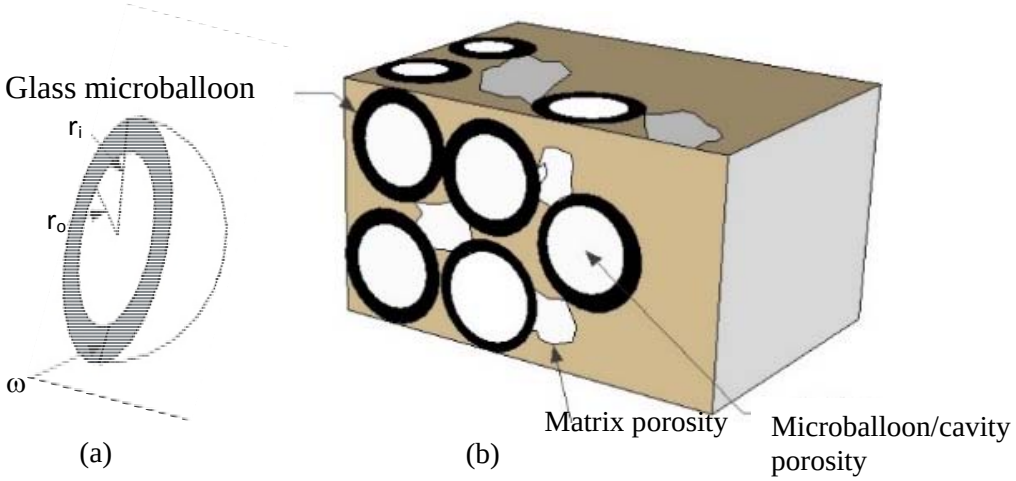

Figure 3.3: Schematic diagram for the structure of (a) Glass microballoon (b) syntactic foam showing microballoons with porosities

The voids may also occur due to non-uniform distribution of resin in the syntactic foam (John et al., 2007). Hence, to calculate the void contents in the syntactic foams, Equation (3.3) is useful to determine this amounts by estimation only.

$$V_{void} = \frac{V_{sf} - \left[W_{sf} \times {}^{W_r}/_{\rho_r} + W_{sf} \times {}^{W_{gm}}/_{\rho_{gm}}\right]}{V_{sf}} \times 100\% \quad (3.3)$$

where V_{sf} and W_{sf} are the volume and weight of syntactic foam; W_r and W_{gm} are the weight of resin and glass microballoon; ρ_r vinyl ester 1161 kgm^{-3} and ρ_{gm} is the standard density of vinyl ester can be used along the calculation when refer the previous report (Tagliavia et al., 2009) and microballoon density respectively.

3.4 Mechanical property testing

Compression testing (ASTM D-695) was performed using MTS test systems with a crosshead speed of 2 mm/min. From the output result, the two parameters of load and crosshead displacement were selected for data analysis and development of stress–strain curves. Figure 3.4(a) shows the photo of one of the specimens during compression testing with the MTS machine.

Tensile testing (ASTM D-638) was carried out using a computer controlled MTS Insight universal testing machine as shown in Figure 3.4(b). At least three specimens of each type of composition of glass microballoon for vinyl ester syntactic foams were tested. Specimens were subjected to tensile loading at a cross speed of 1.25 mm/min. Strain data were measured through an extensometer with a 25 mm gauge length. Load-displacement data obtained from the tests were used to calculate the strength, modulus of elasticity and Poisson's ratio properties of glass microballoon/vinyl ester syntactic foams.

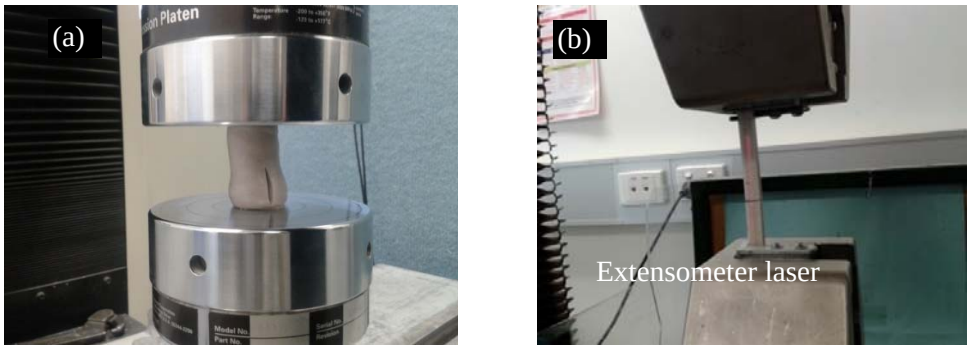

Figure 3.4: (a) MTS Insight compression machine (b) MTS Insight universal tensile machine

The tensile behaviour of the syntactic foam is discussed further in Section 3.5.2. Figure 3.5 shows a typical tensile stress-strain curve for the syntactic foam used in this work. The graph shows that it exhibited linear behaviour, hence for each stress-strain curve, tensile modulus, tensile stress and strain at maximum peak could be determined. The stress-strain curve for compressive testing also is revealed in Figure 3.5. It shows that the trend for mean plateau was observed after achieving the maximum stress for syntactic foam until densification mode was detected. Densification can be described by three important regions of failure. These regions are called region (I)-initial linear deformation, region (II)-plastic mean plateau and region (III)-densification region. The details of these failure modes are also discussed in Section 3.5.2. Basically, syntactic foam is categorised as isotropic or homogeneous materials whose physical properties are similar to a cement or asphalt and easy to break. This characteristic always concerns about the content of glass microballoon which affects the behaviour of syntactic foam.

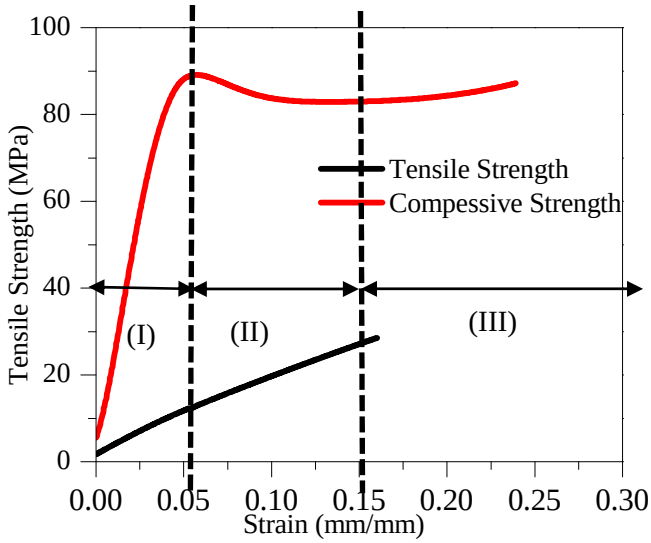

Figure 3.5: Typical curve of a stress–strain for tensile and compression of syntactic foam

3.4.1 Effects of porosity on mechanical properties

Mechanical properties, particularly the compressive behaviour of syntactic foam, can be affected by porosity remaining in the composite materials. During the compression test, a severe shear crack was initiated and had an effect on the glass microballoons and matrix resin. (Gupta et al., 2010) observed that crack formation is increased for a higher volume fraction of glass microballoons due to the brittleness of the composite. As a result, many of the glass microballoons and matrix resin were damaged during the test and they were replaced by each other. For example, resin might be placed inside a broken glass microballoon to develop one of the porosity content. In order to determine the relationship between the mechanical properties and porosity, Phang and Ding (2012) proposed the simple Equation (3.4) below (Phang and Ding, 2012),

$$E_{compressive} = C_1(1-\varphi)^m \quad (3.4)$$

where $E_{compressive}$ is compressive modulus of elasticity, C_1 is constant, $(1-\varphi)$ is relative density, φ is porosity syntactic foam, and m is positive exponential value. This linear equation can be solved by using a logarithm function where m is reacting as the gradient of the graph.

3.5 Results and discussion

3.5.1 Influence of porosity in density properties

The densities of syntactic foams for all specimens are presented in Figure 3.6. From the graph, it can be observed that all the specimens show a decrease in their densities when the glass microballoon content is increased. The data from the graph was calculated by using the rule of mixtures for Equation (3.1). A summary of all specimens is also described in Table 3.1.

All the specimens were as Pure VE, SCFT-01 (2 wt.%), SCFT-02 (4 wt.%), SCFT-03 (6 wt.%), SCFT-04 (8 wt.%) and SCFT-05 (10 wt.%). Generally, the density of syntactic foam becomes lighter when the glass microballoon content in the matrix resin is increased. This did occur due to the glass microballoon filling the gap between the

foam and matrix resin. This shows that the rule of mixtures is supported and followed in this study. From the graph, the specimen SCFT-01 (2 wt.%) with the volume fraction (V_f) 4% has a higher density but it is still lower than pure VE density. The specimen with low density such as 10 wt.% with volume fraction 8 % has low densities in its composition and might be created by voids or porosity in the syntactic foam. In addition, the glass microballoons also contributes to the weight of syntactic foam where the filler percentage is higher than resin. The low density syntactic foam was affected by the influence of porosity and void content. Therefore, the optimum wt.% is difficult to identify but it can be estimated in microlevel using Equations (3.2) and (3.3). Another contribution to this behaviour comes from glass microballoon debris in the matrix resin.

Table 3.1: Physical properties and mechanical properties of syntactic foam.

Specimens	Glass microballoon		Density syntactic foam	Radius ratio	Wall thickness	Cavity porosity	Matrix porosity	Void	Max. Strength (MPa) ±CoV		Modulus of Elasticity (GPa) ±CoV		Specific Max. (MPa/mgm^{-3}) ±CoV		Specific Modulus (GPa/mgm^{-3}) ±CoV	
	(vol.%)	(wt.%)	(kg/m^3)	η	ω (μm)	(%)	(%)	(%)	Tension	Comp.	Tension	Comp.	Tension	Comp.	Tension	Comp.
Pure VE	-	-	1294	-	-	-	-	-	39.28 ±0.03	111.99 ±0.01	10.30 ±0.08	2.25 ±0.03	30.36 ±0.03	86.53 ±0.01	7.96 ±0.08	1.74 ±0.03
SCFT-01	4.01	2.0	1091	0.83	12.23	57.05	1.66	3.02	29.93 ±0.27	89.31 ±0.01	9.72 ±0.02	1.99 ±0.01	27.43 ±0.27	81.86 ±0.01	8.91 ±0.02	1.81 ±0.01
SCFT-02	5.83	4.0	1031	0.79	15.41	48.54	3.14	2.52	22.41 ±0.09	73.80 ±0.01	9.92 ±0.09	1.70 ±0.01	21.73 ±0.10	71.58 ±0.01	9.62 ±0.09	1.81 ±0.01
SCFT-03	6.16	6.0	962	0.85	10.56	62.13	5.12	3.43	23.53 ±0.06	58.84 ±0.06	8.61 ±0.01	1.00 ±0.12	24.46 ±0.06	61.16 ±0.06	8.95 ±0.01	1.65 ±0.01
SCFT-04	7.46	8.0	938	0.86	10.25	63.07	6.94	3.51	22.80 ±0.15	48.31 ±0.1	7.19 ±0.06	0.98 ±0.45	24.30 ±0.15	51.51 ±0.10	7.67 ±0.06	1.04 ±0.12
SCFT-05	7.94	10.0	884	0.87	9.57	65.20	8.58	3.73	23.75 ±0.02	42.59 ±0.02	7.21 ±0.06	0.78 ±0.15	26.87 ±0.03	48.18 ±0.02	8.15 ±0.06	0.88 ±0.15

CoV= Standard deviation divided Mean (σ/μ)

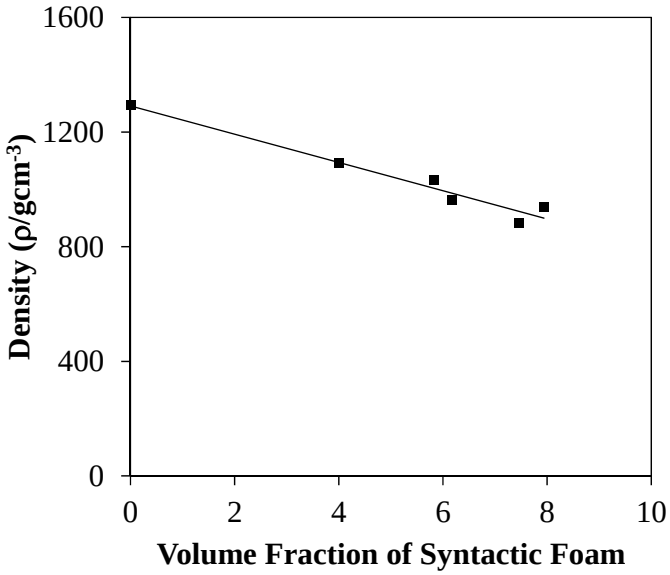

Figure 3.6: Density of syntactic foam as a function of volume fraction of glass microballoon exhibiting a linear trend as per the rule of mixtures

From the graph, the linearity of gradient shows the decreased pattern is considered as particular to the composite materials, where their densities were slightly decreased in order to achieve the low density behaviour. This characteristic was revealed by Swetha and Kumar (2011) in their research in which the density of syntactic foam decreased when the glass microballoon in the epoxy matrix resin increased in three different types of filler. The syntactic foams showed a linear decrease in density with an increase in the weight percentage of glass microballoons as filler incorporated into the vinyl ester resin. This behaviour is also reported elsewhere as the foamy nature of material (Kim and Plubrai, 2004). This result also supports previous reports that showed a trend in decreased density (Bunn and Mottram, 1993, G Subhasha et al., 2006). Therefore, the trend shows that the density of syntactic foam is proportional to the volume fraction of glass microballoon contents and is considered to be evidence proving the rule of mixtures for the composite materials in this study.

The fabrication of syntactic foam in this study has used the open casting method. Hence, the surface of specimens has open bubbles and is rough with an irregular pattern caused by the mixing of glass microballoon/vinyl ester and MEKP dispersed with gas, due to a chemical reaction. This casting method is suitable for the fabrication of syntactic foams used specially to release gas into the air. A similar method was used

in previous work by (Gupta et al., 2010). In order to eliminate the rough surface in the external area of the syntactic foam during the compression testing, the surface must be grinded with a grinder machine to ensure the surface is flat. Surface flatness is necessary, otherwise the mechanism of the compressive will compromise the test process and, as a result, the data will be unsatisfactory.

For the internal area of the syntactic foam, the porosity and voids were randomly distributed across all surfaces. The mechanical properties of syntactic foam can be affected by porosity. Porosity can be identified as one of two types - type I occurs internally in microballoons, while type II is matrix porosity, due to air entrapped in the resin during the fabrication process, as explained in detail elsewhere (Gupta and Ricci, 2006, John et al., 2007, M. Koopman et al., 2006). The voids are considered as one of the type II matrix porosity as mentioned by Gupta et al., (2010). Figure 3.7(a) shows that the total porosity content increased while the glass microballoon content also increased in syntactic foams. The solution for Equation (3.3) provides the positive exponents for both linear graphs. The cavity and matrix porosities meet by crossing with each other at gradient *m*, indicating relative density porosities with 0.88, the details of which are shown in Figure 3.7(b). As a result, it is shown that on average, 12% contains both porosities for all specimens but voids remain in all specimens because it cannot be avoided. Generally, if the specimens have increased the glass microballoon content in syntactic foams, the increased porosity content could affect the mechanical properties.

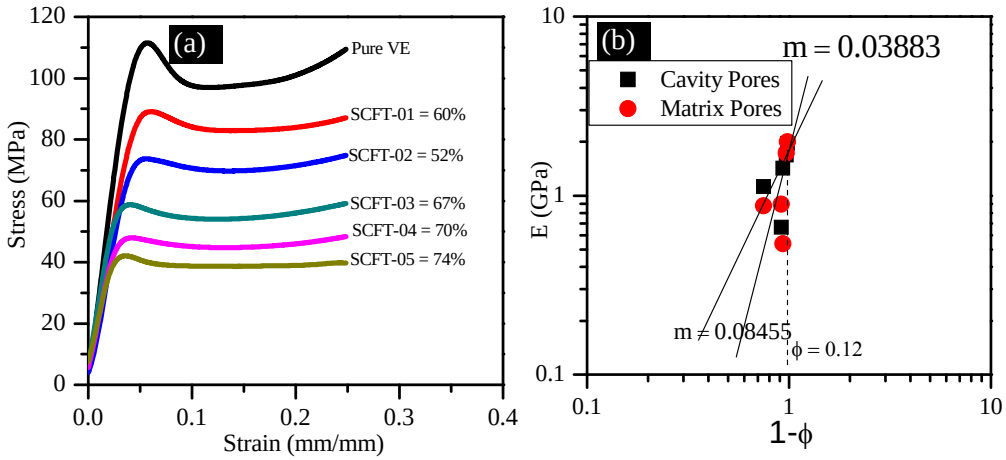

Figure 3.7: Compressive strength related to porosities of syntactic foam a) Total porosity (b) Compressive modulus related to relative density

The particle distribution including their porosities in the vinyl ester/glass microballoon syntactic foams in this study can also be seen by using a SEM machine shown in Figure 3.8(a). Table 3.1 shows the parameters of porosity and voids coexisting in the vinyl ester/glass microballoon syntactic foam, as well as their wall thickness and radius ratio. Generally, the radius ratio and wall thickness are not much different when compared to all specimens. However, both the cavity porosity and matrix porosity have a significant effect on the development of syntactic foams. The specimen for SCFT-01 has less cavity porosity and matrix porosity with 57% and 16%. Even though specimen SCFT-02 has a lower content of cavity porosity, matrix porosity is still high when compared with SCFT-01. The highest content for both porosities was led by specimen SCFT-05 which was 10% higher compared to SCFT-01. This might have been caused by the huge quantity of fractured glass microballoons, which became debris as filler in the syntactic foam. Void contents were also present in all specimens, which contributed to the lower density of the syntactic foam and slightly increased when glass microballoon content was increased.

The void contents were also calculated based on Equation (3.4) and this is presented in Table 3.1. Generally, the void contents are expected to increase when more glass microballoons are added to the syntactic foam, from approximately 2.7% to 3.8%, which is supported by Figure 3.8(b). This can happen during the fabrication of the syntactic foam using a conventional mixer (Islam and Kim, 2007, Tien et al., 2009). The debris of the glass microballoons clearly shows this in Figure 3.8(b).

A similar phenomenon can also be observed in this study, when the void and porosity contents were increased while the glass microballoon content was also increased during the manufacture of the syntactic foams (Gladysz et al., 2006, John et al., 2007, Gupta and Ricci, 2006). John et al., (2007) have explained that this discrepancy can be explained by the partial distribution of resin and microballoons during compression moulding in the case of resin-rich systems. The manufacturing process can be improved by reducing the number of voids when releasing the bubbles or gas from the chemical reaction of MEKP. This can be achieved by using infusion methods.

The enlarged image of both porosities (type I and type II) can be seen clearly in Figure 3.8(c) and (d), respectively. Table 3.1 also shows that the percentage of this type of porosity was increased from 33 % to 53 % when it was calculated here using the Equation (3.2). In some cases, the porosity should be identified as embedded with a small size of glass microballoon and filled with matrix resin. This type of matrix porosity occurred in specimens SCFT-02 to SCFT-05 and could be estimated using Equation (3.2). It was increased approximately, on average with an increase from 1.5 % to 2.0 % individually. Hence, the total porosity also increased when the proportion of glass microballoon had increased.

In this study, the volume of the both types of porosity were calculated and the results show an increasing trend when the glass microballoon content was increased. It is revealed that the lower density is due to increasing the fracture of glass microballoon content, as shown in Figure 3.8(a), especially for specimens SCFT-04 with 8 wt.% microballoons, as supported by Section 3.5.1. The remaining debris also contributed to the lower density, as shown in Figure 3.8(c), for SCFT-01 (2 wt.%). A broken microballoon filled with resin and smaller size microballoons are shown in Figure 3.8(d) for SCFT-02 (4 wt.%). As a result, it is shown that the matrix resin was filled inside the glass microballoons, particularly for SCFT-01, which also contributed to the higher density. This evidence further supports the explanation in Section 3.5.1.

This kind of characteristic is affected overall by the weight of syntactic foam. It became the reason for the vinyl ester resin to be exhibited dominantly in the syntactic foams, as the main matrix. This phenomenon can happen when glass microballoons are fractured during the composite processing and, as a result, their cavities can be filled with higher density materials including glass debris and resin (Gupta et al., 2010). The void percentage was calculated assuming that the microballoons were not broken during moulding. However, the breaking of some microballoons took place during the stirring process, which could not be avoided.

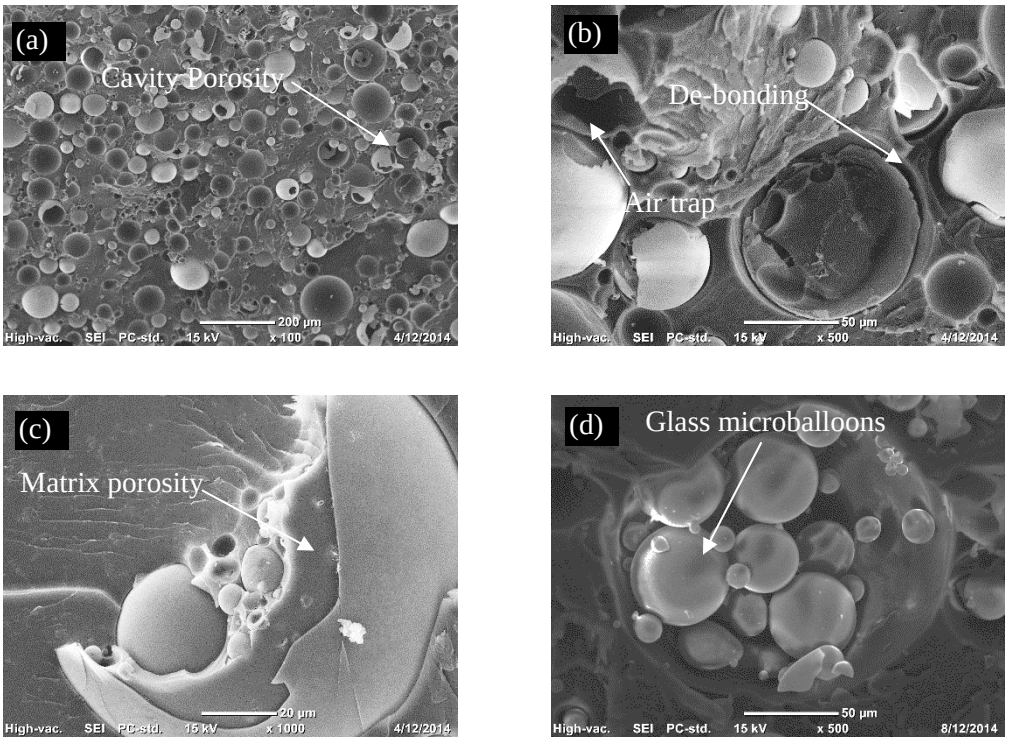

Figure 3.8: A SEM showing (a) Two types of porosity cavities and matrix porosities for SCFT-04 (8 wt.%) (b) Air entrapped for SCFT-02 (4 wt.%) (c) Filled with resin for SCFT-01(2 wt.%) (d) Filled with small glass microballoons for SCFT-02(4 wt.%)

3.5.2 *Influence of porosity in mechanical properties*

The representative compressive stress-strain curves for all types of vinyl ester/glass microballoon syntactic foams are presented in Figure 3.9(a). From the stress–strain profiles, both neat resin and syntactic foams show the same trend for a linear elastic region, followed by a strain softening region, which is characterized by a slight drop in stress. When the compression continues further, the stress starts to rise up again. The increase in stress is faster and significantly higher in the case of neat resin, whereas for syntactic foams it depends on the type and volume fraction of microballoons (Bunn and Mottram, 1993). The compressive modulus values were measured as the slope of the initial linear region of the stress–strain curves, and are presented in Figure 3.9(a).

The compressive strength of composites is defined as the first peak in the stress–strain curves at stage (I). This initial linear deformation region (I) is where stress increases linearly to the first peak (from this gradient line, yield strength or Young's modulus can be defined), followed by a plastic plateau stage (II) where stress slightly increases

as the strain increases; then there is a densification stage (III) where stress rises sharply when the strain is increased slightly. Swetha and Kumar (2011) have also observed that all syntactic foam compositions show this stress plateau, which is a typical feature of most types of syntactic foams (Swetha and Kumar, 2011).

The testing of tensile properties of the vinyl ester/glass microballoon syntactic foam for different compositions of glass microballoon content was carried out. The representative stress–strain curves for vinyl ester/glass microballoon syntactic foam specimens are presented in Figure 3.9(b). These curves show a linear stress–strain relationship, immediately followed by brittle fracture. The stress–strain curves for other types of syntactic foams showed similar features (Gupta et al., 2010, Gupta and Nagorny, 2006). The tensile characteristics values and data, including the CoV (Coefficients of Variation) for all specimens are presented in Table 3.1. The tensile strength from both data, which are presented in Table 3.1 and Figure 3.9(b) show similar tensile strength with the smallest standard deviation. The tensile strength is led by pure vinyl ester at 39 MPa and all specimens show a decrease when the glass microballoon content increases.

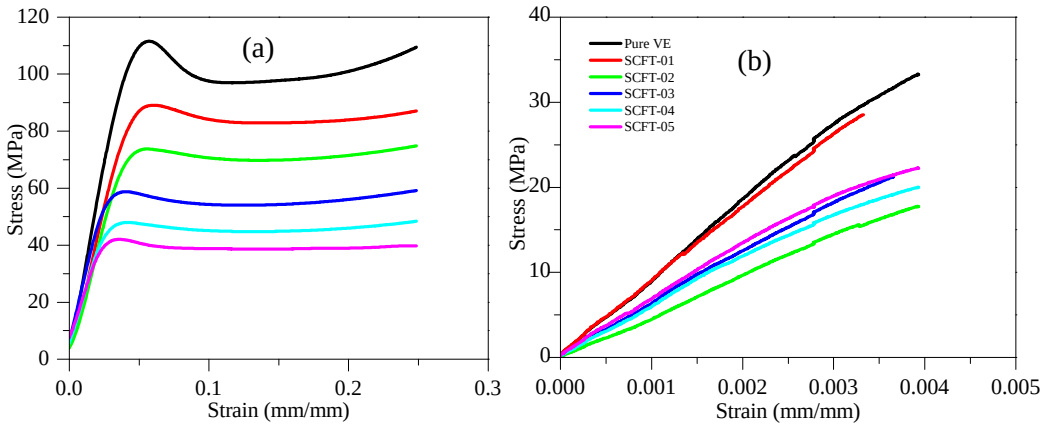

Figure 3.9: Representative mechanical strength curve for vinyl ester matrix syntactic foam (a) Compression (b) Tensile

The decreased tensile strength is observed starting from SCFT-01 at about 10 % from the neat resin, then continuing to reduce for SCFT-02, while no significant change occurs until SCFT-04, as shown in Figure 3.9(b). Similar characteristics are revealed with regards to the reduction of strength value of the syntactic foam, particularly tensile strength in the matrix phase system, which acts as a load bearing phase (Wouterson et al., 2007). They also tested the glass microballoons in epoxy resin as a matrix system. They observed that the matrix-microballoon interface did not appear to

be very strong in these composites, and the presence of a higher volume fraction of microballoons only reduced the volume fraction of epoxy resins in the structure, causing the syntactic foams to have less strength. As mention earlier in Figure 3.5, the compressive and tensile trend were classified as three regions. Although the trend is similar among the pure VE and reinforced VE, the strength showed to be lower due to increasing the filler content in syntactic foam. Again, isotropic behaviour was observed in this case.

The tensile strength and modulus of elasticity values of the vinyl ester matrix syntactic foam, as a function of glass microballoon content, are also shown in Figure 3.10. Overall, the comparison of Young's modulus of all specimens shows that specimen SCFT-02 is higher, with 4 wt,% of glass microballoon content at 9.92 GPa. Generally, the modulus of elasticity decreases while the glass microballoon content in the syntactic foam decreases in the syntactic foam. The reduction of modulus of elasticity could occur due to the porosity contained in the syntactic foam, and the majority of the broken glass microballoons are also filled with voids and porosity. In Table 3.1, it can also be observed that the modulus of elasticity is reduced in the syntactic foam, which is comparable with weight percentage or weight saving for low density syntactic foam Gupta et al., (2010). A similar reduction in modulus of elasticity can contribute in particular to a substantial weight saving application. Huang and Gibson (1993) observed a similar trend for tensile modulus decreasing with an increase in glass microballoon content in syntactic foams. In order to support the weight saving for low density syntactic foam, it is necessary to determine the specific strength of materials. Figure 3.10(c) shows that was led by SCFT-01 with 20 % specific tensile strength higher than other specimens, but with the trend showing a reduction among them. The specific modulus also was higher with SCFT-01 with a content of 2 wt.% of glass microballoons, which is higher than pure VE. Therefore, in order to be applied to a marine application, weight sensitive concerns are very useful for this syntactic foam, particularly SCFT-01 as it will achieve the weight saving matter.

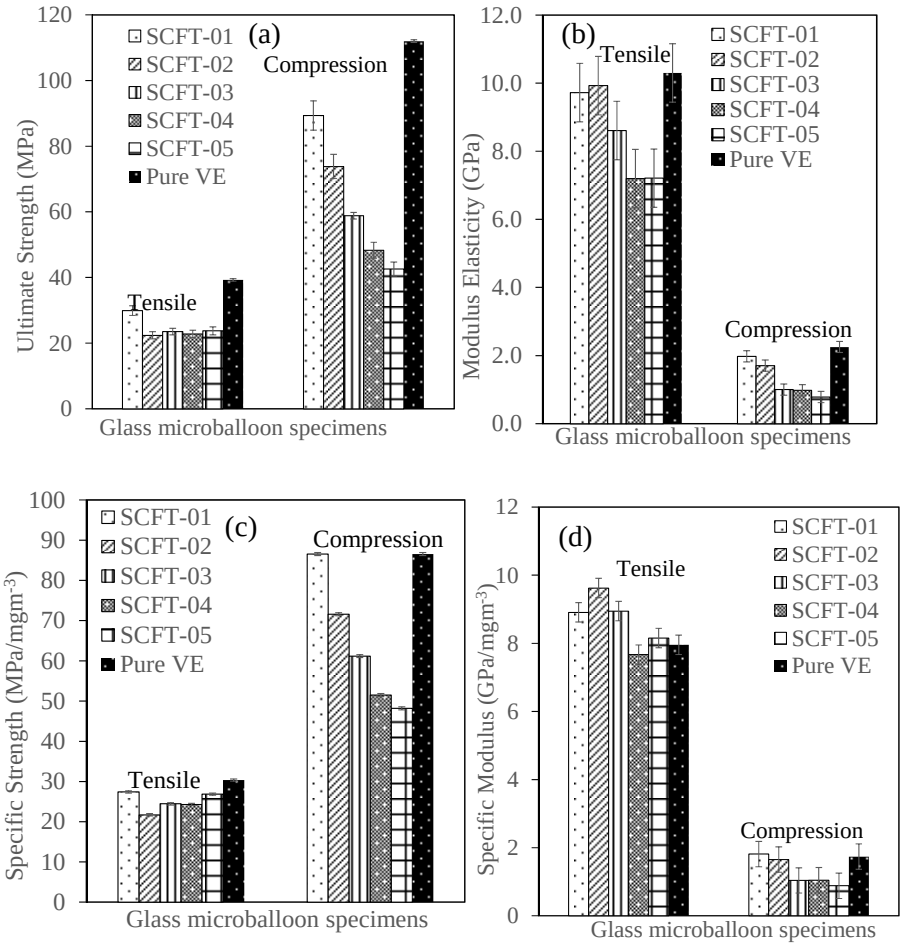

Figure 3.10: Comparison of representative tensile and compression strength with different weight percentages of glass microballoons for (a) Tensile Max. (b) Modulus of Elasticity (c) Specific Strength (d) Specific Modulus

The compressive maximum strength for syntactic foam is measured at the highest peak of the strain-stress curve as shown in Figure 3.10(a). The results show that the compressive strength of syntactic foams decreases with an increasing content of glass microballoons, particularly SCFT-01, which belongs to the lowest η. Gupta et al. (2010) have observed that if a radius ration glass microballoons of $\eta < 0.955$ are used, then the resulting syntactic foam would show substantial benefits in mechanical properties. In this study, it was found that all the specimens showed their lowest in η. It is proven that the modulus of elasticity for compressive strength decreases as the volume fraction of the same type of microballoons increases, as shown in Figure 3.10(b).

The specific compressive strength observed in Figure 3.10(c) shows that the trend also reduces when more glass microballoons are added. The highest specific compressive strength still belongs to SCFT-01 at 86 MPa/mgm^{-3}. This also reflects the lower η andω, which decreases when specific compressive strength decreases. Therefore, even though SCFT-01 had a lowest η, it still has a maximum ω for compressive strength, showing that it is higher than neat resin. Hence, for compressive loading conditions, syntactic foams, particularly SCFT-01, can lead to a significant advantage over the neat resin in terms of weight saving. A summary of the compressive strength results can be seen in Table 3.1. The results indicate that the compressive strength can be tailored over a wide range by selecting microballoons and by using them in different weight percentages. The maximum compressive strengths of the syntactic foams indicate a decrease when glass microballoons are added. The compressive stress for SCFT-01 is higher at 89 MPa but still lower than pure vinyl ester with 112 MPa, while the modulus of elasticity shows a decrease as well as specific compressive strength and specific modulus. Even though the specific compressive strength for SCFT-01 has the same level as pure vinyl ester, it is still 5% lower than the form neat resin. This indicates that adding a small amount of glass microballoons, particularly to SCFT-01 with 2 wt.%, has a significant effect on the low density foams, which is thus useful to be applied to a weight saving application.

The representative SEM microstructure for the fractured surface tensile specimens SCFT-04 and SCFT-05 can be seen in Figure 3.11(a) and (b). It can be observed that microballoon fragments are not present in the syntactic foam because there were several glass microballoons damaged within the matrix resin internal syntactic foam. The tensile fracture mechanism seems to be mainly related to particle–matrix debonding and the fractured matrix resin can be seen clearly for the specimens with a higher resin content, as shown in the higher magnification micrographs presented in Figure 3.11(c) and (d). The fractured surface of the resin exemplifies crack formation and propagation, and severe shear bands are shown in this figure. This is a similar result to that which occurred between epoxy matrix resin and glass microballoons, as studied by Swetha and Kumar (2011). As a result, the pattern of propagation is that of twist hackle lines. Therefore, with a decrease in the volume fraction of the matrix resin in the material, the observation shows that the strength of the composite has decreased,

which contributes to the low density behaviour if the matrix is reduced in the syntactic foam.

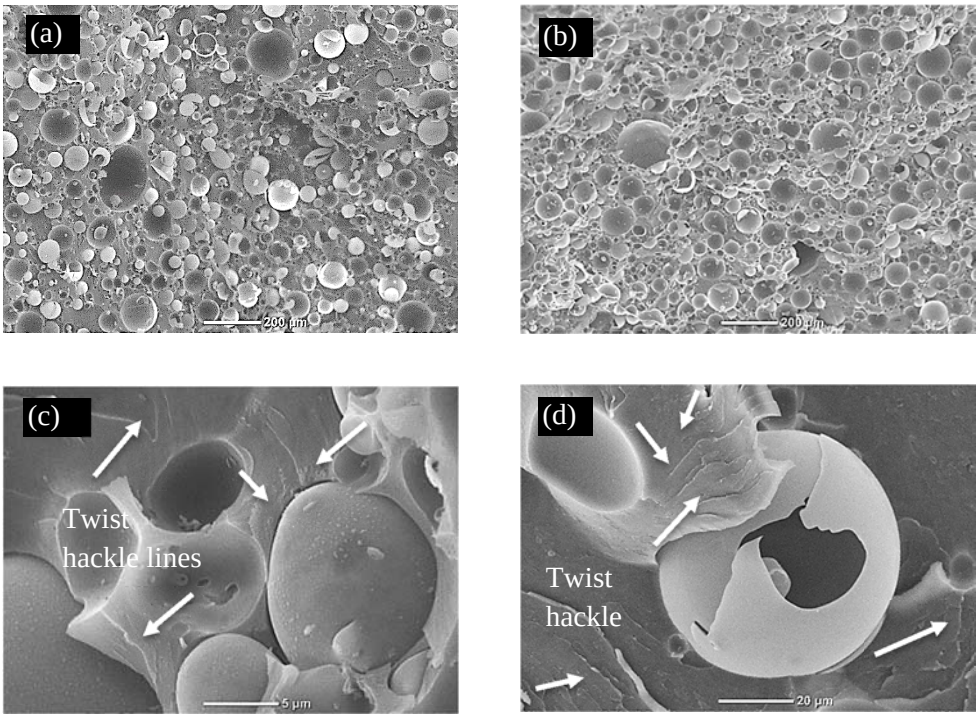

Figure 3.2: Representative of tensile SEM microstructure for (a) SCFT-04 (b) SCFT-05 (c) SCFT-1 (d) SCFT-3 at higher magnification micrograph

3.5.3 *Compressive fracture analysis*

Fractured surfaces of the compressive specimens were studied in detail and it was observed that shear cracks originated from the edges under the bottom side of the specimen. The formation of the shear crack in the matrix is represented as a drop in the stress value of the stress–strain curve. When the specimen is in the plateau region of the stress–strain curve, more shear bands are formed and barrelling of the specimen takes place. At a later stage, along with shear, axial splitting occurs and spalling of the specimen into small pieces is observed. For the specimens SCFT-01 with 2 wt.% to SCFT-03 with 6 wt.% of glass microballoons, the modes are barrelling along with shear yielding alone, until a crack in the middle of the 10 wt.% specimen is observed (schematic shown in Figure 3.12), which is in agreement with earlier results (Li et al., 2009). Figure 3.12(a) represents the schematic of the sample when loaded, i.e., before the start of the stress–strain curve. The drop in the stress value in Figure 3.9(c) and (d) is due to initial crack formation, which is shown in Figure 3.12(b) and actual specimens with crack are shown in Figure 3.12(c) to (e).

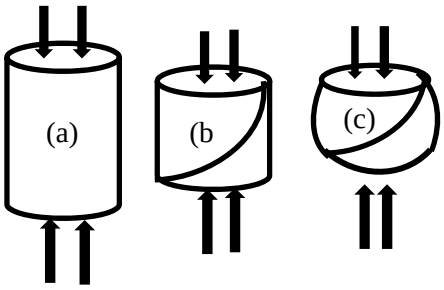

Figure 3.12: Schematic of failure mechanism sequence in syntactic foams (a) Initial stress (b) Internal crack stress concentration (c) Barrelling shape situation

The glass microballoons thus enhance the densification strain of the foams. It is interesting that there is a slight reduction in energy while the variety of the foams increase with different contents of glass microballoons. It is observed that the foam specimens SCFT-01 containing 2 wt.% microballoons deform with a longer time to fracture, as well as having higher stress behaviour at 89 MPa, compared to the other specimens. The limited contents of glass microballoons enhanced the strength of the syntactic foams, which can be seen in the SEM micrograph in Figure 3.11(a). This shows the gaps between the glass microballoons closest to each other, especially for specimen SCFT-03 containing 6 wt.% and SCFT-04 with 8 wt.%. The failure features of these specimens are similar to those presented earlier (John et al., 2007), including the initiation of shear cracks in the specimen and the formation of fragments from the side walls. Inclusion of a higher weight percentage of stiff glass microballoons in the relatively ductile matrix results in increased brittleness of the composite.It can also be observed that these specimens are comparable. Their compressive strength values are deformed with regular distribution of glass microballoons content. While SCFT-5 those containing 10 wt.% glass microballoons occurred many fractured and debris of glass microballoons shown in Figure 3.13(b). The failure features of these specimens are similar to those presented previously (Gupta et al., 2001), which includes the initiation of shear cracks in the specimen and the formation of fragments from the sidewalls. Inclusion of a higher weight percentage of stiff glass microballoons in a relatively ductile matrix results in increased brittleness of the composite. In the plateau region, the samples become barrel shaped and the schematic at the end of the stress–strain curve is represented in Figure 3.12(b) and (c). Similar trends have been observed by Gupta et al., (2001) and G Subhasha et al., (2006) and in epoxy-based polymeric foams with different porosity levels subjected to quasi-static compression (C. Periasamy et al., 2010).

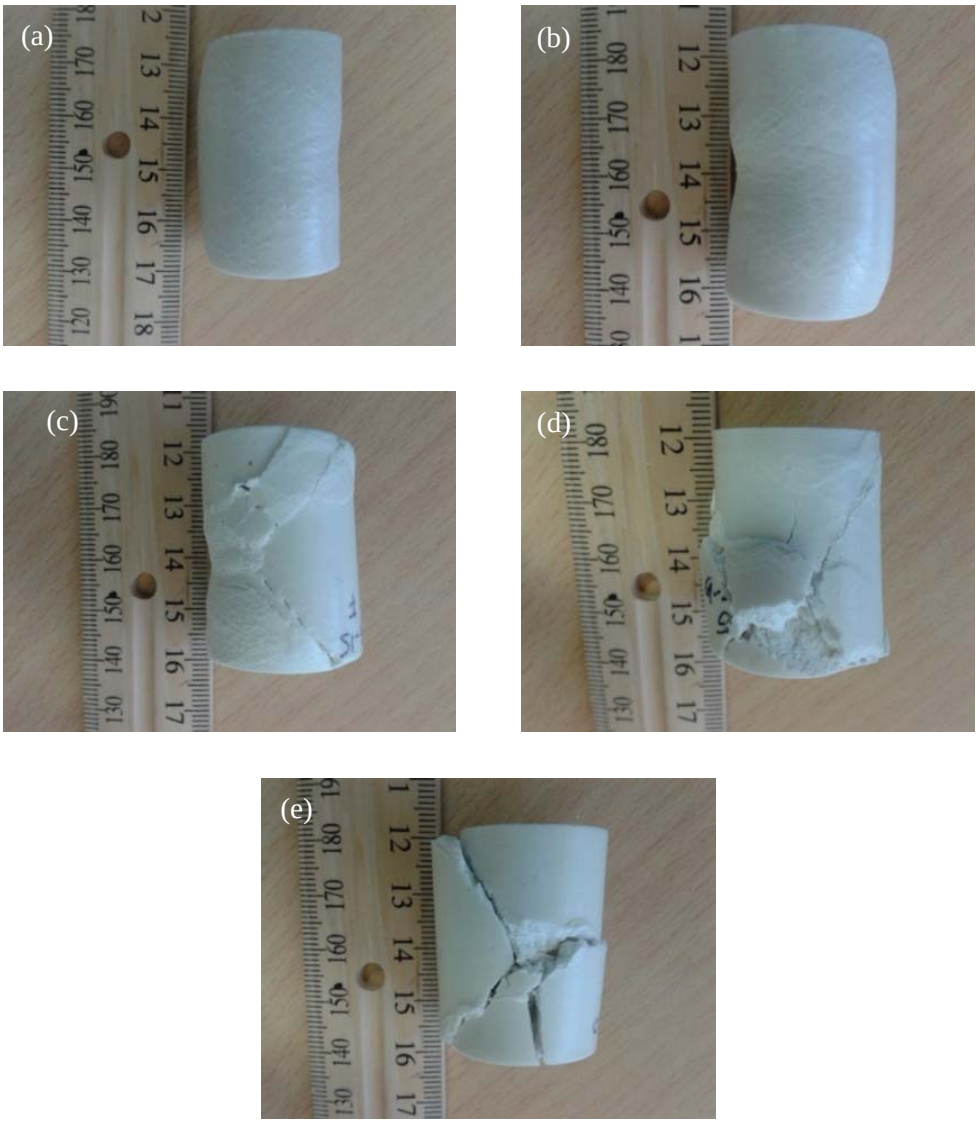

Figure 3.13: Representative specimens of failure mechanism sequence in syntactic foam (a) SCFT-01 and (b) SCFT-02 have barrel shape failure mode (c) SCFT-03 (d) SCFT-04 and SCFT-05 have spalling of syntactic foam

The specimen for 2 wt.% shows the glass microballoons being distributed randomly in the matrix resin. The amount of glass microballoons is less when the density of syntactic foams decreases, while for the specimen with 4 wt.%, the distribution of glass microballoons increases when the density is increased to almost double, when compared with 2 wt.%, as shown in Table 3.1. The specimens with 8 wt.% and 10 wt.% show that the glass microballoons are uniformly distributed around the matrix with increasing density. SEM photos (in Figure 3.14) reveal these phenomena.

The fractured surfaces of some of the glass microballoons and the vinyl ester matrix syntactic foams are shown in Figure 3.14. It can be observed that extensive microballoon damage occurs during the compressive fracturing of the material. Matrix material such as vinyl ester in Figure 3.14(b) reveals that the matrix has also deformed severely. Plastic deformation marks can be seen on the entire matrix surface, including where the microballoons were embedded before the fracture occurred. Microballoons have fractured in the form of small fragments, which are present all over the fractured surface. The fracturing of microballoons and the generation of debris has also been observed in epoxy matrix syntactic foams (Gupta et al., 2002). The plastic deformation marks observed in the matrix are considerably more severe in vinyl ester matrix foams because of the higher failure strain of these composites.

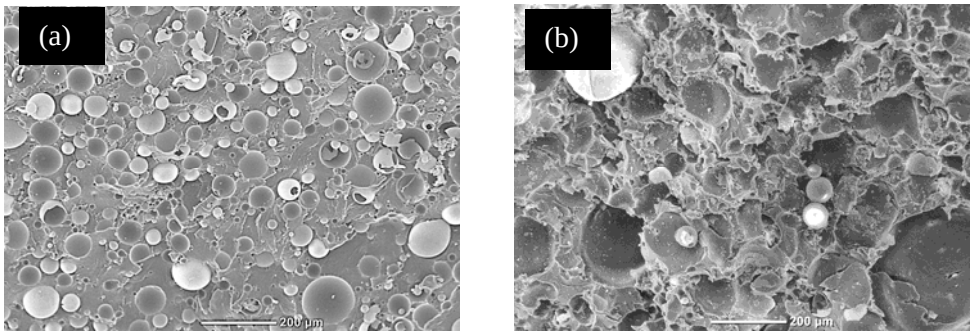

Figure 3.14: Representative fracture surface of (a) SCFT-04 (glass microballoon 8wt.%) (b) SCFT-05 (glass microballoon 10 wt.%)

3.5.4 Relation of Young's modulus with particle parameters (ω,η)

For better understanding of the relationship between all the parameters for syntactic foam and modulus of elasticity, the theoretical model for tensile testing results is good for analysis (Gupta et al., 2010). They found that several studies have been concerned with a number of models to predict the modulus of elasticity for composite materials. Only a few of these report about syntactic foam is being affected by attending to porosity enclosed inside glass microballoons, which then contributes a higher weight percentage or volume fraction (Bardella and Genna, 2001, M. Koopman et al., 2006, Gladysz et al., 2006, Huang and Gibson, 1993, Li et al., 2009). The diluted dispersion of glass microballoons in the matrix resin can be estimated by using a differentiation scheme. Numerical differentiation has been proposed to estimate the elastic properties of syntactic foam for higher compositions (C. Periasamy et al., 2010). In other words,

experimentally the diluted dispersion of glass microballoons was extended to the composite strength for higher volume fractions.

This diluted dispersion can be achieved by adding a small quantity or an incremental quantity of glass microballoons until it reaches the desired quantity. Before achieving this quantity, the composite material must set its condition as a homogenous effective medium, also called an infinitely diluted dispersion particle (Gupta et al., 2010). This mechanism is explained and determined by Gupta et al. (2010) in the Equation (3.5) and (3. 6),

$$\frac{dE}{E} = f_E\left(E_b, \phi_b, E_m, \phi_m, \quad \eta\right)dw \tag{3.5}$$

$$\frac{d\emptyset}{\emptyset} = f_\emptyset\left(E_b, \phi_b, E_m, \phi_m, \quad \eta\right)dw \tag{3.6}$$

where f_E is Young's Modulus function and f_ϕ is Poisson's ratio function consisting of E_b modulus of elasticity of glass microballoon, ϕ_b – Poisson's ratio of glass microballoon, E_m – modulus of elasticity of matrix resin, ϕ_m – Poisson's ratio of matrix resin, η - radius ratio of glass microballoon, and dw – different composition. These equations also assume that there is space available when glass microballoons are added to the composite for the entire homogenous effective medium, and that it will replace the matrix resin cavity. As a result, the composition of composite materials will increase and volume will decrease due to the pre-existing particles. In order to enhance the understanding of Equation (3.5), corrected equation and replaced the dw with $dw/(1-w/w_m)$ where w_m is the maximum packing volume fraction of particles and can be assumed as a random packing factor 0.637 (Gupta et al., 2010). When both equations are integrated with the initial values for all parameters, Young's modulus for the composite can be determined. The relative modulus of the elasticity of vinyl ester syntactic foam, with respect to the modulus of elasticity vinyl ester matrix resin, has been implemented and can also be used in this study.

Therefore, to explain the relationship for these equations, the graph between E/E_m on the y-axis versus $(1-\eta)$ can be plotted, while the x-axis shows the wall thickness of glass microballoons in Figure 3.15. In this study, the graph shows that the trend is non-linear for different weight percentages of glass microballoons and for the wall

thickness of both batches A and B. It can be observed that the relationship between both parameters is non-linear with relative modulus of elasticity (E/E_m), whereby a relative maximum at 1.15 for batch A and 1.01 for batch B occurred for the weight percentage (8 – 10 wt.%), respectively. Based on this result, the theoretical values of $\eta < 0.955$ resulted in composites with relative modulus of elasticity (E/E_m) >1 as proposed by (Gupta et al., 2010). As the value of $(1 - \eta)$ increases, the dependence of relative Young's modulus on the wall thickness decreases, which means that the slope of the curves also decreases. Hence, these results also support the value of ω and η in Table 3.1, which shows decreases as well.

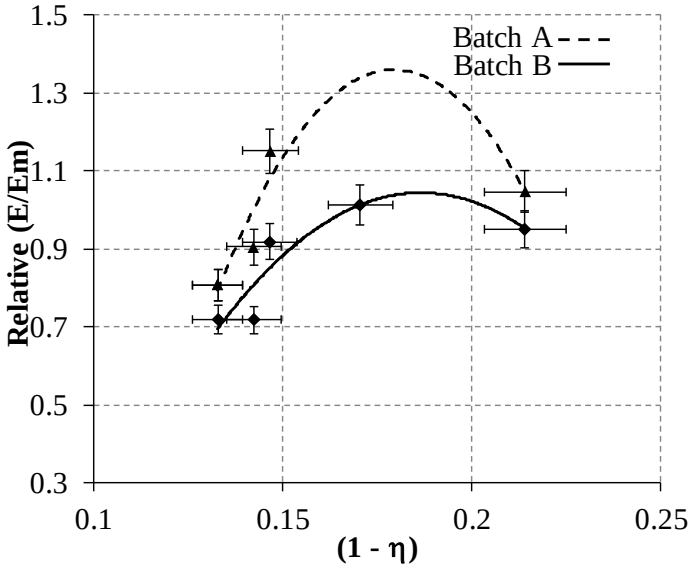

Figure 3.15: Relationship between Young's modulus (E/E_m) and particle composition ($1-\eta$)

It has been observed that the results match well for syntactic foams containing 2–6 wt.% microballoons; however, the predicted values are higher than the experimental results for foams containing 8 and 10 wt.% glass microballoons. Table 3.1 shows syntactic foams containing 8 and 10wt.% glass microballoons, while the void volume fraction is higher, which was not included in the model. Hence, the composition in the experimental results is lower than the predicted values. In other words, glass hollow particles with a density approximately higher than 190 kgm^{-3} (see Table 3.1) lead to syntactic foams being stiffer than the vinyl ester neat resin material for any value of ω.

3.5.5 Difference between tensile and compressive moduli

A comparison shows that the tensile modulus of elasticity values in Figure 3.9(b) are 70-80 % higher than the compressive modulus of elasticity values for the same type of syntactic foam. Such difference was also observed in previously published data (Kishore et al., 2005, Gupta et al., 2004, Gupta and Nagorny, 2006, Tagliavia et al., 2009). Two possible reasons are identified for such a difference. The first reason is the particle–matrix interfacial de-bonding. Existence of any de-bonding causes a difference in the extent of stress transfer between particle and matrix. It has been shown in some recent studies that the tensile modulus of elasticity is sensitive to the presence of de-bonding (Tagliavia et al., 2009). In comparison, under compressive loading conditions, de-bonding does not play an important role because the matrix is compressed on the particle and separation occurs only in a small region in the direction transverse to the applied load. De-bonding seems to be present in these composites as observed in Figure 3.11. Therefore, the presence of de-bonding would result in an increase in the tensile modulus of elasticity, which is similar to the experimental observations made in the present study.

The second reason that plays an important role is the possibility of particle fracture under compressive loading conditions. In Figure 3.9(b) it is shown that compressive modulus of elasticity measurements can be taken in the region where the load is approximately 40–90 MPa. The mean plateau region for all specimens shows linearity except for that of pure vinyl ester. The trend for the mean plateau also creates a different gradient from one specimen to another. One of the reasons for this trend is that if more glass microballoons are added, the linearity of the mean plateau shows greater flatness, as for example in specimens SCFT-04 and SCFT-05. The density analysis was conducted using a multipycnometer machine with the Quantachrome model as presented in Table 3.1. It can be seen that the density is higher for the lower glass microballoon content and low density belongs to the higher glass microballoon content. The low density particles of the higher glass microballoon content have thinner wall thickness and are weaker in comparison to the lower glass microballoon content.

As a result, the porosity takes place and fills in the broken glass microballoon space and also contributes to lower density when higher compressive loading is achieved. Beside this phenomenon, similar things occur to the void content where it takes up the empty space and contributes to the lower density behaviour. In addition, the data on working pressure for glass microballoon survival are provided by the manufacturer and show only a maximum at 500 psi, which is equivalent to 3 MPa when calculated. From these values, it appears that the fraction of weaker microballoons can potentially fracture in the measurement range of 40-90 MPa under compressive stress–strain.

3.6 Summary

This detailed experimental study of the synthesis and characterisation of glass microballoon/vinyl ester syntactic foam provides a number of findings. It is revealed that the density of syntactic foam varied and decreased while the glass microballoon contents increased, which followed the rules of mixture. The parameters such as wall thickness, ω and radius ratio, η play important parts in contributing to low density foam behaviour. Porosity and void content were calculated and it was discovered that cavity porosity was higher than matrix porosity but void contents remained constant in all specimens. Tensile and compressive characteristics of the vinyl ester matrix syntactic foam were investigated and it was revealed that tensile strength was 70-80 % higher than compressive strength when glass content was reduced.

Chapter 4

Fabrication and Characterisation of Syntactic Foam Core Sandwich Composites

4.1 Introduction

The design concept behind composite sandwich panel construction is that the skin carries the in-plane compressive load while the primary function of the light weight syntactic foam core is to maintain the two glass fibre reinforced plastic (GFRP) skins at a desired distance. In this study, the skin of the sandwich panel consisted of GFRP with vinyl ester resin acting as a binder. Furthermore, sandwich panels can be developed using GFRP as the skin and polyol-isocyanate foam as the core, which have previously been used as entry doors and partitions (Shen et al., 2013). In this study, four stages were created to investigate the syntactic sandwich panels. First, the sandwich panels' syntactic foam was fabricated using core-made from constituent materials while their skin made from glass fibre reinforced plastic (GFRP). Secondly, their mechanical behaviour was investigated in relation to the constituent properties and fabrication conditions. Thirdly, to characterise the fracture mechanism of the syntactic foams, a microstructure analysis was introduced using a scanning electron microscope (SEM).

4.2 Materials and experiment methods

The fabrication of syntactic foam as a core material has already been explained in detail in Chapter 3. The same composition of glass microballoons was used in this study, between 2 to 10 wt.%.

4.2.1 Fabrication of glass fibre reinforced plastic sheet

The fabrication of syntactic foam sandwich panels was performed in two stages as part of the pre-mould process. Firstly, the skins of the sandwich panels were prepared. The hand layup technique was used in this study to apply the vinyl ester resin to the

unidirectional GFRP. The size of the GFRP was cut into 370 mm x 400 mm and stacked at a 3-layer thickness. It was then placed onto the rectangular shaped glass as the bottom base, and the vinyl ester was poured onto it using a small squeegee to facilitate uniform resin distribution and the removal of air pockets (Mostafa et al., 2013). Then, the top of this area was covered by a rectangular-shaped piece of glass to ensure a uniform flatness. Furthermore, a small weight was pushed onto the glass until the vinyl ester spread to the edge of the rectangular glass. The GFRP was cured at room temperature for 24 hours at a humidity of 85%RH. The demoulding process was performed after it was cured, and it was then placed into an oven for final curing at a temperature of 80ºC.

4.2.2 Compressive sandwich panel specimens

The second preparation was involved with fabricating the syntactic foam as a core, using different weight percentage of glass microballoons. The types of specimens depended on the mechanical properties that needed to be investigated for the sandwich panels. Shen et al., (2013) have performed three types of testing on sandwich panel foams, which involved compression, tensile and flexural testing. In this study, the ASTM standard applied in the compression test was ASTM C-365. Cylindrical-shaped PVC tubes with dimensions of diameter ϕ = 30.0 mm and length L = 60.0 mm were used for the compression moulds. First, the moulds had to be cleaned using acetone, and the surface was coated with mould wax to ensure that the syntactic foams could be easily removed. The GFRP skin was placed at the bottom of the PVC mould with masking tape as a seal to avoid slurry leakage. This synthesis method consisted of mixing different measured quantities of glass microballoons in the vinyl ester resin and stir mixing them until a slurry of uniform viscosity was obtained. The mixing time was approximately 4 to 5 minutes.

Then, the required amount of glass microballoons, based on the weight percentage, was weighed separately and added slowly to the resin mixture. The mixture was then transferred to a PVC mould. The specimens along with the mould were allowed to cure for 24 hours at room temperature and then removed from the mould. The fabrication of the compressive specimens is depicted in Figure 4.1. To ensure complete curing, the sample was post-cured at 80°C for 4 hours in a hot air oven.

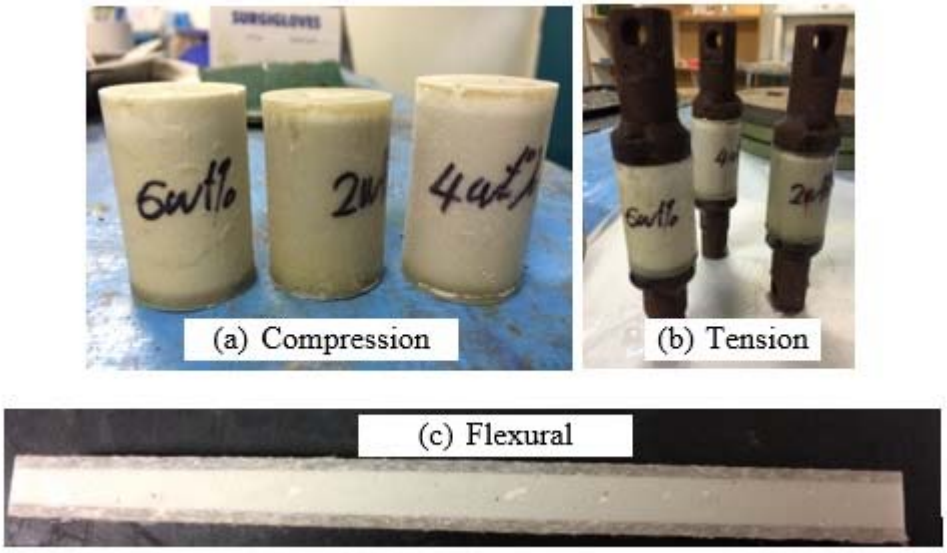

Figure 4.1: Representative specimens of syntactic foam sandwich panels

The compression test was performed using MTS test systems with a constant test speed of 2 mm/min. Figure 4.2 depicts the photograph of one of the specimens tested during the compression test in the MTS machine. From the output result, two parameters were selected for data analysis, namely the load and crosshead displacement, to develop the stress–strain curves. Then, it was necessary to re-calculate the actual values of stress and strain using the area formula for a cylindrical shape for each sample.

4.2.3 Tensile sandwich panel specimens

The tensile specimens for this study followed the dimension size from the compression sample size and were based on ASTM C297. Similar to the compressive specimens, the GFRP skin stuck together on the top and the bottom while the slurry was poured and mixed with the vinyl ester resin. The evaporation from the styrene gas produced from the MEKP hardener made it difficult for the skin to stick to the top of the syntactic foam cores. Therefore, a rectangular glass plate was placed on top of all of the specimens while being cured at room temperature, 25°C. After the demoulding process, all of the specimens were pasted to the tensile loading bloc using an epoxy adhesive type techniglue R5, mixed with hardener techniglue H5 at a concentration ratio of (1:1).

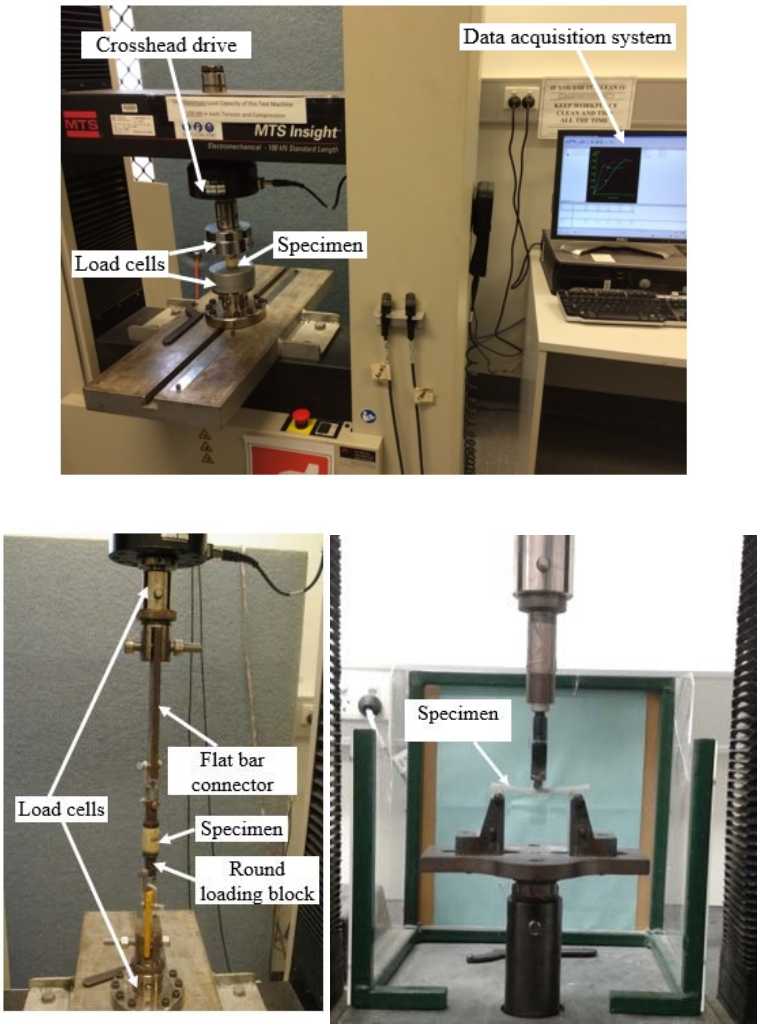

Figure 4.2: Representative overview of the mechanical testing setup using the MTS Insight machine

4.2.4 Flexural shear sandwich panel specimens

Additionally, the specimens for the flexural sandwich specimens were prepared from the same GFRP skin as the compressive specimens. The sandwich panels with the GFRP skin and syntactic foam core were prepared based on ASTM C 393/393M-11. This method is required for a 3–point loading (TPB) with a mid-span and a total span length supported at 150 mm. Similar to the preparation for compressive core syntactic foam, the glass microballoon was measured with different weight percentages before it was poured and cast into the GFRP skin. The GFRP skin for both sides were stuck to each other using masking tape.

4.3 Results and discussion

4.3.1 Compressive property

The specimens can be identified as SCSW-1, SCSW-2, SCSW-3, SCSW-4 and SCSW-5 for syntactic foam cores with glass microballoon contents of 2 wt.%, 4 wt.%, 6 wt.%, 8 wt.% and 10 wt.%, respectively. The properties of the syntactic foam sandwich panels exhibited ductile behaviour when the glass microballoon contents were increased. The compressive strength showed decreased when added more glass microballoon (high wt.%) due to occurred the porosity and void including de-bonding with matrix resin in syntactic foam. This property is depicted in Figure 4.3 for all of the specimens. The SCSW-1 and SCSW-2 specimens exhibited a barrelling shape while the SCSW-3 to SCSW-5 specimens showed cracks at the edges of the skin. Furthermore, Shen et al., (2013) have determined that the sandwich panels for FRP/polyol–isocyanate foam have brittle behaviour during compressive testing.

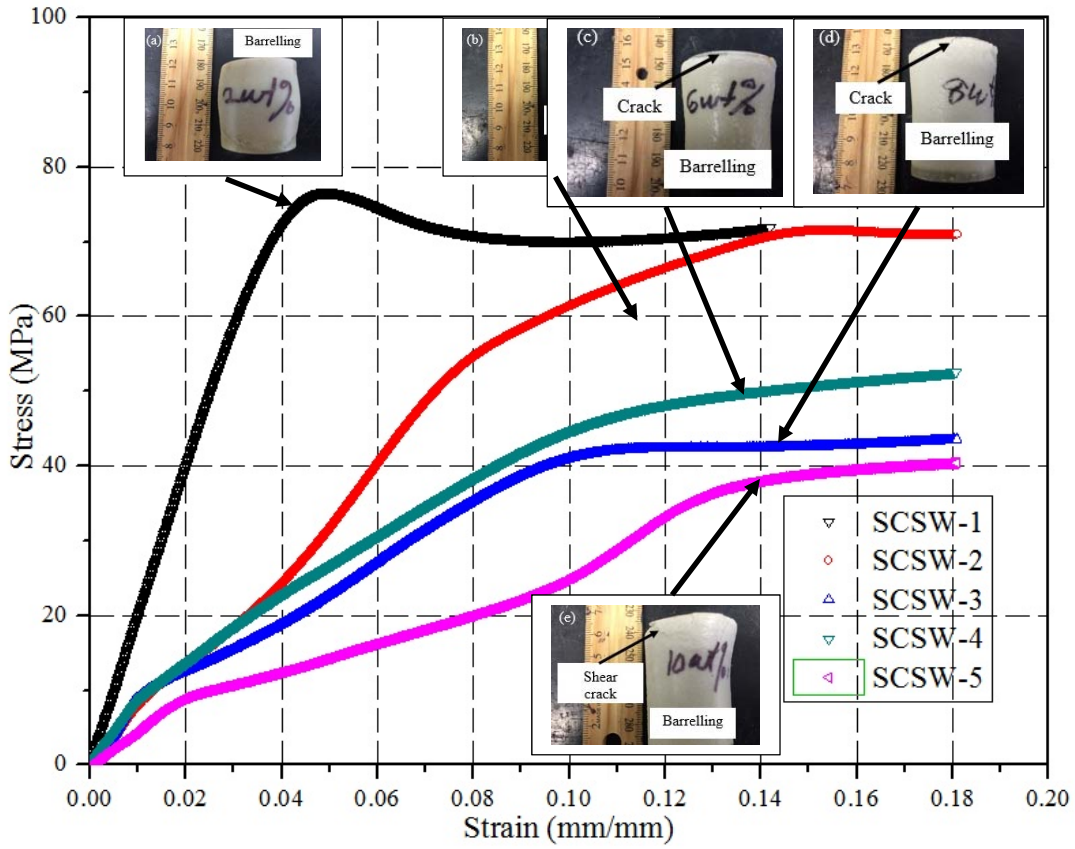

Figure 4.3: Representative overview of the stress-strain curve for compressive strength

The compressive result for all of specimens indicates an initial linear elastic region followed by a mean plateau plastic region and a densification stage at the end of loading. Table 4.1 presents the modulus of elasticity (E_c), maximum yield stress (σ_c), maximum yield strain (ε_c) and their coefficients of variation (CoV's).

Table 4.1: Compressive characteristics for the syntactic foam sandwich panels

Specimens	Glass Microballoon content	Modulus of Elasticity (E_c)	Stiffness, kc	Max. Yield Stress (σ_c)	Max. Yield Strain (ε_c)	CoV-E_c	CoV-σ_c	CoV-ε_c
	(wt.%)	MPa	MPa	MPa	mm/mm			
SCSW-1	2	1614.18	0.07	77.04	0.20	0.04	0.01	0.02
SCSW-2	4	831.15	0.07	72.20	0.19	0.02	0.03	0.01
SCSW-3	6	402.85	0.04	43.56	0.19	0.05	0.03	0.02
SCSW-4	8	361.22	0.05	52.55	0.18	0.01	0.05	0.02
SCSW-5	10	194.92	0.04	40.41	0.18	0.08	0.01	0.01

*CoV = Standard of deviation divided Mean (σ/μ)

Generally, the compressive modulus of elasticity reduces with an increase in the glass microballoon contents in syntactic foam cores, which is demonstrated by SCSW-1. The Ec is decreased due to brittleness and ductility of specimens when amount of glass microballoons where top of the specimens start to crack especially at the edge area. The ductility of the specimens can be clearly observed in SCSW-5, particularly the fractured area at the edge, when the glass microballoon content is increased, as indicated in Figure 4.4. The stiffness trend indicates that it is not significantly affected by the different weight percentage of glass microballoons. However, the compressive maximum yield stress and the maximum yield strain decrease when the glass microballoon contents increase in the syntactic foams. Hence, all specimens indicate that their compressive properties decrease when the microballoon contents increase.

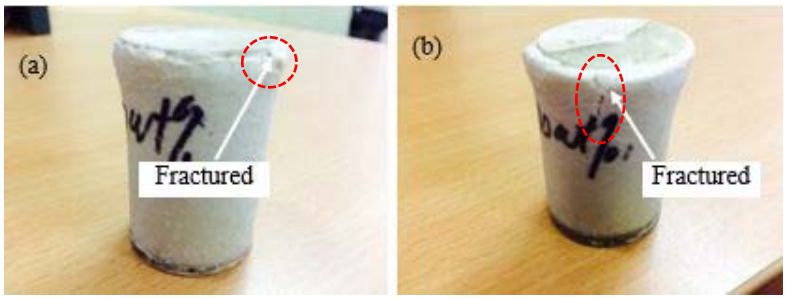

Figure 4.4: Fractured specimen at top edge after compressive testing for (a) SCSW-4; and (b) SCSW-5

The compressive fracture mechanism can be divided into two types, which are known as barrelling and spalling. The specimens with low glass microballoon contents of 2 wt.% to 6 wt.% demonstrated the barrelling mode. However, increasing the glass microballoon contents caused the syntactic foam behaviour to change to the spalling mode, thus making it easy to fracture, especially near the top skin area. Furthermore, this crack started from the internal foam when the air void increased due to the higher glass microballoon contents (Nambiar and Ramamurthy, 2007). Nambiar and Ramamurthy (2007) have determined that the size and number of air voids could be varied with the foam volume unless the machine could determine the desired void contents in the specimens.

4.3.2 Tensile property

Generally, the tensile strength of the syntactic foam sandwich panels depicted in Figure 4.5 decreased when the glass microballoon contents increased. The detailed conditions of the failure modes state that the only acceptable failure modes for this test method are those internal to the sandwich construction (i.e., the core failure and the core-to-FRP skin bond failure) (Materials, 2004). Based on ASTM C297/297M, four types of standard failure mode properties could be evaluated from the tensile testing: (a) core failure, (b) adhesive failure; i) Adhesive failures that occur at the bond to the loading blocks are not acceptable failure modes and the data shall be noted as invalid ii) Failure of Core-Facing Adhesive—Failure in the adhesive layer used to bond the facing to the core, with adhesive generally remaining on both the facing and core surfaces. Adhesive Failure of Core-Facing Adhesive—Failure in the adhesive layer used to bond the facing to the core, with adhesive generally remaining on either the facing or the core surface, but not both, (c) Cohesive failure: Cohesive Failure of Core-Facing Adhesive—Failure in the adhesive layer used to bond the facing to the core, with adhesive generally remaining on both the facing and core surface, and (d) Facing tensile failure: Facing Tensile Failure—Tensile failure of the facing, usually by delamination of the composite plies in the case of a fibre-reinforced composite facing. Based on this finding, testing the specimens detected only failure modes (a) and (c).

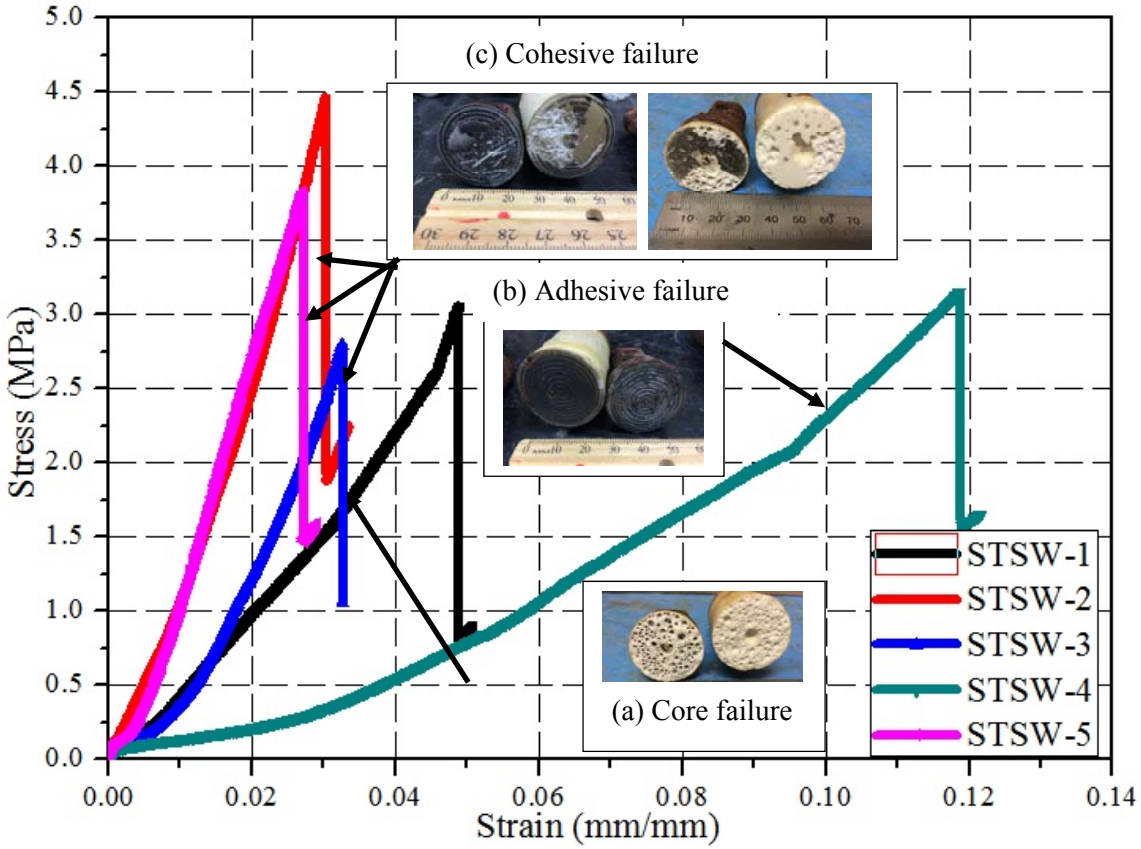

Figure 4.5: Representative overview of the stress-strain curve for tensile strength

Compared to the peak stress values of the stress-strain curves, it can be observed that specimen STSW-2 exhibited the highest ultimate strength of 4.5 MPa. The photographs reveal that the failure mode condition, due to the bonding failure between the skin and the core, clearly occurred for specimen STSW-2, as indicated in Figure 4.5. Therefore, it is not considered acceptable for determining the tensile strength in this case. Based on the observation of the STSW-3 and STSW-4 specimens in Figure 4.7, they exhibit syntactic foam core failure. The photographs illustrate that several air bubbles or voids occurred internally in the syntactic foam due to inadequate mixing during the preparation of the specimens. This failure mode is considered to be evidence of the tensile failure and supports the previous section on the compressive results for SFSW-1. Similar to the compressive result, the modulus of elasticity (E_t), ultimate stress (σ_t), strain (ε_t) and coefficients of variations (CoVs) are presented in Table 4.2.

Table 4.2: Tensile characteristics for the syntactic foam sandwich panels

Specimens	Glass microballoon content	Modulus of Elasticity (E_t)	Ultimate Strength (σt)	CoV-E_t	CoV-σ_t
	(wt.%)	MPa	MPa		
STSW-1	2	124.06	3.06	0.04	0.09
STSW-2	4	195.34	4.46	0.02	0.04
STSW-3	6	132.69	3.14	0.01	0.03
STSW-4	8	129.53	3.15	0.01	0.06
STSW-5	10	153.38	3.83	0.03	0.01

*CoV = Standard of deviation divided Mean (σ/μ)

From Table 4.2, it can be observed that no trend exists in the tensile modulus of elasticity, and the slope is highest for STSW-2 at 195.34 MPa. For specimens with a core failure mode, the modulus of elasticity should range from 120 – 135 MPa. It can be observed that specimen STSW-2 failed due to bonding failure, which is the area between the skin and the core, which is also known as cohesive failure. Furthermore, STSW-4 had the lowest modulus of elasticity of 129.53 MPa, which was due to adhesive failure. A comparison of the difference in the modulus of elasticity between the compressive and tensile strengths may identify two possible reasons. Gupta et al., (2010) determined that one of the reasons was due to particle–matrix interfacial de-bonding. The existence of any de-bonding causes a difference in the extent of stress transfer between the particle and the matrix (Gupta et al., 2010). It has been shown in recent studies that the tensile modulus of elasticity is sensitive to the presence of de-bonding (Tagliavia et al., 2009). In comparison, under compressive loading conditions, de-bonding does not play an important role because the matrix is compressed on the particle, and separation occurs only in a small region in the direction transverse to the applied load. However, the presence of de-bonding could result in a slight decrease in the tensile modulus of elasticity, which occurred in this study. The second reason that plays an important role is the possibility of particle fracture under compressive loading conditions. It can be observed in Figure 4.5 that the compressive modulus of elasticity measurements can be obtained in the region where the load is approximately 40 - 60 MPa. Below this load level, it is difficult to determine the linearity of the stress–strain graphs. One of the reasons for this trend is that the sides of the compression specimens cannot be made perfectly parallel to each other, thus resulting in non-linearity at the onset of testing. This effect is minimised through careful sample preparation; however, it is difficult to completely eliminate it. Therefore, it can be concluded that based on

the compressive and tensile testing for the modulus of elasticity, the foam is considered to be a bi-modulus material, where the tension modulus is different from the compression modulus of elasticity in the same direction. Shen et al., (2013) determined that $E_t > E_c$ in FRP/polyol–isocyanate foam sandwich panels used in civil construction. Furthermore, most of the materials are bi-modulus materials that are widely used in concrete for civil engineering and cast iron for mechanical engineering (Cai, 2010).

4.3.3 Flexural property

4.3.3.1 Flexural properties of the GFRP skin

Both the GFRP skin and sandwich panel properties were tested in this study. The GFRP skin coupons had a rectangular shape of length, L ~ 195 mm, width, W ~ 14 mm and thickness, t ~ 2 mm. This GFRP skin property was useful for calculating the deflection of the sandwich panels.

A summary of the results for flexural 3-point bending of the GFRP skin is listed in Table 4.3. It can be observed that all 6 coupons exhibited stress-strain with an ultimate individual stress between 6 – 8 MPa. The gradient of the linear graph of the stress-strain provided the modulus of elasticity for the skin. Figure 4.6 shows that GFRP-6 had the highest E_s of 3.43 MPa. The low significant effects of the skin thickness may impact the possibility of achieving a higher modulus of elasticity. Generally, it was approximately 30% higher when compared to the E_s values for all of the coupons, as indicated in Table 4.3.

The influence of the skin thickness in this study should only slightly affected the higher modulus of elasticity for the 3-point bending (TBP) test for all coupons. Table 4.3 indicates that the difference in the thicknesses between GFRP-2 and GFRP-6 was only 3 mm; however, the value of E_s was 25% higher than the rest, which was similar to the ultimate strength between the thick and thin thicknesses of the skin. Although GFRP-2 had a higher strength than GFRP-6, the thickness was not considerably different when compared to the rest. Therefore, the variation in the thickness of the skin had a lower impact on the ultimate strength and the modulus of elasticity of the skins. Shen et al., (2013) have determined that the bending strength is larger than the tensile

strength for skin sandwich panels made from glass board REI FRP due to the thickness and uneven surface of the skins.

Table 4.3: TPB Flexural characteristics for the GFRP skin

Specimens	Length	Thickness	Width	Ultimate Stress	Max. Load	Modulus of Elasticity	Stiffness	Tangent modulus
	L(mm)	t(mm)	w(mm)	σ_{ult} (MPa)	P (kN)	MPa	kN/mm	MPa
GFRP-1	192.00	2.00	13.49	7.71	0.208	2.78	49.72	48590
GFRP-2	193.00	1.98	14.70	7.56	0.220	2.58	47.53	43936
GFRP-3	196.00	2.03	15.37	6.12	0.190	2.40	52.39	42975
GFRP-4	194.00	2.05	13.43	6.46	0.177	2.72	54.76	49914
GFRP-5	195.00	1.97	14.65	6.94	0.200	2.60	50.09	47171
GFRP-6	195.00	1.95	11.20	7.13	0.155	3.43	65.52	83210

Using Table 4.3, the coefficients of variants (CoVs) can be calculated by dividing each individual value by the mean. The CoV of the ultimate stress, and the CoVs of the modulus of elasticity and load maximum can be defined as 0.09, 0.13 and 0.12, respectively. Overall, GFRP-1 had the highest ultimate stress of 7.71 MPa, GFRP-2 had the maximum load of 0.220 kN, and GFRP-6 had the highest modulus of elasticity at 3.43 MPa. Furthermore, the behaviour of the GFRP skin can be described by investigating their extension during the flexural testing. Figure. 4.6(b) illustrates that their properties vary with the thickness from 1.95 mm to 2.05 mm for GFRP-1 to GFRP-6.

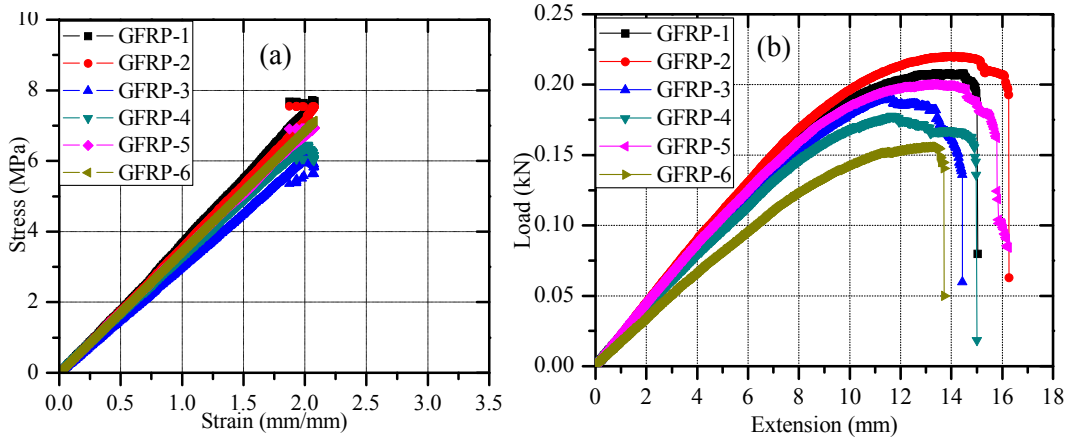

Figure 4.6: Representative plot graph of the GFRP skin for (a) Flexural testing; and (b) Load (kN) – Extension (mm)

The maximum load was achieved for GFRP-2 of 0.220 kN with an extension of 14.0 mm before it reached failure at 16.27 mm. Furthermore, the lowest load of 0.15 kN was achieved by GFRP-6 with an extension of 13.44 mm before it reached failure at 13.72 kN. Specimens GFRP-1, GFRP-3 and GFRP-5 indicated that the loads varied from 0.18 kN to 0.21 kN. Generally, in this study, the thicknesses of the GFRP skin were not comparable with the load and extension during the flexural testing. From the stress–strain flexural testing results, the tangent modulus and the stiffness of the skin can be obtained (Maharsia et al., 2006). The tangent modulus or modulus of elasticity in bending can be calculated using Equation (4.1) (ASTM, 2003) as follows:

$$E_B = \frac{L^3 m}{4wt^3} \tag{4.1}$$

where L is the span length; m is the stiffness; w is the width of the skin; and t is the thickness of the skin. The stiffness of the skin can be obtained from the slope of the load-extension curve. Generally, the stiffness of the GFRP skins increased when the modulus of elasticity increased. The influence of the fibre glass sheet in the vinyl ester resin resulted in a different higher level of the strength of the skin, which also contributed as one of the factors. Furthermore, the randomness of the fibre orientation indicated an increase in the modulus of elasticity in the phenolic microsphere, used as the filler in the epoxy resin (Wouterson et al., 2007).

4.3.3.2 Flexural properties of syntactic foam sandwich panels

According to ASTM C393/393M, the failure mode can be classified as (a) unsymmetrical shear failure in the foam; (b) symmetrical shear failure in the foam; (c) de-bonding at the core-to-GFRP skin interface; (d) local collapse at the top GFRP surface; (e) local buckling of the top GFRP, which was attributed to the in-plane forces caused by the rounded surface of the loading cylinder making contact with the GFRP sheet; and (f) local de-bonding between the top GFRP skin and the foam. The flexure for the syntactic foam sandwich panels are depicted in Figure 4.7. In this study, the core shear was revealed as exhibiting different failure rates in the flatwise and edgewise positions. Tensile cracks of the core can be observed at the bottom of specimen Figure 4.7. On the top of specimen TFSW-1, compressive failure was also revealed due to de-bonding unsymmetrical shear failure between skin and core, as shown in Figure 4.7 (a). Furthermore, tensile cracks of the core failure were observed

at the bottom and side of specimen TESW-1, as shown in Figure 4.7 (b). However, the occurrence of un-symmetrical skin in the edgewise position prevented premature failure and made the syntactic foam sandwich panels fail in a ductile failure mode. Flexural core failure, due to brittle syntactic foam with composition 10 wt.%, was clearly shown in Figure 4.7 (c) for specimen TFSW-5. These cracks originated at the bottom of the (tensile) skin and progressed with the application load. However, the GFRP composite skins bridged the cracked core together to prevent the intermediate failure during the compressive mode. Figure 4.8 presents the typical stress–strain curves of the test specimens with shear failure. Generally, the slope of the graph slightly decreased when glass microballoons were added. From the graph, it can be observed that specimens TFSW-1 and TESW-1 had similar higher shear stress with higher loading force between 200 - 220 MPa and 3174-3175 N, respectively. The majority of test specimens exhibited shear failure of the foam during flexural testing. A small subset of the specimens failed because of de-bonding and local collapse of the GFRP skin; therefore, the shear failure was assumed to be the dominant failure mechanism for three-point bending tests.

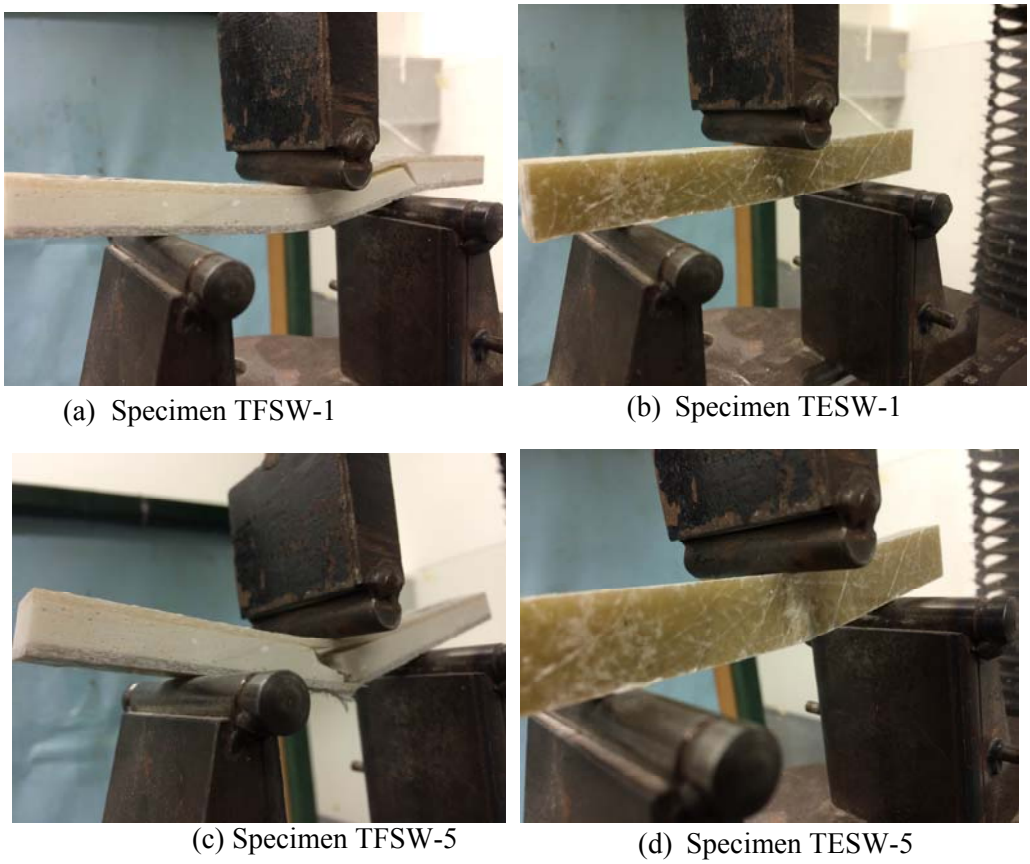

(a) Specimen TFSW-1 (b) Specimen TESW-1

(c) Specimen TFSW-5 (d) Specimen TESW-5

Figure 4.7: Representative failure of syntactic foam sandwich panels

The formula for the core shear ultimate strength could be determined by Equation (4.2), which was obtained from ASTM C393/C393M (ASTM, 2012). Furthermore, the formula for the facing stress could be derived using Equation (4.3). Hence, the calculated values explained the behaviour of the syntactic foam sandwich panel, as indicated in Table 4.4.

$$\tau_{ult} = \frac{F_{max.}}{(D + c)B} \tag{4.2}$$

$$\sigma_{fc} = \frac{F_{max.}S}{2t(D + c)B} \tag{4.3}$$

where $F_{max.}$ is the maximum force prior to failure (N); D is the thickness of the syntactic foam sandwich panels (mm); c is the core thickness (mm); t is the nominal facing thickness (mm); B is the width of the syntactic foam sandwich panels; and S is the span length (mm).

From Table 4.4, the ultimate stress, τ_{ult} and the facing stress, σ_{fc} increased with the highest thickness of sandwich panels, in particular the flatwise shear stress mode, for TFSW-1. By comparison, a different result was shown for the edgewise mode position for the TESW-5 event even though it was thicker than this specimen with τ_{ult} = 6.89 MPa and σ_{fc}= 258.46 MPa, respectively. This phenomenon is the failure mode that occurred, which resulted from a delamination between GFRP skin and syntactic foam core. It might be the case that the foam core, with a very thin layer of foam, remained adhered to the skin due to matrix de-bonding behaviour.

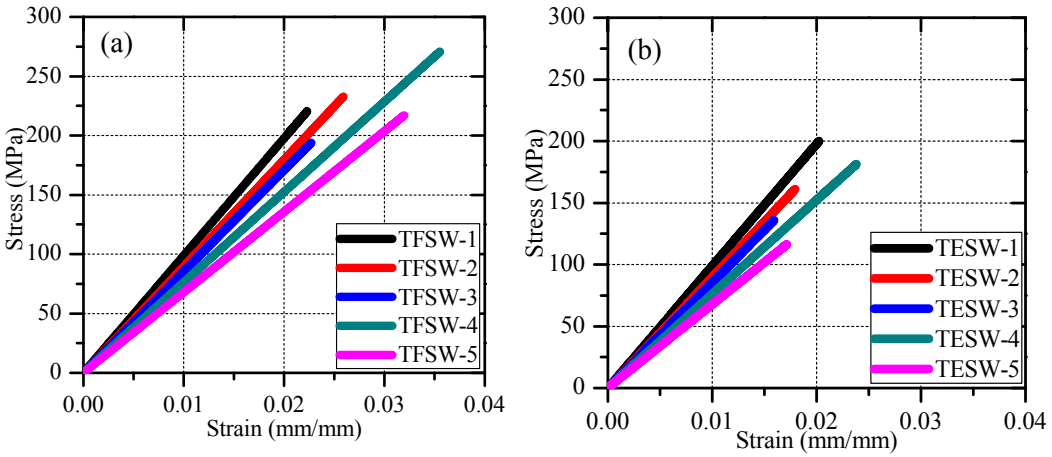

Figure 4.8: Representative result of the stress-strain curve for flexural strength; (a) Flatwise (b) Edgewise

Table 4.4: Three-point bending (TBP) flexural characteristics for the flatwise (TFSW) and edgewise (TESW) syntactic foam sandwich panels

Specimens	t	L	B	l	$\sigma_{max.}$	F_{max}	τ_{ult}	σ_{fc}
	mm	mm	mm	mm	MPa	(N)	(MPa)	(MPa)
TFSW-1	13.00	75	11.25	120	220	3174	11.29	423.29
TFSW-2	10.86	75	13.95	120	233	2807	9.71	364.11
TFSW-3	12.17	75	13.98	120	194	3570	10.08	377.92
TFSW-4	9.65	75	14.70	120	271	2785	9.88	370.33
TFSW-5	11.27	75	15.45	120	217	2989	9.20	344.95
TESW-1	13.30	75	11.80	120	200	3175	10.51	394.10
TESW-2	12.07	75	10.96	120	161	1924	7.59	284.55
TESW-3	14.60	75	12.40	120	136	2770	7.92	297.04
TESW-4	10.30	75	15.30	120	181	2135	7.12	266.93
TESW-5	14.80	75	11.14	120	116	2196	6.89	258.46

Note: t: Foam thickness, L: span length, B: Nominal width, l: Nominal length, $\sigma_{max.}$: Max. Stress, $F_{max.}$: Max. Load, τ_{ult}: Ultimate core shear strength, σ_{fc}: Facing Stress, E_m: Modulus of Elasticity

4.3.3.3 Flexural stiffness properties for syntactic foam sandwich panels

An evaluation of the flexural stiffness of the syntactic foam sandwich panels is determined using the flexural stiffness for flatwise equation, particularly for beams. The flatwise beam equation, which considers both the skin and core properties for the flexural behaviour of glue-laminated fibre composite sandwich beams (Manalo et al., 2010). Manalo et al., (2010) also introduced the flatwise beam sandwich panel equation for flexural stiffness (EI) is depicted in Equation (4.4), while the flexural stiffness for edgewise beams is shown in Equation (4) as follows:

$$EI_{flatwise} = \sum_{i=1}^{n}\left[\left(\frac{Bt_s^3}{12} + Bt_s d_s^2\right)E_{sk} + \left(\frac{Bt_c^3}{12} + Bt_c d_c^2\right)E_{co}\right] \quad (4.4)$$

$$EI_{edgewise} = \frac{nD^3}{6}\left(t_s E_{sk} + \frac{t_c}{2}E_{co}\right) \quad (4.5)$$

where B is the width of panel; t_s is the thickness of the skin; t_c is the thickness of the core; ds and dc are the distances from the centre of the skins and the core to the neutral axis of the glued section, respectively; E_{sk} and E_{co} are the moduli of elasticity of the skin and core, respectively; and D comprises the thickness sandwich panels, while n is the number of glue-laminated composite sandwiches. In this study, n =1 was fixed because there was only 1 layer, and dc = 0 at the centre of the core syntactic foam. All of the calculations were performed by assuming that there was no occurrence of the interlayer slip, and the laminated sandwich acted as a solid perfect bonding, or was directly mounted between the skin and the core to avoid the secondary effects on the syntactic foam sandwich panels. While the effective stiffness formula, EI effectiveness, which was derived from the deflection formula (Manalo et al., 2010). Furthermore, the effective stiffness of a syntactic foam beam using Equation (4.6) (Islam and Kim, 2007)as follows:

$$\mathrm{EI_{eff.}} = \frac{\mathrm{EI_{flatwise}}}{\mathrm{B}} \tag{4.6}$$

The TPB testing had a similar mechanism for simple supported beams to determine the deflection in this study. Hence, the deflection for a simple beam could be derived using Equation (4.7), which is commonly used for static mechanical engineering calculations.

$$\nu_{\mathrm{Def.}} = \frac{\mathrm{FS^3}}{48\mathrm{EI_{flatwise}}}, \nu_{\mathrm{Def.}} = \frac{\mathrm{FS^3}}{48\mathrm{EI_{edgewise}}} \tag{4.7}$$

where F is the force perpendicularly directed to the specimens; and S is the midspan. According to Islam and Kim (2007), the flexural modulus for beams can be determined by using Equation (4.8) as below;

$$E_{flex} = \frac{S^3 M}{4BD^3} \tag{4.8}$$

where M is the slope of the Load-Deflection graph. The resulting parameters E_{co}, $EI_{flatwise}$ and EI_{eff} are listed in Table 4.5.

From Table 4.5, the modulus of elasticity (E_{flex}) generally decreased when the glass microballoons content increased for the syntactic foam sandwich panels. This result

was observed when the thickness of the syntactic foam sandwich panels was thinner compared to all of the specimens, e.g., FLSW-4 had a lower stiffness (EI) and a lower effective stiffness (EI_{eff}) for both flatwise and edgewise positions.

Table 4.5. Predicted and calculated EI, EI_{eff}, flexural stiffness for the syntactic foam sandwich panels

Specimens	Modulus of Elasticity	Flexural Stiffness	Effective Stiffness
	E_{flex} (MPa)	EI (x 10^6 Nmm^2)	EI_{eff} (x 10^6 Nmm^2)
FLSW-1	972.08	16017600.17	1423786.68
FLSW-2	840.54	10012245.71	717723.71
FLSW-3	842.77	17942471.31	1283438.58
FLSW-4	686.65	6377686.12	415213.94
FLSW-5	637.85	8774060.80	567533.04
FESW-1	1288.17	23840673.95	2020396.10
FESW-2	1134.19	14572267.61	1329586.46
FESW-3	1171.28	30133449.99	2430116.93
FESW-4	578.76	6450756.01	421618.04
FESW-5	1051.17	25307707.61	2271787.04

The reduction was nearly 53% when compared for all stiffness values, and it had a significant effect on the syntactic foam sandwich panels as well. Shear deformation could have contributed to the total deformation of the composite syntactic foam sandwich panels in the flatwise position due to the decreased thickness ratio. Modulus of elasticity also varied with different levels of thickness of core syntactic foam. Generally, all of the specimen showed a decrease in the modulus of elasticity when glass microballoons were added as core syntactic foam. The result was that the highest E_{flex} led characterised by lower glass microballoon content with 2wt% for flatwise and edgewise specimen FLSW-1 and FESW-1. A similar result was also observed in the previous section for modulus elasticity stress-strain curve flexure properties. The decreasing of modulus in a flatwise position clearly indicated that the GFRP skin near the neutral axis of the section did not contribute as much stiffness as the outermost skin. There was no trend for edgewise modulus of elasticity but it could be seen that the thin core thickness had a lower modulus of elasticity belonging to FESW-4 at 578.76 MPa. This clearly shows that the modulus of elasticity in the flatwise and edgewise position was not only effected by core thickness but also by the glass microballoon content as its isotropic materials behaviour was adopted in the syntactic foam.

4.3.3.4 Load-Deflection properties for syntactic foam sandwich panels

The load and midspan deflection behaviour of the individual syntactic foam sandwiches under 3-point static bending is depicted in Figure 4.9. This demonstrates that the load of specimen FLSW-3 increased by nearly 3 times than other specimens with the load going up to final failure for both flatwise and edgewise positions. The deflection shows as being lower at 14 mm and 8.5 mm for flatwise and edgewise positions, respectively. This graph also illustrates that FLSW-3 demonstrated a higher load and extended the stretch by 35% when compared with other foams at 14 mm, and by 45% at 9 mm for flatwise and edgewise, respectively. There was an increase in the deflection proportional to an increase in the applied load, which may be due to the progressive failure of the non-horizontal skin thickness. Generally, the specimens failed at an applied load of between 2500 N to 3500 N for flatwise, and between 1900 N to 3100 N for an edgewise position, with a midspan deflection of 75 mm. The load of specimens for both flatwise and edgewise position FLSW-4, exhibiting lower load deflection failure, also increased linearly with the deflection from 19 to 21 mm but showed an approximate reduction in the stiffness at a load of between 2200 N to 2600 N due to the flexural tensile cracking of the core.

Additionally, Manalo et al., (2010) determined that tensile cracking occurred in the core when it was tested using edgewise testing of the sandwich panels. In this study, the deflection of the syntactic foam sandwich panels slightly increased when the stiffness and the sandwich thickness decreased. Furthermore, Islam and Kim (2007) determined that the low density of syntactic foam indicates strong results in the higher deflection for different starch to water ratios. However, Manalo et al., (2010) indicated that the load-deflection composite sandwich beams, tested in the flatwise position, failed due to the brittle and ductile properties of the sandwich panels. Similar to the syntactic foam sandwich panels, this study determined that the load-deflection increased when the glass microballoon content increased in a core material. Therefore, a significant effect on the properties of the core density as well as increased glass microballoon contents affected the sandwich panel fabrication of the syntactic foam.

In this study, all of the specimens demonstrated failure in brittle fracture mode, which was revealed at the end of testing in the elastic region for both flatwise and edgewise positions. The quality of specimen was justified by checking their brittle and ductility of the core syntactic foam. Ductility is one physical property which is the ability to maintain the plasticisation without cracks or fractures especially specimens 2 – 6wt%, while brittleness was occurred when added more glass microballoon (7-8 wt%). A similar trend was revealed by Maharsia et al., (2006), who fabricated a hybrid syntactic foam using epoxy resin as the matrix resin. The thickness of the core resulted in this specimen having still the highest strength among all of the specimens. The skin thickness for all of the specimens was on average only 2.0 mm; however, because the thickness of this foam is less than 10 mm, it may make it stronger than other foams. The maximum force generated at the top skin of the FLSW-4 specimen had a similar magnitude to that at the bottom skin through this extension. Based on a comparison among the different thicknesses, the following results can be observed. First, using a thicker foam core does not necessarily produce the highest pressure yield before fracture. Table 4.4 indicates that a thicker foam size between 10 -12 mm produces a lower force and is easier to fracture. However, a core foam size of less than 10 mm results in a significantly stronger force. Secondly, this phenomenon may also be attributed to variations in the porosity and number of voids in the syntactic foam. The number of voids and porosity can vary with the foam density.

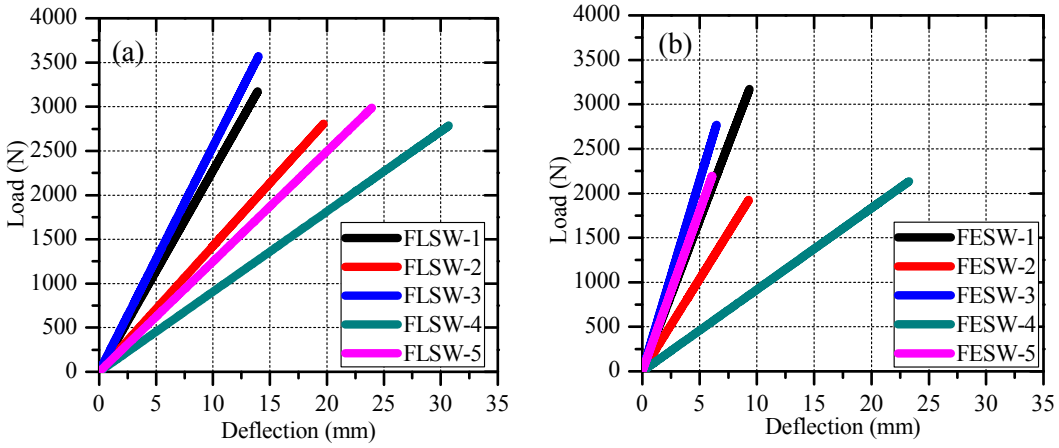

Figure 4.9: Representative graph for Load vs. Deflection; (a) Flatwise (b) Edgewise for syntactic foam sandwich panels

4.4 SEM micrograph

4.4.1 Effects on GFRP skins

A SEM observation of the fibre glass sheet as a skin was also performed in this study. Figure 4. 10 (a) illustrates an overview of a uni-directional fibre glass sheet embedded in vinyl ester resin as the matrix material. It is revealed that several sizes of fibre glass were cut and remained in the matrix resin. Furthermore, fractured and de-bonded fibres, matrix deformation, and de-bonded and crushed fibres were observed. Figure 4.10 (b) confirms the random orientations of the glass fibre sheet because both perpendicularly and longitudinally orientated fibres were observed. The SEM indicates that the direction of fibres tended towards the higher FGS skin, which was stronger in only one direction. Gupta et al., (1999) determined that a fibre orientation with two different directions recorded a better reflection incline in more than one direction. Relatively, this may be caused by the strength of syntactic foam, with or without fibres (Gupta et al., 1999). Additionally, this technique can drastically optimise the void contents in syntactic foam to 4% and result in a higher strength. Thus, it can be clearly demonstrated that fibres will increase the fracture toughness via the creation of an extensive structure and via de-bonding activity. This fibre orientation will lead to an increase in the stress field, which overlaps between the fibres, thus resulting in an enhanced plasticity of the fracture toughness.

4.4.2 Effects on the syntactic foam sandwich panels core

The compressive specimens were used to analyse the fracture microstructure mechanism in this study. Maharsia et al., (2006) used different types of microballoons to explain the mechanism fracture for final compressive testing. Sandwich panels with a lower glass microballoon content (2 wt.%) core, such as SCSW-1, resulted in a higher compressive strength, as indicated in Table 4.1. This result can also be observed in the SEM photograph in Figure 4.10(c), where the vinyl ester resin reacted as a plastic region embedded with fewer debris glass microballoons and void contents. The interfacial bonding between the glass microballoon and the matrix resin remained strong. The absence of debris indicates that a lower crushing and de-bonding phenomenon occurred after compressive testing. In this specimen, it is difficult to

determine the de-bonding between the filler glass microballoon and the matrix resin, and the connection between them remained strong. Based on SEM observations, de-bonding phenomenon was commonly occurred internally between glass microballoon and matrix resin, while core failure was detected at external surface due to poor adhesive between core and skin of the sandwich panels.

The compressive observation continued for specimens with increased glass microballoon content, particularly 4 – 8 wt.%, i.e., specimens SCSW-2 to SCSW-4. The compressive strength for these specimens decreased to nearly 50% of the value of those with lower glass microballoon contents, which was SCSW-1. The spreading of the debris and fractured glass microballoons is illustrated in Figure 4.10 (d). The syntactic foam was more brittle and had numerous pores, which attempted to include their debris into the broken glass microballoon and voids area. Additionally, whiskers from the matrix resin can be observed, including their twist hackle line. Furthermore, the mean plateau region for the compressive curve in Section 5.3.1 indicates that the plasticity of the matrix resin remained, thus achieving a maximum stress longer than the other specimens.

Figure 4.10 (e) depicts that the de-bonding between the filler glass microballoon and matrix resin occurred frequently. The number of crushed glass microballoons and debris kept increasing, as observed in SCSW-3. This phenomenon resulted in the highest number present in any fractured plan and increased the possibilities of crack bridging occurring in the syntactic foams. Azimi et al., (1996) discovered that the same characteristic occurred in hybrid syntactic foams. All of the fractured particles surrounded the glass microballoon and the cavity pore area (Azimi et al., 1996). Severe de-bonding of the glass microballoons was observed in Figure 4.10 (f), where nearly 80% de-bonding occurred for SCSW-5. Furthermore, this phenomenon resulted in a lower strength of compressive failure and difficulty in identifying their mean plateau, and the dissatisfaction modes of the syntactic foams became 48% lower than the highest strength value. The segregation of the entrapped air voids was observed severely in this specimen, which may have resulted in a reduction in strength as well.

4.4.3 Effects on the stiffness syntactic foam sandwich panels

The 3-point bending specimens were used to analyse the stiffness mechanism in this study, particularly specimen FLSW-4. An overview of the aggregates between the FGS skin and the cores for FLSW-4 is depicted in Figure 4.10(g). The figure clearly indicates that the FGS skin can join and stick to the syntactic foam core with minimal tolerance because both the flexural and effective stiffness had lower values of 6377686.12 x 10^6 Nmm^2 and 415213.94 x 10^6 Nmm^2, respectively. The advantages of this sandwich panel were related to the thickness of the cores, which resulted in the crack propagation between the skin and the core having less of an impact during flexural testing. Furthermore, Figure 4.10(g) indicates that the deflection of FLSW-4 withstood a higher force to failure at 3500 N with a deflection of 14 mm. This force was considered to be the highest among all of the specimens and achieved a bearing loading application. Shen and his team suggested that controlling the thickness of the foam and skin can improve the stiffness boundary condition (Shen et al., 2013). Using the higher magnification micrograph, Figure 4.10 (h) indicates that the aggregate size can be measured to be approximately 1-2 μm in size. This phenomenon may occur due to the degradation in the matrix material during the deformation and fracture processes in flexural testing. This result implies that during the loading process, most of the stress in the composite is withstood by the matrix material, the flexural cracking of which determines the composite failure.

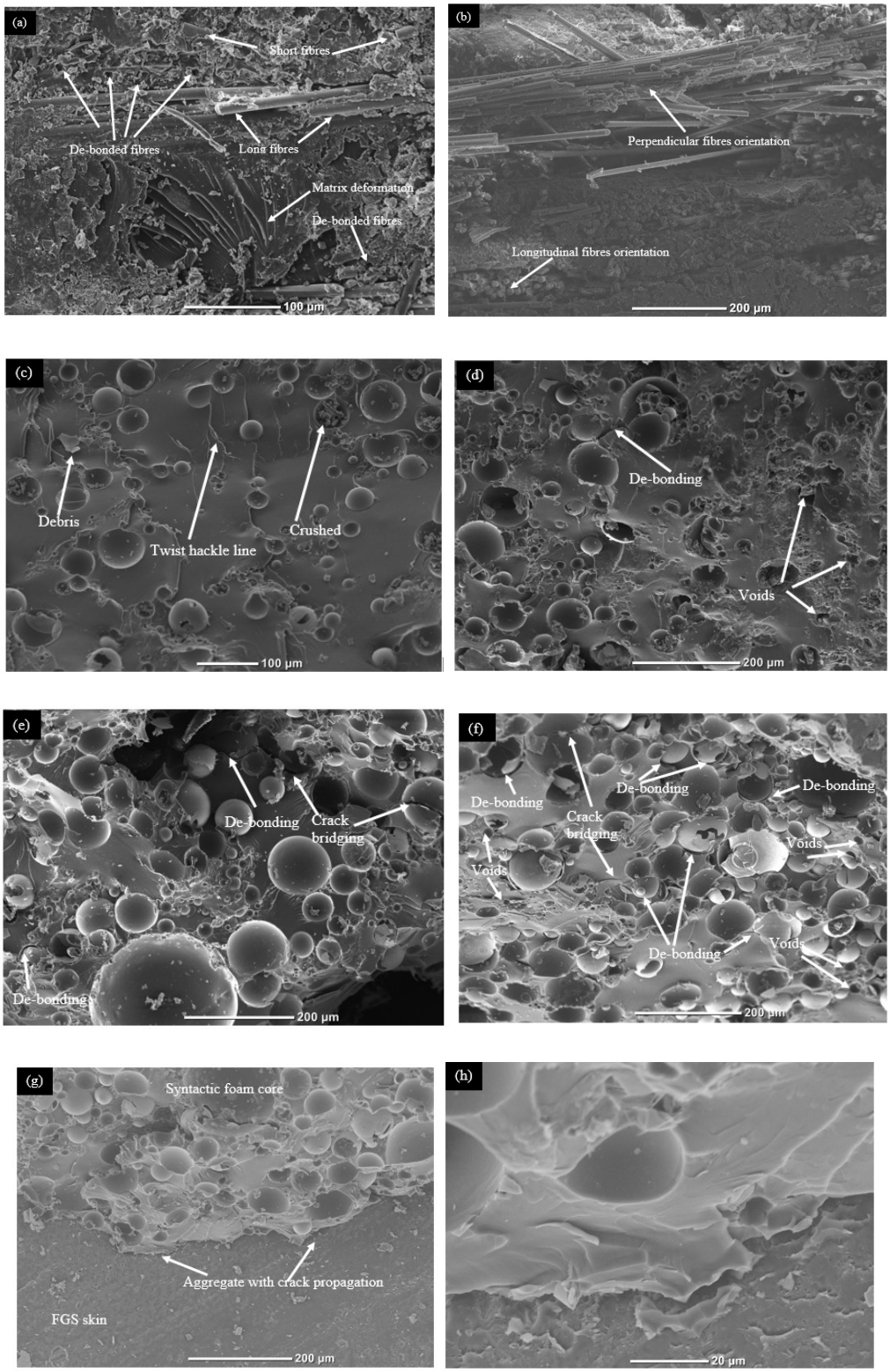

Figure 4.10 (a) Fractured fibres in the matrix resin; and (b) Different fibre orientation embedded in the matrix resin. Fractured glass microballoons distributed in the vinyl ester resin for (c) SCSW-1; (d) SCSW-2; (e) SCSW-3; (f) SCSW-5; (g) Crack propagation during flexural testing for FLSW-4; and (h) Higher magnification view identified the aggregate size of 1 -2 µm

4.5 Summary

The mechanical behaviour of the syntactic foam sandwich panels in relation with the properties of constituent materials was studied. The compressive strength of the sandwich panels was significantly affected by a low density core foam, particularly 2 wt.% of glass microballoon, as well as their modulus of elasticity and maximum stress value. The tensile failure of the syntactic foam sandwich panels was also significantly affected by lower glass microballoon contents (2 wt.%) and the core failure was clearly observed compared to other failure modes, such as cohesive and adhesive failure modes. The selection of the GFRP skin properties also contributed as a primary factor to the fabrication of sandwich panels, as well as the total density of the syntactic foam sandwich panels as a consideration. The flexural shear testing or three-point bending (TPB) of the syntactic foam sandwich panels indicated a higher strength when the glass microballoon contents were increased in the core materials compared to the un-symmetrical shear failure mode.

Chapter 5

Hygrothermal Analysis

5.1 Introduction

The multi-functional composites, which are called syntactic foams, have a broad range of applications either in structural engineering as a damper, insulator and as flame retardant materials. Practically all of them are used as core material in sandwich panels for marine structures (Kumar and Ahmed, 2015). Light weight material, as a way to save weight, is the main objective that needs to be achieved for all applications as mentioned before. Weight sensitivity is exhibited with higher specific properties for syntactic foams, which are made from cenospheres, glass microballoons or hollow particles mixing with polymeric resin, which may be promising in marine applications (Shivakumar et al., 2006, Zhang and Zhao, 2007, Zhang and Ma, 2009, Gupta et al., 2010, Samsudin, 2011, Swetha and Kumar, 2011, Tao and Zhao, 2012). All these kinds of applications are useful for a deep sea environment as buoyancy aid materials (Gupta and Woldesenbet, 2003). Hence, water absorption is highly recommended to be investigated in order to determine the viability of these applications. In most of syntactic foams porosity occurs, which contributes to, and affects the water or moisture absorption characteristics. It is very low moisture absorption coefficient, along with high compressive strength for closed porosity (Gupta and Woldesenbet, 2003). They also found that no significant difference in higher compressive strength for low temperature conditions when compared with dry specimens, while it has detrimental effects in higher temperature conditions for compressive strength when compared with dry specimens. Song and his team found that thermodynamic temperatures affected dynamic compressive behaviour when compared with environmental temperatures (Song et al., 2005). The electrical conductivity was increased in the process of de-ionised water absorption for temperatures ranging between 20 – 200^{o}C, for duration of 18 months (Sauvant-Moynot et al., 2006). In higher humidity, the weight gain increases for different types of water (Grosjean et al., 2009). The strength of phenolic syntactic foam decreased by almost 30% in total when weight gain occurred by 70% within 500 days (Sadler et al., 2009). Moisture absorption for different types of water

reduced flexural properties, particularly modulus of elasticity (Tagliavia et al., 2009). Based on the literature mentioned above, much of it is focused on the effects of the degradation mechanism and residual mechanical properties of syntactic foam for hygrothermal properties, hydrolytic ageing and moisture absorption at environmental temperatures. Moisture diffusion in polymeric composites has been shown to be governed by three different mechanisms (Munikenche Gowda T, 1999, Ben Daly H, 2007, Dash et al., 1999, Alam and Khan, 2006, Saha et al., 1999). The first mechanism involves diffusion of water molecules inside the micro gaps between polymer chains. The second mechanism involves capillary transport into the gaps and flaws, which interfaces between fibre and the matrix. The third mechanism involves transport of microcracks in the matrix arising from the swelling of fibres (particularly in the case of natural fibre composites) (Dhakal et al., 2007). Based on these mechanisms, absorption behaviour can be categorized into several types, including: (1) linear Fick's behaviour, where the moisture weight gains gradually attains equilibrium after a rapid initial take off; (2) pseudo-Fick's behaviour where the moisture weight gains never reached equilibrium after initial take off; (3) two-stage diffusion process with an abrupt jump in the moisture weight gains after initial take off; (4) rapid moisture gain results from filler/matrix de-bonding and matrix cracking; and (5) moisture weight gains follows a decrease trend after the initial take off, an irreversible process as a result of the leaching out of the material from the bulk, following chemical or physical breakdown (Ben Daly H, 2007).

In this study, the focus is on the effect of three types of water, namely Fresh Water (FW), Double Distil (DD) water, and Salt Water (SW), on mechanical properties such as compressive and tensile properties, with respect to water absorption changes. Investigations were also carried out to determine the effects of water absorption on the internal structure of syntactic foam composites with regards to the absence of voids and porosities.

5.2 Materials and experiment methods

5.2.1 Investigation of water absorption for different types of water

The ASTM 5229 was performed in this study to evaluate the behaviour of water absorption for syntactic foams in three different types of water. The specimens were immersed into three types of different aqueous environments originally taken from dam water, called Fresh Water (FW), Double Distil water (DD) which is performed with a two-time condensation process, and red sea salt dissolved with tap water, which is procured from Ocean Company to produce Salt Water (SW). The water was varied in terms of its conductivity due to different resources. The experiment was performed in room temperature (T: 25^{o}C) and all the specimens were immersed in a plastic container, as shown in Figure 5.1. The duration of the immersion process can be longer than 60 days for all specimens.

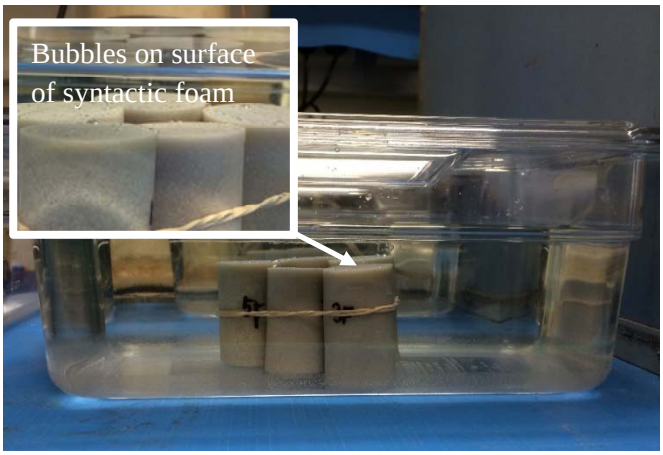

Figure 5.1: The immersion process of syntactic foam in plastic container

The density measurement for this experiment is similar as the one applied with a brief explanation in Chapter 3. The specimens weight was measured prior to determining the density of foam for two different durations, namely after being immersed for 30 days and 60 days for both types of compressive and tensile specimens. From the Rules of Mixture (ROM), the density of cavity porosity can be calculated by using the Equation (5.1),

$$\emptyset_p = 1 - \frac{\rho_{exp}}{\rho_{theo}} \qquad (5.1)$$

where ρ_{exp} and ρ_{theo} are the experimental density and theoretical density, respectively.

For the water absorption measurements, the specimens were withdrawn from the water, wiped dry to remove the surface moisture, and then weighed using an electronic balance accurate to 10^{-4} g to monitor the mass during the ageing process. The moisture content, W(t) absorbed by each specimen is calculated from its initial weight before, w_o and weight of the specimens at time *t*, w_t absorption as follows:

$$W(t) = \left[\frac{Wt - Wo}{Wo}\right] \times 100\% \quad (5.2)$$

Alomayria et al. (2014) used the Fick's behaviour for water absorption behaviour in their study. Therefore, the following formula has been used (Jang-Kyo Kim et al., 2005, T.P. Mohan and Kanny, 2011);

$$\frac{M(t)}{M(\infty)} = 4 \times \left(\frac{D \times t}{\pi \times h^2}\right)^{\frac{1}{2}} \quad (5.3)$$

where M(t) is the water content at time t, $M(\infty)$ is the equilibrium water content, D is the diffusion coefficient and h is the sample thickness. Diffusion coefficient, D is calculated from the slope of moisture content versus the square root of time by:

$$D = \pi \times \left(\frac{h}{4M_\infty}\right)^2 \times \left(\frac{M_2 - M_1}{\sqrt{t_2} - \sqrt{t_1}}\right)^2 \quad (5.4)$$

Assuming that the absorption process is linear at an early stage of immersion, times are taken at the beginning of absorption process, so that the weight change is expected to vary linearly with the square root of time. The actual specimens were measured before starting the water absorption process. The thicknesses of specimens are varied for both compression and tensile testing which are difficult to control during the fabrication process. An average value for thickness: compression is 50mm and tensile is 10mm, while an average surface area: compression is 600mm^2 and tensile is 90mm^2.

5.2.2 Investigation on hygrothermal properties for different types of water

The hygrothermal process began with preparation setup shown in Figure 5.2. The specimens were soaked in the aluminium bowl placed on the heater plate at a setting

temperature between 70-80°C, connected to the thermostat box controller. The thermocouple was also placed in the water to detect the temperature and was connected to the thermostat box controller. All the tensile and compression specimens were immersed in the bowl, as shown in Figure 5.2. During the hygrothermal process, the water needed to be topped up every two days because of the evaporation water condensation process. The specimens were taken out every day to measure the weight gain percentage. Similar to the water absorption process, all the specimens were wiped and dried before being placed on the digital weighing machine to determine their mass. This step was repeated for a duration of 30 days and 60 days before being changed to another type of water, before in turn proceeding to mechanical testing. The specimens that achieved the saturation weight at the end of the process would proceed to mechanical testing with the use of an MTS machine.

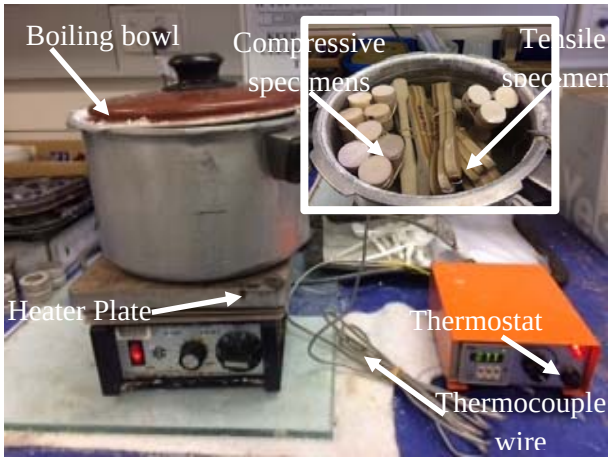

Figure 5.2: Setup equipment for hygrothermal syntactic foam

5.3 Results and discussion

5.3.1 Density property

5.3.1.1 Compressive Specimens

The density property for compressive water absorption, as shown in Figure 5.3, is comparable with theoretical values. Generally, all the specimens had a decreased density when immersed into the FW water, DD water and SW for different wt.% of glass microballoon content. In the graph, the density syntactic foam showed a slight drop when immersed in all water conditions. The dry specimens' density also decreased after more glass microballoon was added from 8wt%-10 wt.%, but their density was constantly maintained at a lower amount of glass microballoon from 2

wt.% - 6 wt.% as well. Among all the specimens, syntactic foam immersed in SW showed a higher density at 1231kgm^{-3}, while the dry specimen was at 1118kgm^{-3} for the 2 wt.% specimen. The density for FW showed a consistently decreased trend with a minimum density at 693 kgm^{-3}, belonging to specimen 10 wt.%. The error bar for graphs show the accuracy of the values for each standard deviation. Syntactic foam immersed in the water treatment changed the densities with a different wt.% of glass microballoon, due to absorbing water which is contributed to the different density. This is attributed to voids and pores contained in syntactic foam, since the water cannot enter the polymeric resin and also hydrate in between glass microballoon and resin, or in the glass microballoon itself. In addition, syntactic foam that had higher glass microballoon content sank in the bottom container, indicating that density was greater than 1gcm^{-3}, while the lower composition floated on the water surface. This also supports the idea that the effect of voids, porosity or debris glass microballoon in syntactic foam contributes to changes in density. Xua and Li (2011) also found that difference in moisture absorption is a possibility, when containing all these parameters.

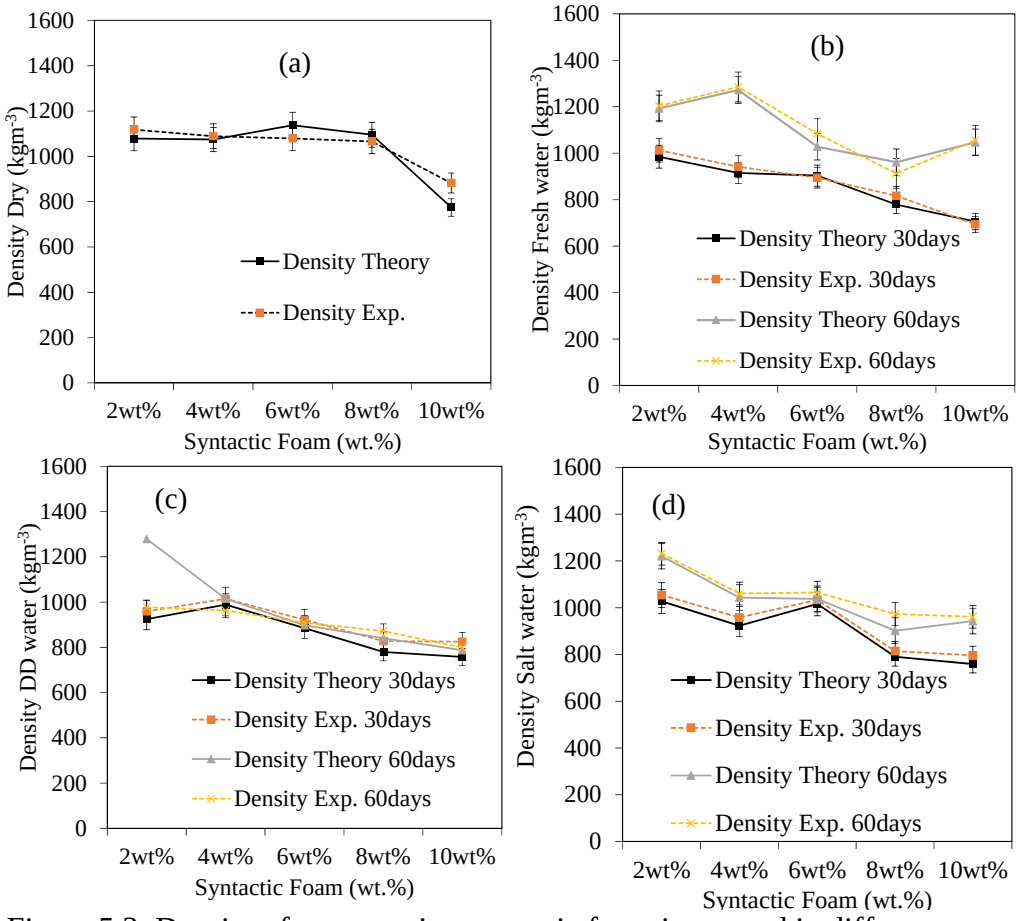

Figure 5.3: Density of compressive syntactic foam immersed in different water conditions; a) Dry specimen. b) Fresh Water (FW). c) Double Distil water (DD). d) Salt Water (SW)

5.3.1.2 Tensile Specimens

Figure 5.4 shows density properties for tensile water absorption at comparable theoretical values. It is revealed that for all the specimens, when immersed in FW water, DD water and SW for different wt.% of glass microballoon content, their density had decreased. From the graph, density syntactic foam shows a slight drop when immersed in all water conditions. Similar to compressive specimens, the dry specimens also showed their density decrease when glass microballoon contents were increased, especially specimen 10 wt.%. Among all the specimens, syntactic foam immersed in DD water showed a higher density 1280kgm^{-3} for 2 wt.% glass microballoon, while the FW specimen density was at 1272kgm^{-3} for 4 wt.% glass microballoon. The density for FW showed a trend consistently constant with a minimum density at 693 kgm^{-3} belong to the specimen with 10 wt.%. The measurement values are verified by examining their errors at each of graphs using error-bar methods. Generally, Figure 5.4 shows that error density measurement for submerged in water treatment is smaller compared with dry specimens. Syntactic foam that had been immersed in the water treatment changed density with a different wt.% of glass microballoon, due to the absorption of water, which is contributed to the different density. The longer it was immersed in the water, starting from day 1 to 30, then finishing at 60 days, the density increased tremendously. This occurred when the tensile specimen's shape was rectangular and it may have been much easier for the water to enter into the porosity and voids area, when compared with compressive specimens with a cylindrical shape.

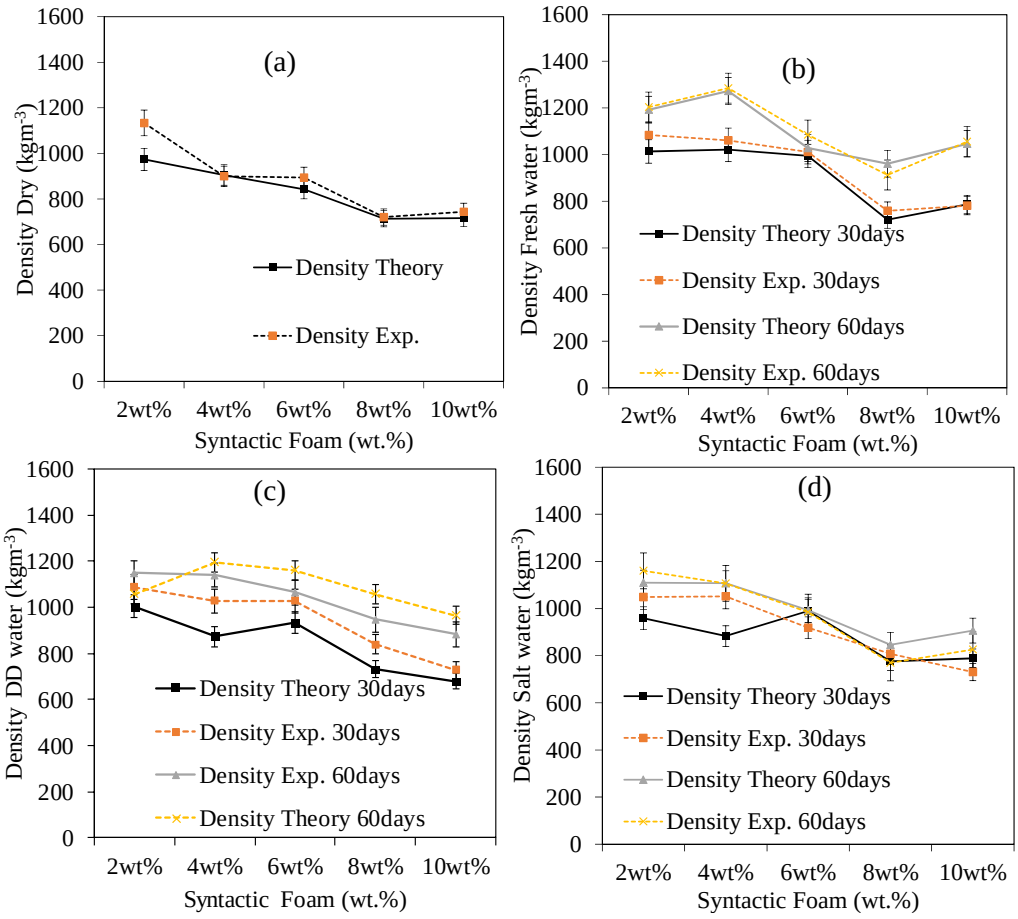

Figure 5.4: Density of tensile syntactic foam immersed in different water condition; a) Dry specimen. b) Fresh Water (FW). c) Double Distil water (DD). d) Salt Water (SW)

5.3.2 Room temperature water absorption of syntactic foam

5.3.2.1 Compressive Specimens

The water absorption graph for compression specimens of vinyl ester/fused borosilicate glass microballoon syntactic foam in room temperature (T: 25°C) is shown in Figure 5.5 (a) – (c). Each curve represents the average data of three specimens. This graph shows that absorbed water content increased with increasing immersion time. During the immersion process, the presence of water in the foam was due to the diffusion of water from the surface to the internal areas of syntactic foam. In this study, a quantitative measure of the water entrapped in the porosity is given as $W(t_1)$ where the water content associated with the first weight measurement taken at t_1 = day one of water immersion. Thus the maximum water absorption due only to diffusion in the matrix material W^m can be calculated as $W^s - W(t_1)$, which is also proposed by G. Tagliavia (2012), where W^s is the weight of specimen when an equilibrium condition

has been achieved. Table 5.1 (a) – (c) shows all these parameters related to porosity content for compressive specimens.

Table 5.1(a): Typical result for FW water absorption analysis of syntactic foam

Material Type	Max. W^s	$W(t_1)$	Max. W^m	Immersion time ($\sqrt{t}$)	Ratio ($\frac{W^m}{\sqrt{t}}$)
	%	%	%	$s^{1/2}$	(%/$s^{1/2}$)
SF2WC-F	0.65918	0.02942	0.62976	2352	0.0002678
SF4WC-F	0.81238	0.04916	0.76322	2388	0.0003196
SF6WC-F	1.17384	0.14394	1.02990	2477	0.0004158
SF8WC-F	1.47386	0.25897	1.21489	2613	0.0004649
SF10WC-F	1.92902	0.41905	1.50997	2726	0.0005539

Table 5.1 (b): Typical result for DD water absorption analysis of syntactic foam

Material Type	Max. W^s	$W(t_1)$	Max. W^m	Immersion time ($\sqrt{t}$)	Ratio ($\frac{W^m}{\sqrt{t}}$)
	%	%	%	$s^{1/2}$	(%/$s^{1/2}$)
SF2WC-D	0.68007	0.20989	0.38117	1972	0.0001933
SF4WC-D	0.60297	0.04529	0.55707	2160	0.0002579
SF6WC-D	1.01042	0.08775	0.92267	2357	0.0003915
SF8WC-D	1.34567	0.16267	1.18300	2380	0.0004954
SF10WC-D	1.56758	0.21987	1.34771	2471	0.0005454

Table 5.1(c): Typical result for SW water absorption analysis of syntactic foam

Material Type	Max. W^s	$W(t_1)$	Max. W^m	Immersion time ($\sqrt{t}$)	Ratio ($\frac{W^m}{\sqrt{t}}$)
	%	%	%	$s^{1/2}$	(%/$s^{1/2}$)
SF2WC-S	0.65725	0.07356	0.58369	2163	0.0002699
SF4WC-S	0.76821	0.12356	0.64465	2354	0.0002739
SF6WC-S	0.97110	0.21328	0.75782	2390	0.0003171
SF8WC-S	1.27061	0.22748	1.04313	2480	0.0004206
SF10WC-S	1.38515	0.39453	0.99062	2612	0.0003793

From Table 5.1(a) to (c), and compared with the Figure 5.5, FW and SW required longer immersion times for saturation with the highest times at 2471$s^{1/2}$ and 2612$s^{1/2}$, respectively, while DD specimens required a shorter time for immersion at maximum 2471$s^{1/2}$. In observing the ratios ($\frac{W^m}{\sqrt{t}}$) for systems with 2 -10 wt.% of glass microballoon, it can be noticed that they exhibited a slight increase in their results within the range between (0.0001933% - 0.0004206%), regardless of practice wall thickness and water environment. Based on the experiment, the contact surface area

between the matrix and the water involved in the diffusion was practically the same and water did not diffuse in glass microballoon particles. For the system with 10 wt.% of glass microballoon, DD water absorption had a high ratio when compared to all water treatment conditions. This may have contributed to the higher cavity/matrix porosity content for the first type, which allowed for larger contact surface areas and faster water diffusion, especially for larger composition glass microballoon content. G. Tagliavia (2012) suggested that specimens with a 60% volume fraction of hollow particles had the highest ratios, regardless of density and water condition, which is important in determining the water up take in the specimens.

Table 5.1(a) – (c) also shows the measured values of maximum W^m, for FW specimens, and this quantity spans the range 0.63 – 1.5% of the initial weight. As the weight percentage increased, W^m also increased for any water treatments, which led to an increase in the porosity content. This phenomenon allowed the water to become entrapped inside the pores cavity as well. The calculation of $\emptyset_p$is based on the overall weight of syntactic foam, therefore it is difficult to identify their size and location in the foam. This porosity may entrap the water or air as soon as the specimen is dipped in the water without any actual diffusion taking place. Figure 5.6 shows the estimation of density porosity content as a percentage in different water conditions. Among all water treatments, DD water had a higher percentage of porosity estimation compared with others from 4 – 9%.

The alkalisation of DD water allowed more water to intersect internally, and thus made a contribution to the porosity being exposed in an area of the syntactic foam. When comparing dry and FW water, the porosity content was not much different. The SW showed the porosity content also increasing from 2.8 – 4.8% when the glass microballoon in the syntactic foam was increased as well. In order to check the accuracy for water absorption (%), the error bar for all graphs was calculated and shows that on average it is still within the 0.25%.

Polymeric resin syntactic foam also showed plasticisation behaviour, which induced some chemical and physical modification; this could attract the water coming into the microstructure of the syntactic foam. This modification changed the physical properties of polymeric composite materials such as swelling, hydrolysis, lixiviation

and others (Lefebvre and V. Sauvant-Moynot, 2009). Lefebvre and Sauvant-Moynot (2009) found that water absorbed in the foam was subjected to irreversible ageing, with three mechanisms related to the material's parametric and behaviour: i) matrix resin hydration, ii) glass microballoon hydration, interface hydration, and iii) pores cavity filling with water.

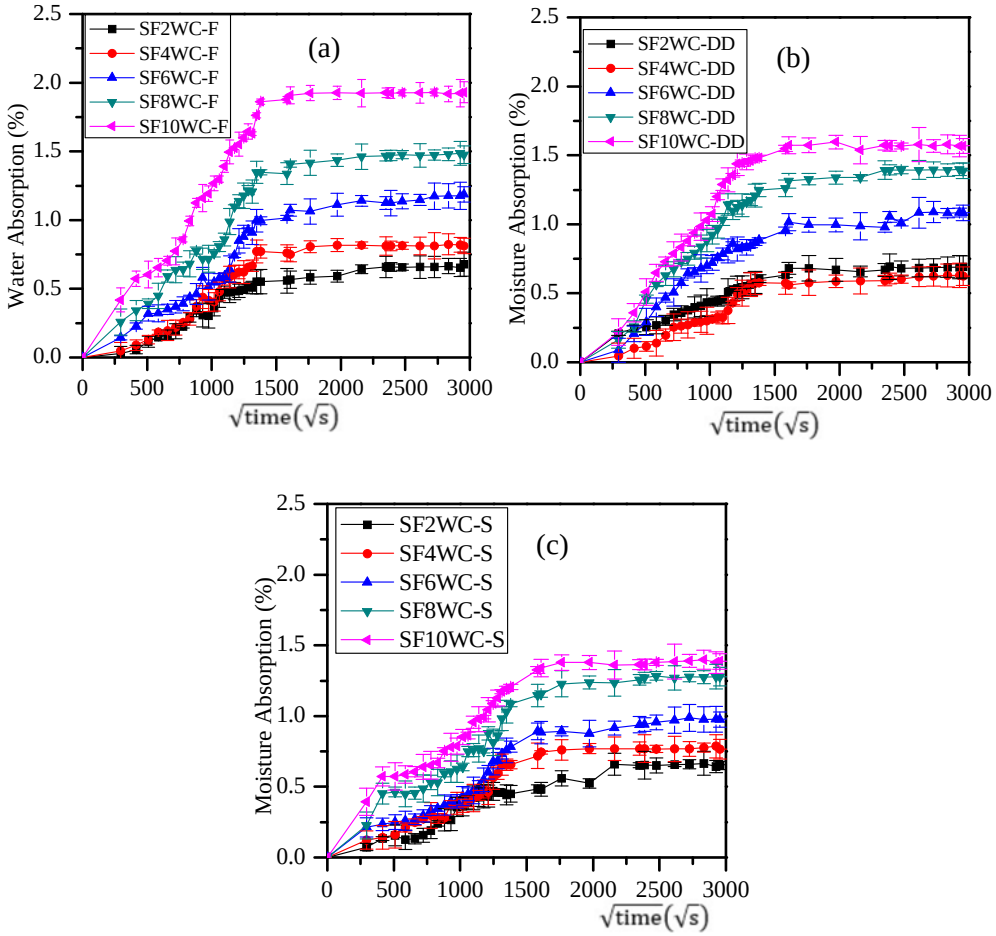

Figure 5.5: Water absorption for compression specimens immersed in different water conditions; a) Fresh Water (FW). b) Double Distil water (DD). c) Salt Water (SW)

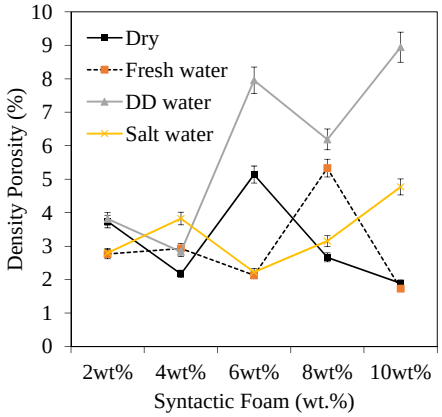

Figure 5.6: Estimation of density of porosity in different water conditions; Dry specimen, Fresh Water (FW), Double Distil water (DD) and Salt Water (SW)

5.3.2.2 Tensile Specimens

Figure 5.7 (a) – (c) shows the plot for water absorption at room temperature (T: 25^{o}C) for tensile specimens of glass microballoon syntactic foam. Each curve represents the average data of three specimens. This graph shows that the absorbed water content increased with increasing immersion time, until the equilibrium condition was achieved at 60 days' time duration. The individual error bar for all graphs also showed that the water absorption (%) for all specimens are not much different which is within the range from 0% to 1.5%. Similar to the compressive specimens, it was the intention to investigate the mechanism of water intake allowable into syntactic foam with the equation of water absorption, $W^s - W(t_1)$ which has also been explained in the previous paragraph. Table 5.2(a) – (c) shows all these parameters related to the porosity content for compressive specimens.

Table 5.2 (a): Typical result for FW water absorption analysis of syntactic foam

Material Type	Max. W^s	$W(t_1)$	Max. W^m	Immersion time ($\sqrt{t}$)	Ratio ($\frac{W^m}{\sqrt{t}}$)
	%	%	%	$s^{1/2}$	(%/$s^{1/2}$)
SF2WT-F	1.7414	0.16169	1.57971	2180	0.0007246
SF4WT-F	2.3527	0.34392	2.00878	1905	0.0010545
SF6WT-F	3.08634	0.41221	2.67413	1950	0.0013713
SF8WT-F	4.57965	0.56573	4.01392	2180	0.0018412
SF10WT-F	5.08716	0.65009	4.43707	1764	0.0025153

Table 5.2 (b): Typical result for DD water absorption analysis of syntactic foam

Material Type	Max. W^s	$W(t_1)$	Max. W^m	Immersion time ($\sqrt{t}$)	Ratio ($\frac{W^m}{\sqrt{t}}$)
	%	%	%	$s^{1/2}$	(%/$s^{1/2}$)
SF2WT-D	2.38990	0.22804	2.16186	2240	0.0009651
SF4WT-D	3.79800	0.43132	3.36668	2477	0.0013592
SF6WT-D	4.70429	0.71120	3.99309	2483	0.0016082
SF8WT-D	6.95298	0.75768	6.19530	2450	0.0025287
SF10WT-D	8.01366	1.04421	6.96945	2645	0.0026350

Table 5.2 (c): Typical result for SW water absorption analysis of syntactic foam

Material Type	Max. W^s	$W(t_1)$	Max. W^m	Immersion time ($\sqrt{t}$)	Ratio ($\frac{W^m}{\sqrt{t}}$)
	%	%	%	$s^{1/2}$	(%/$s^{1/2}$)
SF2WT-S	2.27251	0.26739	2.00512	2424	0.0008272
SF4WT-S	2.65509	0.39199	2.26310	2579	0.0008775
SF6WT-S	2.95429	0.72097	2.23332	2575	0.0008673
SF8WT-S	3.79707	1.06179	2.73528	2520	0.0010854
SF10WT-S	4.58175	1.54066	3.04109	2494	0.0012194

Results from Table 5.2 (a) to (c) compared with Figure 5.6, where the specimens were immersed in DD and SW have the highest saturation with time on 2645s1 / 2 and 2494s1 / 2, respectively. FW specimens required a shorter time for immersion at a maximum of $1764s^{1/2}$ when the glass microballoon content was increased in syntactic foam. The duration of 100 days showed that the water absorption mechanism produced the equilibrium trend between water gain and $(\sqrt{t})$ for all syntactic foam. As a general trend, it can be noticed that in syntactic foams weight gains were higher for DD water as compared with FW and SW water. A larger scattering in the obtained data was revealed for all the tested syntactic foam composition immersed in FW water, including the equilibrium being achieved faster than others. In practice, as the weight percentage of glass microballoon increases, the water uptake also increased. Therefore, the syntactic foam density was expected to have a prominent effect on the weight gain trend because the porosity and voids contents may have absorbed the water inside of them. The glass did not absorb water and the effect of weight gained of any water filling in the pores was eliminated by subtracting the first weight measurement. In this case, the higher composition of glass microballoon specimen's experience with the cavity pores occurred because much glass debris caused the water uptake to increase. This also happened due to the matrix-particle interface area (G.Tagliavia et al., 2012). They also found poor interfacial bonding between matrix and filler during SEM observation. Therefore, the higher composition led to having a higher interface area.

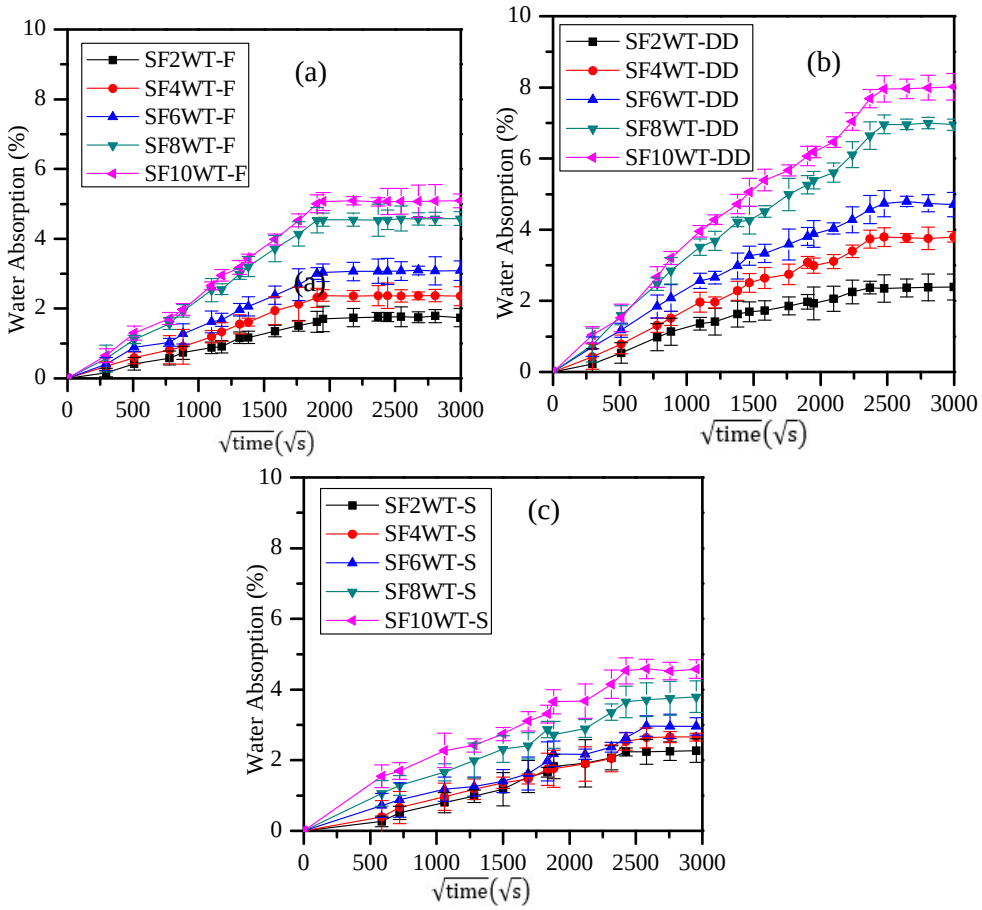

Figure 5.7: Water absorption for tensile specimens immersed in different water conditions; a) Fresh water (FW). b) Double distil water (DD). c) Salt water (SW)

5.3.3 Hygrothermal properties of syntactic foam

5.3.3.1 Compressive Specimens

Hygrothermal trends for all compressive syntactic foam in high temperatures (T: 70°C) are shown in Figure 5.8 (a) – (c). The values shown in this Figure 5.8 are average values based on water absorption by a minimum of three specimens for each composition under each type of water condition. Each curve represents the average data of three specimens. This graph shows that the absorbed water content increased with an increase in immersion time until it achieved the equilibrium condition. Figure 5.5 shows that the equilibrium of water absorption in room temperature can be achieved at $1500s^{1/2}$. However, it took a much longer time at 70°C to attain an equilibrium system, such as that of FW at $2500s^{1/2}$. Generally, a large difference in the water absorption tendency could be seen with change in temperature. For example, in room temperature condition, DD type water absorption was less than 1.6%. But at a high temperature, this increased to 14% maximum water absorption in the syntactic

foam, which means an approximate 6-7 fold for this specimen. Gupta and Woldesenbet (2003) also found that water absorption increased at a high temperature between 5 – 10 fold when immersed in DI in SW conditions. These phenomena can be verified with investigation on their error bar for all graphs. In previous analysis, shows the variation is not much different but when hygrothermal analysis, it is show gaps of error is bigger particularly in double distil water and salt water.

In Table 5.3(a) to (c), when compared with Figure 5.8, DD and SW required longer immersion times for saturation with longest times at $2954s^{1/2}$ and $2998s^{1/2}$, respectively. The data also shows that the percentage of water absorption increased almost 7 times to achieve the equilibrium system in hot water conditions, especially for FW specimens. This is evidence that a higher number of porosity and voids occurred in the syntactic foam, and was present near the surface of the syntactic foam, after it had opened its surface area. Gupta and Woldesenbet (2003) also reported that this phenomenon might be due to the strength of filler with different levels of wall thickness. Therefore, a higher (wt.%) of glass microballoon in syntactic foam contributed more to the matrix-inter facial bonding results (W^m) for all specimens, for example 10wt.% composition in all water treatments.

Table 5.3(a): Typical result for FW hygrothermal analysis of syntactic foam

Material Type	Max. W^s	$W(t_1)$	Max. W^m	Immersion time ($\sqrt{t}$)	Ratio ($\frac{W^m}{\sqrt{t}}$)
	%	%	%	$s^{1/2}$	$(\%/s^{1/2})$
SF2WCH-F	2.15378	0.26666	1.88712	1972	0.0009570
SF4WCH-F	8.35421	0.76653	7.58768	2200	0.0034489
SF6WCH-F	8.50674	0.50031	8.00643	2388	0.0033528
SF8WCH-F	14.95858	0.85576	7.65098	2834	0.0026997
SF10WCH-F	14.72946	0.60691	14.12255	1727	0.0081792

Table 5.3 (b): Typical result for DD hygrothermal analysis of syntactic foam

Material Type	Max. W^s	$W(t_1)$	Max. W^m	Immersion time ($\sqrt{t}$)	Ratio ($\frac{W^m}{\sqrt{t}}$)
	%	%	%	$s^{1/2}$	$(\%/s^{1/2})$
SF2WCH-D	1.13456	0.34733	0.78723	2613	0.0003013
SF4WCH-D	4.0425	0.48518	3.55732	2726	0.0013050
SF6WCH-D	8.03452	1.02652	7.00800	2835	0.0024720
SF8WCH-D	13.21456	1.43501	11.77955	2924	0.0040286
SF10WCH-D	9.02783	0.72755	8.30028	2954	0.0028098

Table 5.3(c): Typical result for SW hygrothermal analysis of syntactic foam

Material Type	Max. W^s	$W(t_1)$	Max. W^m	Immersion time ($\sqrt{t}$)	Ratio ($\frac{W^m}{\sqrt{t}}$)
	%	%	%	$s^{1/2}$	$(\%/s^{1/2})$
SF2WCH-S	1.73542	0.15234	1.58308	2385	0.0006638
SF4WCH-S	7.44368	0.70502	6.73866	2475	0.0027227
SF6WCH-S	6.45632	0.55346	5.90286	2615	0.0022573
SF8WCH-S	6.82311	0.55408	6.26903	2832	0.0022136
SF10WCH-S	8.81456	0.83121	7.98335	2998	0.0026629

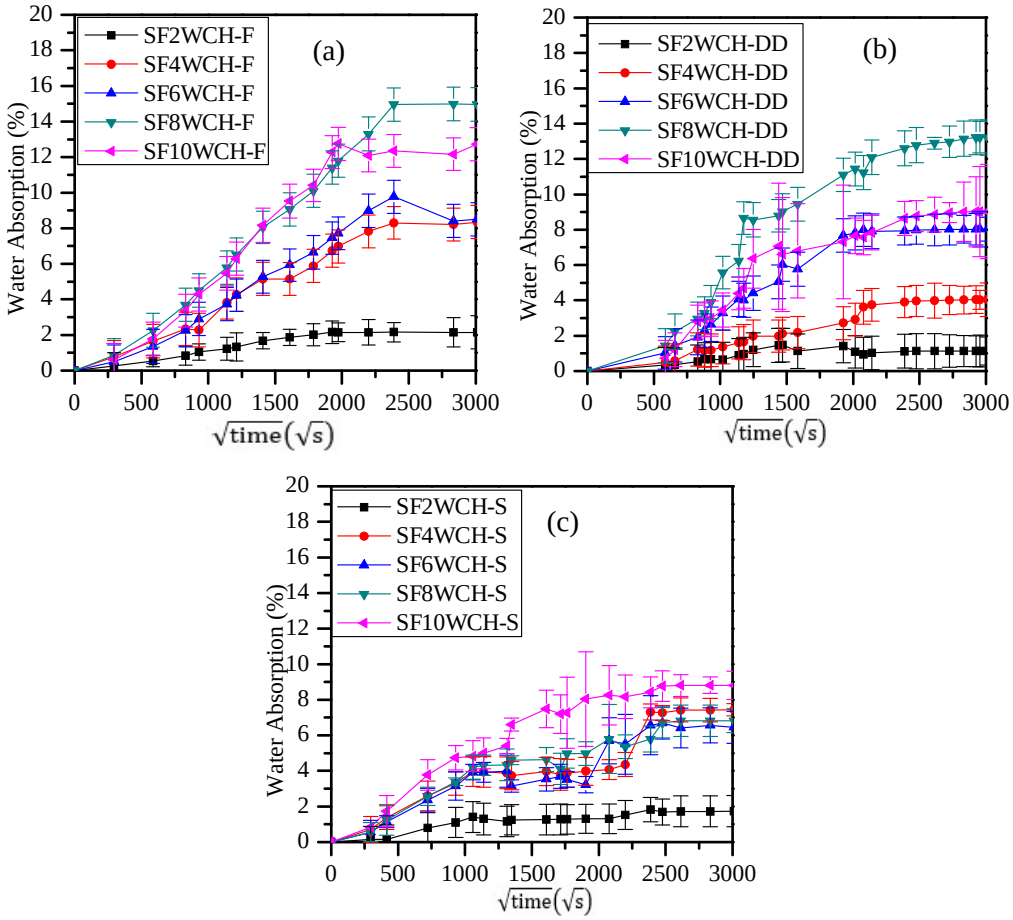

Figure 5.8: Hygrothermal for compressive specimens immersed in different water conditions; a) Fresh Water (FW). b) Double Distil water (DD). c) Salt Water (SW)

5.3.3.2 Tensile Specimens

Similar results have also been reported in tensile hygrothermal specimens as shown in Table 5.4 (a) – (c). All specimens showed an increased percentage of water absorption, almost 5 – 7 times as much, if compared at room temperature conditions. This was attributed to their physical properties and mechanical properties as well. The

immersion time to achieve the equilibrium took longer for all specimens with 10 wt.% of glass microballoon content at 2910$s^{1/2}$. Similar to compression specimens, the gap for error bar was also found bigger for tensile specimens. In terms of physical properties, the investigation into water diffusion in polymeric resin is elaborated on in the next paragraph. The prediction of the water uptake mechanism should involve a model such as the Fick's model. The mechanical properties also contributed to the different weight gained in the syntactic foam for the hygrothermal condition, such as the thin wall glass microballoon that fractured easily, thereby creating additional space for water to accumulate.

Table 5.4(a): Typical result for FW hygrothermal analysis of syntactic foam

Material Type	Max. W^s	$W(t_1)$	Max. W^m	Immersion time ($\sqrt{t}$)	Ratio ($\frac{W^m}{\sqrt{t}}$)
	%	%	%	$s^{1/2}$	(%/$s^{1/2}$)
SF2WTH-F	9.02611	1.54673	7.47938	2511	0.0029786
SF4WTH-F	14.67463	2.23415	12.44048	2596	0.0047922
SF6WTH-F	25.2426	3.54672	21.69588	2678	0.0081015
SF8WTH-F	32.35706	3.43520	28.92186	2757	0.0104903
SF10WTH-F	37.15931	3.87659	33.28272	2910	0.0114374

Table 5.4 (b): Typical result for DD hygrothermal analysis of syntactic foam

Material Type	Max. W^s	$W(t_1)$	Max. W^m	Immersion time ($\sqrt{t}$)	Ratio ($\frac{W^m}{\sqrt{t}}$)
	%	%	%	$s^{1/2}$	(%/$s^{1/2}$)
SF2WTH-D	4.67843	0.88797	3.79046	2612	0.0014512
SF4WTH-D	17.11231	3.44563	13.66680	2666	0.0051263
SF6WTH-D	22.22341	5.33241	16.89100	2731	0.0061849
SF8WTH-D	21.00112	1.00342	19.96692	2835	0.0070430
SF10WTH-D	36.88796	6.99806	29.88980	2741	0.0109047

Table 5.4(c): Typical result for SW hygrothermal analysis of syntactic foam

Material Type	Max. W^s	$W(t_1)$	Max. W^m	Immersion time ($\sqrt{t}$)	Ratio ($\frac{W^m}{\sqrt{t}}$)
	%	%	%	$s^{1/2}$	(%/$s^{1/2}$)
SF2WTH-S	7.59803	1.54321	6.05482	2369	0.0025559
SF4WTH-S	16.13456	2.54362	13.59094	2460	0.0055248
SF6WTH-S	22.22345	4.23452	17.98893	2562	0.0070214
SF8WTH-S	24.25463	3.89765	20.35698	2710	0.0075118
SF10WTH-S	30.11257	4.89765	25.21492	2820	0.0089415

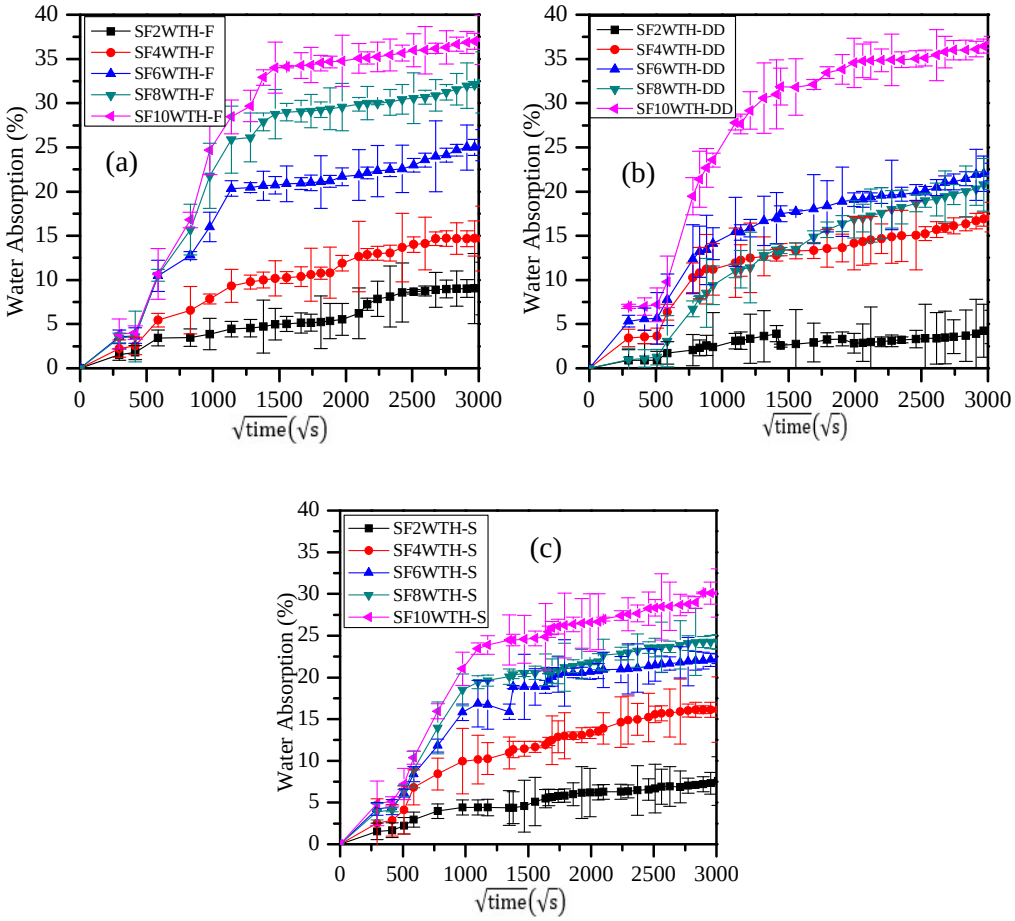

Figure 5.9: Hygrothermal behaviour for tensile specimens immersed in different water conditions; a) Fresh Water (FW). b) Double Distil water (DD). c) Salt Water (SW)

5.3.4 Diffusion parameters of syntactic foam

5.3.4.1 Coefficient of diffusion, D

In this study, the slope in Equation (5.4) was calculated from the first time equilibrium was achieved, and the diffusion coefficient D, calculated from experiment data, is tabulated in Table 5.5 (a). Water diffusivity in the foams is generally higher in FW when compared to other water conditions. This is comparable with increasing the glass microballoon content in syntactic foam as well, when the diffusivity value is increased for composites containing higher porosity content. Specimens SF8WT and SF10WT had large gaps with 3 times higher D values when compared with the lower glass content in the FW condition. However, D values for all compositions were slightly smaller in the SW condition, even though the glass microballoon content was increased. The reason for such a large discrepancy could be attributed to the high

matrix porosity content of SF8WT and SF10WT (see Table 5.1 and 5.2 for both compressive and tensile specimens). This is the cause of the large value for Max. W^m in FW and DD water conditions.

Similar results have been detected when the specimens were immersed in a high temperature (T:70^{o}C) for the hygrothermal condition. Generally, the water diffusion coefficient, D was increased for all water systems in a high temperature condition. It was revealed that D had a higher value for specimens SF8WT and SF10WT when immersed in both of FW and DD conditions (see Table 5.4 (b)).

Table 5.5(a): Typical result for diffusion coefficient, D water absorption in room temperature

Diffusion property	SF2WT (x 10^{-9} mm^2/s)		SF4WT (x 10^{-9} mm^2/s)		SF6WT (x 10^{-9} mm^2/s)		SF8WT (x 10^{-9} mm^2/s)		SF10WT (x 10^{-9} mm^2/s)	
	D	CoV	D	CoV	D	CoV	D	CoV	D	CoV
FW	6.94	0.31	17.37	0.25	17.23	0.46	24.08	0.02	58.03	0.14
DD	5.70	0.74	6.40	0.86	2.11	0.43	36.83	0.28	46.80	0.09
SW	4.25	0.06	3.83	0.24	1.31	1.04	1.13	0.58	14.86	1.23

*CoV: Coefficient of variance

Table 5.5(b): Typical result for diffusion coefficient, D hygrothermal water absorption temperature

Diffusion property	SF2WT (x 10^{-9} mm^2/s)		SF4WT (x 10^{-9} mm^2/s)		SF6WT (x 10^{-9} mm^2/s)		SF8WT (x 10^{-9} mm^2/s)		SF10WT (x 10^{-9} mm^2/s)	
	D	CoV	D	CoV	D	CoV	D	CoV	D	CoV
FW	7.85	0.41	13.57	0.21	15.21	0.05	35.71	0.01	67.63	0.22
DD	6.45	0.23	5.95	0.75	5.88	0.51	57.36	0.54	61.52	0.10
SW	3.22	0.14	2.11	0.31	7.42	0.01	4.34	0.51	21.73	0.66

Table 5.5 (a) and (b) shows a higher diffusion coefficient, D and a maximum of water absorption, W^m, if immersed into FW, followed by DD water and SW conditions. The reduction of these values, particularly the SW condition, were due to changes in the main physicochemical sources in addition to the specimen surface hydration. A similar reduction of D values in SW was also reported by G.Tagliavia et al., (2012) when a different composition of glass microballoon content was used in syntactic foam. This contributes to the global amount of water absorption and the preponderance of each mechanism depends on ageing conditions, and the durability of each component. In details, for foam immersed in SW condition, because the ionic species of salt are larger in size than those of normal water, the presence of salt ions in the water interferes with the diffusion of water in the foam, and ionic species of the salt have a much slower

diffusion rate compared with that of water. The occupancy of pores in the foam may further reduce the diffusion rate in the foam particularly for the higher glass microballoon content syntactic foam. Xua and Li (2011) have also reported that the diffusion rate is slower in salt water condition when compared with rain water, with a difference of 0.34 % in water absorption of glass microballoon/SMP resin. A similar finding was also revealed by Gupta and Woldesenbet (2003), who noted that deposition of salt may give allowance for the pores to be occupied in the foam and contribute to slower D values. However, for syntactic foams which are immersed in FW and DD conditions, the water uptake is more than the SW condition. This is because in chemistry knowledge, both waters were enriched with a lot of nutrients in organic ions such as NO_3^-, SO_4^{2-}, F^-, NH_4^+, Ca^{2+}, Mg^{2+}, Na^+, K^+) and organic species (CH_3COO^-, $HCOO^-$, $CH_2(COO)_2^{2-}$, $C_2O_4^{2-}$, as reported by Song and Gao (2009). The water resources from rain contains more aggressive ions that may easily hydrate the polymer matrix in the syntactic foam (Song and Gao, 2009). Hence, a larger amount of organic material will be deposited in the open pores, causing a greater weight gain than that of smaller inorganic ions in SW.

5.3.4.2 Fick's Law of syntactic foam

Fick's law was applied in this study in order to explain the behaviour of syntactic foam when immersed in the different types of water conditions, either in room temperature (T:25^{o}C) or hygrothermal temperature (T: 70^{o}C). By using the Equation (5.3), the graph was plotted between non-dimensional parameters, $M(t)/M(\infty) - D_t/h^2$ for y-axis and x-axis, respectively. Figure 5.10, Figure 5.11 and Figure 5.12 show the representative results for character of syntactic foam by using Fick's law approached immersed in FW, DD and SW water conditions for compression specimens. For all compositions of syntactic foam (2wt.% - 10 wt.%), it can be seen that the experimental data were in good agreement with Fick's law. As one can see, all materials showed an almost linear relationship between water absorption and the square root of the immersion time at the beginning of the absorption process. Among all specimens in FW, SF4WT-FW take longer to absorb the water and to achieve the equilibrium system, at water absorption 0.996. The SF2WT-FW specimen showed the dimensionless D_t/h^2 started at an earlier stage with 0.3. Specimens SF8WT-FW and SF10WT-FW showed lower water absorption rates of less than 0.993, which showed

the presence of cavity porosity to discard the water coming inside of the syntactic foam to achieve the equilibrium system. The error for Fick's law for all graph showed below the range of 1% but the data almost scatted in all conditions.

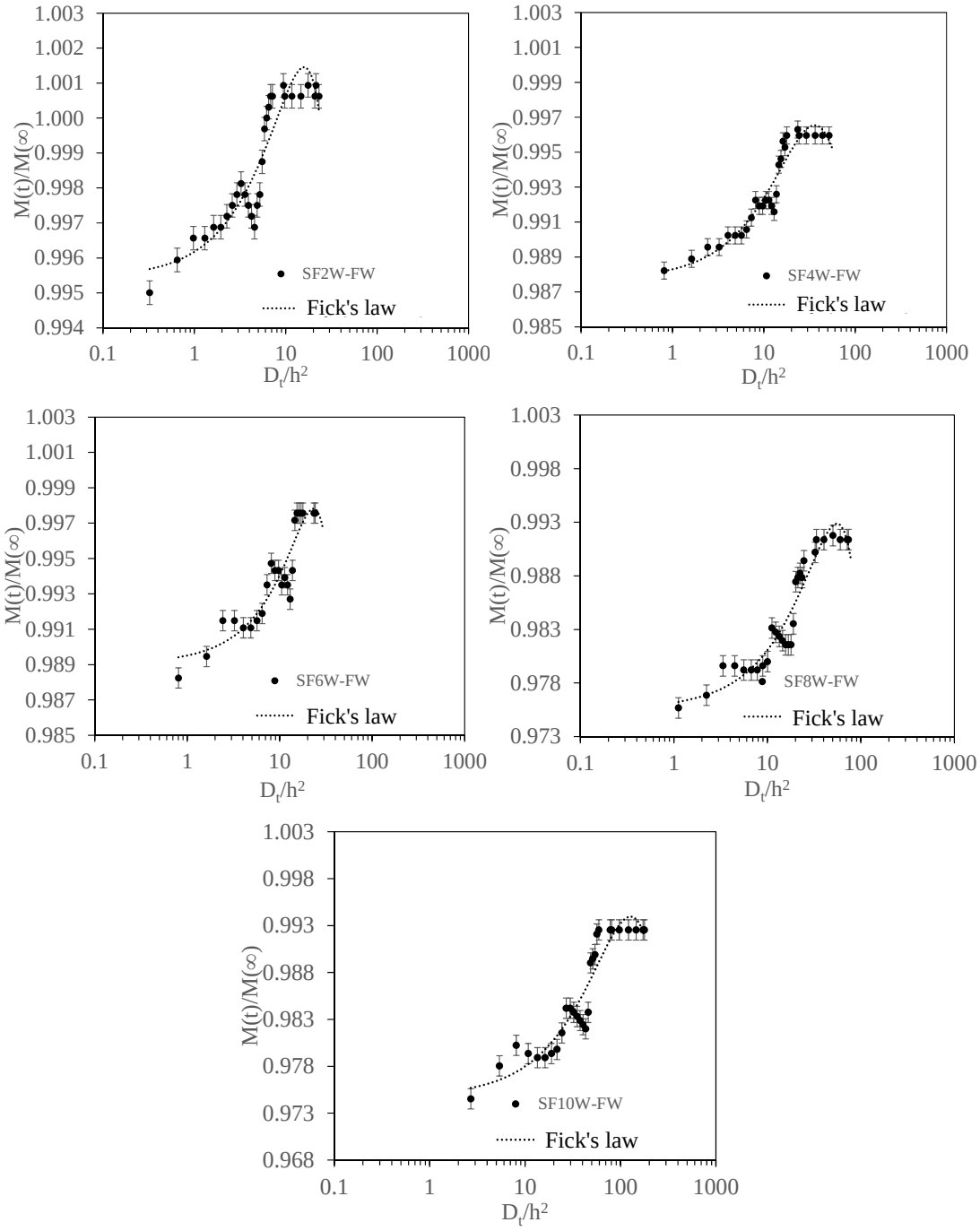

Figure 5.10: Correlation of FW experimental results of syntactic foam based composites with Fick's law

Based on Figure 5.11, the results were compared with Fick's law to explain the behaviour of syntactic foam composites immersed in DD water. Generally, the slope

of the graph was linear at the beginning of the process of water absorption in room temperature. Among all the specimens, SF8WT-DD and SF10WT-DD took longer to get to a saturated condition when immersed in DD water. This delay might be due to the presence of porosity content in syntactic foam, which contributed to the content of glass microballoon. The data also showed a scattering of a similar trend, in particular a 0.991 to 0.999 weight ration among of them. Therefore, the saturation time could be achieved when the weight gained was revealed at 0.999 to 1.005. Specimen SF6WT – DD showed that the dimensionless diffusion rate was faster than others at 0.1.

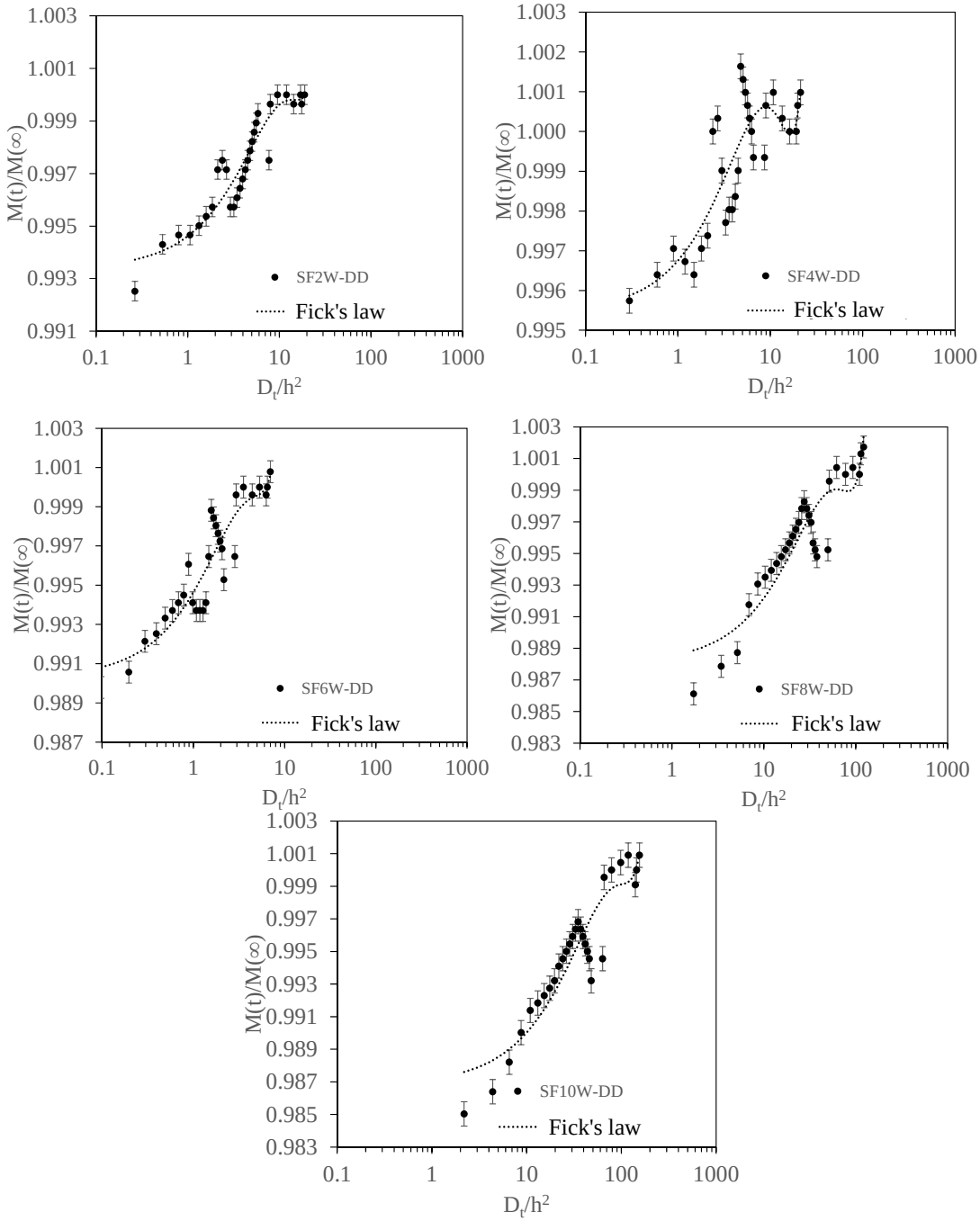

Figure 5.11: Correlation of DD experimental results of syntactic foam based composites with Fick's law

The diffusion rate for the salt water condition (SW) syntactic foam is show in Figure 5.12. Specimens SF6WT-S and SF8WT-s showed their diffusion rate was faster than others at 0.1. Specimen SF8WT-S also showed a shorter diffusion rate to achieve the equilibrium system starting at 2. Furthermore, specimens SF2WT-S and SF4WT-S showed their diffusion rates took longer to achieve the saturated condition at 70. Kumar and Ahmed (2015) also found that the D_t/h^2 value is between 0.01 - 1 for syntactic foam sandwich composites.

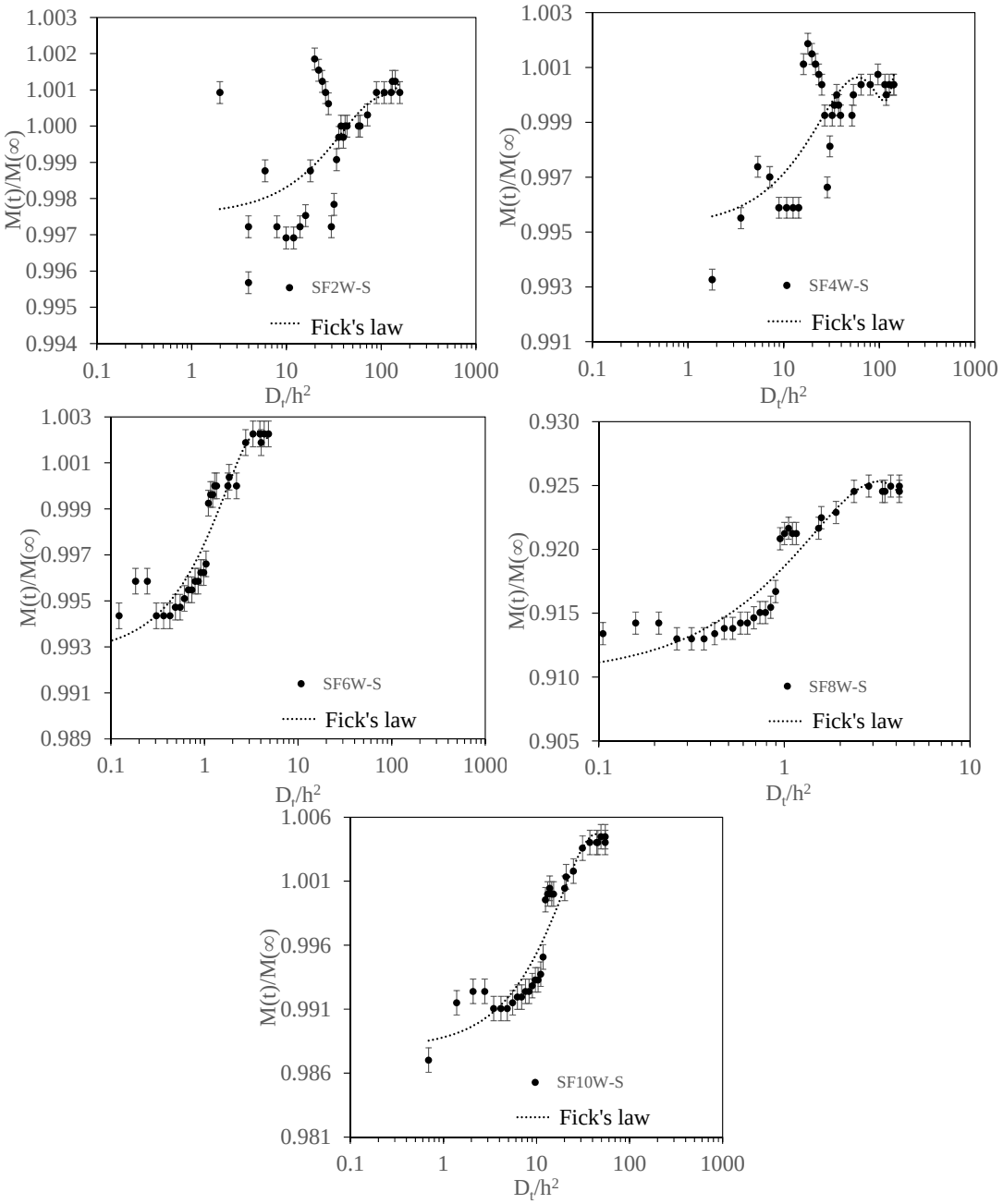

Figure 5.12: Correlation of SW experimental results of syntactic foam based composites with Fick's Law

5.3.5 Effect of water absorption on mechanical properties

5.3.5.1 Compression testing

Results of the compression test after being immersed for 30 days in all water conditions at room temperature are shown in Figure 5.13 (b-d). Dry specimens and syntactic foams immersed in all water conditions at room temperature were compressed to strain as high as 0.20% for compressive properties, respectively. From Figure 5.13 (a), it is observed that the stress-strain for the dry specimens behaved similarly to the syntactic foam immersed in FW, DD and SW water conditions. These curves showed elastic characteristics at a low strain level. After the elastic region, the stress became nearly constant for considerable strain during further compression, which is referred to as the densification stage. At the end of the densification stage the stress started increasing again. This behaviour was revealed to be more likely for lower glass microballoon content, which had taken longer to fracture, compared with higher microballoon content, which was much lower in rigidity and allowed the more intact microballoon to be crushed. It was revealed that the variations of compression strength with ultimate compression strength after being exposed to FW, DD water and SW, was comparable to dry specimens, respectively. Among all specimens, the highest strength belonged to SF2WC, except in the DD water condition belonging to the SF4WC specimen. On the other hand, similar shape also showed the corresponding stress–strain curves for each environmental condition, which was investigated after immersion for 60 days. Each value represented the average data of three specimens. This indicated a decreasing trend in compression strength and compression modulus with an increasing immersion time; however, there was a trend of an increasing maximum compression strain as immersion time increased after being exposed to aqueous environments. In Figure 5.4 (c), the compressive strength for SF2WC and SF4WC had a closer ultimate peak strength at 80 MPa. The influence of DD water through internal surface syntactic foam after 60 days may have occurred. Generally, all the specimens had a higher ultimate compressive strength after being treated for 60 days and being immersed in all water conditions.

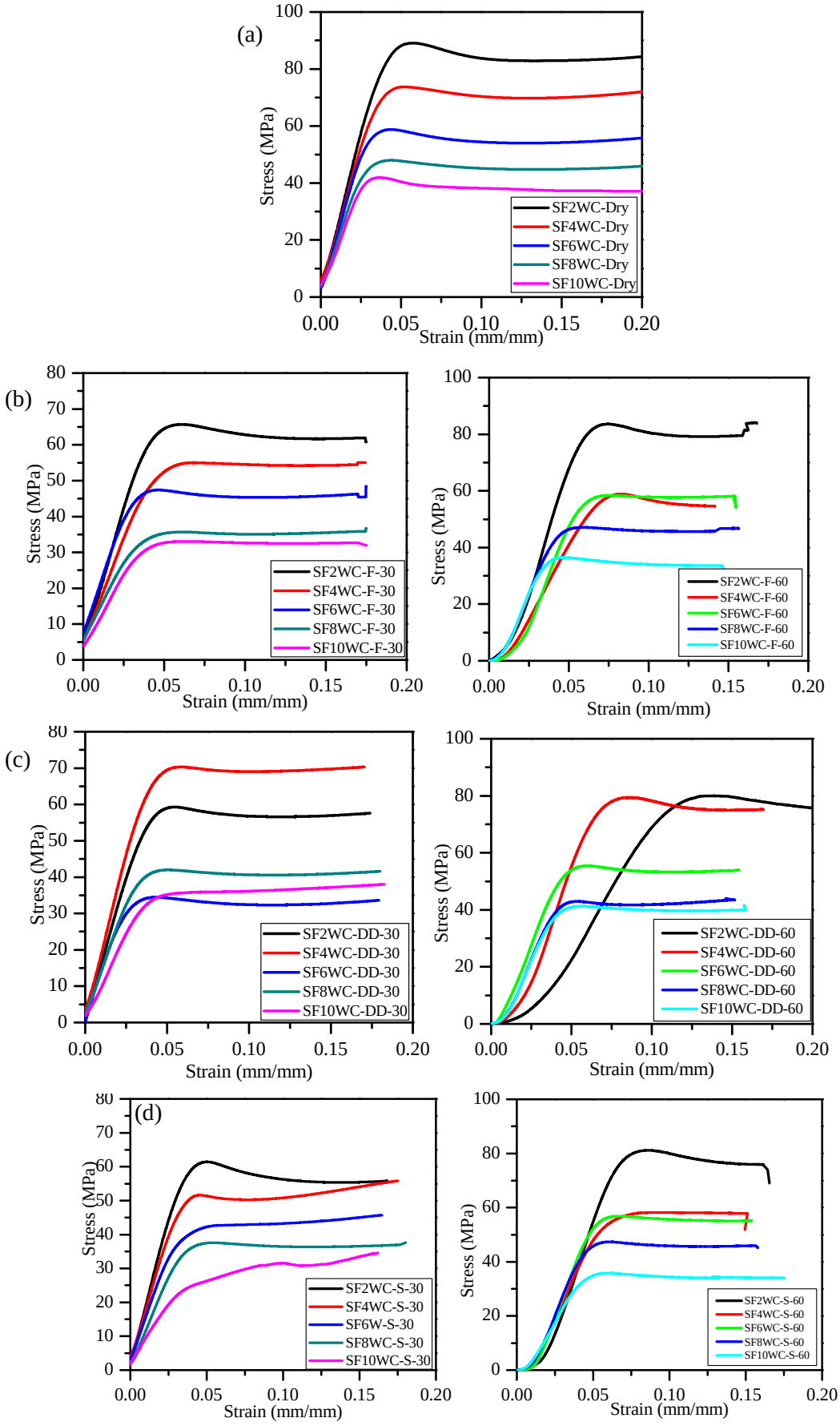

Figure 5.13: Typical water absorption compressive graph at room temperature, T: 2ºC for (a) Dry (b) FW (c) DD (d) SW

These compression results also showed a similar trend in terms of the details displayed for all mechanical properties as shown in Figure 5.14 (a – d) for 30 days and 60 days of being immersed in all water conditions. The peak strength in Figure 5.14 (a) shows that decrease for syntactic foam treated in all water conditions was comparable to dry specimens after being immersed for both 30 and 60-day duration times. However, if compared for all water conditions, specimens immersed in FW and SW showed a higher strength for both 30 and 60 days. A comparison for the compressive modulus is shown in Figure 5.14 (b). The trends show an increase of at least one-third after 60 days, particularly when immersed in DD and SW conditions, but it was still lower than dry specimens. Specific compressive strength showed an incremental trend when immersed in DD and SW but FW had a decreasing trend, particularly for specimens with higher glass microballoons content for a duration of 60 days. This is due to the higher density syntactic foam contributing to these results. Not much different was observed for specific compressive modulus strength results, as shown in Figure 5.14 (d).

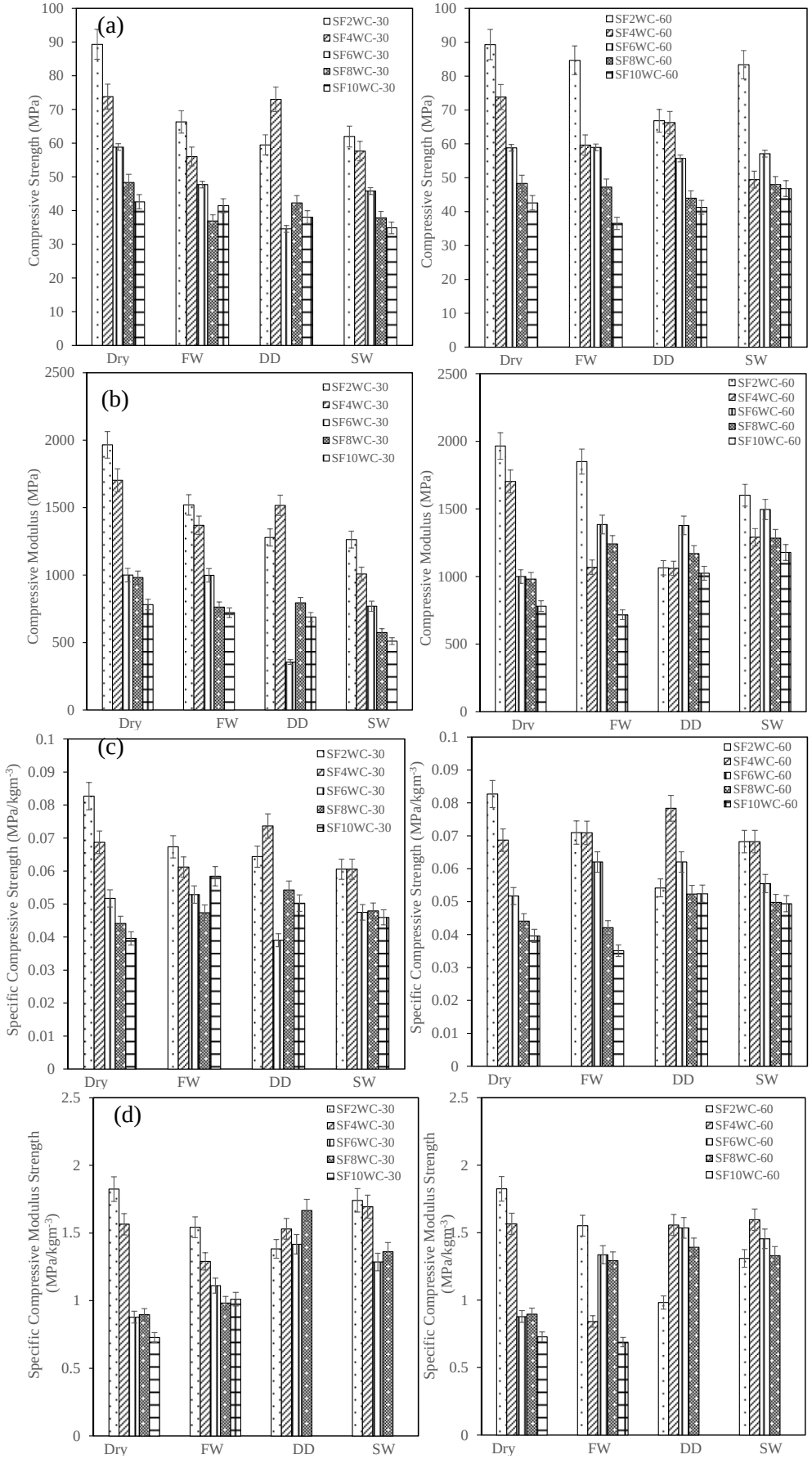

Figure 5.14: Typical results for compressive strength after being immersed in room temperature

5.3.5.2 Tensile testing

The tensile stresses and strain test results are shown in Figure 5.15. The graph exhibits the tensile stress-strain curves of the foams immersed in all water at room temperature and shows a decrease in tensile strength when more glass microballoon content was added, compared to dry specimens. The specimens SF2WT had a higher strength in all water conditions for a duration of 30 days, especially for FW with value 30MPa. Moreover, specimens with higher glass microballoon content, such as SF8WT and SF10WT immersed in SW, showed the lowest strength values between 8 -10 MPa. This indicated that the immersed foams in SW had more ductility than in other water due to the moisture content in the foams, which had more salinity in chemical reaction. This may have caused more severe plasticization of syntactic foam but weaker in strength.

While specimens were immersed in all water conditions for a 60-day duration, they exhibited very large decreases in tensile strength with a highest value of 20 MPa only. This discrepancy might have been due to hydrolytic ageing of glass microballoon, especially when immersed in FW and DD water, which had more OH^- content when compared with SW. In addition, it caused also more weakening between the matrix and glass microballoon interface when immersed for a long duration, regardless of the water condition. Sauvant-Moynot et al., (2006) had the same finding and reason for a decrease in stiffness, namely as being due to an interface problem.

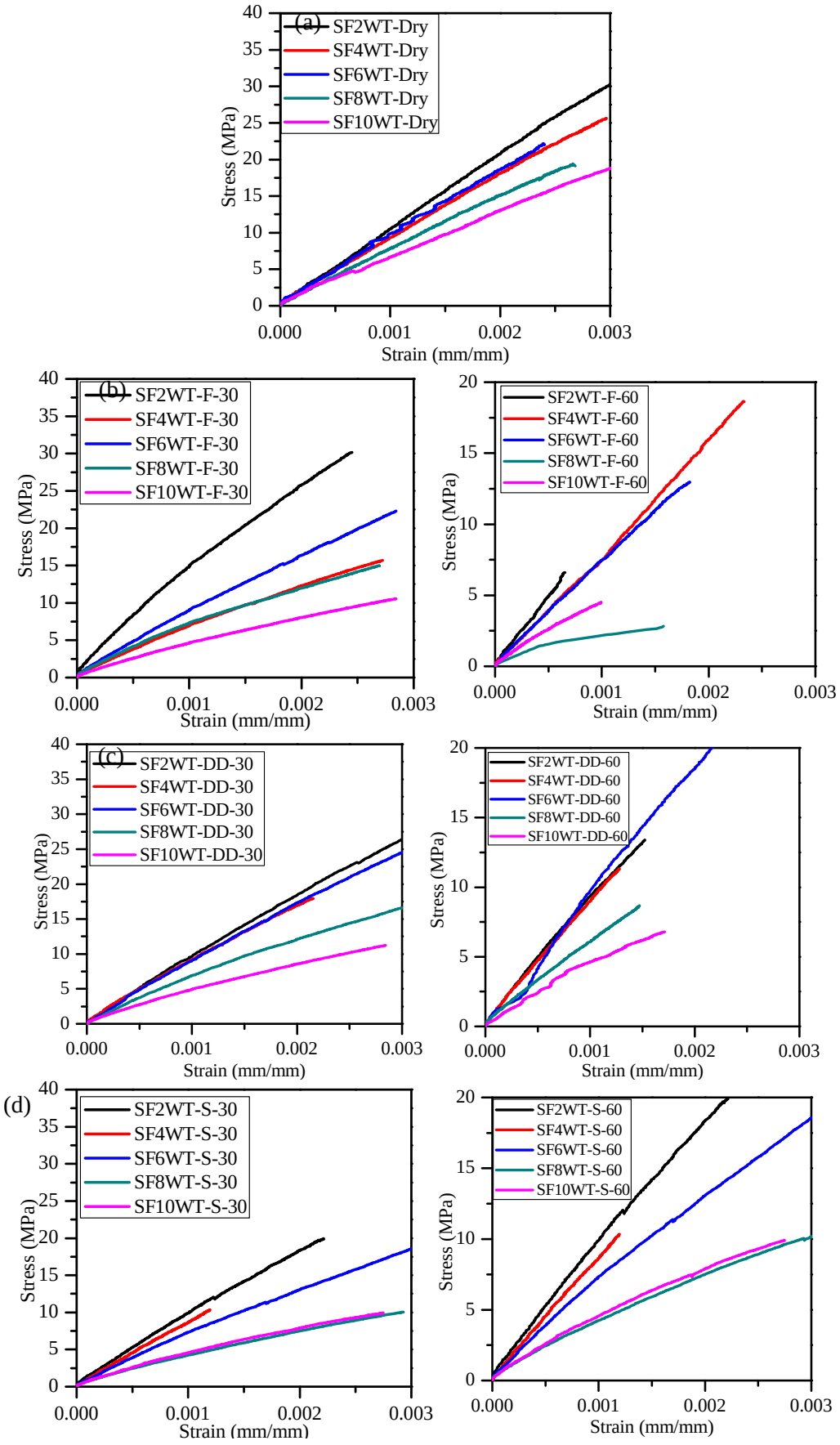

Figure 5.15: Typical water absorption tensile graph for (a) Dry (b) FW (c) DD (d) SW at a duration of between 30 and 60 days

The behaviour of mechanical properties for all specimens immersed in FW, DD and SW could also be explained by Figure 5.16 in detail. The maximum tensile strength increased when immersed for 30 days in FW and DD water conditions, led by specimen SF2WT. Generally, maximum tensile strength showed a decrease when more glass microballoon content was added in all water conditions. It was also revealed that the tensile modulus showed a decrease for all specimens and had a similar trend for dry specimens. This might have been due to a de-bonding problem that occurred between matrix and resin, and as a result the connectivity is was loose, which was detected during the tensile testing of the specimens. Moreover, specific tensile strength showed an increasing trend when immersed in FW and DD water, especially for SF2WT specimens with 0.04 MPa/kgm^{-3}, but decreased in the SW water condition. Even though specimen SF2WT had the highest specific tensile modulus with 16 MPa/kgm^{-3} when immersed in DD water, other specimens showed a trend still going down. The porosity could have contributed to these results because the lighter materials, such as the higher microballoon content, has a higher chance of having more porosities if compared with the higher resin specimens such as the SF2WT specimen.

Similar results were found for the specimen immersed for a duration of 60 days in all water conditions, as shown in Figure 5.16 (a). Generally, the maximum tensile strength had a lower value when compared with the dry specimens. When immersed in DD water, the specimen SF6WT had the highest values while SF10WT had the lowest value with 22 MPa and 5 MPa, respectively. The tensile modulus showed a decreasing trend for both immersed in FW and SW conditions, but DD still led for this characteristic behaviour. Specimen SF6WT had increased by 20 % when compared to dry and FW water, while it increased by 50% when compared with SW. Similar to maximum tensile strength, the specific tensile strength also showed an increase of between 2% – 8% when immersed in both of FW and DD water. While specimen SF10WT showed not much difference when compared in DD and SW water conditions with 0.008 MPa/kgm^{-3}, this was related to the higher possibility porosity content in the syntactic foam. The specific tensile modulus in Figure 5.16 (d) showed a slight increase for specimen SF2WT and the highest value belonged to SF4WT at 12 $MPakgm^{-3}$, which was closer to a dry specimen while specimen SF10WT slightly decreased in all water conditions.

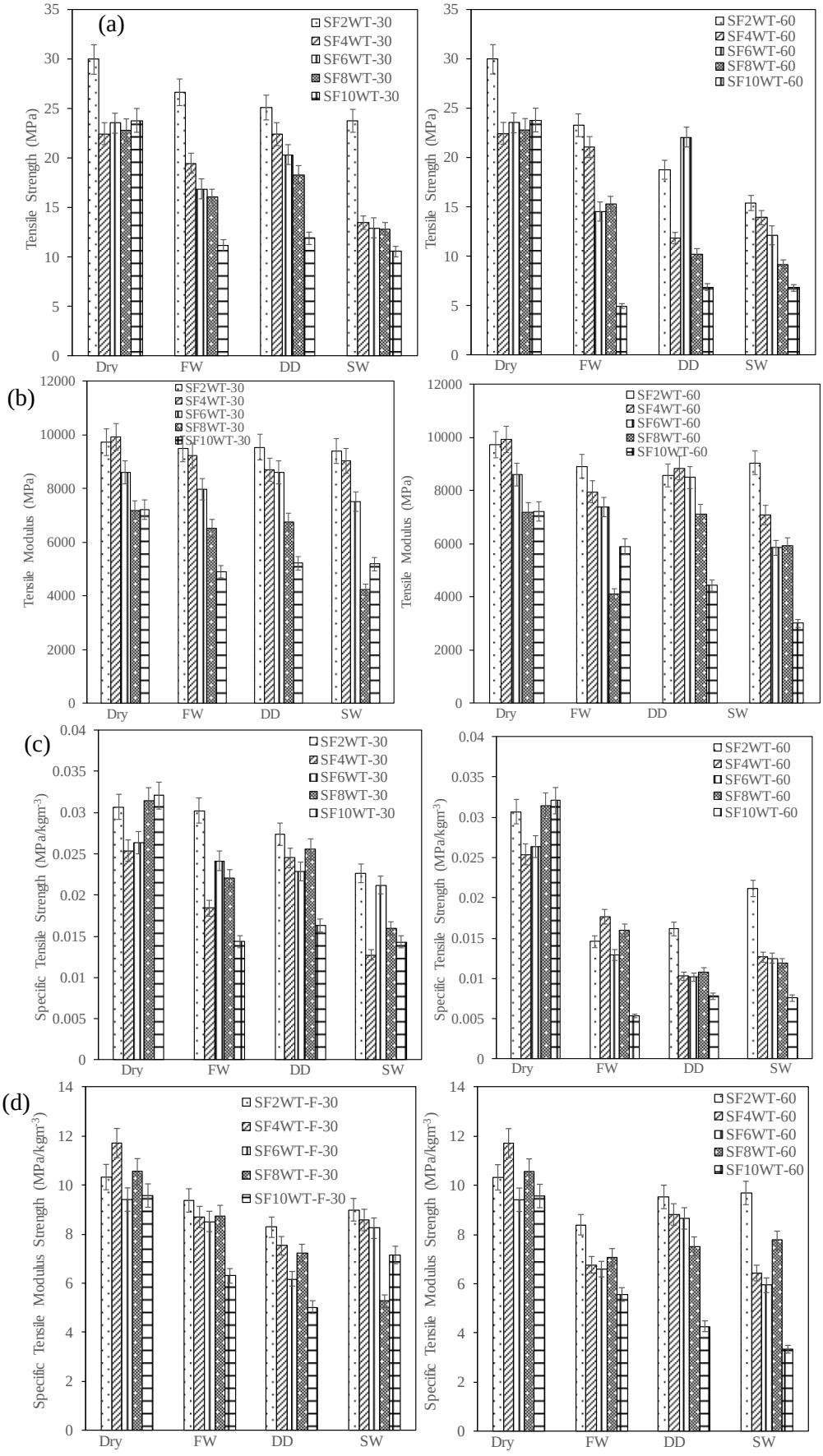

Figure 5.16: Typical results for tensile strength after immersed in room temperature

5.3.6 Effect of hygrothermal on mechanical properties

5.3.6.1 Compression testing

Results of the compressive test syntactic foams immersed in FW, DD and SW at temperature, T: 70^{o}C were compressed to strain at least as 0.15%. Result of the compression test are shown in Figure 5.17 (a –c) for both 30 days and 60 days. From Figure 5.17, it is observed that the stress–strain for the 30 day specimens behaved similarly to the syntactic foams immersed for 60 days for FW, DD and SW. These curves showed elastic characteristics at a low strain level. After the elastic region, the stress became nearly constant for considerable strain during further compression, which is referred to as the densification stage. At the end of the densification stage the stress started increasing again. This type of behaviour was common for all syntactic foams, which had a much lower rigidity and more intact microspheres to be crushed when compared to the immersed foam. Meanwhile, foams immersed in FW and SW for 60 days exhibited a decrease in yield compressive strength, scattered in one group of stress, which is ascribed to water absorption and de-bonding and damage at interfaces (Alomayria et al., 2014). However, the excepted specimen SF2WT kept its strength at 80 MPa in all water conditions at long time duration. In this figure also, a comparison of the yield compressive strength for hydrolytic foams and salinity foam is shown clearly. This revealed that, for hydrolytic specimens, a decrease in the yield compressive strength was seen as compared to the salty specimens. Furthermore, foams immersed in FW 60days showed a further decrease in yield compressive strength by 25% for immersed specimens and 15-20% for DD specimens, as compared to those of the specimens immersed in SW.

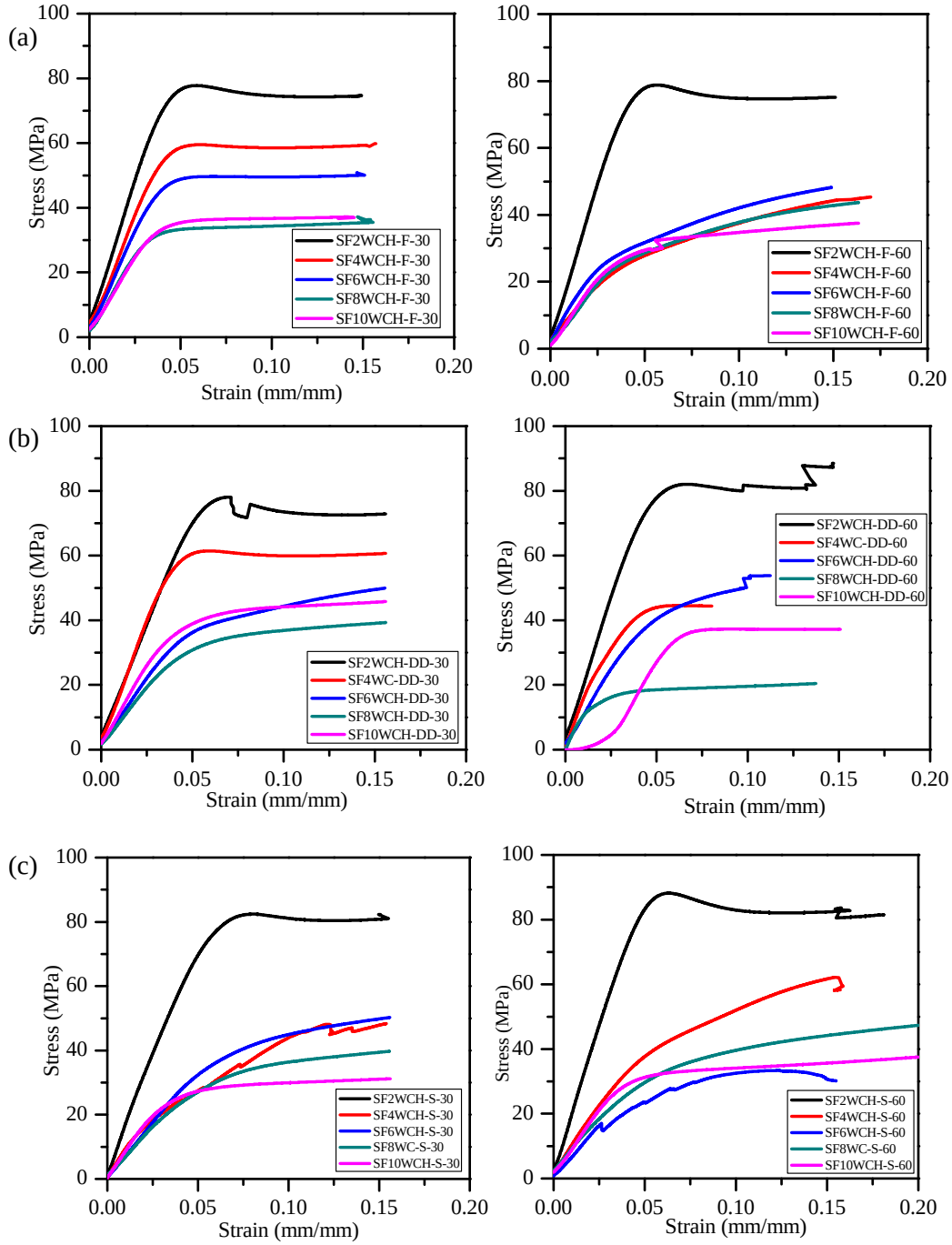

Figure 5.17: Typical hygrothermal compressive graph for (a) Dry (b) FW (c) DD (d) SW at a duration of 30 and 60 days

The mechanical properties of syntactic foam can be explained in detail in Figure 5.18. As shown in this graph, the majority of all specimens had a decrease in their compressive strength after being immersed for 30 days and 60 days in all water conditions when compared with dry specimens. However, specimens SF2WT, SF6WT and SF8WT showed an increase in 30 days while SF2WT, SF4WT, SF8WT and SF10WT also showed an increase in their strength in 60 days. Additionally, the

compressive strains of hydrolytic foams at the yield compressive strength increased. This indicates that the stiffness of all types of foams was lowered due to the presence of moisture in the specimens. FW and DD made the foam softer and brittle than the SW did, regardless of the dry foams. This caused a considerable decrease in modulus of elasticity as shown in Figure 5.18 (b). These results are attributed to the moisture content in the foam and the possibility of material property degradation. The foam in water might undergo a faster degradation than in air (Xua and Li, 2011). Consequently, syntactic foam specimens could be compressed to a higher degree of strain without generation of cracks. Additionally, another reason for decrease in stiffness is hydrolytic ageing of glass, which is not only a direct factor in glass microballoon breakage, but also an indirect factor as a promoter for weakening the matrix-glass microballoon interface (Sauvant-Moynot et al., 2006).

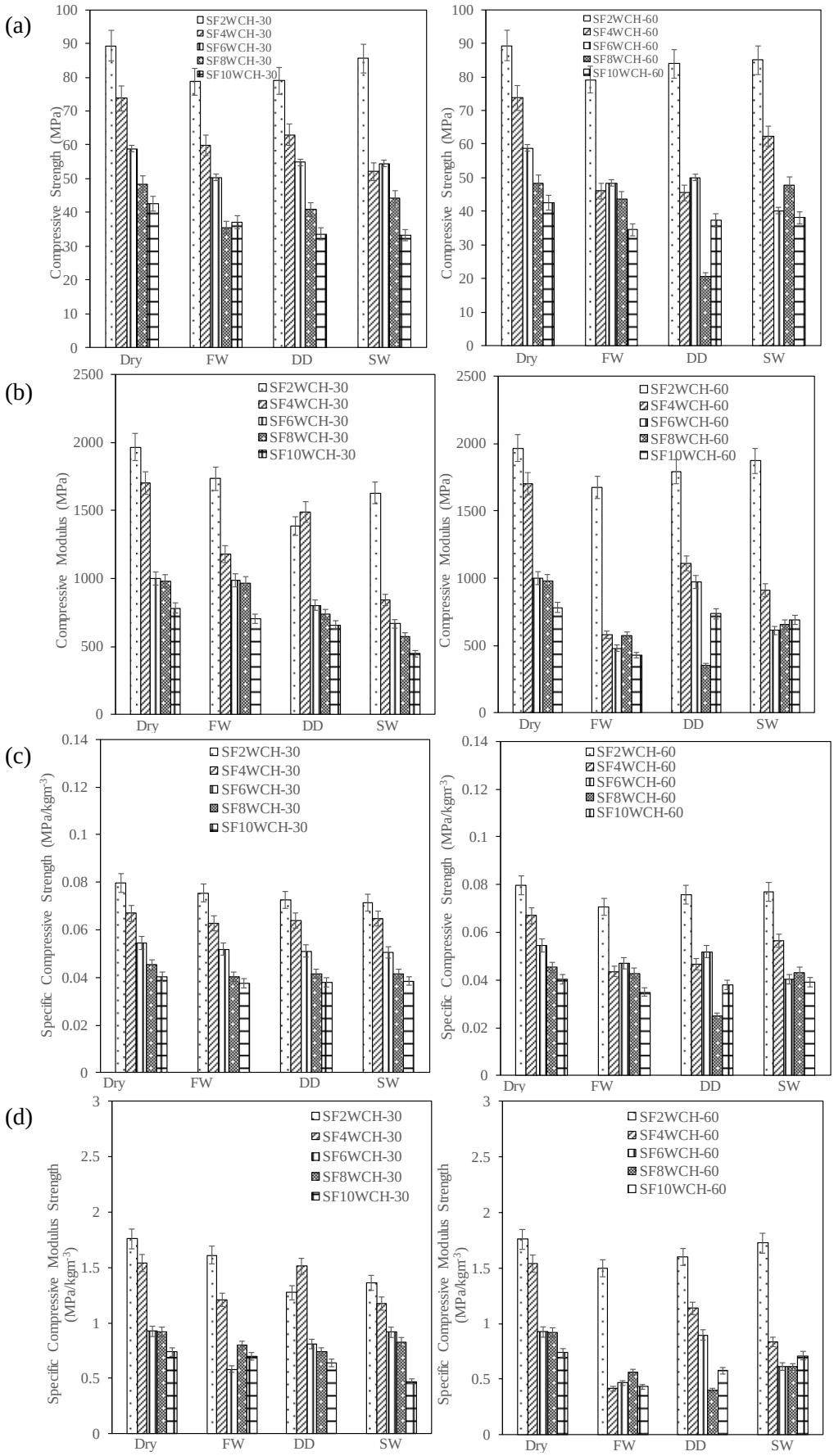

Figure 5.18: Typical results for hygrothermal compressive strength after being immersed in temperature, T: 70ºC

5.3.6.2 Tensile testing

Results of the tensional test are shown in Figure 5.19. The tensile stress-strain curves of the foams immersed in water exhibited a decrease in tensile strength when glass microballoon content was added for a duration of 30 days and 60 days. Moreover, foams immersed in SW showed a larger decrease in tensile strength than those in FW and DD water for both durations. This indicates that the immersed foams had more ductility than dry foams due to the presence of moisture in the foams, which may have caused plasticisation of the matrix resin. Moreover, SW made the foam more ductile than DD and FW waters. The reason for the decreased ductility was the same as that in the compression tests. In addition, the presence of porosity and voids in syntactic foam also contributed to the ductility of specimens regardless of the water condition.
The behaviour of syntactic foam can be elaborated in detail in Figure 5.20. Comparison of yield strength includes modulus of elasticity, and the specific strength for both tensile and modulus are explained in this graph. Yield strength SF2WT was a little bit higher at 32 MPa when immersed in SW if compared with dry specimens but both FW and DD were still below this result after 30 days. However, while SF4WT showed a higher result at 33 MPa when immersed in DD water, the rest was still lower than this value after 60 days.

In comparing modulus values, it can be seen that all types of syntactic foams were affected due to the presence of moisture in the specimens after being immersed in high temperature conditions. Specimens SF4WT, SF6WT, SF8WT and SF10WT showed an increased tensile modulus for all water conditions in 30 days, namely a 5 – 15 % reduction. However, SF2WT still had a higher value at 9531 MPa, which was still below the dry specimen value. When immersed in high temperature conditions for 60 days, it was revealed that tensile modulus decreased, especially for specimens SF2WT, SF4WT, SF8WT and SF10WT. These behaviours could be attributed to two factors: the moisture content entrapped in the porosity regime in the specimens, and the possibility of material property degradation.

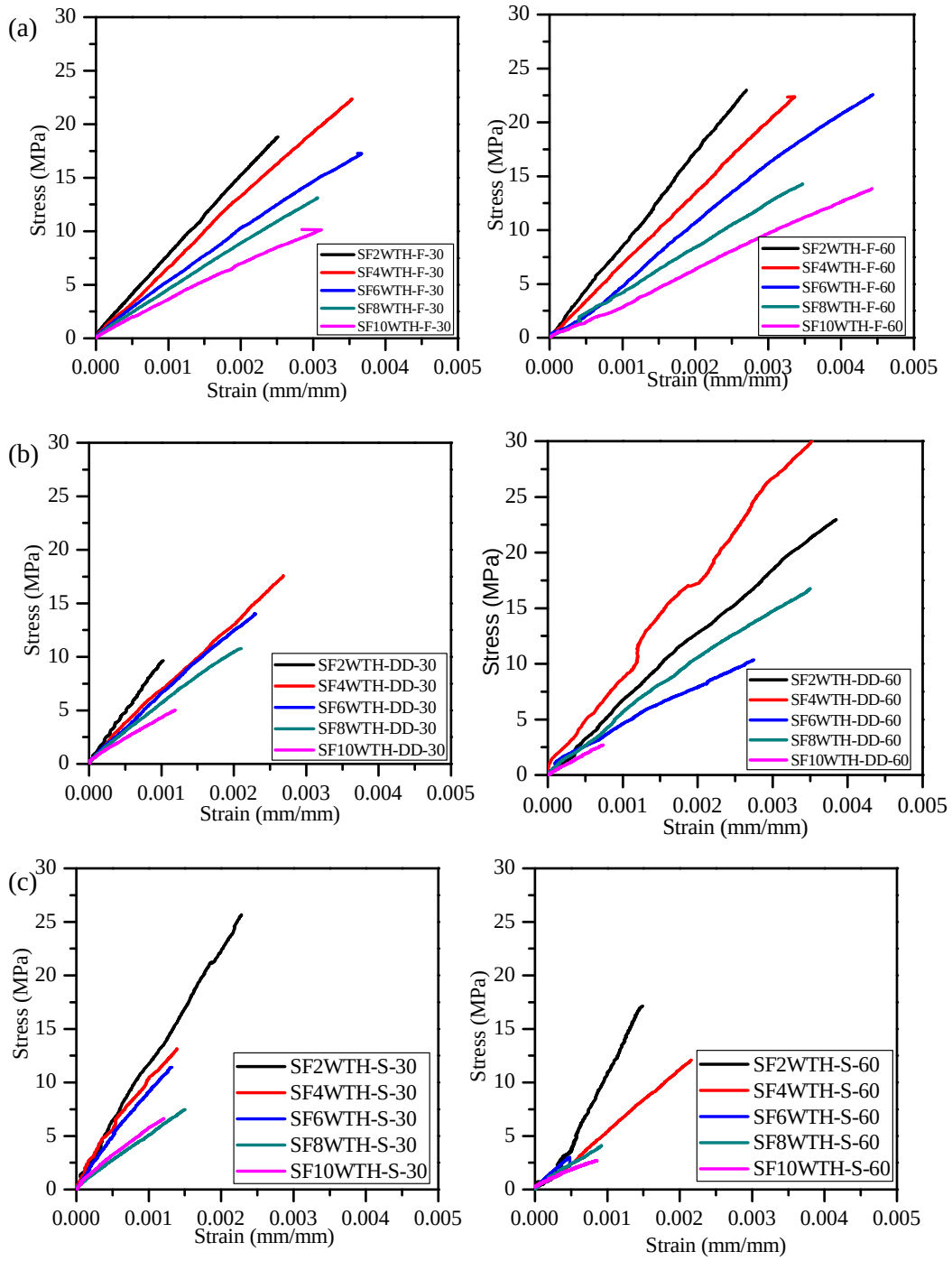

Figure 5.19: Typical hygrothermal tensile graph for (a) Dry (b) FW (c) DD (d) SW at a duration of 30 and 60 days

According to Figure 5.8, the water absorption for compression in the high temperature specimens, T: 70ºC was much higher than room temperature at around a 16% maximum. Conversely, for tensile specimens, according to the Figure 5.9, the water absorption was around 35% maximum when compared to the room temperature conditions.

A considerable decrease in modulus revealed that water absorption had infused in the specimens, allowing for cavity and matrix porosity and leading them to contain the water inside. Due to being brittle and easily cracked, the strength as well as modulus were reduced in the high temperature tested specimens, which indicated an occurrence of some additional events in the material. It must be noted that the thermal and water absorption into the porosity area induced strains generated the syntactic foam to come off the glass microballoon, which could then fracture. Due to the fracture of the glass microballoons, it could develop cavity or matrix porosity, and as a result not only the strength and modulus of the modulus of syntactic foam would go down, but further water absorption would also increase. In addition to this, it must be remembered that when more glass microballoon was added, the potential for it to break was higher and it generated more porosity. Therefore, the hygrothermal strain could cause rupture of the matrix resin in some places near the glass microballoon, which would reduce the strength of syntactic foam specimens. Finally, contributions from the hygrothermal could also expand air being trapped in the porosity and void which would then slightly reduce the strength and modulus of the elasticity of the specimens.

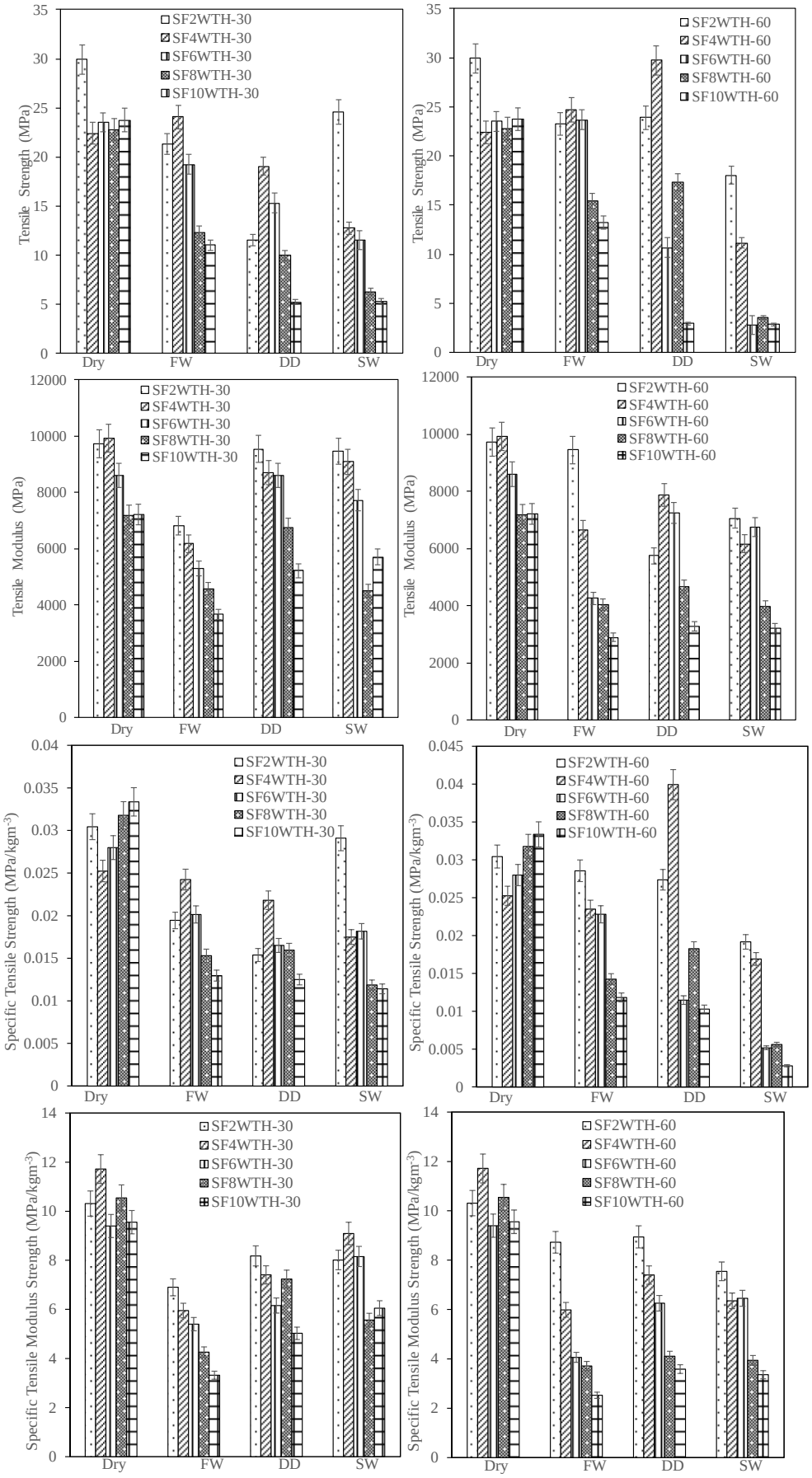

Figure 5.20: Typical results for hygrothermal tensile strength after being immersed in temperature, T: 70^{o}C

5.3.7 Fractographic examination of tested compressive specimens

Fractographic examinations of tested compressive specimens (see Figure 5.21) shows the various toughening mechanism present in syntactic foam after being immersed in FW, DD and SW water conditions. Fractured, crushed and de-bonded glass microballoons, and matrix deformation were observed. The de-bonded glass microballoon was clearly revealed in the specimens in SW water where the matrix gap was larger than other specimen immersed in FW and DD water, as shown in Figure 5.21 (a). Generally, porosity and voids content occurred in all the specimens. The effect of the hygrothermal on the specimens was obvious when being immersed in SW in high temperature conditions. As mentioned in a previous section, Fick's law can be related to the hydrolysis. Ray (2006) reported that this thermal stress or hygrothermally generated porous and weaker interface could allow capillary flow of water absorption in the composites at higher conditioning temperatures. The occurrence of porosity entrapped with water inside of glass microballoon or voids could also reasonably cause matrix deformation cracking, resin de-bonding and microballoon de-bonding (Ray, 2006. As can be seen in Figure 5.21 (b)-(c), many occurring de-bonding failure modes clearly indicated that in the previous section 5.3.3, the water absorption was higher in the hygrothermal process, which might be due to degradation phenomena. The probable reasons for such degradation may be related to the weakening effects of higher thermal and moisture induced swelling stresses at the interface and/or in the matrix resin. It may also be hypothesized that this conditioning environment could result in either breakdown of chemical bonds or secondary forces of attraction at the interface.

(a)

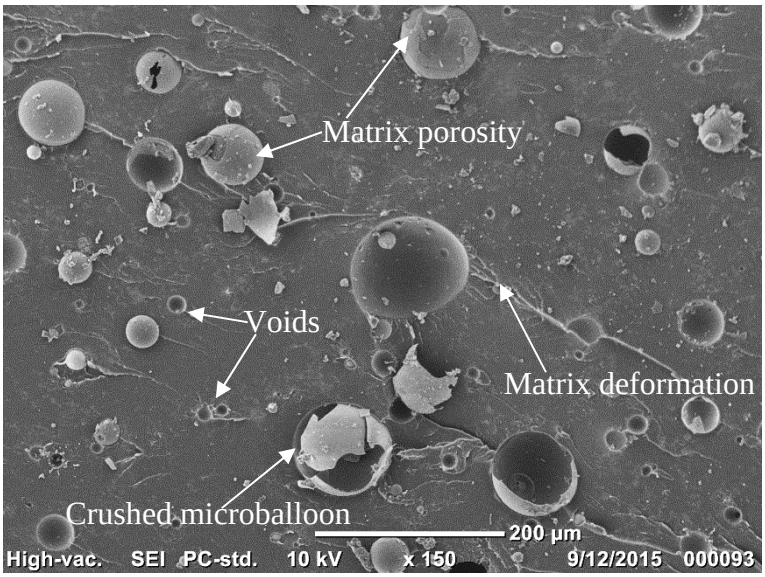

(b)

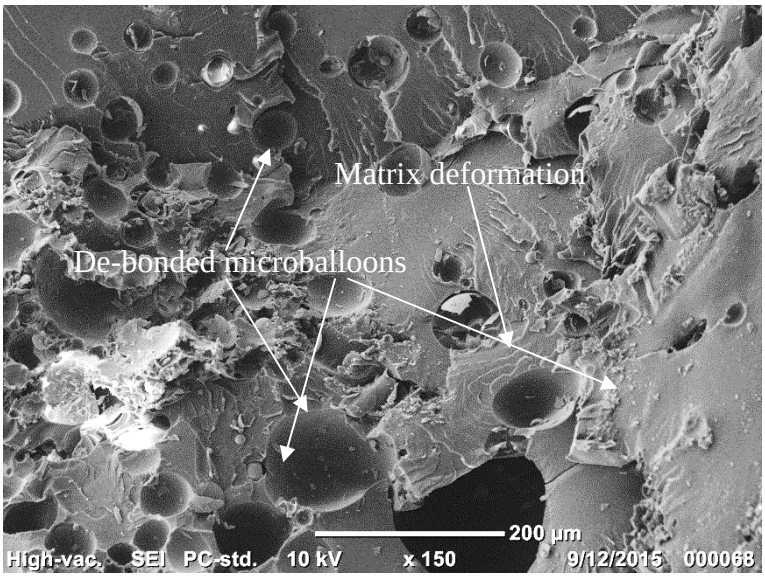

(c)

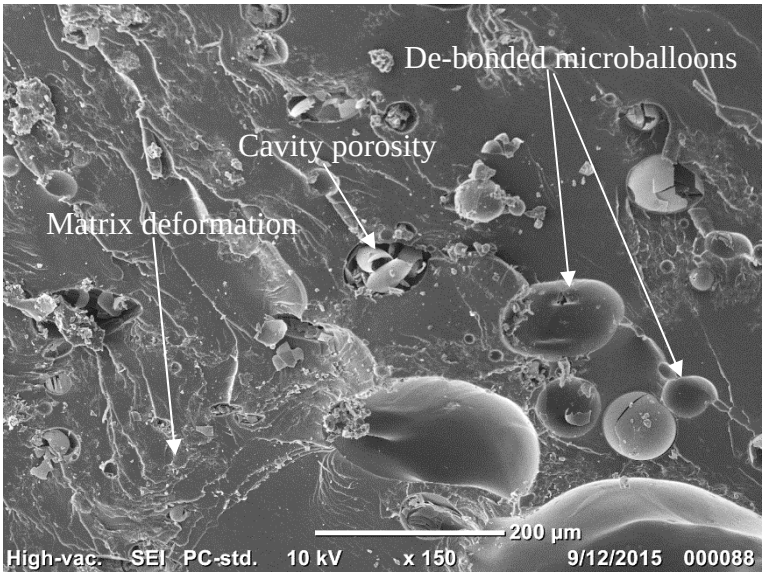

Figure 5.21: SEM images of the fracture surface of the specimens after being immersed in (a) SW (b) FW (c) DD

5.4 Summary

In this study, the water absorption of syntactic foam at room temperature (T: 25^{o}C) and high temperature hygrothermal conditions (T: 70^{o}C) influenced many factors to an important extent. Water absorption rates varied due to the effect of density of syntactic foam because the pores and void containment attributed to higher glass microballoon content. The diffusion rate or coefficient D, can be estimated by using Fick's law, which also predicted that the equilibrium stage could be achieved better at high temperature conditions when compared to room temperature. The diffusion rate also varied when immersed with different water condition, such as SW being slower than FW and DD waters because the effect of the pores activity. The mechanical properties of syntactic foam when immersed in different types of waters at room temperature and under hygrothermal conditions also varied with duration at 30 days and 60 days. It can be seen that the modulus of elasticity for both compressive and tensile properties showed decreases when more glass microballoon content was added and when immersed for a long duration such as 60 days. This phenomenon can also be attributed to pores and voids expanding their size when compared to the dry specimens. Hence, this is further evidence that porosity and voids containment occurring in the syntactic foam affects the mechanical and thermal properties in engineering applications.

Chapter 6

Thermo-Mechanical Properties and Finite Element Modelling of Syntactic Foam Specimens

6.1 Introduction

Lightweight materials can be developed for wider range of engineering application if the materials are tailored with significantly sound mechanical properties and excellent thermal characteristic. In marine applications, s closed cell foams are used as thermal insulation and sealing materials either in combination with polymeric or with a metallic matrix (Gladysz et al., 2006, Rohatgi et al., 2006). This foam is also known as low density foam, which is used in buoyancy aid facilities for offshore applications (Tien et al., 2009). Many studies have reported that the presence of porosity inside a thin wall thickness shell promises to give a better result during environmental test conditions such as moisture absorption and thermal analysis (Sauvant-Moynot et al., 2006, Gupta and Woldesenbet, 2003). At the same time, the stress concentration factor (SCF) around the hole for homogenous material, such as syntactic foam, can be determined experimentally using strain field measurements.

In this study, the investigation on the degradation of syntactic foam using Thermogravimetric (TGA) and Thermomechanical analyses (TMA) was required to determine thermal properties and the behaviour. Both properties are the focus of a parametric study and particularly being affected by the porosity and voids content..

6.2 Materials and experimental methods

6.2.1 Investigation on Thermogravimetric analysis (TGA)

TGA testing was carried out using NETZSCH TG 209F1 Libra equipment. The weight of the specimens were between 4 mg to 8 mg, and different weight percentage of glass microballoon, were used for the analysis. The specimens were heated from 30 ^{o}C to 800 ^{o}C at a rate of 10 ^{o}C/min. A differential thermogravimetric analysis (DTGA) curve was achieved from the TGA analysis. The heating conditions were maintained constant along the experiment.

6.2.2 Investigation on Thermomechanical analysis(TMA)

The linear dimension at different temperatures for the thermal expansion characteristics of the prepared specimen were evaluated by a thermomechanical analyser (TMA) using TA Instrument (Model TGA Q500), as shown in Figure 6.1. An expansion type probe was used to measure the temperature-dependent dimensional changes. A preload loading of 0.02 N was applied in all tests. A minimum of 3 coupons were prepared for each compositions. The samples were cut into pieces with dimensions L: 3 mm x W: 3 mm x t: 2 mm. The external gas air input was used for cooling the TA unit system after finishing the testing. The heating rate in each run was kept at 3 ^{o}C/min and the temperature range was changed from ambient to 80 ^{o}C. Time, temperature and change in specimen height were recorded during the test. The slope of tangent, also called coefficient of thermal expansion (CTE), between Dimension change-temperature plot was determined and predicted as shows in Equation (6.1) (Shunmugasamy et al., 2012, Kim et al., 2011).

$$\alpha = \frac{1}{l} \times \frac{\Delta l}{\Delta T} \tag{6.1}$$

where l initial length of specimen, $\frac{\Delta l}{\Delta T}$ slope of the graph.

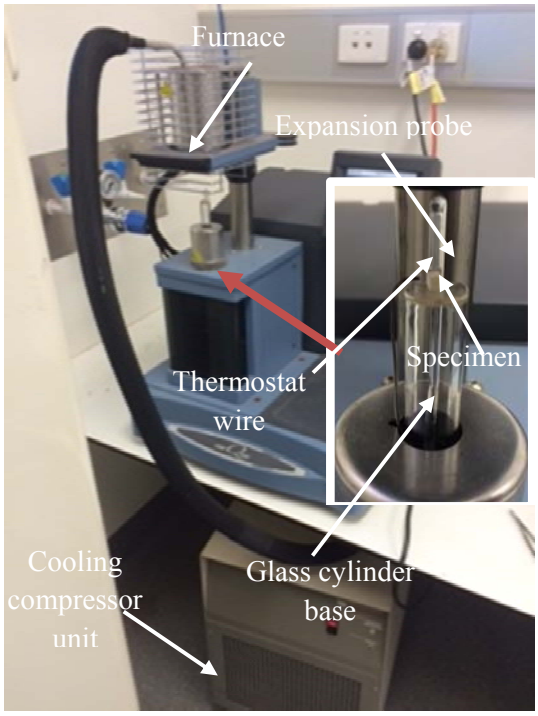

Figure 6.1: Overview of the TMA analyser machine

6.2.3 The Coefficient of thermal expansion (CTE) model, α

The rule of mixture (ROM) is commonly used to obtain upper bound of various properties of composites material. Shunmugasamy et al., (2012) have duplicated the relationship equation between ROM and CTE, as shown in Equation (6.2) below:

$$\alpha = \alpha_m \beta_m + \alpha_g \beta_g \tag{6.2}$$

where $\alpha_m \alpha_g$ is CTE for matrix resin and glass microballoon, respectively. The mixture of specimens in this study was weight percentage (wt.%), therefore β_m , β_g used wt.% of matrix resin and glass microballoon, instead of using volume fraction (Shunmugasamy et al., 2012).

Kerner's and Tuner's models have been modified from previous reports by Shunmugasamy et al., (2012) to include the physical parameters of glass microballoon, such as wall thickness and radius ration, but excluding the porosity and voids. Therefore, in this study additional parameters have been included, starting with the derivation from Turner's model, as shown in Equation (6.3) below:

$$\alpha = \frac{\alpha_m \beta_m K_m + \alpha_g \beta_g K_g}{\beta_m K_m + \beta_g K_g} \tag{6.3}$$

$$K = \frac{E}{3(1-2\nu)} \tag{6.4}$$

Where K is a bulk moduli composite, considering K_m, K_g, modulus of elasticity for matrix resin and glass microballoon, while E is Young's modulus and ν is Poisson's ratio of glass microballoon, respectively. An effective modulus of elasticity of glass microballoon can be assumed if the glass microballoon sphere has the same properties as the hollow glass microballoon, which is modified with porosities and voids content in syntactic foam, as shown in Equation (6.5) (Nji and Li, 2008) and (Li and Muthyala, 2008) below:

$$E_{eff} = \frac{E_g(1-2\nu)\left(1-\emptyset_g^3\right)(1-\emptyset_m)(1-\emptyset_v)}{(1-2\nu)+\left(\frac{1+\nu}{2}\right)\emptyset_g^3+\left(\frac{1+\nu}{2}\right)\emptyset_m+\left(\frac{1+\nu}{2}\right)\emptyset_v} \tag{6.5}$$

where $\emptyset_g, \emptyset_m, \emptyset_v$ are percentages of cavity porosity, matrix porosity and voids content, respectively. In order to have a mutual understanding about the existing

model, the standard specification has been used. Proposed value for modulus of elasticity glass microballoon E_g can be used at 60 GPa (Tagliavia et al., 2009). The final modified Turner model can be written up and divided by three equations as below in Equations (6.6) and (6.7):

$$\text{Cavity porosity, } \alpha_{\phi_g} = \frac{\alpha_m \beta_m E_m \left[\left(1-2\nu_g\right)+\left(\frac{1+\nu_g}{2}\right)\emptyset_g^3\right]+\alpha_g \beta_g E_g\left(1-2\emptyset_g^3\right)(1-2\nu_m)}{\beta_m E_m \left[\left(1-2\nu_g\right)+\left(\frac{1+\nu_g}{2}\right)\emptyset_g^3\right]+\beta_g E_g\left(1-2\emptyset_g^3\right)(1-2\nu_m)} \quad (6.6)$$

$$\text{Matrix porosity, } \alpha_{\phi_m} = \frac{\alpha_m \beta_m E_m \left[\left(1-2\nu_g\right)+\left(\frac{1+\nu_g}{2}\right)\emptyset_m^3\right]+\alpha_g \beta_g E_g(1-2\emptyset_m^3)(1-2\nu_m)}{\beta_m E_m \left[\left(1-2\nu_g\right)+\left(\frac{1+\nu_g}{2}\right)\emptyset_m^3\right]+\beta_g E_g(1-2\emptyset_m^3)(1-2\nu_m)} \quad (6.7)$$

$$\text{Voids, } \alpha_{\phi_v} = \frac{\alpha_m \beta_m E_m \left[\left(1-2\nu_g\right)+\left(\frac{1+\nu_g}{2}\right)\emptyset_v^3\right]+\alpha_g \beta_g E_g(1-2\emptyset_v^3)(1-2\nu_m)}{\beta_m E_m \left[\left(1-2\nu_g\right)+\left(\frac{1+\nu_g}{2}\right)\emptyset_v^3\right]+\beta_g E_g(1-2\emptyset_v^3)(1-2\nu_m)} \quad (6.8)$$

where ν_g is Poisson's ratio of glass microballoon, which can be used as 0.21, while the modulus of elasticity, E_m vinyl ester matrix resin, is used as 22.82 GPa (Gupta et al., 2010) and ν_m is Poisson's ratio as 0.35 (Poveda et al., 2010). In this prediction, the void content can be ignored from the modelling in Turner's model because air/gas trap in syntactic foam is not required for higher percentages (< 5 %) in terms of its contribution to the evaluation. Thus, the CTE values investigation only focused on radius ratio's (η), cavity porosity (ϕ_g) and matrix porosity (ϕ_m).

6.2.4 Glass transition temperature, T_g measurement

According to the ASTM E1545 standard, thermomechanical analysis (TMA) was determined from a change in T_g via the measurement of dimensional variation in the sample with temperature (ASTM, 2016). T_g is determined from the intersection of two tangential lines drawn along discontinuities in the dimensional change versus

temperature profiles (Zhou and Lucas, 1999). In this study, the compression and tensile specimens were immersed in water at a temperature of 70 ^{o}C for longer than 60 days. T_g from the dry specimens was measured and compared with specimens after water treatment, for example fresh water, salt water and double distil water. The specimens were cut into L: 3 mm x W: 3 mm x t: 2 mm from each type of T_g analysis.

6.2.5 Theoretical study on kinetic energy for polymer degradation

The kinetic energy for polymer degradation commonly uses the Equation (6.9) introduced by Flynn (Flynn, 1989).

$$\frac{d\alpha}{dt} = k(T)f(\alpha) \tag{6.9}$$

where α represents conversion factor (α=0 -1), t is the time, k(T) is temperature rate constant and f(α) is the reaction model, which describes the dependence of the reaction rate on the extent of the reaction. The temperature dependence of k(T) could be represented by the Arrhenius Equation (6.10).

$$\frac{d\alpha}{dt} = Ae^{\frac{-Ea}{RT}}f(\alpha) \tag{6.10}$$

where E_a is activation energy of the process. A is the pre-exponential factor, R is the universal gas constant and f(α) depends on the decomposition mechanism. The simplest and most frequently used model for f(α) is shown in Equation (6.11),

$$f(\alpha) = (1-\alpha)^n \tag{6.11}$$

where n is order of reaction, while the rate of conversion, dα/dt can be written as,

$$\frac{d\alpha}{dt} = k = k(T)f(\alpha) \tag{6.12}$$

The combination of Equation (6.10 – 6.12) gives the following relationship, as shown in Equation (6.13),

$$\frac{d\alpha}{dt} = k = (1-\alpha)^n Ae^{\frac{-Ea}{RT}} \tag{6.13}$$

and the first order reaction (n =1) and Equation (6.13) can be expressed as,

$$\frac{d\alpha}{dt} = k = Ae^{\frac{-Ea}{RT}} \tag{6.14}$$

Therefore, the Arrhenius equation can also be shown as Equation (6.14) above. In a chemical kinetics reaction, the rate constant quantifies the speed of a chemical

reaction. It is also quantified by a frequency factor or a factor is the pre-exponential constant in the Arrhenius equation, which can be expressed as in Equation (6.15),

$$\ln(\mathrm{k}) = \frac{-\mathrm{E_a}}{\mathrm{RT}} + \ln(A) \tag{6.15}$$

Then, a reaction obeys the Arrhenius equation as a plot of ln(k) versus T^{-1} will give a straight line, or slope and an intercept can be used to determine E_a and A. The final activation energy can be defined as (-R) multiplied by the slope of the graph.

$$\mathrm{E_a} = -\mathrm{R}\left(\frac{\Delta\ln(k)}{\Delta\ln(\frac{1}{T})}\right) \tag{6.16}$$

Studying kinetic energy, particularly activation energy, can be described in the form of many methods. There are several methods that can determine kinetic energy (Das et al., 2014). The well-known method called the Broido Method is useful to determine the kinetic parameters, which can be derived from mass loss versus temperature (Broido, 1969). Equation (6.17) shows the derivation of the Broido Method,

$$\ln\left(\ln\frac{1}{\mathrm{Y}}\right) = -\frac{\mathrm{E_a}}{\mathrm{R}}\left(\frac{1}{\mathrm{T}}\right) + \ln\left(\frac{\mathrm{R}}{\mathrm{E_a}}\frac{\mathrm{Z}}{\mathrm{R_H}}\mathrm{T_m^2}\right) \tag{6.17}$$

where (1/Y) is the fraction of the number of initial molecules not yet decomposed, R is the universal gas constant ($8.31451 JK^{-1}mol^{-1}$), T_m is the temperature of the maximum decomposition rate unit Kelvin (K), R_H is the heating rate ($Kmin^{-1}$) and Z is frequency factor s^{-1}.

6.2.6 The determination of Stress concentration factor (SCF) around a hole drilled on a material sample.

The SCF for a few "simple" geometries has been determined by researchers (analytical equations) (Warren and Richard, 2002). Warren and Richard (2002) have compiled these into a tables for easy reference. Determining the SCF for complex geometries can be difficult because there are highly localized effects due to sample geometry and the loading conditions. In order to predict the "actual" stress resulting from a geometric stress raiser, a theoretical stress concentration factor needs to be determined. The SCF can be determined experimentally from the strain field measurements around the concerned location. For the finite plate containing a hole and loaded in tension, the maximum stress becomes less than three times the nominal stress at the zone containing the hole (Warren and Richard, 2002). Thus, the stress concentration factor

is equivalent to 3, which is used for the finite plate. This plate will decrease the width and the Equation (6.18) can be used to determine the SCF for the strain gage values.

$$\sigma_{\max .} = K_t \sigma_{nom} \tag{6.18}$$

where $\sigma_{max.}$ is the maximum stress, K_t is the SCF, and σ_{nom} is the applied uniform stress. The stress concentration factor from the experiment can be determined by using Roark's formula, as shown in Equation (6.19).

$$K_t = 3.00 - 3.13\left(\frac{2r}{D}\right) + 3.66\left(\frac{2r}{D}\right)^2 - 1.53\left(\frac{2r}{D}\right)^3 \tag{6.19}$$

where the parameters for r and D are shown in Figure 6.2 for each of the specimens. This was measured using the Vernier caliper with scientific error -/+ 0.0001mm.

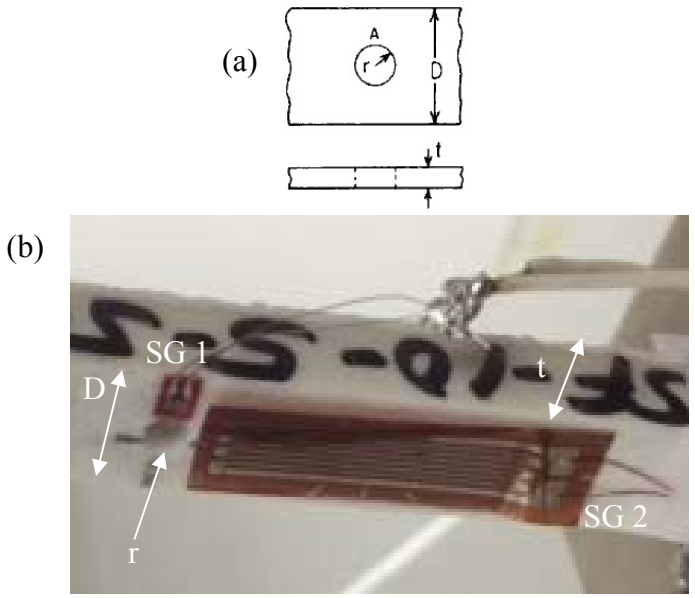

Figure 6.2: The parameters t, r and D for (a) Geometry (Warren and Richard, 2002) and (b) Actual specimens.

The illustration of the SCF measurement near to the hole is shown in Figure 6.3 (a). The direction of SG 1 is in the Z axis-direction and SG2 follows the Y axis –direction. The coordinate system is also shown in Figure 6.3 (b), which exactly followed the CREO FEA (WCS) coordinate system.

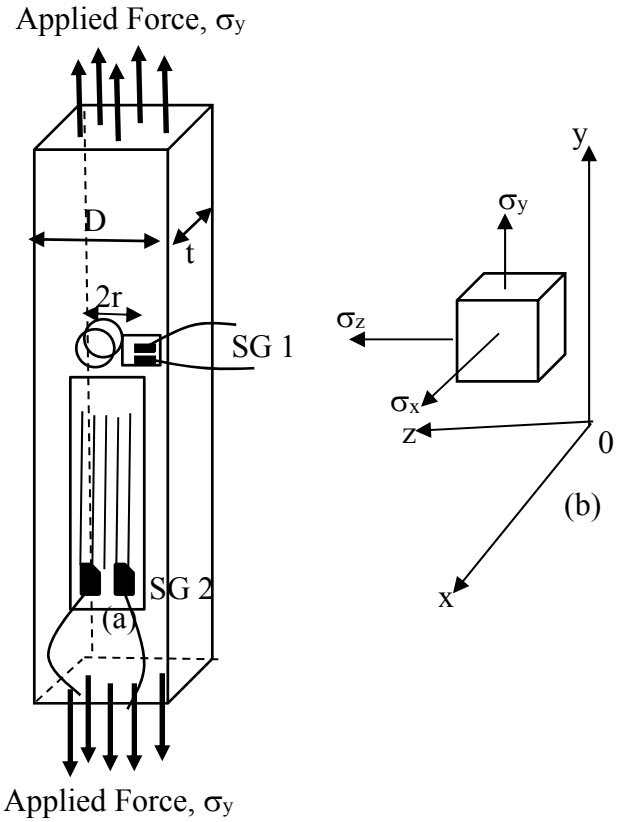

Figure 6.3: The illustration of the SCF measurement using (a) SG1 and SG2 (b) CREO (WCS) coordinate system.

6.2.7 The Finite element analysis (FEA) modelling

A detailed FEA was performed for simulation of test samples used for measurement of SCF as indicated in Figure 6.4 (a). The flexural specimen, taken from the sandwich syntactic foam, which has two homogeneous layers, which is shown as two skin layers for top- bottom and core in the middle, as shown in Figure 6.5 (a). FEA was done CREO 3.0 Parametric/Simulate software. The actual parameters and properties of the sandwich samples which were provided in Chapter 4 were used to set-up the FEA model. The considered sandwich panels were symmetric, i.e., its skins had an identical thickness *t*. The thickness of the core was denoted by the symbol c as the syntactic foam. With reference to the terminology used by Allen, the sandwich panels can be classified as thick skins and non-antiplane core (Allen, 1969). The deflection of a thick-skinned and non-antiplane core has computed. The first solution was the approximation that the field along the sandwich core is linear, and the second solution used the Total Potential Energy theorem. Because this study was most likely to use the actual size of the specimens, as it was beneficial to continue with this solution. The constitutive model utilised for this study was considered as a crushable foams plasticity model (Deshpande and Fleck, 2000).

The composite samples were modelled as a plane stress problem. The syntactic foam was considered as isotropic material and used the existing experimental data for modulus elasticity and Poisson's ratio of the specimens. An isotropic material can be simulated with the rigid body system. Also from the previous report, the longitudinal strain y axis-direction was used in this model to simulate the object, which is required for rigid body systems proposed by (Kulesa and Robinson, 2014). Kulesa and Robinson (2014) have used this stress to perform a thermal simulation for syntactic foams. In their study, the isotropic hardening model was used, where the yield stress is cantered at the origin in the vertical stress plane and evolves geometrically. The input data from the hardening curve showed the uni-axial compression yield stress as a function of the corresponding plastic strain. In order to calculate the finite strains, the true stress and logarithmic strain values should be determined first. On this observation, they found yield surface evolves are in a self-similar manner and it is governed by the equivalent plastic strain. In this simulation, the refined model mesh used 5 mm for a minimum element size and an AutoGEM reference for all properties, as indicated in Figure 6.4(b). The force is applied in the direction of Y axis-. The meshs contained 2677 Tetra elements. A constraint was created to ensure it was fixed at the bottom as shown in the Figure 6.4. The material properties for Young modulus and Poisson's ratio were used as indicated in Chapter 3. The applied force for this model was taken from -1.0 to -1.2 kN in the Y axis-direction through the WCS system.

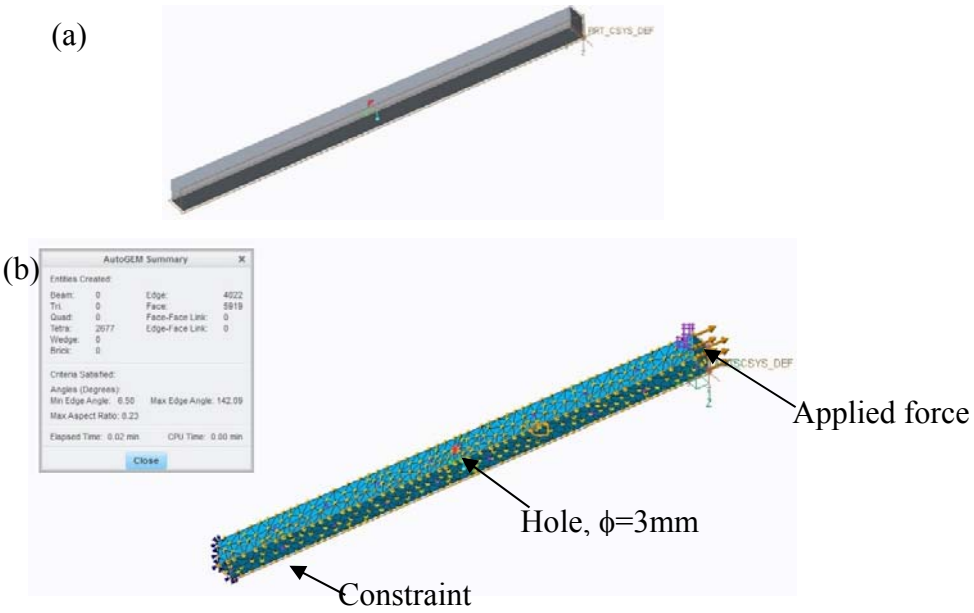

Figure 6.4: Typical tensile specimens are illustrated in CREO 3.0 Parametric software for (a) Tensile dimensioned (b) AutoGEM with redefined summary.

The flexural testing analysis used in this model has dimensioned as the actual specimens. The refined model had 2887 terra elements. A control size element was 5 mm. The geometrical flexural 3-point bending meshing results are depicted in Figure 6.5(a). The material assignment option was used in the material properties for this model, which used the syntactic foam core taken from the library mode. The constraint was focused on the GFRP skin in which the stress distribution may be higher than in any other area.

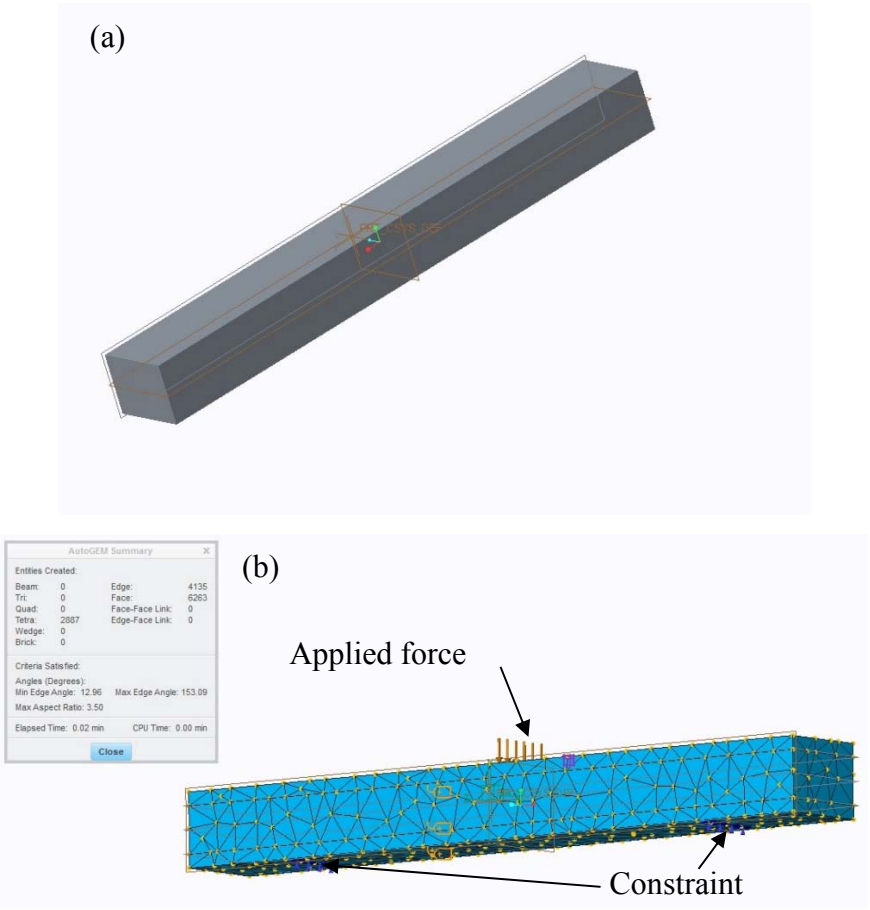

Figure 6.5: Typical flexural 3-point bending specimen is illustrated using CREO 3.0 Parametric software for (a) Flexural dimensioned (b) Redefined automesh.

6.2.8 The Stress concentration factor (SCF) for tensile specimens

The tensile specimens were selected for SCF analysis in accordance with ASTM D-638-10 (ASTM, 2010). Specimen with one attached strain, gauge for different weight percentages of glass microballoon with 2 wt% to 10 wt.% were prepared for testing. Two strains, gauges have been attached closer to one hole placed in the middle of the 10wt.% composition specimen only. A hole with a 3mm approximate diameter has been drilled to a 1 mm depth on the surface of the specimen, and a strain gage supplied

by Bestech Australia Pty Ltd was bonded with glue. The strain gauge was manufactured by Tokyo Sokki Kenkyujo Co. Ltd. with the general specification: type FLG-02-11, gage factor 2.05, length 0.2 mm and width 1.4 mm, resistance 120 Ω (Bestech, 2015). The tensile test was performed in a 10 kN capacity MTS Insight Electro-mechanical testing machine using a crosshead speed of 2.0 mm/min. An extensometer was also provided at the gauge length to measure the experimental longitudinal and transverse deformations to determine the ultimate strength and modulus, as well as to calculate the SCF of the glass microballoon/vinyl ester syntactic foam. Then, strain data were measured with a strain gauge device, which was connected to the laptop and which recorded the data acquisition with Easy V3.4.2 DAQ project software. The experimental set-up was used in conducting the tensile test with strain gauges as shown in Figure 6.6.

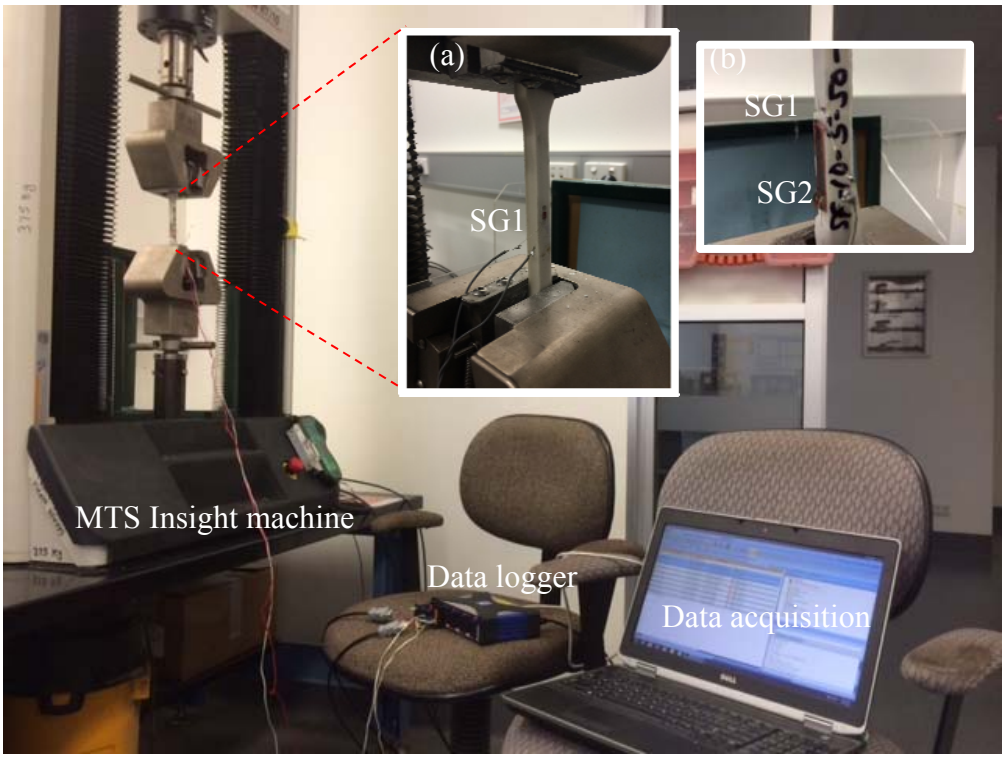

Figure 6.6: The SCF tensile measurement set-up (a) one strain gauge (b) two strain gauges.

6.2.9 The flexural syntactic foam core sandwich panel

The flexural syntactic foam sandwich panel has been used for the evaluation, using the FEA modelling method. The specimens were prepared and explained in Chapter 4 with a different composition of glass microballoons as core materials. The strain gauges, also supplied by Bestech Australia Pty. Ltd, were attached with glue in the middle of the top (SG1) and bottom (SG2) of the skin sandwich panel as shown in Figure 6.7. The strain gauge was manufactured by Tokyo Sokki Kenkyujo Co. Ltd. with the general specification: type FLG-02-11, gage factor 2.05, length 0.2 mm and width 1.4 mm, resistance 120 Ω (Bestech, 2015).

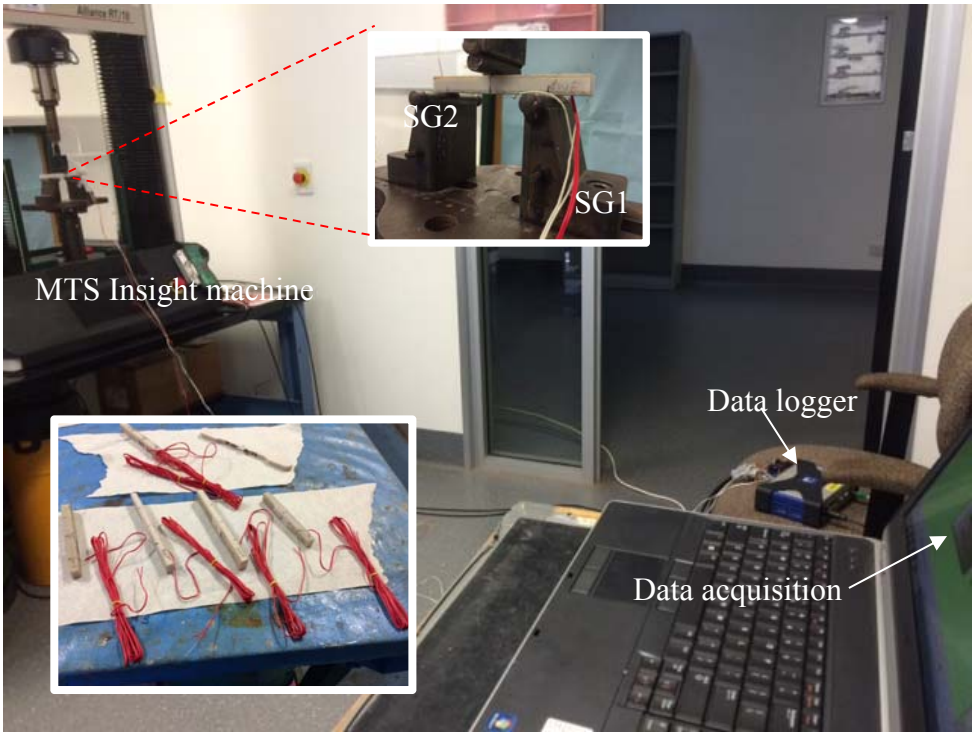

Figure 6.7: Typical flexural sandwich panels with SG attachment for simulation set-up

6.3 Results and discussion

6.3.1 Glass transition temperature, T_g analysis

All syntactic foam composition dry specimens has dropped its glass transition temperature T_g and found it was lower than the neat resin at 118 °C, as shown in Figure 6.8. In earlier studies, a similar trend was observed where T_g of vinyl ester resin decreased when they were filled with granite powder to fabricate the composites

(Baskaran et al., 2014). The decrease of T_g is attributed to the interfacial reactions between glass microballoons and vinyl ester resin. It was observed that the glass microballoon weight percentage had an effect on the glass transition temperature as well as an effect on the wall thickness. For example, starting from syntactic foam containing 2 wt.% of glass microballoon had a T_g value at 105 ^oC and decreased to 78^oC for 5 wt.% of glass microballoon. A similar T_g trend result was also reported by (Tien et al., 2009) for glass microballoon with epoxy resin matrix syntactic foam. This trend can be related to the effect of glass microballoon composition and wall thickness on the total glass content of the specimens. As mentioned in Chapter 3, the wall thickness varies between the 9.57 and 15.41 µm used in this study. Therefore, the effect of both weight percentage of glass microballoon and wall thickness is for a potential decrease of the T_g for dry specimens.

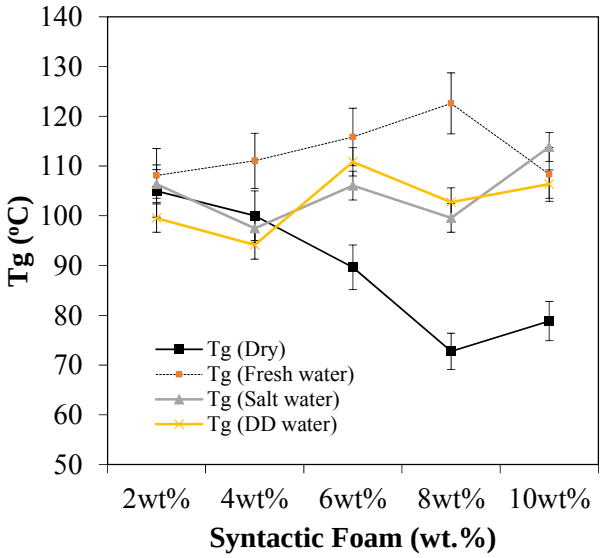

Figure 6.8: T_g changed with different weight percentages of glass microballoon.

After changes in the water treatment conditions, particularly for the hot water condition, T_g for all specimens increased when compared to the dry specimens. Hygrothermal fresh water specimens had a higher T_g at 122 ^oC for 8 wt.%, followed by hygrothermal salt water with 114 ^oC, and then hygrothermal double distil water with 108 ^oC for 10 wt.% and 6 wt.%, respectively. The increase in T_g for fresh water raised a concern about excessive water between the glass microballoon and matrix resin. T_g values for both hygrothermal salt water and double distilled water specimens increased constantly when more glass microballoon content was added in the syntactic

foam. This may have resulted from the different water salinity content between salt and distilled waters. The conductivity of these waters was also lower than the fresh water, at below 1msev. The nature of water interacting with the matrix resin can be described in terms of molecule interaction. The water molecules are diffused into the resin and effectively might disturb the inter-chain bonding through Van der Waals' force and the initial hydrogen bonds in the matrix resin. Zhou and Lucas (1999) also reported that this is called Type I bonded water forms with the chain network. The detailed result for T_g is shown in Table 6.1. The data show that a comparable result for dry specimens and after hygrothermal treatment for FW, DD and SW specimens. The dry specimens with the highest T_g belong to SF-2WT and the trend was going down with a minimum T_g at 72.52 ^oC for SF-8WT. This clearly showed that the decrease in T_g affected the addition of glass microballoon content. FW hygrothermal specimens showed a different trend, exhibiting an increase in the T_g when more glass microballoon was added. The maximum T_g value for FW hygrothermal was 122.58 ^oC belonging to SF-8WT. This means that the influence of FW water with the addition of the hot temperature condition may have contributed to the higher T_g but dropped to 108.41 ^oC when 10 wt.% glass microballoon. There was no trend indicated for both DD and SW water conditions. The highest T_g for DD water and SW water was 110.86 ^oC belonging to SF-6WT and 113.98 ^oC belonging to SF-10WT, respectively. This also showed that the SW hygrothermal condition was much more severe to DD hygrothermal even though more glass microballoon was added in the syntactic foam.

Table 6.1: Typical result for T_g analysis syntactic foam after hygrothermal process

Specimens	Dry	FW	DD	SW
	^oC	^oC	^oC	^oC
SF-2WT	104.94	108.12	99.31	106.38
SF-4WT	100.05	111.07	94.12	97.44
SF-6WT	89.31	115.92	110.86	106.07
SF-8WT	72.52	122.58	102.75	99.14
SF-10WT	79.72	108.41	106.45	113.98

Figure 6.9 also shows the plot for T_g measurement after hygrothermal treatment for three types of water such as FW, SW and DD water. Similar to the result in Table 6.1, Figure 6.9 (a) fresh water shows the highest T_g led by SF-8WT or glass microballoon with 8 wt.% at 122.58 ^oC. This indicates that the extension of the immersion process,

will make T_g increase due to the influence of water absorption in the specimen through glass microballoons at different compositions. This can be related to the porosity content which affects the T_g value in the specimen. The hydroxyl water group of fresh water also contributed to the higher T_g value compared to other types of water. At the same time, the immersion specimens in salt water and double distil water showed a T_g up and down trend for different wt.% of glass microballoon. The specimen with 10 wt.% for hygrothermal salt water showed the highest T_g value at 113.98°C. The porosity content and wall thickness also increased in this specimen if compared with others (please refer to Chapter 3 for a detailed discussion).

This was similar to the specimen with 6 wt.% after hygrothermal, double distil water treatment, which had a higher T_g value with 110.86 °C. The analogy could also be made for the contribution to increasing the T_g values, when a comparison study was made between a solid and a hollow particles composite. For a solid particle filled composite, for example in the form of ceramic microballoons, thermal stability changed during variation in the weight percentage of the microballoon content. In hollow particles, such as glass microballoons, it was possible to control the variation in the particle-resin interface area, which was related to the wall thickness. This approach allowed isolation of the effect of the glass content and the interface area independent of each other. A comparison of the measured values of T_g for syntactic foam containing different weight percentages and wall thickness had a significant impact on the T_g values. Hence, a change in T_g was mainly attributed to the different weight percentage of constituent materials, as well as wall thickness.

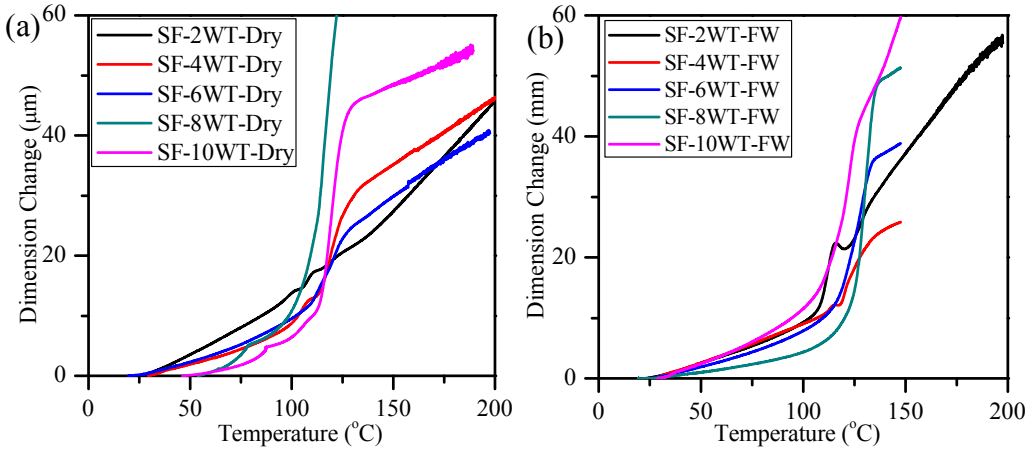

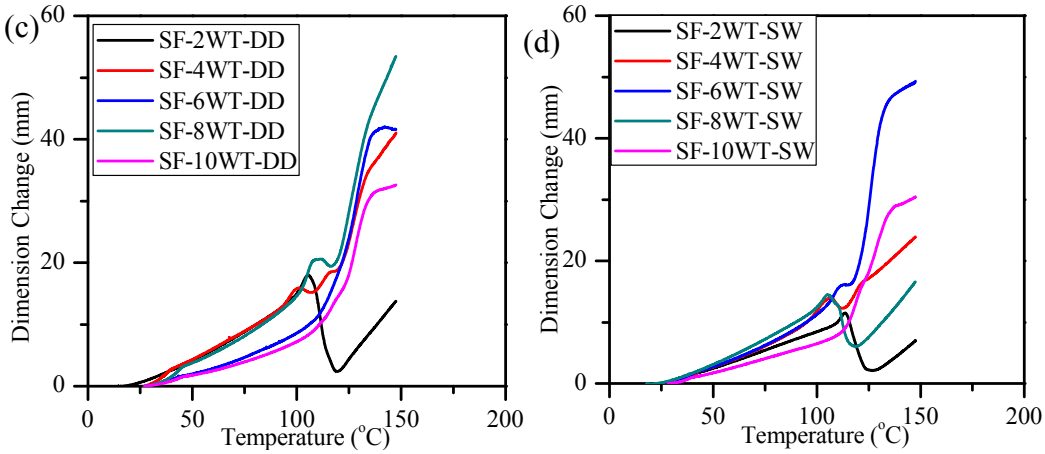

Figure 6.9: Typical T_g change of syntactic foam after hygrothermal treatment; (a) Dry (b) FW (c) DD (d) SW

6.3.2 Weight loss analysis

The thermogravimetric result for syntactic foam and its comparison with pure vinyl ester is shown in detail in Table 6.2. The mass loss residue for all specimens after decomposition shows that pure vinyl ester had a higher residual with 21.95 %, compared to the syntactic foams. It was observed that for all syntactic foams, the mass loss residue showed a reduction as well as a temperature reduction when the wt.% of glass microballoon was increased. It was also observed that increasing the wt.% of glass microballoons led to an increase in the porosities content in syntactic foam rather than affect a reduction in the $T_{peak.}$ The increasing glass microballoon content with thin wall thickness showed the reduction of mass loss. Hence, the reduction of the wt.% of vinyl ester resin by means of using a higher wt.% of filler provided composites with a lower thermal stability.

Table 6.2: Typical result for thermogravimetric analysis syntactic foam

Specimens	T_{onset}	T_{end}	T_g max	Mass loss residue	Temperature residue	T_{peak}
	°C	°C	°C	%	°C	°C
Pure VE	381	457	118.00	21.95	433.69	434
SF-2WT	382	456	108.11	21.13	435.90	436
SF-4WT	380	455	111.00	19.11	432.98	433
SF-6WT	381	450	115.92	19.83	426.17	429
SF-8WT	374	444	112.59	19.40	426.50	426
SF-10WT	386	447	113.82	19.05	420.85	423

Figure 6.8 showed the typical result from a TGA analysis comparison between pure vinyl ester and syntactic foam 2 wt.%. For vinyl ester, degradation occurred in the single stage around 110 ºC. Compared with syntactic foams, specimens had a higher degradation temperature at 140 ºC for SF-2WT and a minimum temperature at 90 ºC when more glass microballoon content was added. This occurred due to much debris or flakes from glass microballoons, and their potential to increase the cavity and matrix porosity in the syntactic foam. In all syntactic foams, the release of moisture led to a slight weight loss of between 50 ºC to 100 ºC. At approximately 150 ºC – 200 ºC, the degradation profile of the composites started according to the thermogravimetric analysis. Between 200 ºC and 380 ºC, degradation of the syntactic foam followed, which relates to constituent decomposition. A similarly, observation detected degradation for different volume fractions of glass microballoon when added to epoxy matric resin syntactic foam (Tien et al., 2009). Continued decomposition was evident from 400 ºC until the temperature reached nearly 453 ºC at which point a constant mass was achieved.

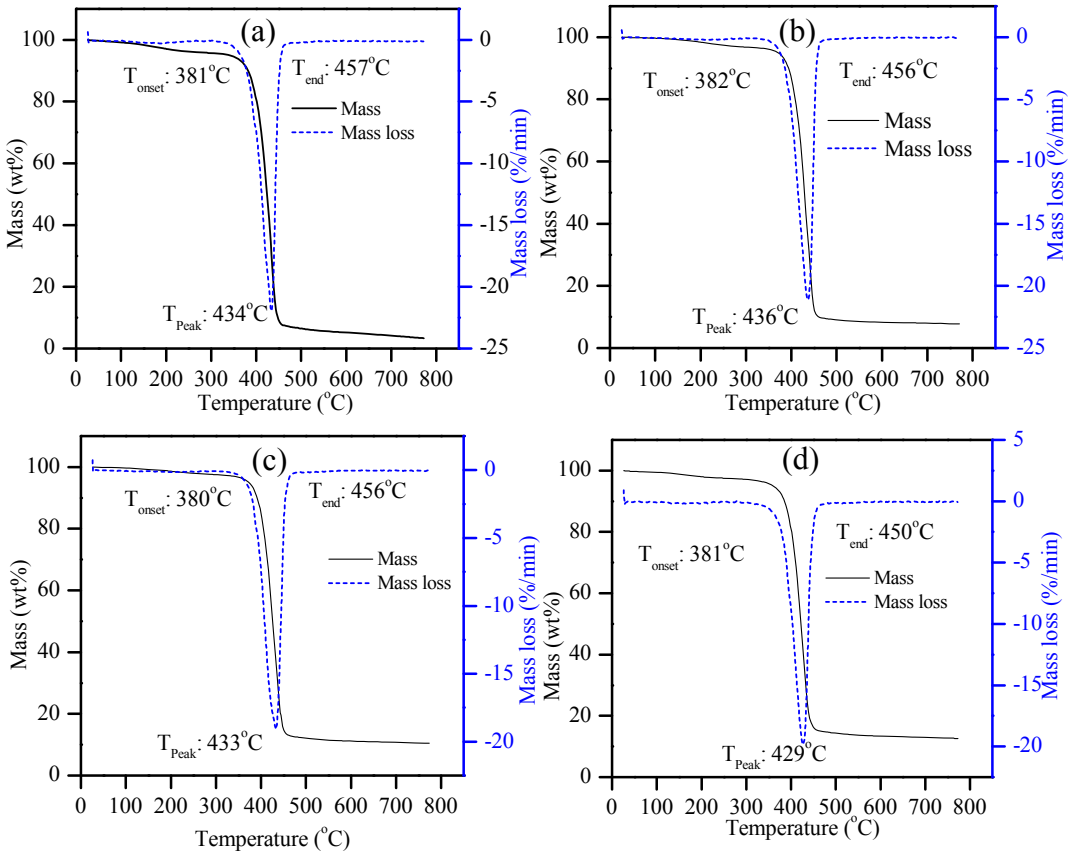

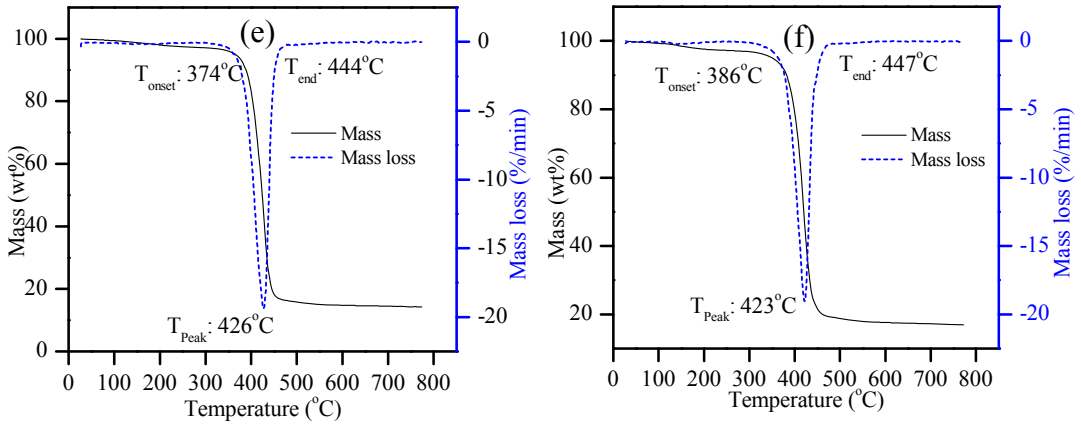

Figure 6.10: Typical results for TGA/DTGA for (a) Pure vinyl ester (b) SF-2WT. (c) SF-4WT, (d) SF-6WT, (e) SF-8WT, (f) SF-10WT

6.3.3 Kinetic parameter study

The Broido method with Equation (6.14) was used to evaluate the kinetic parameters. Broido assumes that the degradation from the first order reaction with the plot graph ln(ln(1/Y)) versus (1/T) for the stage of thermal degradation would produce the linear line fitting. A plot of ln(ln(1/Y) versus (1/T) gives a linear line by using a linear fitting approach. The slope of the plot shows the activation energy of the degradation with intercept at the ln(ln(1/Y) axis. The values of the decomposed temperature range, frequency factor (S^{-1}), activation energy (E_a) and regression value (R^2) are shown in Table 6.3. A lower activation energy was required to decompose neat resin rather than syntactic foams. The trend showed that the maximum activation energy for decomposing the specimen with 6 wt.% glass microballoon produced 36.68 $kJmol^{-1}K^{-1}$. The activation energy produced needed more energy to decompose with a composition of 2 wt.% - 4 wt.% of glass microballoons. This was due to the matrix bonding between resin and filler, which had a strong relationship, which was difficult to separate for the decomposition process. Figure 6.8 (b) and Table 6.2 also show that the decomposition was completed at T_{peak} 456 ^oC until it reached 500 ^oC – 600 ^oC to finish when compared with other compositions. Wouterson et al., (2007) also found that decomposition for short fibre reinforced glass microballoon/epoxy resin syntactic foam was achieved between 550 ^oC – 600 ^oC. It required less activation energy for the specimen with the higher glass microballoon content, especially for the 10 wt.% specimen. This was due to the syntactic foam displaying softer and brittle behaviour with the crystallinity of the matrix resin, also resulting in lower energy.

Table 6.3: Kinetic parameter study on syntactic foam using the Broido method

Specimens	Decomposition temperature range	Frequency factor	Activation energy	Regression value
	(T/°C)	$s^{-1}(10^{-5})$	(E_a/kJmol^{-1}K^{-1})	(R^2)
Pure VE	380 - 460	6.01	32.60	0.88212
SF-2WT	380 - 455	7.17	36.47	0.84256
SF-4WT	380 - 456	7.16	36.68	0.85827
SF-6WT	380 - 450	6.30	33.57	0.84049
SF-8WT	370 - 440	6.35	33.70	0.84044
SF-10WT	385 - 450	5.97	32.28	0.84527

Applying the first-order reaction of the polymer composite due to degradation can be plotted in Figure 6.11 using the Broido method. Generally, all specimens were comparable with neat resin, which showed the degradation trend decreased when the temperature was increased. The degradation process for syntactic foam occurred, starting from positive E_a to negative E_a, due to a two-step decomposition process. Similar results were reported by (Gopalakrishnan and Sujatha, 2011).

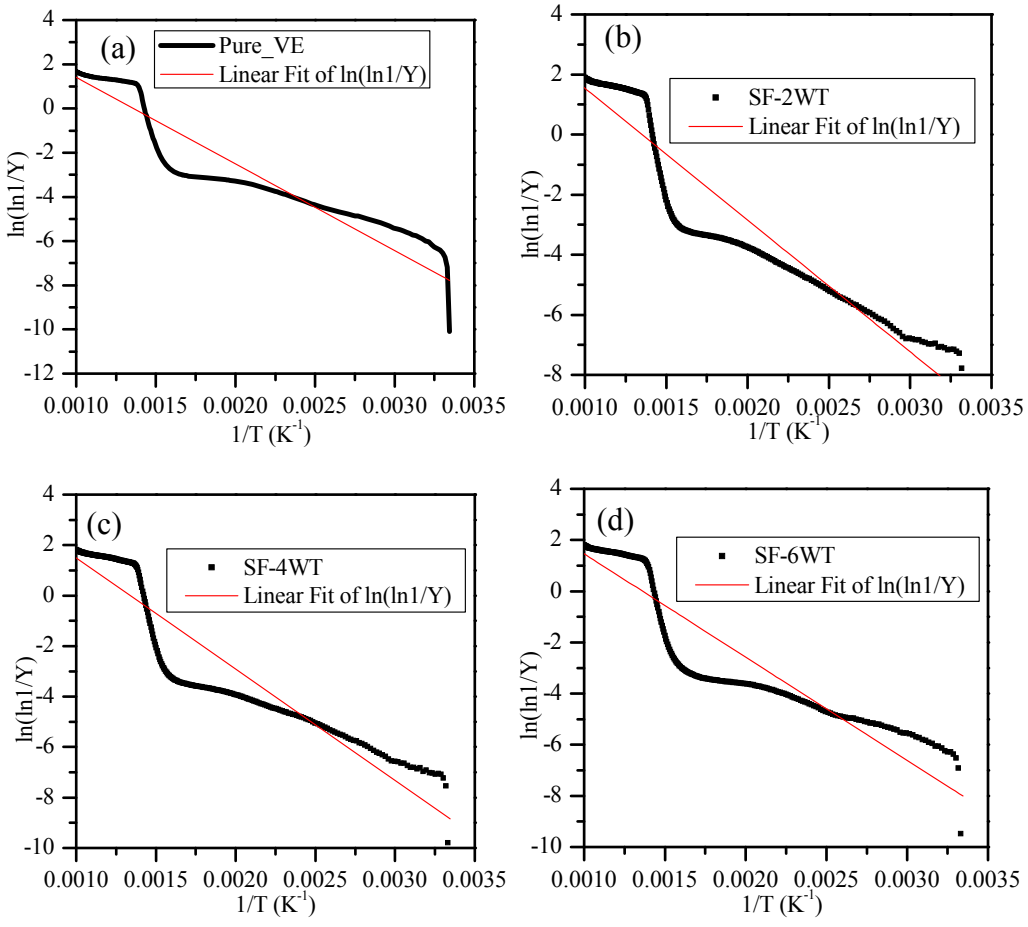

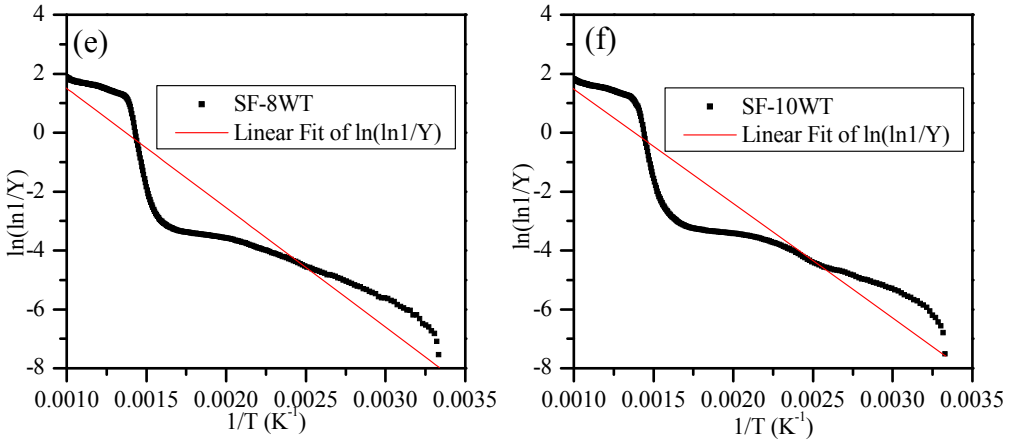

Figure 6.11: Typical results for a decomposition rate with linear fitting over the degree of conversion (1/Y) versus (1/T) for (a) Pure vinyl ester (b) SF-2WT. (c) SF-4WT, (d) SF-6WT, (e) SF-8WT, (f) SF-10WT

6.3.4 Dimension stability affected by physical properties

Figure 6.12 shows the typical result from a thermal dimension change with temperatures ranging between 20 ºC – 75 ºC. It reveals that the dimension change was steepest when it had different glass microballoon content in the syntactic foam but was still led by pure vinyl ester. It further showed that specimen 4 wt.% had a higher dimension change when compared with other specimens, which had a thicker wall thickness with higher porosities as well and the least voids content (see Chapter 3). The thin wall thickness contributed to the smaller dimension change belonging to the specimen with 10 wt.% as well as higher porosities content. These results contradicted previous findings reported by Shunmugasamy et al., (2012), who found that it related only to the wall thickness but they did not mention it in the context of porosity. This finding also agreed with their results that increasing the glass microballoon contents would likely increase the dimension stability in the syntactic foam as well.

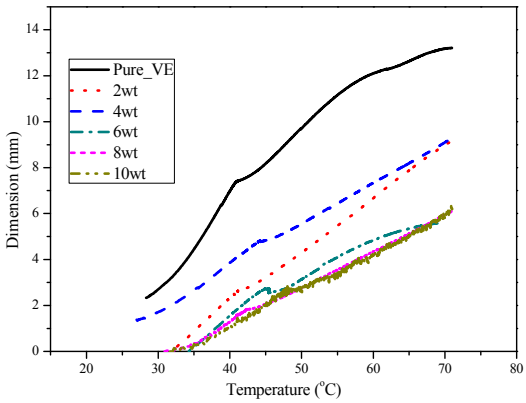

Figure 6.12: Typical result for thermal stability change with temperature

6.3.5 Coefficient of Thermal Expansion (CTE), α affected by physical properties

From the experimental results, CTEs were analysed and compared to understand the effect of the physical parameters of syntactic foam on CTE. The CTE result for all specimens, including pure vinyl ester, is shown in Figure 6.13. It shows that the CTE of glass microballoon syntactic foam decreased when the glass microballoon in syntactic foam was increased. This graph reveals a 30 % - 70 % decrease in the CTE of syntactic foams compared to the neat resin result. The lowest CTE value was observed for 10 wt.% glass microballoon, which contained the lowest average wall thickness, as shown in Table 6.4. The reduction of CTE related to the physical properties of glass microballoons, such as wall thickness, radius ration, porosities and voids, which were interesting to discover for a more concrete understanding of how to obtain the quantitative parameters in this study. The percentage reduction of the CTE can be determined with a different (ratio) starting from pure vinyl ester and a specimen of 2 wt.%, which is also shown in Table 6.4. Incorporation of filling with glass microballoon resulted in up to a 63 % reduction and it kept decreasing to 53 % for a temperature change from 30 ^{o}C to 70 ^{o}C.

Table 6.4: CTE syntactic foam at different temperature

	CTE	T: 30^{o}C	CTE	T: 50^{o}C	CTE	T: 70^{o}C
Specimens	α (μm^{o}C^{-1})	Δ (%)	α (μm^{o}C^{-1})	Δ (%)	α (μm^{o}C^{-1})	Δ (%)
Pure VE	100.18	-	-	-		-
2wt.%	63.70	-36.41	68.59	-31.53	69.50	-30.62
4wt.%	59.15	-40.95	58.99	-41.12	45.80	-54.27
6wt.%	41.58	-58.49	56.88	-43.22	32.80	-67.25
8wt.%	38.89	-61.18	45.38	-54.69	57.06	-43.04
10wt.%	36.71	-63.35	44.61	-55.46	46.77	-53.31

The CTE values between 4 wt.% and 6 wt.%, and between 8 wt.% and 10 wt.% did not have much difference between them, whereas they were almost 5 % and 1 % if compared to each other, respectively. This gap could be contributed to the porosity and voids content occurring in the syntactic foam with a debris of glass microballoons.

The thermal flow through these kinds of mechanisms will affect the CTE value in the syntactic foam and can be seen in the SEM photo in Chapter 5. The specimen with 2 wt.% had the highest CTE value, which also corresponded to the lower glass microballoon. This trend was also detected by Shunmugasamy et al., (2012) who also noted that the CTE value decreased when glass microballoon was added (with a 30 % - 60 % volume fraction) into the vinyl ester matrix resin.

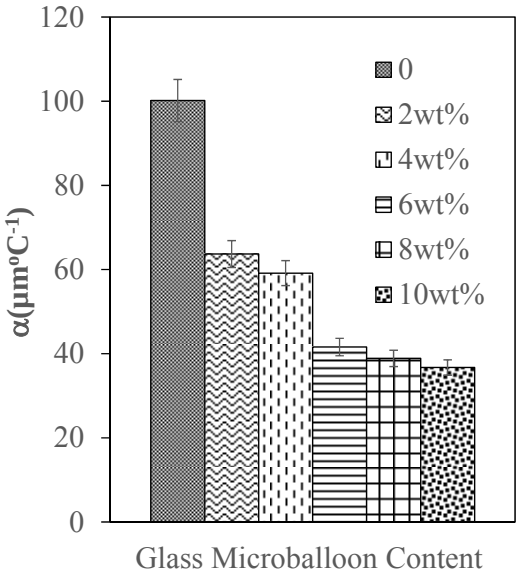

Figure 6.13: Experimental CTE measured values for neat resin and syntactic foam.

6.3.6 Comparative study on CTE using Turner's model

The CTE in the experimental result was analysed and plotted to be normalised in the CTE vinyl ester resin as shown in Figure 6.14. The CTE function was considered at different weight percentages of (wt.%) glass microballoons at temperatures of 30 ºC, 50 ºC and 70 ºC. Generally, the normalised CTE steeply decreased when glass microballoon was added from lower to higher temperature conditions. According to the graph, normalised CTE at a temperature of 70 ºC shows to be more stable when compared to other temperatures, particularly in combination with more than 4 wt.% glass microballoon. It shows that a lower thermal heat resistance application was also useful and not only for weight saving composite material, with varied wall thickness as reported by Shunmugasamy et al., (2012). Starting from 2 wt.%, the behaviour showed a more polymerised condition with 20 %, which is different from pure resin CTE. The variation between three different temperatures did also have almost no gap between 1 to 5 %, when close to each other. Normalised CTE rapidly changed at

between 6 – 8 wt.% but until 10 wt.% it was suitable to be used for lower heat transfer applications at 30 °C.

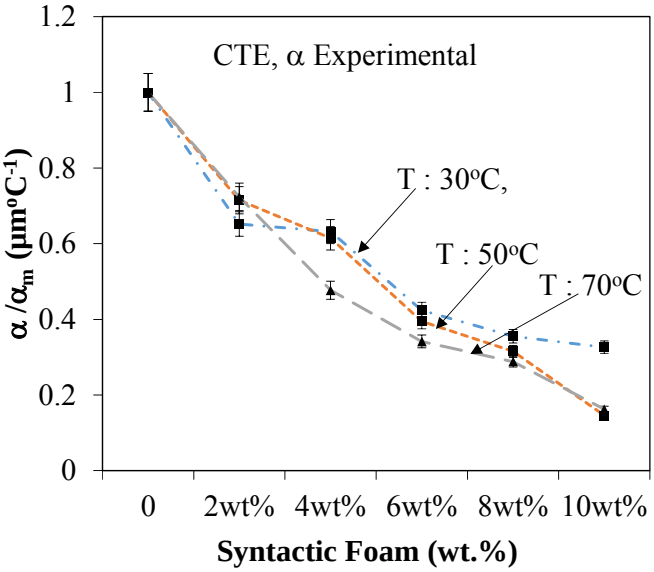

Figure 6.14: Normalised CTE function of wt.% glass microballoon.

The dimension changed at various temperatures, which shows that a temperature of 30°C, obtained from a specimen with 2 wt.%, had a lower expansion rate, with the highest slope of dimension change-temperature plot at 0.2006 μm/°C. This characteristic behaviour made polymeric resin the dominantly crystallised influence in syntactic foam. Furthermore, the specimen of 4 wt.%, between temperatures 30 °C and 50 °C, exhibited a similar CTE value of $\alpha = 58$ μm°C^{-1}.

The modified Turner's model was used to predict the CTE values function with different glass microballoon (wt.%), as shown in Figure 6.15. The CTE value also varied within a different parametric investigation, whereby radius ratio (η), cavity porosity (ϕ_g), and matrix porosity (ϕ_m) were estimated at three different temperatures: 30 °C, 50 °C and 70 °C. Generally, the CTE value decreased when the glass microballoon content was increased at different temperatures, thus following the experimental values. Similar work has also revealed that a parametric study on the wall thickness of glass microballoons decreased their CTE values when the filler content was increased in syntactic foam (Shunmugasamy et al., 2012). From the graph, it can be predicted that Turner's model showing CTE values was varied in terms of radius ration, η and syntactic foam for different wt.% of glass microballoons. The CTE decreased from 70 - 37 μm°C^{-1}, which led to a milder effect on the radius of the glass

microballoon. Turner's model CTE trend value closely matched the experimental results, particularly specimens 4, 8 and 10 wt.% for a temperature at 30 ^{o}C. At temperatures of 50 ^{o}C and 70 ^{o}C, Turner's CTE model values were nearest to the experimental results at 4 wt.% glass microballoons. In conjunction with additional glass microballoons, the estimation of CTE in Turner's model will have a reduction from 66 % to 36 % with varied temperature conditions, as shown in Table 6.5.

Turner's prediction model, when related to porosity in this study, revealed that the CTE trend for both cavity porosity and matrix porosity were close to each other, as shown in Figure 6.12. This is also evidence that both porosities were present in all specimens and that it increased their percentage in Table 6.1 when many fractured glass microballoons in the syntactic foam occurred. At a temperature of 30 ^{o}C, Turner's model predicted a lower CTE when compared to the experimental result. Within this behaviour, α was decreased from 28 $\mu m^{o}C^{-1}$ to 19 $\mu m^{o}C^{-1}$ but still below the α experimental with 38 $\mu m^{o}C^{-1}$. Also in this model, many CTE values were much higher than the experimental CTE value with elevated temperature conditions especially at 50 ^{o}C – 70 ^{o}C. This model could predict that the CTE value was close to the experiment for the composition of glass microballoons of between 2 wt.% - 4 wt.%, while a higher composition of glass microballoon thus contributed more porosity. As a result, a gap occurred between the experimental CTE result and Turner's porosities model especially at a temperature of 70 ^{o}C with large gap CTE, α: 48 -57 $\mu m^{o}C^{-1}$. The reduction of the CTE could be calculated by using this model from 78 % to 44 % and 80 % to 45 % for cavity porosity and matrix porosity, respectively as shown in Table 6.5. Therefore, this model predicted that the CTE was higher in porosity at a high temperature even though there was a decreasing trend towards being inclusive in terms of glass microballoon content.

In this study, the average diameter glass microballoon, with a range of 72-75 μm was used with the average r_o and r_i that could be estimated at a range of between 36-38 μm size, respectively. Hence, the wall thickness of this microballoon could be calculated by using the equation introduced by (Tien et al., 2009). The thermal stability of this syntactic foam could be varied in terms of wall thickness, due to a different radius of glass microballoon. Similar results have also been detected in previous studies where

the thin wall thickness (1-η) < 0.4, decreased the CTE sharply, which was similar in this report. This could be happening when the porosities regime was dominantly in the syntactic foam, which was contributed to an increase in the CTE value. Therefore, porosity also contributed to a change in phase- transformation, which occurred internally in the syntactic foam. It can be seen in Figure 6.15 that the dimensional change occurred nonlinearly up to a glass transition temperature, T_g of syntactic foam. Beyond this temperature, the behaviour of syntactic foam totally changed in terms of the dimensional variation and it changed to a fairly linear graph. Saha et al., (2008) also found similar results for epoxy resin composite. The potential changes in phase with the dimensional stability of the various types of glass microballoon when mixed with an epoxy resin (Saha et al., 2008).

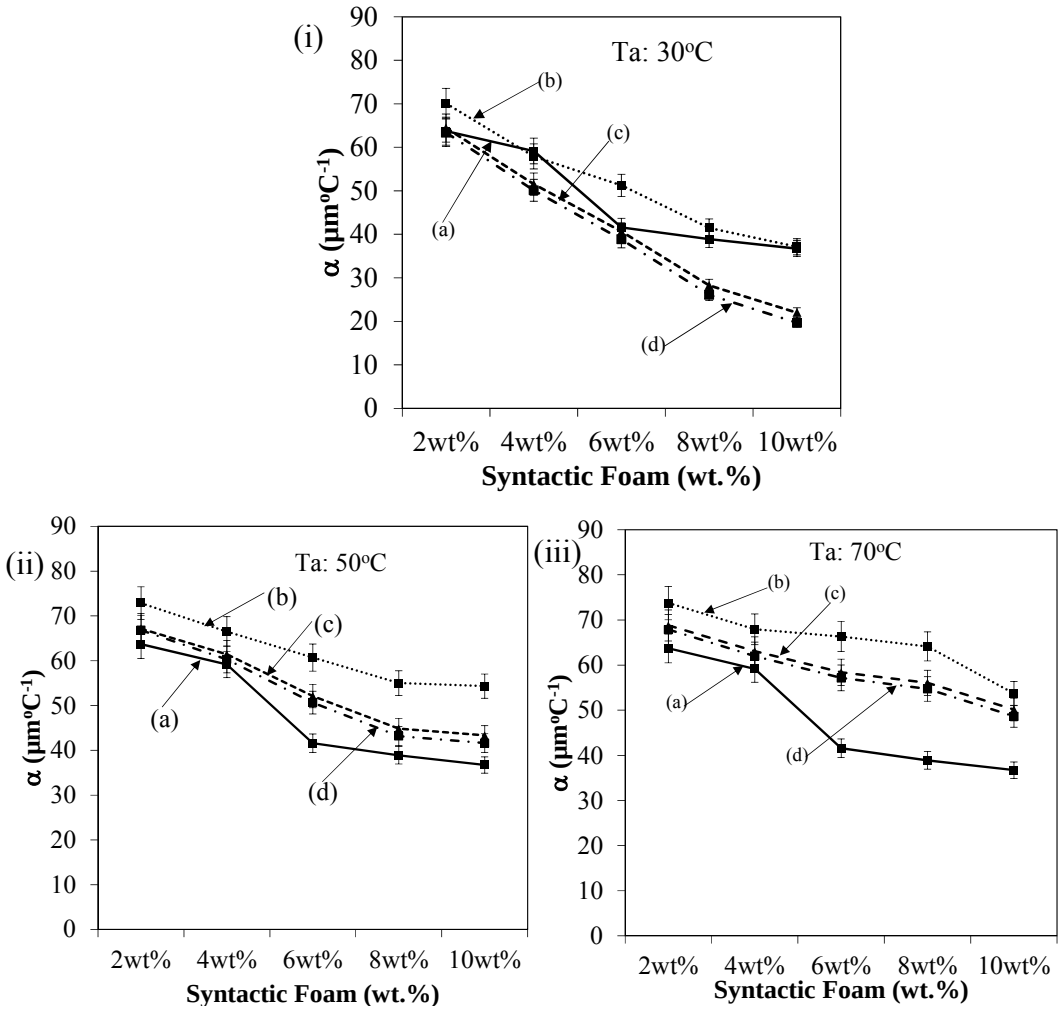

Figure 6.15: Typical comparison of CTE values using Turner's model (a) Experimental (a) Radius ratio (η), (c) Cavity porosity (ϕ_g), (d) Matrix porosity (ϕ_m), at (i) Ta: 30°C, (ii) 50°C and (iii) 70°C.

Table 6.5: Difference (Δ) of α CTE Tuner's model at temperature 30°C, 50°C and 70°C.

Specimen Different at 30°C	Tuner's Model Radius ratio, η Δ (%)	Tuner's Model Cavity Porosity, ϕ_g Δ (%)	Tuner's Model Matrix Porosity, ϕ_m Δ (%)
2wt%	-30.08	-35.70	-36.77
4wt%	-42.21	-48.55	-49.99
6wt%	-48.84	-59.45	-61.24
8wt%	-58.63	-71.79	-73.97
10wt%	-62.93	-78.02	-80.38
Different at 50°C			
2wt%	-27.26	-32.97	-33.32
4wt%	-33.63	-38.69	-39.83
6wt%	-39.43	-47.99	-49.44
8wt%	-45.10	-55.23	-56.91
10wt%	-45.78	-56.76	-58.48
Different at 70°C			
2wt%	-26.39	-31.32	-32.26
4wt%	-32.19	-37.03	-38.12
6wt%	-33.79	-41.70	-42.95
8wt%	-35.97	-44.04	-45.38
10wt%	-46.42	-49.93	-51.44

6.3.7 Comparison of SCF between experimental and one strain gage

A tensile property test of vinyl ester/glass microballoon syntactic foam for different compositions of glass microballoon content was carried out. The specimens were named as SCFT-01, SCFT-02, SCFT-03, SCFT-04 and SCFT-05. The representative stress–strain curves for all specimens were comparable between experimental and simulation, using a strain gauge, which is presented in Figure 6.16. These curves showed a linear stress–strain relationship immediately followed by brittle fracture. The tensile stress–strain curves for other types of syntactic foams showed similar features (Gupta et al., 2010, Gupta and Nagorny, 2006). The maximum tensile strength from the overall specimens belonged to SCFT-01 for both strain gauge (SG) and experimental (EXP) with 32.74 MPa and 30.72 MPa, respectively. However, it was led by pure vinyl ester at 40 MPa and for all specimens showed a decreased when the glass microballoon content was increased.

The tensile strength was observed to have decreased for both SG and EXP values between 20.51 – 20.56 MPa for SCFT-02. But then it increased 5 % for SCFT-03 to 25 MPa and decreased again for SCFT-04. Generally, the tensile strength trend showed a continued decrease starting from SCFT-02 to SCFT-05 with the strength at 11.5 MPa. Hence, the specimens of tensile strength were observed to fracture more easily due to de-bonding of the glass microballoons in the matrix resin when they were added into the matrix resin as well. The reduction of the strength value of syntactic foam might be concerned with the matrix phase in the system which may act as a load bearing phase (Wouterson et al., 2007). They tested glass microballoon in epoxy resin as a matrix system. From their observation, it was found that the matrix-microballoon interface did not appear to be very strong in these composites, and the presence of a higher volume fraction of microballoons only reduced the volume fraction of the epoxy resins in the structure, causing a lower strength of syntactic foam.

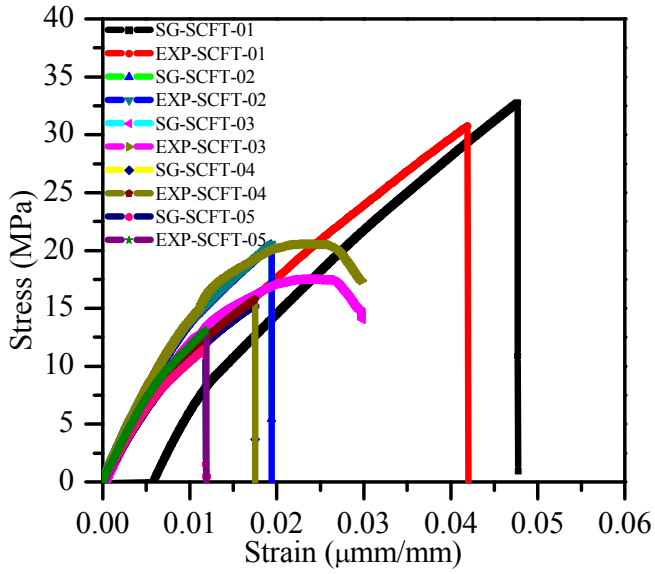

Figure 6.16: Tensile stress-strain curve between experimental and strain gage value

Figure 6.17 shows the comparison modulus of elasticity between tensile specimens for EXP and SG. Generally, the modulus of elasticity decreased for all specimens with the highest belonging to SCFT-01 SG with 1472 MPa, while the higher modulus elasticity for EXP belonged to SCFT-03 at 1586 MPa. The range of modulus elasticity for all specimens was between 703 and 1586 MPa. It was observed that these values showed a reduction when more glass microballoon was added in the syntactic foam. It is clear that the increase of glass microballoon content affected particularly the matrix-glass

microballoon interface bonding in these composites. The reduction for modulus of elasticity SG was more constant when compared with EXP. This may have been due to the slope for the tensile stress-strain curve showing not much difference, which was captured with a strain gauge data logger system. Similar to Wouterson et al., (2007) findings, the increased weight percentage of glass microballoons only reduced the volume fraction of vinyl ester. Gupta and Nagorny (2006) also found that the modulus elasticity decreased when the glass microballoon content was increased. This is also contribution from the difference types of wall thickness and density (Gupta et al., 2010, Gupta and Nagorny, 2006). Therefore, the strength of the composite was reduced when the matrix content decreased.

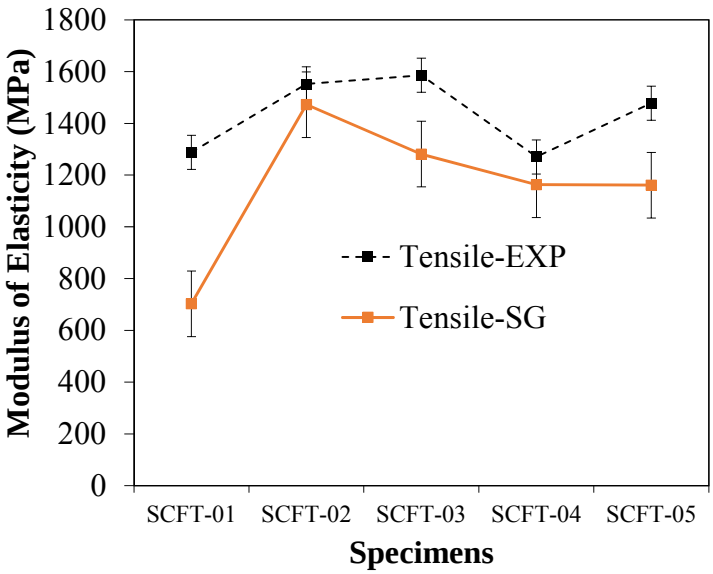

Figure 6.17: Comparison of typical modulus of elasticity between experimental and strain gage value

Figure 6.18 represents the observation for the fractured tensile specimens in this study. It can be observed that the fractured specimens were broken within the extensometer range of 250 mm in length, except for specimen SCFT-04. From the SEM observation showed at Figure 6.18 (a), the tensile fractured mechanism seems to have been mainly related to particle–matrix de-bonding. The matrix propagation occurred between matrix and glass microballoons (Swetha and Kumar, 2011). As a result, the majority of fractured patterns for all specimens was identified at a narrow section of the bottom area except for the SCFT-03 specimen, which occurred in the tensile grip jaw area. Therefore, with a decrease in the volume fraction of the matrix resin in the material structure, the strength of the composite was observed to have decreased. This also

contributed to the low density behaviour if the matrix content in the syntactic foam decreased. Among all specimens, the SCFT-05 one was observed to fracture close to the SG area. The SCF for all specimens that were calculated using Equations (6.18) and (6.19) with the maximum strength and modulus elasticity is shown in Table 6.6. Generally, the trend of SCF for both SG and EXP constantly decreased for SCFT-01 to SCFT-03 but it increased again towards SCFT-05. This phenomenon may be related to the increase in glass microballoon content in syntactic foam. Based on Figure 6.18, specimen SCFT-05 shows the strain gauge unit, and the fractured are was close to the neck.

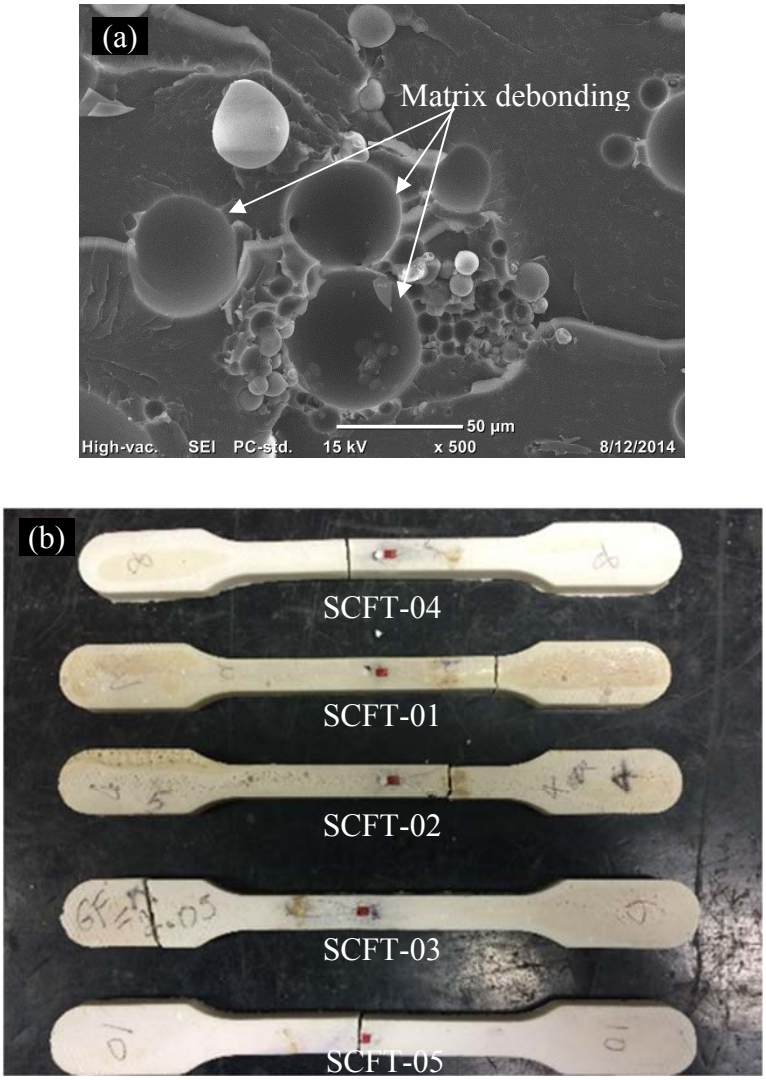

Figure 6.18: (a) Matrix particle debonding of tensile specimen (b) Representative of the tensile fractured specimens

Therefore, it shows that the SCF that was measured directly at the hole area had a higher SCF value 2.25 as well. Specimens SCFT-02 and SCFT-04 also fractured near the hole area at approximately 10 mm and the SCF value was more accurate for both SG and EXP. The specimens SCFT-01 had a neck fracture at more than 10 mm from the hole and SG detector unit. Then for specimen SCFT-03, the fracture was far away from the hole and the SG unit and showed a different value of 1.36 %.

Table 6.6: SCF and mechanical properties of syntactic foam.

Specimens	Stress Concentration Factor, SCF		Max. Stress, σ (MPa)		Modulus of Elasticity (MPa)		Diff. SCF (SG-EXP.)
	SG	EXP.	SG	EXP.	SG	EXP.	%
SCFT-01	2.24	2.25	32.74	30.72	702.57	1288.10	0.40
SCFT-02	2.23	2.24	20.51	20.56	1472.20	1552.50	0.40
SCFT-03	2.21	2.18	17.52	15.50	1281.03	1585.93	1.36
SCFT-04	2.22	2.19	15.27	15.77	1162.61	1270.28	1.35
SCFT-05	2.25	2.22	11.55	12.69	1160.89	1477.94	1.30

The local strain value for all specimens can also be compared with the experimental values shown in Figure 6.19. In this graph, both SCF values for SG and EXP are exhibited between the ranges 2.15 to 2.30. The specimens SCFT-03 showed a lower SCF, which might have been due to the fracture not being in the extensometer range area, which had a 25 mm range. This is considered out of the range but it is still more than 2.0.

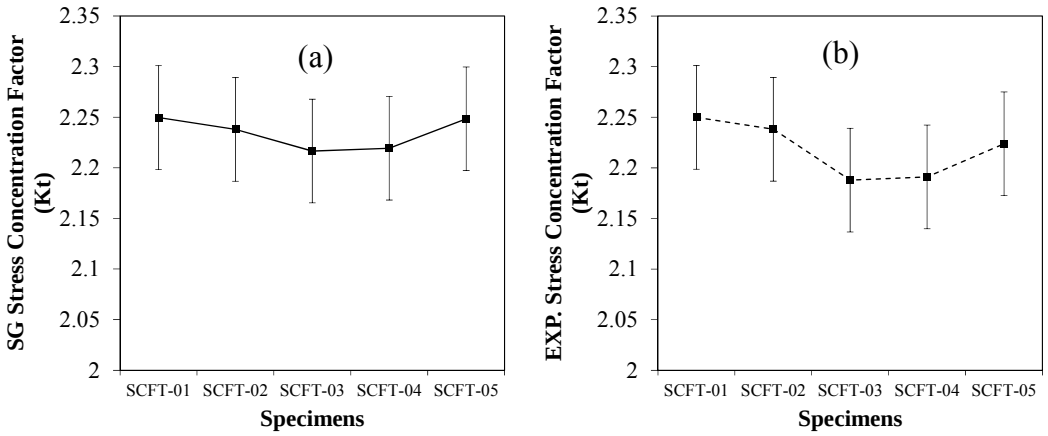

Figure 6.19: Representation of the variation of SCF between (a) SG and (b) EXP

6.3.8 FEA modelling comparison of tensile properties for SCF at a hole

The longitudinal and transverse values of the stress-strain relationships with a failure mode of a specimen under tensile loading are displayed in Figure 6.20. Similar to Section 6.3.7, tensile with one strain gauge, the values of the stress and strain in the curve are the average values of the specimens with two strain gauges attached. The strain gage specification and gage factor indicated that the unit is in "μmm/mm" provided by manufacturer company BESTECH. It should be noted that the calculation of tensile stress and modulus values was based on the equations suggested in the corresponding standard. The calculated tensile modulus was found to be 2.6 GPa and -8.6 GPa for SG1 and SG2, respectively. In this figure, it can be observed that the specimen exhibited an elastic behaviour with a maximum tensile strength of -15.3MPa. The estimated strain at this failure stress was about 5635 μmm/mm and -1680 μmm/mm for SG1 and SG2, respectively. From these results, it can be seen that the micro strain at SG1 was compression mode while the micro strain behaviour at SG2 became tensional mode.

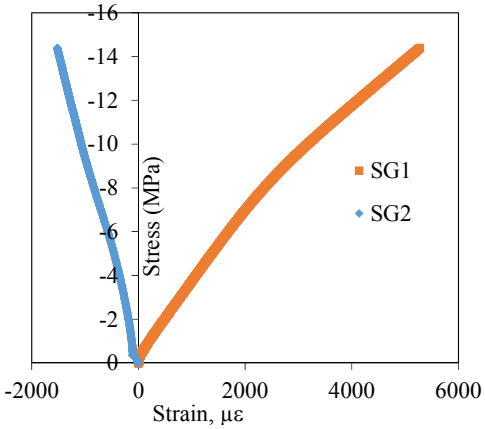

Figure 6.20: Representation of a comparison between SG1 and SG2 tensile stress-μstrain curves

The result of longitudinal and transverse tests show FEA predictions with strain gauge measurements of the hole with a distance using WCS (world coordinate system) [X: 8.55, Y: 92.041, Z: -5.2585] mm from an SG unit using PTC CREO software. At this FEA, the external forces were varied with comparable actual forces in the tensile experimental results. The prediction of micro strain attached to SG1 and SG2 could be determined as micro strain, in Y-axis & Z-axis directions, as shown in Figure 6.21 (a) and (b), respectively. Amongst the scale strain levels SG1, the maximum micro strain

value was the red colour with 0.03095 μmm/mm, while the minimum micro strain was the dark blue colour with -0.00234 μmm/mm. Figure 6.19(b) showed the micro strain attached to the SG2 at Z-axis directions. The maximum micro strain value was also detected at the edge of the hole with 2893 μmm/mm and a minimum value of -0.00234 μmm/mm. This revealed the stress concentration near the hole, particularly at the edges of both sides. This occurred when the tensile achieved its ultimate strength, and at this point the interconnection between glass microballoons was weakened and many porosities, including void such as broken microballoon, could arise in the specimen at 10 wt.%. A detailed discussion has been presented in Chapter 3 of the SEM micrograph observation. SG1 detected a similar phenomenon where the bulk moduli were lower than the SG2 results. Balch and Dunand (2006) suggested using a solution developed by Bardella and Genna for syntactic foam stiffness, and in particular that shear and bulk moduli for homogenised materials could be solved using the four-phase consistent method. Furthermore, when the load was increased in tensile testing, particularly in the longitudinal strain, delamination and matrix cracks could occur particularly at the transverse strain, Z- axis (Balch and Dunand, 2006). At this location, it was very critical along the edge corners of the hole, which may have affected the SCF values as well. The experimental values, when compared to the physical actual specimen, showed that the cracking could also transpire for the middle specimen near the hole area. Hence, it is clear that the stress concentration in this highlighted area indicated that cracks were imminent in this region.

The investigation using FEA modelling was continued in the form of a comparison longitudinal-transverse loading by plotting the graph Load-μstrain as shown in Figure 6.21. Both the FEA micro strain values and the local micro strain SG were increased for both longitudinal and transverse modes. Estimates of around 90 % and 70 % in experimental values followed the FEA values for SG1 and SG2, respectively. This figure shows the linear load-micro strain relationship up to the final failure and is in good agreement with the predicted load-μstrain relation based on the FEA method. It should be noted that the failure in the FEA model was assumed to adopt the μstrain according to the failure of the specimen, derived from the tensile test, and was used to calculate the stress at the failure point. It was also assumed that the material parameter such as modulus of elasticity, E = 1.47 GPa and Poisson's ratio, $\gamma = 0.45$ were exactly the same as the experimental values that had been used in the FEA modelling. In the

graph, the values are more scattered nearest to the FEA linear fitting line and only several points were not aligned at the beginning of testing. On the other hand, µstrain values are scattered everywhere with a minimum strain of -0.0016 µmm/mm for the transverse Load-µstrain plot in Figure 6.22 (b).

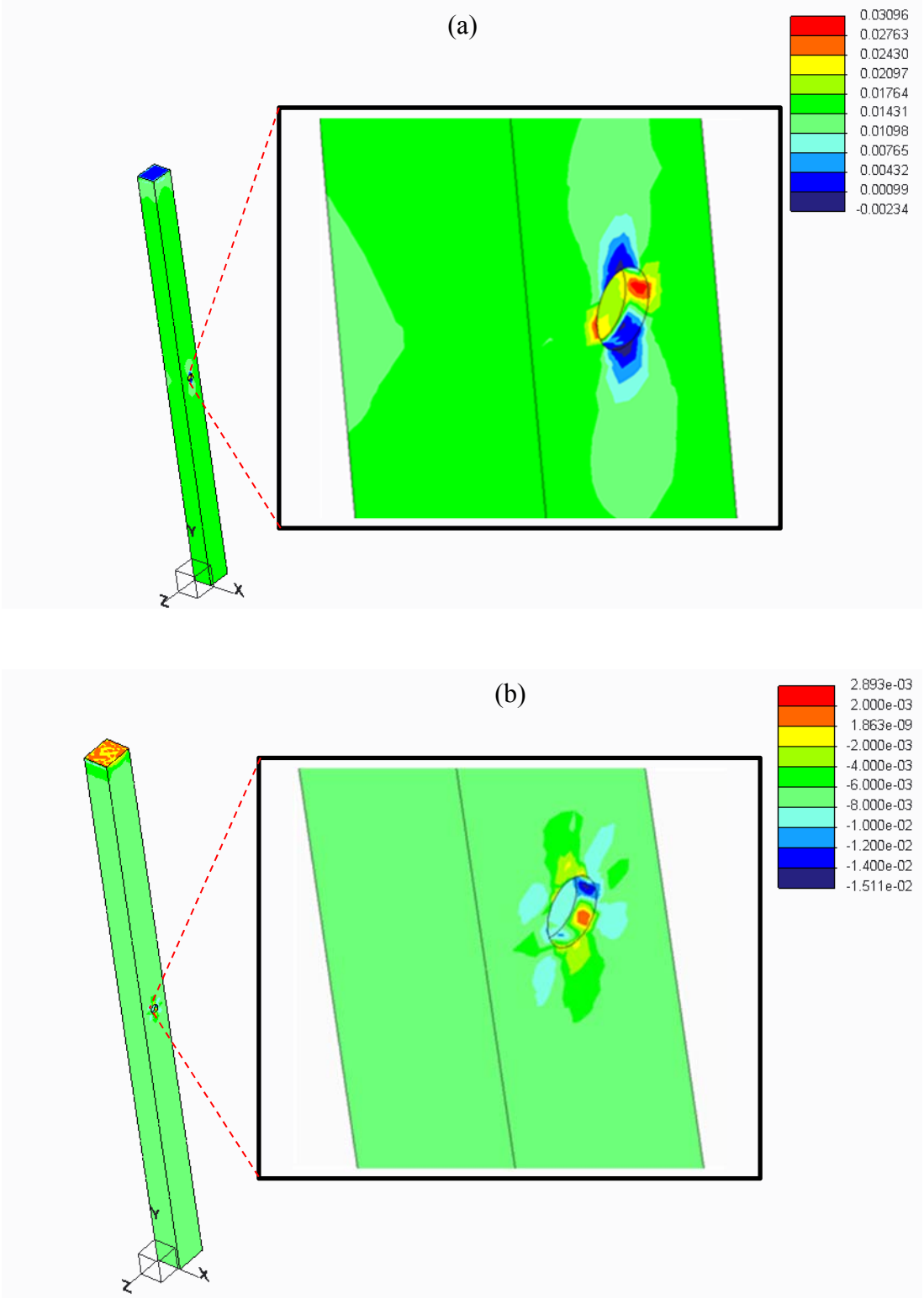

Figure 6.21: Representative FEA modelling for micro strain analysis longitudinal and transverse (a) SG1, (b) SG2

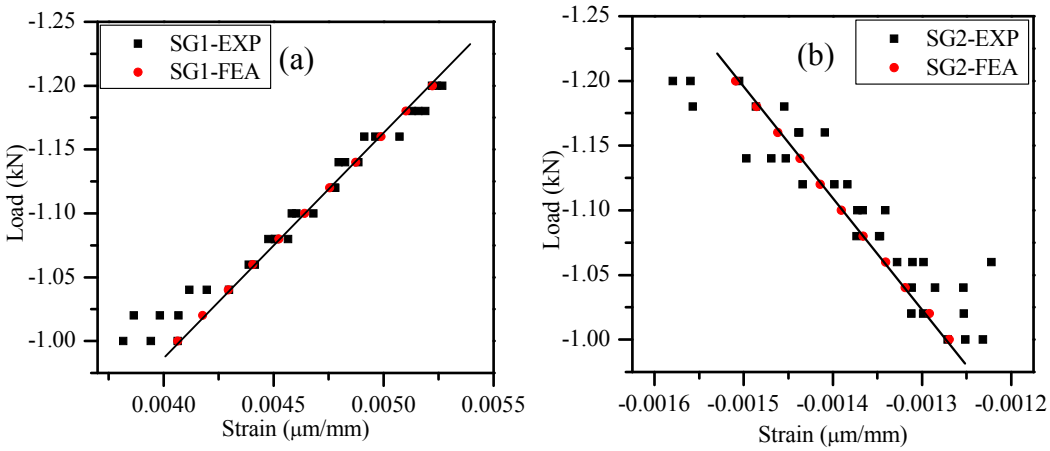

Figure 6.22: Comparison of micro strain values between experimental and FEA analysis (a) Longitudinal-Y axis (b) Transverse-Z axis.

6.3.9 FEA modelling comparison of flexural properties of sandwich panel

The material properties used for this FEA model analysis of the behaviour of a 3-points bending (TPB) test were similar to those used in simulating its tensile behaviour. However, the difference was the addition of GFRP (glass fibre reinforced plastic) skin, which was directly mounted into the syntactic foam core sandwich panels. A detailed discussion on this matter has already been provided in Chapter 4 for flatwise specimens. Similar to tensile FEA simulating, the redefined and auto meshing was also used in the PTC CREO simulator for this investigation. Less skill in preparation of the specimens using the handy layup method affected the mechanical properties in this study. As a result, some specimens may have had a varied core thickness as well as length but the mid span had a fixed value at 75 mm. During flexural tests, SG1 and SG2 were located exactly nearest to the middle top of the specimens in the plunger area and the backs of the specimens were also perpendicular to this area. The applied load in this experiment was transmitted from the loading ram ASTM E1545 - 11(2016)ps to the specimens. Therefore, an area load (pressure load) was suitable for use in simulating the loading condition in the FEA analysis. Figure 6.23 shows the typical results for 3-points bending for a comparison between SG1 and SG2.

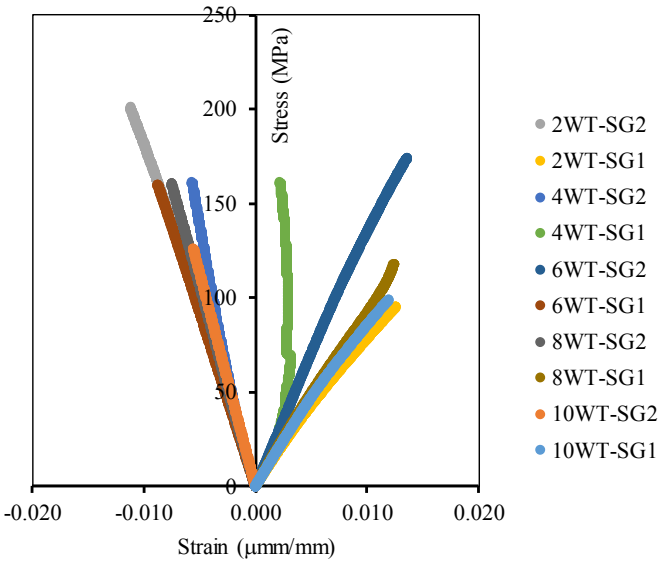

Figure 6.23: Representation of a comparison between SG1 and SG2 flexural stress-µstrain curve

From the Table 6.7, the flexural strength shows a decrease when glass microballoon content was increased as core materials in the syntactic foam sandwich panels. It also shows that all the parameters did not contribute much to the flexural strength but the wide specimens' strength decreased. The increasing glass microballoon content also played an important role in decreasing the modulus of elasticity sandwich panels. The thin specimen, for example 8WT, had an effect on the inertia value, while the thicker one increased their inertia.

Table 6.7: Typical flexural properties of syntactic foam sandwich panels.

Specimens	Thickness	Width	Length	Max. Stress,	Load Max.	Modulus of Elasticity	Moment Inertia
	t (10^{-3} m)	D (10^{-3} m)	L (10^{-3} m)	σ (MPa)	N	E (MPa)	I (10^{-6} m^2)
2WT	12.39	14.24	120	205	3993	1936	2257
4WT	11.03	14.03	110	164	2485	1725	1569
6WT	12.86	12.60	140	198	3665	1122	2233
8WT	9.73	15.11	145	191	2464	1099	1160
10WT	11.30	17.35	144	110	2668	778	2086

The failure mode pattern of flexure specimens, tested under a 3-points bending test and a FEA analysis using CREO simulation software, is revealed in Figure 6.24. The failure mode observed in the flexural test, which was characterised by compressive failure, was also revealed to be due to de-bonding unsymmetrical shear failure between

the skin and core areas that were in direct contact with the loading ramps, as shown in Figure 6.24 (a), with a detailed explanation in Chapter 4. The crack formation under the flexure testing, due to compression, could clearly be seen in the simulated failure mode shown in Figure 6.24 (b). It was apparent from the simulated failure that the side area (the initial compression zone) was imminent. In the figure, the cracked portion is represented by a blue and red-coloured strip at the side edge area. It is worth noting that whilst the surface contact with the loading rams provided a concave green-coloured shape, the middle area produced a small convex line at the side of the sandwich panels. This simulation confirmed the results obtained from the load-strain relationship (Figure 6.23) that whilst this region is compressed during the initial loading, the increase of the loading until failure shifted the surface into tension mode, as revealed in Figure 6.24 (c), for the support beam condition. This FEA failure mode was detected when the stress is fully distributed along the bottom of specimen on the 2-support points area. These weak points with the young green coloured clearly indicated that if loading is increased it will occur more dented under the neat of specimen.

Figure 6.25 shows the load-μstrain relationships obtained from both the flexural testing and the FEA simulation. It should be noted that the micro strain values indicated in the figure are the values at the top of the skin (SG1), while another strain gauge (SG2) was located exactly perpendicular with the loading ramp at the bottom mid-span section of the sandwich panel. As can be seen in Figure 6.23(a), the linear fitting line represented as the FEA simulation was correlated with the experimental micro strain SG1, and then with tabulated data. The peak load obtained from the experiment SG1 was found to be 2 kN at failure strain 0.00989 μstrain. On the other hand, the predicted failure load using the FEA simulation at 2 kN is showed a 0.01191 μstrain. In this case, the μstrain value predicted from the FEA simulation was 17 % higher than the experimental value. This difference of the value was found to be reasonable, indicating that the FEA simulation predicted the flexural behaviour of syntactic foam sandwich panels well. The peak load obtained from the experiment SG2, for example at 1.2 kN, was at failure strain -0.002665 μstrain. A similar observation applied to the FEA simulation at this loading condition where the strain failure could be -0.002743. The differences in value between SG2 and the FEA

simulation was about 2.7 %. Again this value reasonably indicated that the FEA was in good agreement for another comparison μstrain value.

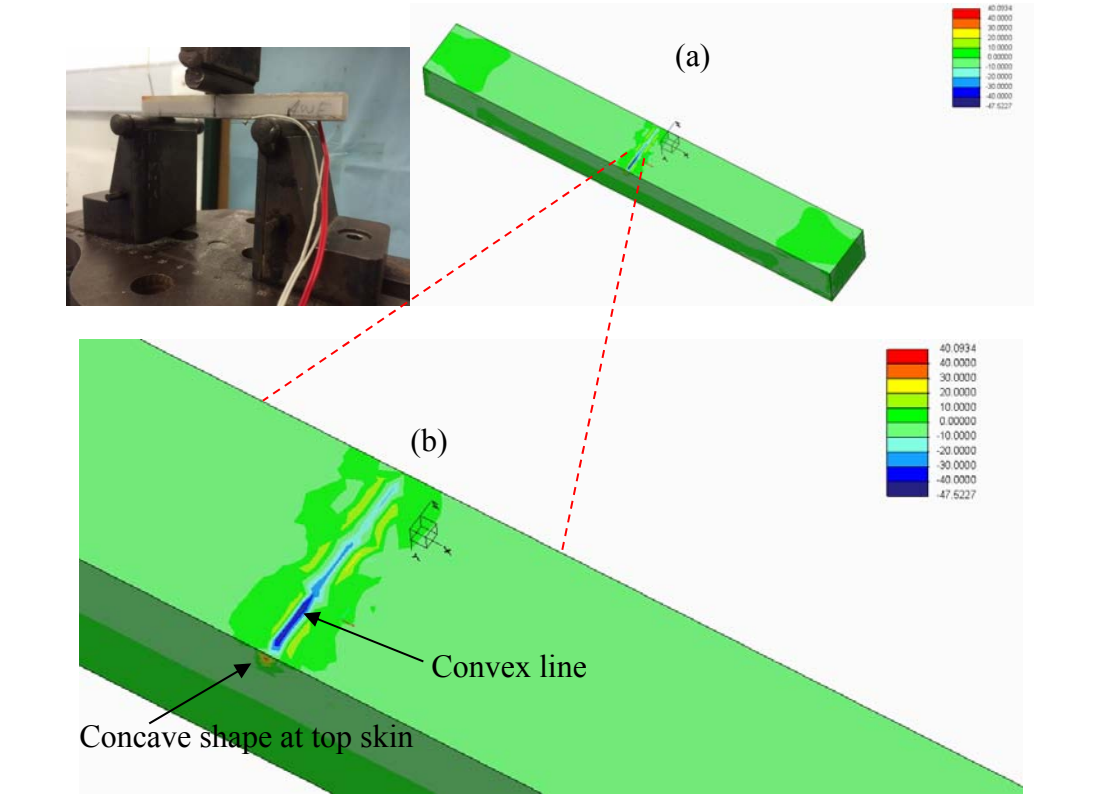

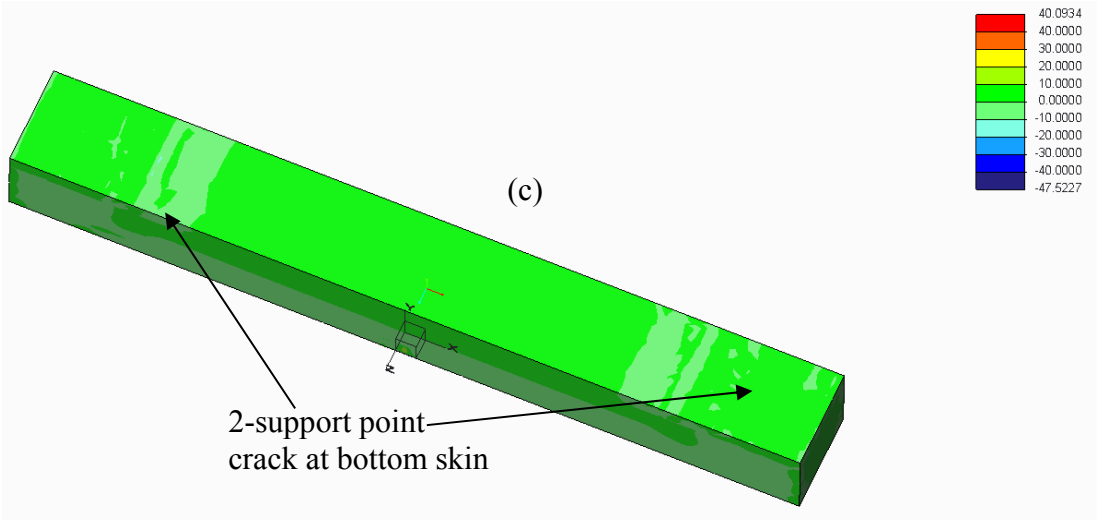

Figure 6.24: Comparison of the flexural failure mode of syntactic foam core sandwich panel (a) Actual flexural testing (b) FEA flexural simulation (c) Support beam dented

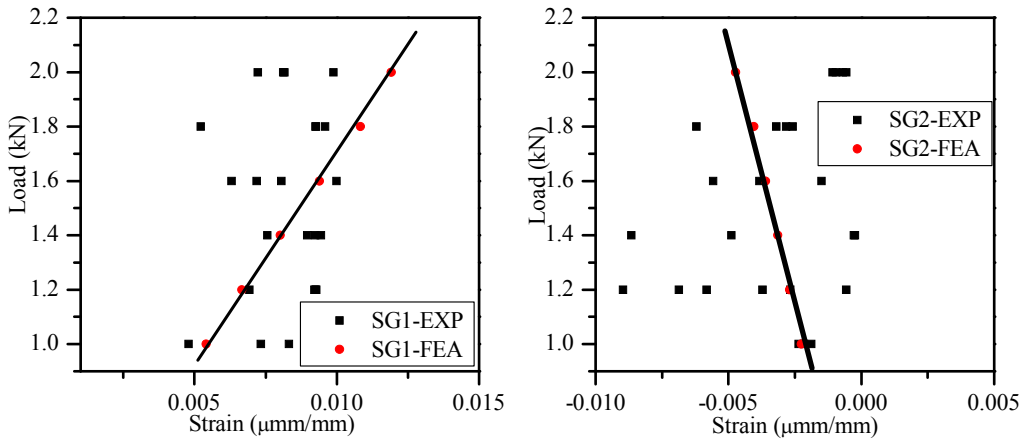

Figure 6.25: Comparison of flexural testing and FEA simulation for (a) SG1 and (b) SG2

6.4 Summary

In this chapter, two categories of analyses were carried out: thermomechanical properties, and a comparison for stress concentration factor (SCF) of syntactic foams, using a Finite Element Analysis (FEA) simulation approach with PTC CREO 3.0 software to finalise the behaviour of syntactic foam. The thermomechanical properties of syntactic foam were investigated in the form of TGA and TMA analyses. In this parametric TGA study, the results for T_g of syntactic foam with different (wt.%) of glass microballoon were increased after a hygrothermal process in which three different types of water were compared with dry specimens. Within the TGA/DTGA curve it was also found that onset temperature (T_{onset}), peak temperature (T_{peak}) and end temperature (T_{end}) showed varied temperatures when more glass microballoon content in syntactic foam was added. Moreover, their composition properties such as weight loss residue, as well as their temperature residue, also decreased until all specimens changed properties in the ash coal type.

The TMA analysis on kinetic energy, was conducted according to the first-order reaction Broido method, which is commonly used in polymer composites that have been discovered. In this study, it was revealed that the parameter, such as activation energy (E_a), decreased when the degradation temperature increased. Within this finding, E_a was varied and depended on the (wt.%) of glass microballoon in syntactic foam. The lower activation energy was required to complete the decomposition process. A linear expansion study was done, especially with a focus on the thermal

dimension stability of syntactic foam, and the result showed a decrease when more glass microballoon in syntactic foam was added. The lower thermal stability at a higher temperature could be very useful for an insulator product particularly in marine and aerospace engineering applications. The linear dimension stability, also called coefficient of thermal expansion (CTE), decreased when the glass microballoon content increased. The modification of Turner's model was applied in this study for the the comparison of CTE in three different temperatures: 30 ^{o}C, 50 ^{o}C and 70 ^{o}C for syntactic foam. The modification included parametric study involvement with the effect of radius ration, porosity and voids content in syntactic foam. As a result, the porosity content contributed much more to the CTE value, especially gap of ratio, which was different from the matrix porosity. The prediction of strain value between local strains from the experimental strain gauge was compared with the FEA simulation when their varied load in longitudinal and transverse axes was applied to tensile and flexural sandwich panel's syntactic foam. For the tensile specimen, the determination of the stress concentration factor (SCF) used one strain gauge, which was attached near the hole in the middle of the extensometer length. The results show that the SCF values were comparable between experiments with extensometer and SG values, with different percentages from 0.40 % to 1.36 %. The investigation of SCF for two SG were investigated using a specimen of 10 wt.%, which was attached near the hole area at the same position as previous tensile specimens. The comparison and prediction were made between experimental values and the FEA analysis results. It can be estimated that the experimental values of around 90 % and 70 % followed the FEA values for SG1 and SG2, respectively. The investigation on the strain value for flexural sandwich panel syntactic foam were also carried out using the FEA approach to predict the properties' behaviour in this study. It was found that the micro strain for SG1 for FEA was 17% higher than the experimental value, even though they were at the same loading setting. However, the prediction for the micro strain of SG2 was only 2.7 % different, which was considered a good agreement to predict the properties of syntactic foam core sandwich panel for different loading values. The previous report indicated that, SCF from FEA results is within 7% compared to the theoretical values and less than 14% error for countersunk rivet holes in orthotropic plates (Darwish et al., 2013). Another reasonable prediction simulation work also been made agreement with less 5% difference for their work on characterisation of the mechanical properties of pultruded fibre-reinforced polymer tube (Guades et al., 2014).

Chapter 7

Conclusions and Recommendations

7.1 Conclusions

The detailed experimental study of the synthesis and characterisation of glass microballoon/vinyl ester syntactic foam has provided a number of findings in Chapter 3. It is useful to report an important finding in relation to the prediction and interpretation of the properties of glass microballoon/vinyl ester syntactic foam in this study. In this study, it was revealed that the density of syntactic foam varied and decreased when the glass microballoon content increased, which followed the rule of mixture. The parameters such as wall thickness, ω and radius ratio, η played important roles in contributing to the low density foam behaviour. Porosity and void contents were calculated and it was found that cavity porosity was higher than matrix porosity but void content remained constant in all specimens. This might be due to care being taken during sample preparation, while gentle conventional stirring was enough to ensure that fewer glass microballoons were broken. Tensile and compressive characteristics of the vinyl ester matrix syntactic foam were investigated and it was revealed that the tensile strength was 70-80% higher than the compressive strength when glass content was reduced. Both in terms of compression and tensile strength, the comparison result could be attributed to the measurement procedure and the possibility of particles fracturing under compressive loading, even at low load levels. The maximum strength for both testing was led by SCFT-01 (2 wt.% of glass microballoons). Even though SCFT-01 had a lower tensile modulus when compared to all specimens, it still had a higher compressive modulus. Compressive moduli of this foam were found to be lower than that of neat resin, but the specific compressive modulus was higher. Both the specific tensile and specific compressive strengths had a higher value for SCFT-01 when compared with the other specimens, which is useful for light weight material. It was observed, from the relative modulus of elasticity results, that when the microballoons of $\eta < 0{:}955$ were used in this study, the resulting syntactic foams would show substantial benefit in mechanical properties. Both the compressive and tensile strength for VE110 vinyl ester / glass microballoons led when

compared with other glass microballoon type syntactic foams. Hence, these beneficial results showed that vinyl ester matrix syntactic foams are promising for structural applications due to their weight saving properties and that they could be applied to marine structures.

The fabrication and characterisation of syntactic foam core sandwich panels made from glass fibre reinforced plastic (GFRP) skins and foam core with different weight percentages of glass microballoon contents (2–10 wt.%) were demonstrated in Chapter 4. The mechanical behaviour of the syntactic foam core sandwich panels in relation to the properties of constituent materials was studied. The compressive strength of the sandwich panels was significantly affected by a low density foam core, as well as their modulus of elasticity and maximum stress value, particularly with 2 wt.% of glass microballoons. The tensile failure of the sandwich panels was also significantly affected by lower glass microballoon content (2 wt.%). The core failure was clearly observed compared to other failure modes, such as cohesive and adhesive failure modes. The selection of the GFRP skin also contributed as a primary factor to the fabrication of sandwich panels, as well as to considering the total density of the sandwich panels. The flexural testing of the syntactic foam sandwich panels indicated a higher strength when the glass microballoon content was increased in the core materials compared to that in unsymmetrical shear failure mode. Porosity content, de-bonding of glass microballoon and crack bridging might have contributed to the different values of the flexural stiffness of sandwich panels. The different thickness of syntactic foam core also played an important role in the deflection between GFRP skin and syntactic foam core with varied content of glass microballoons. The results of the load-deflection behaviour of syntactic foam core sandwich panels indicated a significant effect on the core properties with higher deflection when the glass microballoon content was increased, specifically to 8 wt.% and 10 wt.%.

The behaviour of syntactic foam was further explained in Chapter 5 in terms of its properties in marine applications such as water absorption in room temperature and high temperature, which is also called as hygrothermal. This started with the properties of density syntactic foams when it was immersed in three different types of water such as Fresh Water (FW), Double Distil (DD) water and Salt Water (SW). The density was varied after their weight was determined at the end of being immersed for a duration

of 30 days and 60 days. The capability of syntactic foam having decreased its density for water uptake showed when glass microballoon content from 2 wt.% to 10 wt.% for all water conditions was added. The density of syntactic foam in terms of its compressive strength for a duration of 30 days showed an average of below 1000 kgm^{-3} while for tensile strength it showed an average below 1100 kgm^{-3}. It was revealed that density of compressive syntactic foam was higher in FW and SW for a duration of 60 days while tensile specimens were also higher in FW and DD water. This was attributed to voids and pores contained in syntactic foam, since the water could not enter the polymeric resin nor hydrate in between glass microballoons and resin, or in the glass microballoons themselves. In addition, SEM photos also revealed that some specimens had cavity porosity, which was filled up with small glass microballoons, and debris from broken microballoons could discard the water to spread in syntactic foam as well.

Water uptake behaviour for compressive specimens of syntactic foam in room temperature showed an increase in their maximum weight (W^s) when glass microballoon content was added until the equilibrium condition was achieved. Syntactic foam had the highest maximum weight in FW condition with 1.92902 % for SF10WC-F (10 wt.% of glass microballoons), if compared with other waters. The maximum diffusion rate (W^m) was also highest in FW condition with a value of 1.50997 % and lowest rate was in SW condition with a value of 0.99062%. Tensile specimens showed the water uptake was achieved at the highest maximum weight in DD water with 8.01366 % for SF10WT-D (10 wt.% of glass microballoons), if compared with other types of water. The maximum diffusion rate and weight gained was also higher in DD water with 6.96945% and 8% for SF10WT-D (10 wt.% of glass microballoons), respectively. The lower water gain revealed in SW condition had a maximum of around 5 % only. The alkalisation properties of DD water may have contributed to this result. Other factors considered were poor interfacial bonding between matrix and microballoon and plasticisation behaviour of polymeric syntactic foam.

Results for hygrothermal compressive specimens of syntactic foam showed that the maximum weight was increased on average to a temperature almost 7 times higher than the room temperature. Moreover the equilibrium condition that could be achieved

from the water uptake also showed an increase, especially when immersed in FW and DD water. This might be attributed to the presence of porosity and voids near the surface of syntactic foam, which opened the surface area in hot conditions. Hygrothermal tensile specimens had a higher result, almost four times as high, if compared with compressive specimens for the maximum weight and maximum diffusion rate in the matrix material. The physical properties comparison with different shapes of specimens, such as rectangular for tensile strength, allowed the surface to absorb more water, which included an increasing in porosity content in syntactic foam. The highest W^s was detected in FW condition with a value of 37.15931% for specimen SF10WTH-F (10 wt.% of glass microballoons). The highest diffusion rate percentage belonged to the same group of specimens.

With regards to water diffusivity in the foams, D is generally higher in FW when compared to other water conditions. This is comparable with an increase in the glass microballoon content in syntactic foam as well, when the diffusivity value was increased for composites containing higher porosity content. However, D values for all compositions were slightly smaller in the SW condition, even though the glass microballoon content was increased. The reason for such a large discrepancy could be attributed to the high matrix porosity content in the syntactic foam. Similar results were detected when the specimens were immersed in a high temperature for hygrothermal testing. The reduction of diffusion rate, D in SW was related to enrichment with organic ions that made syntactic foam, particularly glass microballoons, more closed to each other's. In addition, the plasticisation of matrix resin was more severe in hygrothermal, especially when de-bonding occurred, and the gap would be closed and reduced for water entrapped in the porosity area as well.

The majority of specimens followed Fick's law with the agreement to achieve the equilibrium stage either in room temperature or higher temperatures for all water conditions. In the FW condition, the specimens achieved a linear equilibrium relationship between the water absorption rate $M(t)/M(\infty)$ and D_t/h^2 at the initial stage. Specimen SF4WT-FW (4 wt.% of glass microballoons) took longer to absorb the water and to achieve the equilibrium system while Specimens SF8WT-FW(8 wt.% of glass microballoons) and SF10WT-FW (10 wt.% of glass microballoons) showed lower water absorption rates. Among all the specimens, SF8WT-DD (8 wt.% of glass

microballoons) and SF10WT-DD (10 wt.% of glass microballoons) took longer to get to a saturated condition when immersed in DD water. Specimens SF6WT-S (6 wt.% of glass microballoons) and SF8WT-S (8 wt.% of glass microballoons) showed their diffusion rate was faster than others at 0.1 in the SW system.

Again this phenomenon also showed the presence of cavity porosity can discarded the water entering the syntactic foam to achieve the equilibrium system, when observed through an SEM micrograph. Variations of compression strength in room temperature conditions (T: 25 ^{o}C) were revealed with the ultimate compression strength after being exposed to FW, DD water and SW, which was comparable to dry specimens, respectively. The compressive behaviour was revealed to be more likely for lower glass microballoon content, which had taken longer to fracture, compared with higher microballoon content, which was much lower in rigidity and allowed the more intact microballoons to be crushed. This indicated a decreasing trend in compressive strength and compressive modulus with an increasing immersion time; however, there was a trend of an increasing maximum compressive strain as immersion time increased after being exposed to aqueous environments. It was also revealed that the tensile modulus showed a decrease for all specimens and had a similar trend for dry specimens. This might have been due to a de-bonding problem that occurred between matrix and resin, and as a result the connectivity was loose, which was detected during the tensile testing of the specimens.

The compressive strength in hygrothermal conditions, for hydrolytic specimens, showed a decrease in the yield compressive strength as compared to the salty specimens. Furthermore, the mechanical properties of foams immersed in FW 60 days showed a further decrease in yield compressive strength by 25% for immersed specimens and 15-20% for DD specimens, as compared to those of the specimens immersed in SW. Additionally, the compressive strains of hydrolytic foams at the yield compressive strength increased. This indicates that the stiffness of all types of foams was lowered due to the presence of moisture in the specimens. FW and DD made the foam softer and more brittle than the SW did, regardless of the dry foams. The tensile stress-strain curves of the foams immersed in hygrothermal water conditions exhibited a decrease in tensile strength when glass microballoon content was added for a duration of 30 days and 60 days. Moreover, foams immersed in SW showed a larger

decrease in tensile strength than those in FW and DD water for both durations. This indicates that the immersed foams had more ductility than dry foams due to the presence of moisture in the foams, which may have caused plasticisation of the matrix resin. Moreover, SW made the foam more ductile than DD and FW water. The reason for the decreased ductility was the same as that in the compression tests.

In addition, the presence of porosity and voids in syntactic foam also contributed to the ductility of specimens regardless of the water condition. An extended explanation can be made by comparing modulus values, and it could be seen that all types of syntactic foams were affected due to the presence of moisture in the specimens after being immersed in high temperature conditions. These behaviours could be attributed to two factors: the moisture content entrapped in the porosity regime in the specimens, and the possibility of material property degradation. A considerable decrease in modulus revealed that water absorption had infused in the specimens, allowing for cavity and matrix porosity and leading them to contain the water inside. Due to being brittle and easily cracked, the strength as well as modulus were reduced in the high temperature tested specimens, which indicated an occurrence of some additional events in the material. It must be noted that the thermal and water absorption into the porosity area induced strains and generated the syntactic foam to come off the glass microballoons, which could then fracture.

The thermomechanical properties and Finite Element Analysis (FEA) simulation of syntactic foam were investigated in Chapter 6. In this parametric TGA study, the results for T_g of syntactic foam with different weight percentages of glass microballoons were increased after a hygrothermal process in which three different types of water were compared with dry specimens. Within the TGA/DTGA curve it was also found that onset temperature (T_{onset}), peak temperature (T_{peak}) and end temperature (T_{end}) showed varied temperatures when more glass microballoon content in syntactic foam was added. Moreover, their composition properties such as weight loss residue, as well as their temperature residue, decreased until all specimens changed properties in the ash coal type. In the Thermomechanical Analysis (TMA) analysis, the linear dimension stability, also called coefficient of thermal expansion (CTE), decreased when the glass microballoon content increased. The modification of Turner's model was applied in this study for a comparison of CTE in three different

temperatures (30 ^{o}C, 50 ^{o}C and 70 ^{o}C) for syntactic foam. The modification included parametric study involvement into the effect of radius ration, porosity and voids content in syntactic foam. The porosity content contributed much more to the CTE value, especially gap of ratio, which was different from the matrix porosity. The prediction of strain value for Stress Concentration Factor (SCF) between local strains from the experimental strain gauge was compared with the FEA simulation, when their varied load in longitudinal and transverse axes was applied to the specimens (tensile and flexural). The results show that the SCF values were comparable between experiments with extensometer and SG values, with different percentages from 0.40 % to 1.36 %. The FEA investigation was further extended using a specimen with 10 wt.% for simulation in this study. It could be estimated that the experimental values of around 90 % and 70 % followed the FEA values for SG1 and SG2, respectively. Furthermore, FEA analysis on flexural sandwich panels of syntactic foam was compared for different compositions of glass microballoons with experimental values. It was found that the micro strain for SG1 for FEA was 17% higher than the experimental value, even though they were at the same loading setting. However, the prediction for the micro strain of SG2 was only 2.7 % different, which was considered a good agreement to predict the properties of sandwich panel syntactic foam for different loading values.

7.2 Recommendations

It is proposed that further investigation can be carried out in more detail on characteristic properties of syntactic foam, particularly for marine applications. The following recommendations are suggested:

a) An investigation into environmental degradation behaviour such as moisture resistance, UV index and sunlight testing should be conducted, in the form of outdoor weathering tests, to ensure that it can be applied for marine potential applications. Hence, the mechanical properties of syntactic foam should also be tested after they have been periodically exposed to natural weathering.

b) Further understanding about interface bonding between glass microballoons and matrix resin should be investigated using DMA (Dynamic mechanical

analysis) testing through fatigue and delamination analysis. By conducting this testing, the fatigue life of syntactic foam could be monitored to gain more insight into further mechanical properties of syntactic foam.

c) An analytical investigation or micro analysis of a statistical approach can be conducted with a focus on all testing items, particularly mechanical properties of syntactic foam. These analyses could statistically prove the mechanical property improvement of glass microballoons as filler and also as core material of sandwich panel.

References

Abbess. 2011. Sandwich syntactic foams [Online]. http://www.abbess.com/vacuum/node/147. [Accessed].

Adkins, L. & Good, F. Ashland. High performance epoxy vinyl ester resins (EVERs) with improved processing. Proceedings of the ACUN-3 International Composites Conference, 2001 Sydney. University of New South Wales.

Alam, M. K. & Khan, M. A. 2006. Comparative study of water absorption behaviour in bio pol and jute-reinforced bio pol composite using neutron radiography technique. Reinforce Plastic Composite 25, 11.

Allen, H. 1969. Analysis and design of structural sandwich plates, Franklin Book Co.

Alomayria, T., Assaedia, H., Shaikh, F. U. A. & Lowa, I. M. 2014. Effect of water absorption on the mechanical properties of cotton fabric-reinforced geo polymer composites. Journal of Asian Ceramic Societies, 2, 223-230.

Altuna, F. I., Esposito, L. H., Ruseckaite, R. A. & Stefani, P. M. 2010. Thermal and mechanical properties of anhydride-cured epoxy resins with different contents of bio based epoxides soybean oil. Journal of Applied Polymer Science, 120, 789-798.

ASTM 2002. Standard Test Method for Compressive properties of rigid plastics. Standard D 695-02a. 100 Barr Harbor Drive, PO Box C700, West Conshohocken, PA 19428-2959, United States.

ASTM 2003. Standard test methods for flexural properties of unreinforced and reinforced plastics and electrical insulating materials. ASTM D790-03. 100 Barr Harbor Drive, PO Box C700, West Conshohocken, PA 19428-2959, United States.

ASTM 2010. Standard test method for tensile properties of plastics. D638-10. 100 Barr Harbor Drive, PO Box C700, West Conshohocken, PA 19428-2959, United States.

ASTM 2011. Standard test method for flatwise compressive properties of sandwich cores. C365/C365M - 11a. 100 Barr Harbor Drive, PO Box C700, West Conshohocken, PA 19428-2959, United States.

ASTM 2012. Standard terminology relating to plastics. D883-12. 100 Barr Harbor Drive, PO Box C700, West Conshohocken, PA 19428-2959. United States.

ASTM 2012. Standard test method for core shear properties of sandwich constructions by beam flexure. C393/C393M. 100 Barr Harbor Drive, PO Box C700, West Conshohocken, PA 19428-2959, United States.

ASTM 2016. Standard test method for assignment of the glass transition temperature by thermomechanical analysis. In: 11(2016), A. E.-. (ed.). ASTM.

Ayers, S. R. 2001. Material Foundations for the Application of Fibre Composites Materials in Civils and Structural Engineering. PhD, USQ.

Balch, D. & Dunand, D. 2006. Load partitioning in aluminium syntactic foams containing ceramic microspheres. Acta Material 54, 1501-1511.

Balch, D. K., O'Dwyer, J. G., Davis, G. R., Cady, C. M., Gray, G. T. & Dunand, D. C. 2005. Plasticity and damage in aluminium syntactic foams deformed under dynamic and quasi-static conditions. Materials Science and Engineering: A, 391, 408-417.

Bardella, L. & Genna, F. 2001. Elastic design of syntactic foamed sandwiches obtained by filling of three-dimensional sandwich-fabric panel. International Journal of Solids and Structures, 38, 307-333.

Bardella, L., El-Hadek, M. A. & Tippur, H. V. 2003. Discussion on the paper Simulation of porosity by microballoon dispersion in epoxy and urethane: Mechanical measurements and models. Journal of Materials Science Letters, 22, 1643-1646.

Baskaran, R., Sarojadevi, M. & Vijayakumar, C. T. 2014. Utilization of granite powder as filler for vinyl ester resin. Malaysian Polymer Journal, 9, 39-44.

Ben Daly H, B. B. H., Hfaied N, Harchay M, Boukhili R. 2007. Investigation of water absorption in pultruded composites containing fillers and low profile additives. Polymer Composite, 28, 355-364.

Bestech 2015. Sensor and Teaching Equipment Product catalogue. In: BESTECH (ed.).

Boon, A. & Palfreyman, A. 1998. Derakane Epoxy Vinyl Ester Resins - High Performance Resins for Challenging Structural Applications. Midland: The Dow Chemical Company, The Dow Chemical Company.

Broido, A. 1969. A simple, sensitive graphical method of treating thermogravimetric analysis data. Journal Polymer Science, 7, 761-1773.

Bunn, P. & Mottram, J. T. 1993. Manufacture and Compression Properties of Syntactic Foams. Composites Part A: Applied Science and Manufacturing, 24, 565-571.

C. Periasamy, Jhaver, R. & Tippur, H. V. 2010. Quasi-static and dynamic compression response of a light weight interpenetrating phase composite foam. Material Science Engineering A, 527, 2845-2856.

Caeti, R., Gupta, N. & Porfiri, M. 2009. Processing and compressive response of functionally graded composites. Materials Letters, 63, 1964-1967.

Cai, K. Effects of the Properties of Bi-modulus Material on Stiffness Design. Proceeding of Intelligent Computation Technology and Automation (ICICTA), 11-12 May 2010, Changsha, China.

Calahorra, A., Gara, O. & Kenig, S. 1987. Thin film parylene coating of three-phase syntactic foams. Journal of Cellular Plastic, 23, 383-398.

Challa, G. 1993. Polymer Chemistry, Chichester, Ellis Horwood Ltd.

Clements, L. 1995. Overview of Composite Materials. Society for the Advancement of Materials and Process Engineering. Tutorial Notes. 40th International SAMPE Symposium. Covina.

Cochran, J. 1998. Ceramic hollow spheres and their applications. Solid State & Materials Science, 3, 474-479.

Cotgreave, T. C. & Shortall, J. B. 1978. The fracture toughness of reinforced polyurethane foam. Journal Material Science, 13, 722-730.

Das, A. M., Ali, A. A. & Hazarika, M. P. 2014. Thermal degradation and kinetic study of vinyl ester monomer grafted silk fibroin. International Journal of Engineering and Technical Research (IJETR), 2, 69-78.

Darwish, F., Tashtoush, G. & Gharaibeh, M. 2013. Stress concentration analysis for countersunk rivet holes in orthotropic plates. European Journal of Mechanics A/Solids, 37**,** 69-78.

Dash, B., Rana, A. K., Mishra, H. K., Nayak, S. K., Mishra, S. C. & Tripathy, S. S. 1999. Novel, low cost jute-polyester composites: Part 1: processing, mechanical properties, and SEM analysis. Polymer Composite, 20, 1-5.

Davey, S. W. 2004. A Foundation Investigation of Vinyl ester/Cenosphere Composites Materials for Civil and Structural Engineering PhD, University of Southern Queensland Australia.

Deshpande, V. & Fleck, N. 2000. Isotropic constitutive models for metallic foams. Journal Mechanic Physics Solids, 48, 1253-1283.

Devi, K., John, B. & Ninan, C. N. K. 2007. Effect of low-density filler on mechanical properties of syntactic foams of cyanate ester. Polymer, 48, 3183-3191.

Dhakal, H., Zhang, Z. & Richardson, M. 2007. Effect of water absorption on the mechanical properties of hemp fibre reinforced unsaturated polyester composites. Composite Sciences Technology, 67, 1674-1683.

Division, P. I. L. E. G. M. 2011. Spherical Typical Product Characteristics Valley Forge, PA 19482 USA: Potters Industries LLC.

Dwivedi, D. K., Kaith, B. S. & Singha, A. S. 2003. Preparation of polystyrene matrix based composites using flax-g-copolymers as reinforcing agent and evaluation of the mechanical behavior. International Journal Plastic Technology, 7, 119-125.

Eric, G. 1999. Marine Composites, Annapolis, Maryland, Eric Greener Associates, Inc.

Flynn, J. H. 1989. Encyclopedia of Polymer Science and Engineering, New York, Wiley.

Gladysz, G., Perry, B., McEachen, G. & Lula, J. 2006. Three-phase syntactic foams: structure-property relationships. Journal of Material Science 41, 4085-4092.

Gopalakrishnan, S. & Sujatha, R. 2011. Comparative thermoanalytical studies of polyurethanes using Coats-Redfern, Broido and Horowitz-Metzger methods. Der Chemica Sinica, 2, 103-117.

Grosjean, F., Bouchonneau, N., Choqueuse, D. & Sauvant-Moynot, V. 2009. Comprehensive analyses of syntactic foam behaviour in deep water environment. Journal of Materials Science, 44, 1462-1468.

Guades, E., Aravinthan, T. & Islam, M. M. 2014. Characterisation of the mechanical properties of pultruded fibre-reinforced polymer tube. Materials and Design, 63, 305-315.

Gupta, N. & Nagorny, R. 2006. Tensile properties of glass microballoon-epoxy resin syntactic foams. Journal of Applied Polymer Science, 102, 1254-1261.

Gupta, N. & Ricci, W. 2006. Comparison of compressive properties of layered syntactic foams having gradient in microballoon volume fraction and wall thickness. Materials Science and Engineering A, 427, 331-342.

Gupta, N. & Woldesenbet, E. 2003. Hygrothermal studies on syntactic foams and compressive strength determination. Composite Structures, 61, 311-320.

Gupta, N., Karthikeyan, C. S. & Kishore, S. S. a. 1999. Correlation of processing methodology to the physical and mechanical properties of syntactic foams with and without fibres. Materials Characterization, 43, 271-277.

Gupta, N., Priya, S., Islam, R. & Ricci, W. 2006. Characterization of mechanical and electrical properties of epoxy-glass microballoon syntactic composites. Ferroelectrics, 345, 1-12.

Gupta, N., Woldesenbet, E. & Kishore 2002a. Compressive fracture features of syntactic foam-microscopic examination. Journal of Material Science, 37, 3199-3209.

Gupta, N., Woldesenbet, E. & Mensah, P. 2004. Compression properties of syntactic foams: Effect of cenosphere radius ratio and specimen aspect ratio. Composites: Part A, 35, 103-111.

Gupta, N., Woldesenbet, E., Kishore & Sankaran, S. 2001. Studies on compressive failure features in syntactic foam material. Journals of Materials Science, 36(18), 4485-4491.

Gupta, N., Woldesenbet, E., Kishore & Sankaran, S. 2002b. Response of syntactic foam core sandwich structured composites to three-point bending. Journal of Sandwich Structures and Materials, 4, 249-272.

Gupta, N., Ye, R. & Porfiri, M. 2010. Comparison of tensile and compressive characteristics of vinyl ester/glass microballoon syntactic foams. Composites Part B: Engineering, 41, 236-245.

Hiel, C., Dittman, D. & Ishai, O. 1993. Composite sandwich construction with syntactic foam core: A practical assessment of post-impact damage and residual strength. Composites 24, 447-450.

Hinves, J. & Douglas, C. 1993. The development of a hybrid advanced composite-syntactic foam structural component for use in undersea vehicles. IEEE, III, 468-472.

Hodge, A., Kaul, R., McMahon, W. & Reinarts, T. 2000. Sandwich composite, syntactic foam core based application for space structures. 45th International 11 SAMPE Symposium and Exhibition (Proceedings).

Huang, J. S. & Gibson, L. J. 1993. Elastic moduli of a composite of hollow spheres in a matrix. Journal Mechanic Physics Solids 41, 55-75.

Huo, S., Chevali, V. S. & Ulven, C. A. 2013. Study on Interfacial Properties of Unidirectional Flax/Vinyl Ester Composites: Resin Manipulation on Vinyl Ester System. Journal of Applied Polymer Science, 128, 3490-3500.

Ishai, O., Hiel, C. & Luft, M. 1995. Long-term hygrothermal effects on damage tolerance of hybrid composite sandwich panels. Composite 26, 47-55.

Islam, M. M. & Kim, H. S. 2007. Novel syntactic foams made of ceramic hollow micro-spheres and starch: theory, structure and properties. Journal of Materials Science, 42, 6123-6132.

Jang-Kyo Kim, Chugang Hu, Ricky S.C. Woo & Sham, M.-L. 2005. Moisture barrier characteristics of organoclay-epoxy nanocomposites. Composites Science and Technology, 65, 805-813.

John, B., Nair, C. P. R. & Ninan, K. N. 2010. Effect of nanoclay on the mechanical, dynamic mechanical and thermal properties of cyanate ester syntactic foams. Materials Science and Engineering: A, 527, 5435-5443.

John, B., Nair, C. P. R., Devi, K. A. & Ninan, K. N. 2007. Effect of low-density filler on mechanical properties of syntactic foams of cyanate ester. Journal of Materials Science, 42, 5398-5405.

Juska, T. & Puckett, P. 1997. Matrix Resins and Fibre / Matrix Adhesion., New York, Marcel Dekker Inc.

Karthikeyan, C. S., Sankaran, S. & Kishore 2005. Flexural behaviour of fibre-reinforced syntactic foams. Macromolecular Materials and Engineering, 290, 60-65.

Karthikeyan, C., Sankaran, S. & Kishore 2004. Elastic behaviour of plain and fibre-reinforced syntactic foams under compression. Materials Letters, 58, 995-999.

Karthikeyan, C., Sankaran, S., Kumar, M. & Kishore 2001. Processing and compressive strengths of syntactic foams with and without fibrous reinforcements. Journal of Applied Polymer Science 81, 405-411.

Kenig, S., Raiter, I. & Narkis, M. 1984. Three-phase silicone based syntactic foam. Journal Cell Plastic, 423-429.

Kim, H. S. & Oh, H. H. 2000. Manufacturing and impact behaviour of syntactic foam. Journal Applied Polymer Science, 76, 1324-1328.

Kim, H. S. & Plubrai, P. 2004. Manufacturing and failure mechanisms of syntactic foam under compression. Composites Part A: Applied Science and Manufacturing, 35, 1009-1015.

Kim, H. S., Sung, H. & Mohamad, A. K. 2001. Fracture and Impact behaviour of hollow micro-sphere/epoxy resin composites. Composites Part A 32, 1311 - 1317.

Kim, M.-K., Kwon, K.-J. & Han, Y.-K. 2011. Synthesis of cardo based poly (arylene ether)s for flexible plastic substrates and their properties. Bull. Korean Chem. Soc., 32, 3311-3316.

Kirk-Othmer, R. 1996. Polyesters, Unsaturated. In: Encyclopaedia of Chemical Technology. 4 ed. New York: John Wiley and Sons.

Kishore, Shankar, R. & Sankaran 2005. Gradient syntactic foams: Tensile strength, modulus and fractographic features. Materials Science and Engineering A, 412, 153-158.

Koopman, M., Chawla, K., Carlisle N & Gladysz, G. 2006. Microstructural failure modes in three-phase glass syntactic foams. Journal of Material Science 41, 4009-4014.

Kulesa, A. T. & Robinson, M. J. 2014. Analytical study of structural thermal insulating syntactic foams. Composite Structures, 119, 551-558.

Kumar, S. A. & Ahmed, K. S. 2015. Effects of ageing on mechanical properties of stiffened syntactic foam core sandwich composites for marine applications. Journal of Cellular Plastics, 0, 1-30.

Lawrence, E. & Pyrz, R. 2001. Viscoelastic properties of polyethylene syntactic foam with polymer microballoons. Polymer Composites, 9, 227-237.

Lawrence, E., Wulfsohm, D. & Pyrz, R. 2001. Microstructural Characterisation of a syntactic foam. Polymer Composites, 9, 449-457.

Lefebvre, X. & V. Sauvant-Moynot, D. C., P. Chauchot 2009. Durability of Syntactic Foams for Deep Offshore Insulation: Modelling of Water Uptake under Representative Ageing Conditions in Order to Predict the Evolution of Buoyancy and Thermal Conductivity. Oil & Gas Science and Technology - Rev. IFP, 64, 165-178.

Li, G. & Muthyala, V. D. 2008. A cement based syntactic foam. Materials Science and Engineering A, 478, 77-86.

Li, P., Petrinic, N., Siviour, C. R., Froud, R. & Reed. 2009. Strain rate dependent compressive properties of glass-microballoon epoxy syntactic foams. Journal of Material Science Engineering A 515, 19-25.

Lin, T. C., Gupta, N. & Talalayev, A. 2008. Thermoanalytical characterization of epoxy matrix-glass microballoon syntactic foams. Journal of Materials Science, 44, 1520-1527.

Lin, T., Gupta, N. & Talalayev, A. 2009. Thermal conductivity of multiphase particulate composite materials. Journal Material Science, 44, 1540-1550.

Mae, H., Omiya, M. & Kishimoto, K. 2008. Effects of strain rate and density on tensile behavior of polypropylene syntactic foam with polymer microballoons. Materials Science and Engineering: A, 477, 168-178.

Maharsia, R. R. & Jerro, H. D. 2007. Enhancing tensile strength and toughness in syntactic foams through nanoclay reinforcement. Materials Science and Engineering: A, 454-455, 416-422.

Maharsia, R., Gupta, N. & Jerro, H. D. 2006. Investigation of flexural strength properties of rubber and nanoclay reinforced hybrid syntactic foams. Materials Science and Engineering: A, 417, 249-258.

Mallick, P. 1997. Introduction: Definitions, Classifications and Applications., New York, Marcel Dekker Inc.

Manalo, A. C., Aravinthan, T. & Karunasena, W. 2010. Flexural behaviour of glue-laminated fibre composite sandwich beams. Composite Structures, 92, 2703-2711.

Marsh, G. 2007. Tooling up for large wind turbine blades. Reinforced Plastics, 51, 38-43.

Materials, A. S. F. T. 2004. ASTM Standard C297M-04. Standard test method for flatwise tensile strength of sandwich constructions. USA.

Mathias, L. 2016. Monomer bisphenol-A. Polymer Learning Centre.

Meteer, C. L. & Philipps, T. E. 1999. Syntactic foam core material for composite structures. USA patent application.

Meteer, C. L. 2011. Syntactic foam core material for composite structures, International patent classification.

Methven, J. & Dawson, J. 1982. Reinforced foams. In: HILYARD, N. (ed.) Mechanics of Cellular Plastics London: Applied Science Publishers Ltd.

Mills, N. 2007. Engineering and Biomechanics Applications and Design Guide. Polymer Foams Handbook, 79-90.

Mostafa, A., Shankar, K. & Morozov, E. V. 2013. Insight into the shear behaviour of composite sandwich panels with foam core. Materials and Design 50, 92-101.

Muller, J. 2014. Subsea Market Expected to reach 115 billion by 2020. Offshore Magazine.

Munikenche Gowda T, N. A., Chhaya Rajput 1999. Some mechanical properties of untreated jute fabric-reinforced polyester composites. Composite Part A: Applied Science and Manufacturing, 30, 277-284.

Nambiar, E. & Ramamurthy, K. 2007. Air-void characterization of foam concrete. Chemical Concrete Res, 37, 221-330.

Narkis, M., Gerchcovich, M., Puterman, M. & Kenig, S. 1982. Syntactic foams III. Three-phase materials produced from resin coated microballoons. Journal of Cellular Plastic, 18, 230-232.

Narkis, M., Puterman, M. & Kenig, S. 1980. Syntactic foam II, Preparation and characterisation of three-phase system. Journal Cell Plastic, 20, 320-330.

Nijenhuis, K. T., Addink, R. & Vegt, A. V. d. 1989. A study on composites of nylon-6 with hollow glass microspheres. Polymer Bulletin, 21, 467-474.

Nji, J. & Li, G. Q. 2008. A CaO enhanced rubberized syntactic foam. Composite Part A-Applied Science and Manufacturing, 39, 1404-1411.

Papakonstantinou, C. G., Giancaspro, J. W. & Balaguru, P. N. 2007. Fire response and mechanical behaviour of polysialate syntactic foams. Composites Part A: Applied Science and Manufacturing, In Press, Corrected Proof.

Phang, Z. & Ding, J. 2012. Poly(lactide-co-glycolide) porous scaffolds for tissue engineering and regenerative medicine. Interface Focus, 2, 366-377.

Poveda, R., Gupta, N. & Porfiri, M. 2010. Material Letter, 64, 2360.

Puterman, M. & Narkis, M. 1980. Syntactic foam I, Preparation, structure and properties. Journal Cell Plastic, 223-229.

Qian, J., Liu, Z., Chen, J., Huang, R., Shi, C. & Guo, W. 2014. Synthesis and curing behaviour of novel multifunctional hybrid oligomers. Journal of Applied Polymer Science, 42276, 1-10.

Ratna, D. 2001. Mechanical properties and morphology of epoxidase soybean-oil-modified epoxy resin Polymer International, 50, 179-184.

Ray, D. & Gnanamoorthy, R. 2007. Friction and wear behaviour of vinyl ester resin matrix composites filled with fly ash particles. Journal of Reinforced Plastics and Composites, 26, 5-13.

Ray, D., Bhattacharya, D., Mohanty, A. K., Drzal, L. T. & Mishra, M. 2006. Static and dynamic mechanical properties of vinyl ester resin matrix composites filled with fly ash. Macromolecular Materials and Engineering, 291, 784-792.

Rittel, D. 2005. Adiabatic shear failure of a syntactic polymeric foam. Materials Letters, 59, 1845-1848.

Rizzi, E., Papa, E. & Corigliano, A. 2000. Mechanical behaviour of a syntactic foam: experiments and modeling. International Journal of Solids and Structure, 37, 5773-5794.

Rohatgi, P., Kim, J., Gupta, N., Alaraj, S. & Daoud, A. 2006. Compressive characteristics of A356/fly ash cenosphere composites synthesized by pressure infiltration technique. Composite Part A: Applied Science and Manufacturing, 37, 430-437.

Sadler, R., Sharpe, M. & Panduranga, R. 2009. Water immersion effect on swelling and compression properties of eco-core, PVC foam and balsa wood. Composite Structures, 90, 330-336.

Saha, A., Das, S., Bhatta, D. & Mitra, B. 1999. Study of jute reinforced polyester composites by dynamic mechanical analysis. Applied Polymer Sciences, 71, 1505-15013.

Saha, M. C., Nilufar, S., Major, M. & Jeelani, S. 2008. Processing and performance evaluation of hollow microspheres filled epoxy composites. Polymer Composites, 29, 293-301.

Salleh, Z., Islam, M. & Ku, H. 2014. Study on compressive properties of syntactic foams for marine applications. Journal of Multifunctional Composite, 21-27.

Samsudin, S. S. 2011. Development and characterization of epoxy syntactic foam filled with epoxy hollow spheres. Express Polymer Letters, 5, 653-660.

Sauvant-Moynot, V., Gimenez, N. & Sautereau, H. 2006. Hydrolytic ageing of syntactic foams for thermal insulation in deep water: degradation mechanisms and water uptake model. Journal of Materials Science, 41, 4047-4054.

Seamark, M. 1991. Use of syntactic foam for subsea buoyancy. Cellular Polymers, 10, 308-321.

Shao, B. & Yan, X. 2011. Reliability analysis of locally thinned submarine pipelines in Cheng Dao oil field. Applied Mechanics and Materials, 94-96, 1527-1530.

Shen, S. Y., Masters, F. J., Upjohn, H. L. & Ferraro, C. C. 2013. Mechanical resistance properties of FRP/polyol-isocyanate foam sandwich panels. Composite Structures, 99, 419-432.

Shivakumar, K., Argade, S. & Sadler, R. 2006. Processing and properties of a lightweight fire resistant core material for sandwich structures. Journal Advance Materials, 38, 1-17.

Shunmugasamy, V. C., Pinisetty, D. & Gupta, N. 2012. Thermal expansion behaviour of hollow glass particle/vinyl ester composites. Journal of Materials Science, 47, 5596-5604.

Shutov, F. 1996. Syntactic Polymer Foams. Advances in Polymer Science, 63-123.

Song, B., Chen, W. & Yanagita, T. 2005. Temperature effects on dynamic compressive behaviour of an epoxy syntactic foam. composite Structures, 67, 289-298.

Song, F. & Gao, Y. 2009. Chemical composition, sources, and deposition fluxes of water-soluble inorganic ions obtained from precipitation chemistry measurements collected at an urban site in northwest China. Journal of Environmental Monitoring, 14, 3000-3008.

Subhasha, G., Liu Q., & Gao, X. L. 2006. Qua static uni axial compression behaviour of hollow glass microspheres epoxy based syntactic foams. International Journal Impact Engineering 32, 1113-1126.

Sultaniaa, M., Yadawb, S. B., Raia, J. S. P. & Srivastavaa, D. 2010. Laminates based on vinyl ester resin and glass fabric: A study on the thermal, mechanical and morphological characteristics. Materials Science and Engineering A, 527, 4560-4570.

Swetha, C. & Kumar, R. 2011. Quasi-static uni-axial compression behaviour of hollow glass microspheres/epoxy based syntactic foams. Materials & Design, 32, 4152-4163.

T.P. Mohan & Kanny, K. 2011. Water barrier properties of nanoclay filled sisal fibre reinforced epoxy composites. Composites Part A: Applied Science and Manufacturing, 42, 385-393.

Tagliavia, G., Porfiri, M. & Gupta, N. 2009. Vinyl ester-glass hollow particle composites: dynamic mechanical properties at high inclusion volume fraction. Journal Composite Material, 43, 561-582.

Tagliavia, G., Porfiri, M. & Gupta, N. 2012. Influence of moisture absorption on flexural properties of syntactic foams. Composites: Part B, 43, 115-123.

Tao, X. & Zhao, Y. 2012. Compressive failure of Al alloy matrix syntactic foams manufactured by melt infiltration. Material Science Engineering A, 549, 228-232.

Tien, C., Gupta, N. & Talalayev, A. 2009. Thermoanalytical characterization of epoxy matrix-glass microballoon syntactic foams. Journal Material Science, 44, 1520-1527.

Trelleborg 2007. Subsea Buoyancy Products. Engineered System. Houston, United State America Trelleborg CRP Limited.

Updegraff, I. 1982. Unsaturated Polyester Resins. In: LUBIN, G. (ed.) Handbook of Composites. New York: Van Nostrand Reinhold.

Vasanth, C., Dinesh, P. & Gupta, N. 2012. Thermal expansion behaviour of hollow glass particle/vinyl ester composites. Journal Materials Science, 47, 5596-5604.

Verweiji, H., With, G. D. & Veeneman, D. 1985. Hollow glass microsphere composites: preparation and properties. Journal of Material Science, 20, 1069-1078.

Warren, C. & Richard, G. 2002. Stress Concentration Factor. Roark's Formula for Stress and Strain, McGraw-Hill.

Watkins, L. 1988. Syntactic foam buoyancy for production risers. Seventh International Conference on Offshore Mechanical and Artic Engineering. Houston, Texas.

Wouterson, E. M., Boey, F. Y. C., Hu, X. & Wong, S. C. 2007. Effect of fiber reinforcement on the tensile, fracture and thermal properties of syntactic foam. Polymer, 48, 3183-3191.

Wouterson, E., Boey, F., Hu, X. & Wong, S. 2004. Fracture and impact toughness of syntactic foam. Journal of Cell Plastics, 40, 145-154.

Wouterson, E., Boey, F., Hu, X. & Wong, S. 2005. Specific properties and fracture toughness of syntactic foam: effect of foam microstructures. Composites Science and Technology, 65, 1840-1850.

Xua, T. & Li, G. 2011. Durability of shape memory polymer based syntactic foam under accelerated hydrolytic ageing. Materials Science and Engineering A, 528, 7444-7450.

Yung, K., Zhu, B., Yue, T. & Xie, C. 2009. Preparation and properties of hollow glass microsphere-filled epoxy-matrix composites. Composites Science and Technology, 69, 260-264.

Zaske, O. & Goodman, S. 1998. Unsaturated Polyester and Vinyl Ester Resins. In: GOODMAN, S. (ed.) Handbook of Thermoset Plastics. New Jersey: Noyes Publications.

Zeng, H. B., Pattofatto, S., Zhao, H., Girard, Y. & Fascio, V. 2010. Impact behaviour of hollow sphere agglomerates with density gradient. International Journal Mechanical Science, 52, 680-688.

Zhang, L. & Ma, J. 2009. Processing and characterization of syntactic carbon foams containing hollow carbon microspheres. Carbon, 47, 1451-1456.

Zhang, L. & Zhao, Y. 2007. Mechanical response of Al matrix syntactic foams produced by pressure infiltration casting. Journal Composite Material, 41, 2105-2117.

Zhou, J. & Lucas, J. P. 1999. Hygrothermal effects of epoxy resin. Part II: variations of glass transition temperature. Polymer, 40,5513-5522.